HAL
open science

# Sand Tectonics : a material-based approach to architectural design and fabrication

Ahmed Hussein Abouelkheir

## To cite this version:

Ahmed Hussein Abouelkheir. Sand Tectonics : a material-based approach to architectural design and fabrication. Art and art history. Université Paris-Est, 2021. English. NNT : 2021PESC1105 . tel-03676526

**HAL Id: tel-03676526**

**https://theses.hal.science/tel-03676526v1**

Submitted on 24 May 2022

**HAL** is a multi-disciplinary open access archive for the deposit and dissemination of scientific research documents, whether they are published or not. The documents may come from teaching and research institutions in France or abroad, or from public or private research centers.

L'archive ouverte pluridisciplinaire **HAL**, est destinée au dépôt et à la diffusion de documents scientifiques de niveau recherche, publiés ou non, émanant des établissements d'enseignement et de recherche français ou étrangers, des laboratoires publics ou privés.

UNIVERSITÉ PARIS-EST

malaquais / École nationale supérieure d'architecture Paris-Malaquais

# THÈSE

préparée au sein du laboratoire Géométrie Structure Architecture
de l'École nationale supérieure d'architecture Paris-Malaquais

présentée pour l'obtention du diplôme de
DOCTEUR DE L'UNIVERSITÉ PARIS-EST
École doctorale: Ville, Transports et Territoires
Spécialité: Architecture

par

**Ahmed Hussein Abouelkheir**

Intitulée

## SAND TECTONICS

## a material-based approach to architectural design and fabrication

Soutenue le vendredi 02 juillet 2021 devant le jury composé de :

Nicolas Pauli, président du Jury, Professeur, ENSA Montpellier
Antonella Mastrorilli, rapportrice, Professeure, HDR, ENSAP Lille
Bernard Maurin, rapporteur, Professeur, HDR, Université de Montpellier
Marine Bagneris, examinatrice, Maîtresse de conférences, ENSA Marseille
Salvator-John Liotta, examinateur, Maître de conférences, Université Libre de Bruxelles
Maurizio Brocato, directeur de thèse, Professor, HDR, ENSA Paris Malaquais

To Hussein and Mervat,

my parents,

for their unconditional love and support.

## Résumé

Le comportement d'auto-formation des matériaux est utilisé comme outil physique pour la génération de formes en architecture. Néanmoins, l'utilisation de matériaux auto-formant est, le plus souvent, limitée à la phase de conception tandis que dans la phase de construction, un autre matériau avec ses propres capacités mécaniques est utilisé. Il existe une opportunité pour un nouveau système de matériaux en architecture, qui fusionne les processus de conception et de fabrication, qui réside dans le sable, ce dernier présente un comportement d'autoformation lorsqu'il est sec et des capacités mécaniques lorsqu'il est lié. Des études antérieures ont examiné les caractéristiques morphologiques du comportement d'autoformation du sable. Plus récemment, le projet de recherche *35 Degree* a développé une méthode de solidification du sable et de ses formes émergentes avec une solution saline. La méthode de solidification a donné naissance à un nouveau matériau nommé Hyposand et a établi une conception intégrée au système de fabrication, éclairé par l'auto-organisation du sable et la cristallisation du sel appelée '*Sand tectonics*'. Les propriétés et les caractéristiques mécaniques de Hyposand n'ont cependant pas été examinées, l'interrelation entre la conception, la fabrication, la géométrie et la modélisation est limitée aux formes coniques, quant à la fabrication robotique n'a pas été pensée.

Cette thèse vise donc à développer la tectonique du sable pour examiner ses potentiels dans la conception et la réalisation architecturales. Un cadre théorique et technique de recherche est utilisé pour relier les études de matériaux, de conception et de fabrication à travers des méthodes d'expérimentation physiques et numériques. Pour construire les fondements théoriques de la recherche, le rôle des matériaux et de leurs processus de formation dans la genèse de la forme est passé en revue. Pour mettre en œuvre le cadre de recherche, les propriétés, la microstructure et les caractéristiques mécaniques d'Hyposand sont étudiées. Les principes géométriques des surfaces à angle constant sont analysés. Trois méthodes de modélisation paramétrique associant la géométrie et le comportement des matériaux aux contraintes de conception et de fabrication sont proposées. Les méthodes manuelles et robotiques de formation des matériaux sont présentées, leurs méthodes de fabrication sont développées, et leur flux de travail numérique-physique est présenté.

Parmi les contributions potentielles, figure la réalisation d'un matériau à haute résistance, moulable et recyclable pour les structures compressives et les coffrages réutilisables. De plus, six techniques de fabrication utilisant des cadres théoriques et techniques suggérés sont présentées à travers un certain nombre de prototypes physiques et numériques. Les prototypes démontrent la contribution et l'avenir potentiel d'un nouveau domaine de conception et de recherche.


**Mots-clés** : sable, sel de sulfate de sodium, conception par les matériaux, conception et fabrication numérique, modélisation paramétrique, surfaces d'égale pente, axe médian, weighted Voronoi.

## Abstract

Materials self-formation behavior is used as a physical tool for form generation in material-based design approaches. Though, the use of self-forming materials is, most frequently, limited to the design phase, while in construction, another material with mechanical capacities is used. An opportunity for a new material system in architecture that merges design and fabrication processes lies in sand, which exhibits self-formation behavior when loose and mechanical capacities when bonded. Previous studies examined the morphological characteristics of sand self-formation behavior. More recently, the 35 Degree research project developed a method to solidify sand and its emergent forms with a saline solution. The solidification method gave rise to a new material named Hyposand and established an integrated design to fabrication system informed by sand self-organization and salt crystallization termed ‘sand tectonics’. However, the properties and mechanical characteristics of Hyposand were not examined, the interrelation between design, fabrication, geometry, and modeling was limited to conical forms, and robotic fabrication was not thought.

This thesis aims at developing sand tectonics to examine its potentials in architectural design and making. A theoretical and technical framework of research is used to interrelate material, design, and fabrication studies through physical and digital experimentation methods. To construct the theoretical foundations of the research, the role of materials, and their formation processes in the form’s genesis is reviewed. To implement the research framework, the properties, microstructure, and key mechanical characteristics of Hyposand are investigated. The geometrical principles of constant angle surfaces are analyzed. Three methods of parametric modeling that associate material geometry and behavior with design and fabrication constraints are proposed. Manuel and robotic methods of material formation are presented, their fabrication methods are developed, and their digital-physical workflow is introduced.

Among the potential contributions is achieving high strength, castable and recyclable material for compressive structures and reusable formworks. Moreover, six making techniques employing suggested theoretical and technical frameworks are presented through a number of physical and digital prototypes. The prototypes demonstrate the contribution and the potential future of a new design and research field.


**Keywords**: sand, sodium thiosulfate salt, material-based design, digital design and fabrication, parametric modeling, surfaces of constant slope, medial axis, weighted Voronoi.

## Acknowledgment

To my supervisor, Professor Maurizio Brocato, I would like to express my sincere gratitude for his guidance and critical feedback throughout my research. His experience in architecture, engineering, and material science led to the interdisciplinary character of my work. His openness, trust, and understanding have been of substantial importance to the development of the sand tectonics research and my thesis's completion. His interest in engaging the topic of research in the educational courses at the ENSA Paris-Malaquais greatly improved the development of the topic and my teaching skills.

To my Professor Magdy Moussa of Alexandria University, who passed away before the end of this thesis, I would like to express my genuine appreciation for his great support and trust from the beginning of my undergraduate studies until our last discussion. He was an inspiring teacher and a remarkable friend who encouraged me to pursue my interest in architecture and research.

I also want to extend my appreciation to Jean-Marie Delarue, the Professeur at ENSA Paris-Malaquais and member of the GSA laboratory, for his inspiring discussions on the geometry of sand piles, which were crucial in developing the modeling methods in this work. His dedication to and profound knowledge of the topic is inspiring for me to further develop the topic.

The GSA laboratory provided a place for the exchange of knowledge and skills in geometry, structure, and architecture, which enriched the multidisciplinary approach of my work. It also provided a place of friendship and sympathy even during the most unsociable times of my dissertation. I would like to thank my colleagues at the GSA, Thierry Ciblac for his advices and support in teaching and research, Mohamed Mansouri for the discussions on the modeling techniques, Ahmed Elshafeii for the discussions on mathematics and architecture, especially the weighted Voronoi problem, and Blerta Lepo for her help in the analysis of the results of the mechanical tests. I would especially like to thank Roberta Zarcone for her advices on the digital, and mechanical aspects of this research, and strong support to bring the dissertation to completion.

The GSA laboratory partially funded the experiments presented in this work. The author acknowledges the infrastructure provided by the laboratory and the ENSA Paris-Malaquais. Thanks, Benoît Vérant, Stéphane Papin, and Bruno Weiss, for providing the necessary tools at the school for the fabrication and documentation of the physical models. Special thanks to Professor Ashraf Ragab of Alexandria University, for having hosted the compression test campaign at the Advanced Materials' Services laboratory, Professor Gilles Foret of Ecole des Ponts ParisTech, for organizing the flexural test campaign at Navier laboratory, Professor Stefano Dal Pont, and Dr. Edward Andò of Grenoble Alpes University for organizing the X-ray tomography tests at 3SR laboratory.

I want to thank my partners at Encode Studio, Dr. Ebtissam Farid and Dr. Mohamed Zaghloul, and my colleagues at the studio Mohamed Abdelkhalek and Mohamed Dawood for their countless intense discussions and fruitful advice in developing the physical and digital methods of design and fabrication.

My deepest gratitude goes to my parents, Professor Hussein Ezzat and Mervat Naguib, who gave me a passion for architecture. Their unconditional love, faith, patience, and support was essential to accomplish this work. This gratitude is extended to my sister May, for her love and irreplaceable support along the hard moments of this journey, including the organization of workshops, model making, and manuscript revisions. I also thank my parents-in-law, Francine, and Dominique de Latour, for their support and kindness during the last months of writing.

Finally, I thank my wife, Anne, for her consistent love and encouragement during this endeavor. Beyond her endless patience and family support, she has contributed to finalizing this thesis through nightly editing sessions. Our family has grown, and I thank Naël, who brought me the greatest joy in coming into the world. His arrival in the last month of this journey is a marvelous gift.

Ahmed Hussein
Paris, December 2020

# Contents

THÈSE ..... 1

Résumé ..... 3
Abstract ..... 4
Acknowledgment ..... 5
Contents ..... 7
Glossary ..... 11
Abbreviations ..... 12

Introduction ..... 13

Main objective ..... 14
Specific objectives ..... 15
Methodology ..... 17
Limitations ..... 19
Structure of the thesis ..... 19

1 Literature review: Role of material in architectural design ..... 22

1.1 The role of materials in the tectonic concepts ..... 23
1.2 The role of materials in the design process ..... 27
*1.2.1 Representational role of materials in the formal approach of design ..... 27*
*1.2.2 Mechanical role of materials in the structural approach of design ..... 27*
*1.2.3 Behavioral role of materials ..... 30*
*1.2.4 New materiality: the integrated role of materials in form making ..... 32*
1.3 Towards sand tectonics in architecture ..... 34
*1.3.1 The work of Jean-Marie Delarue and Frei Otto ..... 34*
*1.3.2 The 35 Degree project ..... 38*
*1.3.3 Robotic formation of sand ..... 40*
*1.3.4 Discussion of the use of sand self-formation in architecture ..... 41*
*1.3.5 Research objectives and methodological framework ..... 42*

2 Materials fundamentals: characteristics and behaviors of sand and salt ..... 44

2.1 The physical characteristics of sand grains ..... 44
*2.1.1 Types of sand ..... 45*
*2.1.2 Grain size ..... 46*
*2.1.3 Grain shape ..... 46*
*2.1.4 Environmental advantages of desert sand ..... 47*
2.2 Sand phase changing behavior ..... 48
*2.2.1 Sand phase changing behavior ..... 48*
*2.2.2 Formation processes of wet sand ..... 49*
*2.2.3 Formation processes of dry sand ..... 50*
2.3 Sand self-organization behavior ..... 51

*2.3.1 Morphological aspects of the sand pile ... 52*
*2.3.2 Geometrical principles of sand pile ... 53*
*2.3.3 Sand self-organization in nature and art ... 55*
2.4 Sand solidification methods ... 56
2.5 Sodium thiosulfate pentahydrate salt ... 58
*2.5.1 The phase changing behavior of the ST salt ... 59*
*2.5.2 Characteristics of the ST salt ... 60*

3 Material system: Hyposand fabrication methods ... 63

3.1 Materials preparation method ... 64
3.2 Mixing method of making ... 65
3.3 Spraying method of making ... 66
3.4 New methods of making ... 69
3.5 Aspects of Hyposand ... 71
3.6 Aspects of the STP saline solution ... 73

4 Material characterization campaign ... 76

4.1 Structure of the experimental work ... 76
4.2 Standard method of specimens preparation ... 77
4.3 Specifications of sand types ... 78
4.4 Grain size analysis: sieve test ... 80
*4.4.1 Materials and methods ... 80*
*4.4.2 Results and discussion ... 81*
4.5 Grain size analysis: statistical methods ... 84
*4.5.1 Parameters and methods ... 84*
*4.5.2 Results and discussion ... 88*
4.6 Grains shape analysis: tomography scan ... 92
*4.6.1 Materials and methods ... 92*
*4.6.2 Results and discussion ... 98*
4.7 Compression tests ... 105
*4.7.1 Materials and methods ... 105*
*4.7.2 Results and discussion ... 106*
*4.7.3 Comparison of the compression results to the grain size and shape ... 114*
4.8 Flexural test ... 117
*4.8.1 Materials and Methods ... 117*
*4.8.2 Results and discussion ... 118*
4.9 Thermal conductivity test ... 119
*4.9.1 Materials and Methods ... 119*
*4.9.2 Results and discussion ... 119*
4.10 Comparison of Hyposand with other materials ... 121
*4.10.1 Method of comparison ... 121*
*4.10.2 Results and discussion ... 122*

5 Making system: design and fabrication methods ..... 126
5.1 Design system: material formation methods ..... 127
*5.1.1 Formation parameters ..... 128*
*5.1.2 Formation tools ..... 133*
5.2 Geometry of sand piles ..... 135
*5.2.1 Constant slope ..... 135*
*5.2.2 Conic sections ..... 136*
*5.2.3 Voronoi diagrams ..... 138*
*5.2.4 Medial Axis ..... 140*
5.3 Modeling methods ..... 143
*5.3.1 Boolean method ..... 145*
*5.3.2 Heightfield method ..... 147*
*5.3.3 Medial axis methods ..... 151*
*5.3.4 Medial axis_ Boundary to ridge method ..... 152*
*5.3.5 Medial axis _ Ridge to border method ..... 156*
*5.3.6 Comparative evaluation of the algorithms ..... 158*
*5.3.7 Robotic control code ..... 160*
5.4 Fabrication system: fabrication methods of sand panels ..... 161
*5.4.1 Fabrication process ..... 161*
*5.4.2 Fabrication constraints ..... 164*
5.5 The Digital-physical workflow of sand tectonics ..... 170
5.6 The framework of methods ..... 173
6 Prototyping: design and fabrication techniques ..... 175
6.1 Addition and subtraction techniques ..... 176
*6.1.1 Parameters and design prototypes ..... 176*
*6.1.2 Fabrication prototypes ..... 189*
*6.1.3 Robotic deposition technique ..... 192*
6.2 Tilting technique ..... 197
*6.2.1 Method definition ..... 197*
*6.2.2 Parameters and constraints ..... 200*
*6.2.3 Algorithm of the tilting technique ..... 202*
*6.2.4 Design and fabrication process ..... 203*
*6.2.5 Physical and digital Prototypes ..... 207*
6.3 Displacing technique ..... 214
*6.3.1 Method definition ..... 215*
*6.3.2 Parameters and constraints ..... 216*
*6.3.3 Geometry analysis ..... 216*
*6.3.4 Algorithm ..... 221*
*6.3.5 Design and fabrication processes ..... 222*

*6.3.6 Physical and digital experiments* ..... *225*
6.4 Sweeping technique ..... 228
*6.4.1 Method definition* ..... *228*
*6.4.2 Curved surface discretization and fabrication* ..... *230*
*6.4.3 The making constraints.* ..... *232*
*6.4.4 The making workflow* ..... *234*
*6.4.5 Physical and digital experiments* ..... *238*
6.5 Helicoid technique ..... 243
*6.5.1 Method definition* ..... *243*
*6.5.2 Geometrical principles* ..... *244*
*6.5.3 Physical making method* ..... *244*
*6.5.4 Digital making method* ..... *247*
6.6 Pipe casting technique ..... 249
*6.6.1 Initial tests* ..... *249*
*6.6.2 Experiment 1: the hanging model* ..... *251*
*6.6.3 Experiment 2: the vertical model* ..... *253*
6.7 Discussion of the sand tectonics ..... 254
Conclusion and future work ..... 255
A. Material system ..... 256
*1. Standardization of the processes of making of Hyposand* ..... *256*
*2. Characterization of the Hyposand mechanical properties* ..... *257*
B. Making system ..... 259
*1. Design system* ..... *260*
*2. Geometry* ..... *261*
*3. Modeling methods* ..... *262*
*4. Fabrication system* ..... *263*
Final reflections and future perspectives ..... 265
List of figures ..... 267
List of tables ..... 273
Bibliography ..... 274

## Glossary

This section clarifies some terms used in this study.

The thesis uses three terms in studying the role of material in design: material properties, behavior, and capacity. ***Properties*** refer to quantitative intensive and extensive properties of materials such as granulometry, friction, and strength. ***Behavior*** signifies the dynamic process of self-organization that displays morphological changes under external or internal forces such as self-organization, or phase changing from fluid-like to solid-like states at certain conditions. ***Capacity*** refers to the capability of a material to perform certain functions based on its properties and behavior.

***Self-organization***, interchangeably with the term ***self-formation***, describes the capacity of sand to generate forms and patterns through local interactions between the grains and under the influence of internal and external forces.

***Phase changing behavior*** refers to the behavior of a material, either sand or salt, that exhibits a reversible transition between liquid and solid states.

***Liquid vs. solid states of sand: Liquid*** refers to either dry or wet states of sand where the particles are unbounded and can flow. In contrast, ***solid*** refers to the confined and stable state of grains.

***Dry vs. wet states of sand*:** Dry sand refers to the state of sand where no cohesion occurs between the grains (moisture content is less than 5% by weight), while 'wet sand' is used to describe a range of states from humid to water-saturated sand where cohesion between the grain occurs.

***Hyposand*** refers to the material developed in this work, the mixture of sand and sodium thiosulfatesalt. It is used to describe the solid or liquid state of the mixture. The term is derived from the commercial name of the salt '*hypo*'.

The terms '**formation method**' and '**boundary conditions**' are suggested to describe respectively the process of sand formation (ex: deposition) and the context in which sand is formed (ex: box). Both terms return a designated formation technique, herein, deposition in a box.

## Abbreviations

| | |
|---|---|
| **AR** | Angle of Repose |
| **HF** | Heightfield algorithm |
| **MA** | Medial Axis algorithm |
| **Ma** | Medial axis curve |
| **PCB** | Phase changing Behavior of salt |
| **SCS** | surfaces of constant slope |
| **SPB** | Sand Phase-changing Behavior |
| **SSB** | Sand Self-organization Behavior |
| **ST** | Sand Tectonics |
| **STP** | Sodium Thiosulfate Pentahydrate |

# Introduction

The thesis examines the role of material and making in architectural processes, emphasizing the role of material properties and behavior in the genesis of form. The work speculates how material and formation processes can be instrumentalized not only as a conceptual design tool but also as a means of fabrication. Does correlating design and making through a material logic evoke new meanings and materiality values in architecture beyond optimization and performance? Through an experimental approach of research, the thesis explores what sand wants to be? What is the form of the material? What architectural possibilities might emerge from a bottom-up process of research starting from the material? The research examines and employs sand morphological, mechanical, and ecological capacities as active agents in the architectural design and fabrication processes of compressive structures.

It is now common knowledge that architects use physical models in which the material itself generates form and structure. In these models, materials that have certain degree of self-formation are employed as agents to represent forces and generate optimized forms and structures (ex: chains to generate catenary structures). Since the self-forming materials function as agents of forces, it is essential to be replaced with building materials in construction to withstand the true forces. As such, the role of the materials is limited to the design phase of form generation but do not engage in the fabrication process. This replacement is mainly due to the nature of the material itself as it can represent forces by its self-forming process but cannot withstand forces due to the lack of appropriate mechanical properties.

Sand exhibits morphological, mechanical, and ecological advantages, which draw the interest of the research. **Morphologically**, sand formability allows the generation of almost natural-looking structures due to its phase changing behavior from liquid to solid and its self-organization behavior that generates constant angle surfaces under gravitational forces. **Mechanically**, sand is a construction material that can support load and withstand shear if bonded. **Ecologically**, sand is an ‘abundant’ natural raw material, especially in desert areas with limited use in construction.

The mechanical properties and ecological aspects of sand are well-established domains of knowledge. However, studies on sand morphological potentials and loose granulate in general are relatively few in architecture. To date, available studies on sand self-formation in architecture are mainly limited to the work of Frei Otto at the Institute for Lightweight Structures at the University of Stuttgart, and Jean-Marie Delarue at the GSA[1] laboratory at Paris-Malaquais school of architecture, among few others. Previous studies that employed the SSB as a design tool highlighted its morphological potentials and studied constant angle geometry of the emergent forms. Recently, the 35 Degree project [1] extended the SSB potentials from

[1] GSA laboratory, (Geometry-Structure-Architecture)

design to fabrication through solidifying the emergent forms with a saline solution. The study is a ‘master by research’ project conducted at the Architectural Association school of architecture by a team of four architects, among whom is the author of this thesis. Based on a material approach of research, the study developed a method for hardening sand with salt, a parametric method for the generation of conical forms, and a fabrication system of sand panels. With the introduction of the industrial robot in architecture in the last decade, there has been an increasing interest in developing architectural systems based on robotic sand forming. The machinic rigour of the robot provided a means to explore new methods of sand formation that are otherwise hard to achieve.

## Main objective

The thesis explores how sand self-organization behavior (SSB) prompts new insights into architectural design and making. The overall purpose is to develop an ecological tectonic system by employing sand and salt behaviors and properties as active agents in architectural design and fabrication processes. The main objective of the thesis is to develop the sand tectonics (ST), a material-based approach to architectural design and fabrication. The term of ‘sand tectonics’ is suggested to represent the unique qualities of sand self-formation, its associated techniques and tools, forms and patterns; it is suggested as a design approach, to be integrated in field of architecture

An organizational framework of research is set to study the interrelation between the trilogy of (i) the **material system** that identifies and characterizes the material itself, (ii) the **design system** that develops material distribution methods, and (iii) the **fabrication system** that extends the design methods to the materialization phase. Besides, structural, ecological, and aesthetic aspects of the ST are thought.

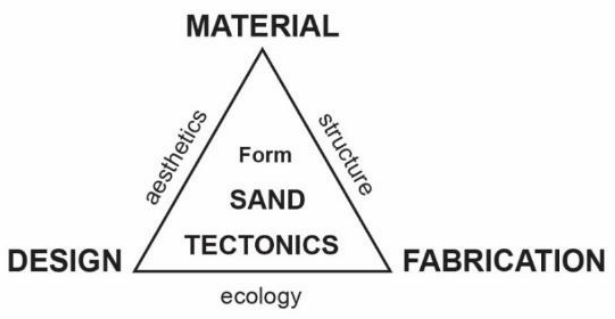


Figure 0.1 The sand tectonics framework

## Specific objectives

To meet the main objective of the thesis, the three systems of the ST are addressed simultaneously as comprehensive research axes with interlinked objectives. The following specific objectives are addressed to develop, assess, and employ the proposed ST:

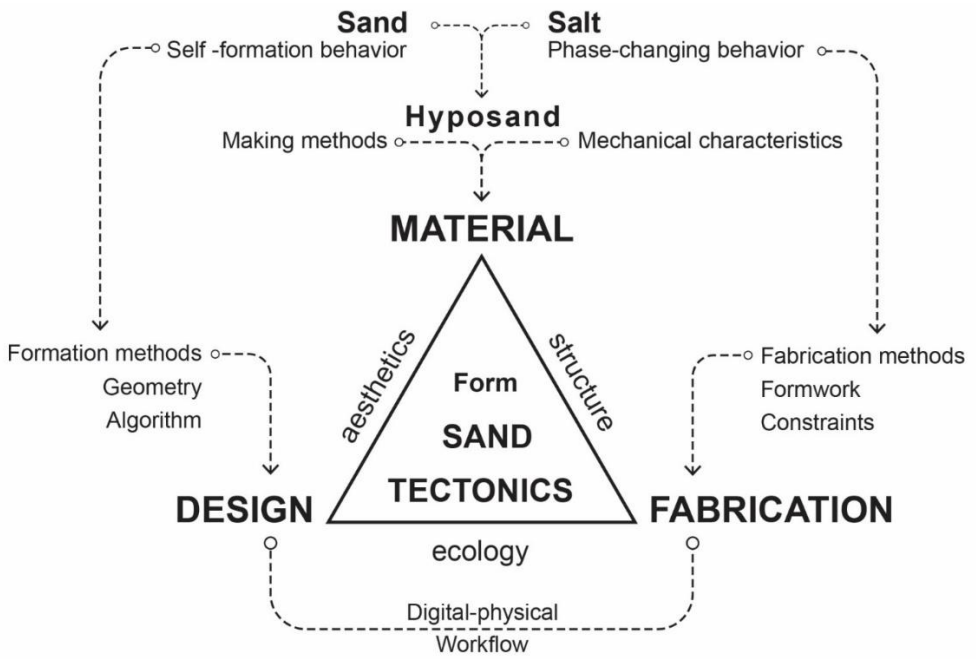


Figure 0.2 The organizational framework of the research

**A-** **The material research** focuses on studying the mixture of sand and salt, herein Hyposand. It aims at deepening the knowledge of the material solidification methods and its key mechanical characteristics to unfold its morphological and construction potentials. To identify the material, it is essential to:

1- **Define the sand and salt characteristics,** including the physical characteristics of sand grains and the phase changing behavior of salt.
2- **Improve the material making methods** that are previously developed in the master research (mixing and spraying), and to explore new methods of making.
3- **Characterize the Hyposand by** identifying its microstructure, mechanical behavior, and the optimum mixing method that returns workable material with high strength.

**B-** **The design research** aims at instrumentalizing the SSB as an active agent in the design process. The objective is to explore the possible morphologies behind the SSB to define the distribution methods and boundary conditions that enable such morphologies. What the sand wants to be is a central question addressed by the design research to examine the interchange between the material agency and the designer authorship in the generation of form. To employ the SSB in the design process, it is necessary to:

4- **Develop physical methods of material formation** as an explorative framework defined by the material logic, the distribution parameters, and the boundary conditions.

5- **Identify the geometrical principles** of the emergent forms to inform the digital methods.
6- **Develop digital methods of material formation** to explore further morphologies that reach beyond the analog limitations. It is necessary to develop the digital tool as a flexible computational framework to adapt to the different distribution methods, the variations of the boundary conditions while considering fabrication constraints and assembly logics.

It is important to note that the design research is not only concerned by the distribution of dry sand but also of the Hyposand liquid mixture that has an important feature of being moldable and able to solidify relatively fast without the need of air contact, which drew the interest of the research to develop design methods that unfolds this feature of the material capacity.

**C-** **The fabrication research** explores the methods of making that are enabled by the material logic, and the distribution methods while considering feasible manufacturing constraints and the assembly logic. To extend the distribution methods of loose sand into solid panels and assemblies it is important to:

7- **Set up the fabrication process** through five consecutive phases (1) paneling of large surfaces to ensure feasible scale of fabrication while maintaining the continuity of the assembled surfaces, (2) design and making of the formwork where the sand is distributed, (3) solidification and thickening of the emergent patterns with the saline solution, (4) assembly of the solid sand panels, and then (5) casting of the panels into solid blocks.
8- **Inform the design and modeling methods** with the fabrication constraints such as the assembly and casting techniques and feasible surface size and shape.

In pursuit of the overall aim of the ST at introducing new insights into architecture by employing the morphogenetic, mechanical, and ecological potentials of sand in the design and making processes, it is imperative to address two extended objectives:

9- **Construct a digital/physical workflow** that integrates the material, design, and fabrication methods in a coherent and flexible process.
10- **Establish prototyping techniques** to examine and apply the developed methods and workflow of the ST into specific design and fabrication techniques through a large number of physical experiments.

## Methodology

The research considers that materials embody their formation processes and that much of the making potential lies in the way the materials are worked. The processes introduced in this work are developed from the observation and analysis of the material characteristics such as the formation and manufacturing techniques allowed by the material. The objective is to remain coherent with the material logic and to unfold its morphogenetic possibilities without forcing external ideas. Following this material approach, the employment of either low- or high-tech tools in making is not the question of the research but rather a response to what the material requires to reach specific forms.

In pursuit of the material approach and to meet the objectives of the thesis, a methodology of design by research is set to tease out formation processes from the materials capacities rather than constructing predefined forms. The purpose is to systemize the processes and to establish order in the almost infinite range of morphological possibilities. Along with the systematic approach, some features of the research are developed through casual observations, which when combined with systematic methods, return positive outcomes that arise casually.

To develop an in-depth understanding of the possibilities and limitations of the proposed ST, an empirical methodology is employed through a large number of material tests, physical and digital experiments, and prototypes. Making prototypes is an inherent part of experimentation that requires iterations and intuition. Feedback between the physical and digital experiments is central to this work to construct a comprehensive dialogue between material behavior, geometry, code, design, and fabrication constraints. Following the research methodology, five major aspects are addressed to experiment and employ the ST framework.

**The first aspect is to develop methods of material fabrication and formation.** An analytical, experimental study is followed to study the properties of the STP salt to identify its mixing, storage, and recovery possibilities, to systemize the mixing and spraying procedures of solidification, to explore new methods of making.

**The second aspect is to characterize Hyposand**. Standard material tests are used to analyze the granulometry and the microstructure of the material and to identify the effect of grain type, size and shape, salt proportion and temperature, curing time, and addition of gravel on the compression strength. Also, flexural tests are thought to identify the effects of humidity on the flexural and compression strengths of the material. Moreover, the thermal conductivity of the Hyposand is measured. Finally, Ashby charts[2] are used to develop an initial comparison between the characteristics of Hyposand and other classes of construction materials.

[2] Ashby plots are a set of scatter graphs that display some properties of different classes of materials. The plots are used in structural and mechanical engineering for material selection in the conceptual design phase (see §4.10).

**The third aspect is developing the physical workflow of making** from material distribution up to assembly of solid sand panels. The workflow is not developed as a specific linear sequence of stages but as a flexible network to enable the interchange between the different design and fabrication methods, which enriches the possibilities of making. The physical workflow consists of two main phases, sand distribution, and panels fabrication. **Firstly, to develop the sand formation methods,** it is essential to construct a fundamental understanding of how the material works and the morphogenetic possibilities of SSB to employ it as a design tool. For this purpose, some aspects of the physics behind the SSB are studied, the conditions that trigger sand morphologies are identified, the generated surfaces of constant slope are geometrically analyzed, the employment of sand behavior in architecture and beyond are mapped. Based on these studies and iterative physical experimentation, manual and robotic sand distribution methods are explored, the SSB parameters are defined, and the interrelations between the emergent forms and their boundary conditions are identified. As a result, six material formation methods are developed, and three types of boundary conditions (containers) are studied. The interchange between the formation methods and the container type in addition to the variation of the design parameters allows a rich network of morphological exploration. **Secondly, to develop the fabrication methods,** the process is broken into five separate tasks, where technical studies and iterative experiments are conducted on each task to improve its workability. Then, the tasks are merged to assess the whole process. The constraints of each task are identified and parametrized to be considered in the digital phase of form generation.

**The fourth aspect is the development of the digital workflow.** The design of custom digital tools is essential to parametrically operate the digital workflow from form generation to production. The digital tools are developed within Rhino and Grasshopper environments to emulate the material behavior under specific boundary conditions and then translate the design parameters into robotic fabrication code using HAL plugin. It is essential to develop the digital workflow as a flexible framework that allows the exploration of possible morphologies informed by a series of parameters inferred from material, geometry, design, fabrication, and assembly logics. For practical reasons, the digital workflow is divided in four main stages: (i) boundary design (ii) form-generation, (iii) manufacturing information, and (iv) robotic control. It is found practical to develop the four stages as separate chunks of code and link them when needed upon design requirements. Each chunk of the code necessitates special geometrical, technical, and computational studies to develop it and to improve its performance.

**The fifth aspect, prototyping,** applies the developed physical and digital methods into specific design and fabrication techniques. Digital and physical methods of prototyping are employed as tools of thinking, verification, testing, and validation of the proposed ST. Six design and fabrication techniques are developed, their workflow is detailed and verified through a number of prototypes. The motivation behind each technique, its geometrical analysis, design strategy, fabrication process and prototypes are detailed.

## Limitations

Since this work is not a funded research and in regard to the laboratory scale and the available resources the following limitations were encountered:

1. **Material characterization campaign**: around 300 specimens are tested in the mechanical characterization campaign, which returns an overview of the key mechanical charachterestics of the material but not a detailed understanding.
2. **Physical prototyping**: the scale of prototypes are restricted to the sizes that are possible to fabricate with the available resources.
3. **Robotic fabrication**: the failure of the available industrial robotic arm during the research restricted the study of robotic sand distribution to initial experiments.
4. **Scope of research:** the scope of this work is defined in the subsection of specific objectives. The following studies are beyond the scope of this work: material insulation, assembly of sand blocks, structural studies of compressive forms, and the construction process. These studies may constitute the objects of future studies to investigate the application of the sand tectonics on large compressive structures.

## Structure of the thesis

The manuscript is structured in two parts and seven chapters. **Part I' *State of the Art'*** constitutes the theoretical foundations and the methodological resources of the research in two chapters. **Chapter 1 *'Literature review'*** examines the role of material and making in the genesis of form and presents four models of material role in architecture based on a selected review of historical references and emergent trajectories. **Chapter 2 *'Materials fundamentals'*** studies the physical characteristics and behaviors of sand, investigates the most relevant applications of SSB in architecture and beyond, reviews the available methods of sand solidification and studies the characteristics of sodium thiosulfate pentahydrate salt. **Part II *'Sand tectonics'*** is the main body of the work, it introduces and characterizes the material system, details the design and fabrication methods, and applies the ST in four chapters**.** **Chapter 3 *'Material system'*** introduces the Hyposand material by identifying its fabrication methods by means of solidifying sand with sodium thiosulfate pentahydrate salt. **Chapter 4 *'Material characterization'*** investigates the mechanical characteristics of Hyposand through a testing campaign. **Chapter 5 *'Making system'*** introduces the design and fabrication methods through the integrated framework of the ST and its digital-physical workflow. Then it introduces the design system by identifying the material formation methods, the geometrical aspects of the emergent forms, the algorithms of surface generation, and the robotic control code. Then, the chapter details the fabrication methods and constraints. Finally, **Chapter 6 '*prototyping'*** introduces six techniques of design and fabrication that integrates the ST in a digital/physical framework of prototyping. It discusses the motivation behind each technique, defines their parameters, constraints, and strategies of design, details their processes, and demonstrates their morphological possibilities through a number of digital and physical prototypes.

PART I

# STATE OF THE ART

# Chapter 1

Literature review:

Role of material in architectural design

# 1 Literature review: Role of material in architectural design

Architecture as a material practice, attains its meaning (typos) and contextual relevance (topos) through the articulation and assembly of materials and structures (tectonics) into an expressive and performative whole [2]. Materialization is an inherent vector in the architectural process, thus the way we conceive it is central to how we (re) think architecture [3]. Since the emergence of the concept' truth to material' by the end of the 19th century, architectural discourse is dominated by the expressive concepts of materiality [4–7]. However, the thesis deals with the physical nature of materiality, which involves the process of transforming matter into material, and the formation of material into forms, yet the thesis considers material expressions but as the natural product of material properties. Hence, active materiality is the main focus of the thesis where form emerges from material capacities and its own language of formation. In this context, morphogenetic, performative, and ecological capacities of materials are considered as the design principles, while aesthetic, and expressive values are considered as emergent qualities of the material processes.

Throughout the history of architecture, the visions of architects and engineers of the role of materials in design changed significantly regarding the availability of new materials, technological advances, and philosophical views at their times. Most research on the role of materials has been carried within the larger scope of the relationship between the triplet tectonic relationship between form, structure, and material [8]. The existing literature has often discussed the role of materials in a form-versus-material framework [9], should the material be an inert that conforms itself to predefined form or should the material operates as a key driver of architectural design?

The thesis questions the impact of materials and their formation processes on the genesis of form with an emphasis on materials capacities, i.e. their mechanical properties and formation behavior. A critical review of the state-of-the-art of the role of materials in design is provided in this chapter. The study questions both the relegated role of material in the representational model of design - that still predominant today - and the agency role of materials in the *new materiality* model to raise the key research issues. Firstly, the triplet relationship between material, technique, and form in the tectonic theory is discussed. Secondly, the formal, mechanical, behavioral role of material in the design processes are analyzed followed by the integrated role that considers material capacity in form making. Thirdly, previous architectural studies that employed sand self-organization behavior are reviewed. Through this study a comprehension of the tectonics principles is founded, key research issues are raised, and subsequently the framework of sand tectonics can be constructed in this work.

## 1.1 The role of materials in the tectonic concepts

The discussions on architectural tectonics have been growing during the last decades, not least in relation to the development of digital technologies and their use in architectural design. This subsection discusses the evolution of the role of materials and techniques in the tectonic theory. First, the term tectonics is defined, its concept is outlined, and its historical background is briefly highlighted. Thereafter the role of materials in the tectonic theory is discussed in three chronological groups, the German, the modernism, and the 'digital' tectonics.

Tectonic theory and architecture are inextricably linked as demonstrated by the etymology of the words. The term tectonics is derived from the ancient Greek word *tektonikos* meaning 'related to building' and *tekton* meaning carpenter or builder. From this comes the Latin *arkhitekton*, from (*arkhi*- 'chief') and (*tekton*- 'builder) meaning the master builder from which the term Architect is derived [10]. The tectonic theory, founded in the 19th century, adapted the term to transform the meaning from that of builder to the concept of an integrated building system. In the literature, tectonic is most commonly conceived as the concept that ties together the science (structure, material, and construction) and art (expression and meaning) of building into a homogeneous whole. The term has evolved over the last two centuries, and through time there have been many different visions on what the term might contain, which is discussed in [2,10] and reviewed through a timeline of key individuals contributions in [11].

The historical background that laid to the foundation of tectonics is discussed in the literature through two influences:

i. Partly due to the new building techniques and writings of French Enlightenment architects who emphasized on the expressive potentials of structural assemblies [10].
ii. Mainly due to the archeological excavations of the Roman and Hellenic architecture in the 18th century, which brought architects to question the Vitruvian dictum of the Renaissance against the actual ruins. The examination allowed a new understanding of the relationship between ornaments, form, and structural issues, which gave rise to a fundamental break with tradition [4,12].

A coherent historical evolution of the tectonic thoughts can be traced in Germany from its initiation by Friedrich Schinkel, foundation by Karl Bötticher and formulation as a theory by Gottfried Semper (among others). The German tectonic discourse signaled a transition moment from classicism to modern architecture by incorporating issues of structure, construction, techniques, and material in the architectural discourse. Eventually, their main contribution lies in two folds, the distinction between symbolic and technical aspects of building, and the study of Classicism not as a style but rather as an artistic encapsulation of technological solutions of its time [13].

Friedrich Schinkel in his concept *Grundformen* distinguished between art (ornaments) and construction and advocated the coordination between historical 'style' and construction technologies of the present. His pupil Karl Bötticher extended his ideas into a more precise theory of tectonics where he emphasized the distinction between construction and art by means of separating the building materiality, function, and structure (*Werkform* – 'Work form') from the expressive layer of ornaments added over the material reality of the building (*Kunstformen* – 'Art form') to which the building owes its meaning [13].

Bötticher interpreted the term tectonic as both the system, which binds all the parts of a building into a single whole [2], and the activity of forming a building where architecture is investigated through the processes, which made up building [14]. Following, Bötticher revisited his theory from a construction approach and recognized three construction systems: the relative (masonry posts and beams), the reactive (masonry arches and vaults), and the absolute (iron structures)[2]. Despite that Bötticher theory was based on his archeological studies of Hellenic architecture [12], the advent of iron technology drew his attention to the mechanical capacity of the new material and its potentials in architecture. In contrary to his contemporaries who engaged cast iron in the Gothic constructions and ornaments, Bötticher argued for the superior mechanical performance of iron and on its potential for a 'change of principle' resulting in a 'new and hitherto unknown system' [15]. Botticher's theory was highly influential in central Europe through the early-twentieth century especially the iron tectonic, which formed the basis for the integrated aesthetic/industrial theme in modern architecture [14] such in the work of Otto Wagner.

In his pioneering contribution to the discussion of tectonics, Gottfried Semper, similar to Schinkel and Bötticher, distinguished between the technical and symbolic issues of building but with greater emphasis on the coherency between material and method of manufacturing[3] which had a lasting impact on associating architecture and technology [17]. Among his seminal writings[4], two main concepts are relative to this research. First, the concept of architecture elements which he introduced in [18] as a new[5] universal conceptual framework for architectural analysis and production[6]. Second his study the evolution of art forms technical arts. In his observations, Semper assumed a parallel between natural and art form which raised the question of what driving forces might be behind the formation process in art [19].

[3] Semper's emphasis on materials and techniques came from his interests in crafts, industry, and metal working. The detailed context in which Semper's theories emerged is examined in [16].

[4] Semper's writings was not translated into English until 1998. A complete bibliography of his writings is available in [18]

[5] In his theory, Semper challenged the Vitruvian triad of utilitas, firmitas, venustas as model of work [2]

[6] According to Patrick Schumacher, the objective of Semper's framework (theory) was to addresses the question of the origin and the development of historical styles [15].

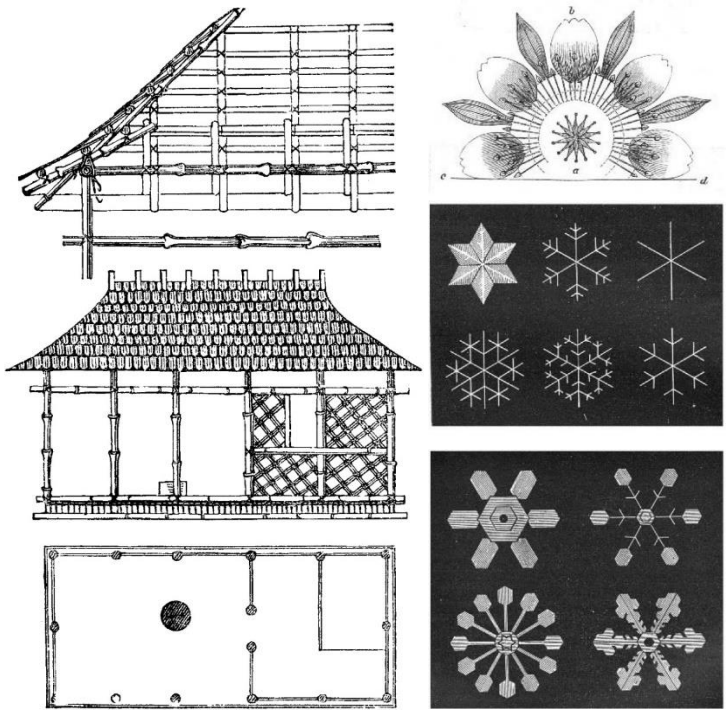

Figure 1.1 Gottfried Semper, Illustrations of the Caribbean hut and study of flowers and snow Crystals [20].

The significance of the work of Semper lies in his attempt to consider art and architecture as the objects of scientific investigation. Until today, the methodological framework of his theory influences architectural scholars such as Bernard Cache in the concept of Objectile Patrik Schumacher in The Autopoiesis of Architecture[15]. While his understanding of art-form like a natural form as a result of formation processes and contextual conditions continues to attract attention from practitioners until today, especially in morphogenetic design. For instance, Spuybroek (Nox) [21] and Neri Oxman [22] interpret the nature of the four elements being either actual building materials and assemblies or states of material properties. Collectively, the German tectonics built a bridge between classicism and modernism and paved the way for engaging the new materials and techniques as motive forces in theory and practice.

Despite that the discussion of tectonic theory at the end of the 19th century focused on the new material and techniques, the discussion in the 20th century, when concrete and steel became major building materials, was much less about materiality but the expression of the materials and their assemblies. In Studies in tectonic culture [1], Kenneth Frampton discussed the concept of ‘knot’ in the work of semper (introduced above) and analyzed the concept of assembly in the work of avant-garde architects of the 20th century. From his study, He claimed that the joint is the key element of the tectonics as it links parts, and materials, and structures of the whole architecture and therefore a crucial point in revealing the logic of a construction and in the meaning of a building. In practice, modernist architects such as Le Corbusier and Mies van der Rohe offered models of concrete and steel tectonics but with emphasis on the material-specific expression of the assembly [23]. In their work, the tectonic was largely

expressed by the logic of composition and the aggregation of elements to form the whole. On the logic of assembly, Le Corbusier claimed that '*Architecture is the masterly, correct and magnificent play of masses brought together in light*', while Mies van der Rohe asserted that: '*Architecture starts when you carefully put two bricks together*'

In the 19th century Bötticher and Semper established the theory of tectonic as a framework for practice, however, now the theorists are attempting to interpret the term from the production of the practice. Since the introduction of the term *digital tectonics* in [24] 2004, its interpretation changed at a great pace due to the advent of technology. The changes can be concluded in two shifts, the phase of CAD and the phase of computation.

In the first digital wave, which employed CAD tools as a representative tool, almost followed the same logic of assembly of modernism, but instead the focus was on geometrical assemblies with little interest in material, structure, or construction logics. This is largely due to the limitations of CAD tools in modeling material properties or structural behavior.

Tectonic ideas here could be summarized as the conceptual framework that organizes the interdependent relationship between the technical elements and the expressive meanings in a homogeneous whole. Despite the diverse viewpoints offered by the tectonic theorists as discussed above, they all reclaimed materiality as a meaningful constituent of architecture, and called for consistency between whole and parts, for expressiveness of structural and material behavior, and for connections between representation and construction, invoking various levels of authenticity. The study of the different tectonic concepts is essential for this work to construct the ST framework. However, since the tectonic concepts are a somewhat utopian framework of abstraction it was essential in this work to examine the relationship between material and formation within a practical framework as will be introduced in the following subsection.

## 1.2 The role of materials in the design process

### 1.2.1 Representational role of materials in the formal approach of design

The formal approach of architectural design is characterized is characterized by a hierarchical process where a form is first conceived and drawn, then subsequently structured and materialized [25]. This hierarchical process of 'form, structure, and material' was established in architecture at least since the advent of drawing techniques and the emergence of the 'architect' as a distinct role from the builder in the Italian Renaissance time [26–28]. The distinction between the architect and the builder yielded to the superiority of the intellectual process of drawing over the physical process of making and subsequently the separation between form and its materialization [15]. The primacy of drawing as the motive force of architecture led to the consideration of material and making as executors of preconceived forms that are well-defined by as set of instructions [26] whether drawn by hand, through computer-aided design (CAD) [9], generated algorithmically [10], or even encapsulated as G-code for computer-aided manufacturing (CAM) [29]. Within this representational approach, that still predominant today, the influence of material on the genesis of form is limited, as it is rarely examined beyond its poetic meanings or its mechanical performance. The modernism, post-modern, deconstruction, and the early digital design architectures provide many such examples of formal approaches that prioritize form over materialization [4].

The formal approaches of design remain the foundation model of contemporary practices that embrace human intellect and authorship as means of form creation. In such, it promotes the Aristotle's 'hylomorphic model' as a paradigm of form creation in which matter is an inert receptacle for superimposed from the outside [30,31]. 1.2.4 discusses recent researches in architecture, which focuses on an opposite framework of design in which materials are not inert receptacles for architectural concepts imposed from the outside, but active participants in the genesis of form[32].

### 1.2.2 Mechanical role of materials in the structural approach of design

Interest in materiality raised multiple times after the Renaissance partly due to theoretical discourses but mostly due to technological advances. This arguably began from the 17$^{th}$ century onwards with the work of early proponents of the Enlightenment such as Claude Perrault whose writings marked the breakout of the classical canons and instead follow reason and scientific thought as the basis for modern architectural theory and practice. Moreover, by the mid of 18$^{th}$ century the by then 'new' archaeological discoveries of Roman and Hellenic architecture brought architects to question the classical canons of Vitruvius against the actual ruins in order to establish a more objective basis on which to work. This together with the technical advancements that followed through the century, incited architects, such as Jean Rondlet and Jean Durant, to accommodate not only new building techniques but also new models of thinking in their work, which laid the way to the foundations for modern architectural theory and practice [4]. Following, both the theoretical discussions and technological advancement by the end of

the 18th century incited the foundation of the tectonic theory and the rise of Structural Rationalism principles in the 19th century, which engaged the expressive and technical roles of materials, as well as the structure and construction techniques within the architectural discourse [2].

Since the industrial revolution, the availability of new engineered materials and construction methods coupled with the advances of structural analysis methods prompted new insights into architectural theory and practice and led to novel structural forms. Since then, the mechanical properties of the new materials and their formation processes incited engineers and architects to employ them as driver forces of design rather than being subordinates to form [33]. The mechanical performance of iron, steel and concrete led to the development of unprecedented structures in terms of span, heights, lightness, and transparency and therefore new building types and construction systems emerged [4]. Unlike engineers who were receptive to iron and employed its stiffness and lightness in the construction of bridges since 1770, architects, accustomed to brick and stone construction, were much slower to adopt the new material. Moreover, the public culture at the time was stuck to the classical aesthetic values of Neoclassicism [13]. Consequently, it took almost 150 years to gradually adopt the performative and aesthetic values of steel in architecture. Steel was first employed as a secondary structural material hidden within the bearing walls in the Pantheon (1790), then as visible structure elements in the interior of the Sainte-Geneviève Library (1838) and finally as a principal external expression in the crystal palace (1851), the Gallery des machines and Tour Eiffel (1889) [4]. The gradual appearance of iron was accompanied by an evolution of its ‘art form’ from imitating stone based classical elements and ornaments up to the establishment of its proper industrial nature as a new ‘art form’ in architecture. In theory, Karl Bötticher advocated for iron tectonics and argued that a modern building method must not imitate historical styles but emerge out of the mechanical performance of iron and its evolving technologies [14]. Iron tectonics would thus constitute the basis for the development of a modern architecture and stand as the most representative style of the 19th century [13].

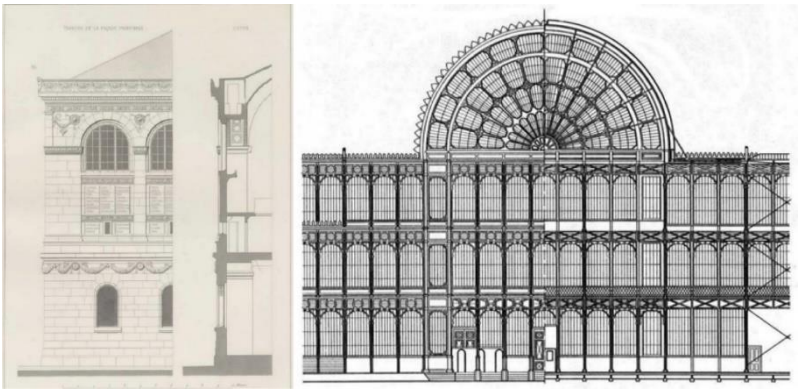

Figure 1.2 Evolution of iron tectonic from structure elements in the interior of Bibliothèque Sainte-Geneviève by Henri Labrouste,1838, Paris [34] (left) to the principal external expression in the Crystal palace by Sir Joseph Paxton, 1851,London.

The relationship between material, form and formation acquired a new richness and variety with the development of reinforced concrete by the end of the 19th century. The plastic behavior of concrete, its mechanical performance, and monolithic nature prompts new insights into its formal and expressive potentials for architecture. The bridges of Robert Maillart and the ribbed shells of Pier Luigi Nervi express the capacity of concrete to form following structural forces where thickness differentiation is articulated in response to the compressive forces. Variations in section and material properties offer significant advantages on both structural and architectural levels. Structurally, the gradation of values between stiffness and elasticity is particularly useful for resisting dynamic loading conditions such as those produced by wind [35]. Architecturally, it returns efficient designs yet aesthetically appealing, which recalls natural forms. Since then, plastic formation coupled with structural optimization was established as a tectonic feature proper to concrete as seen in the beams of Sydney Opera house by Jørn Utzon and more recently the topologically optimized ceiling of the DFAB House by the Digital Building Technologies Group, ETH Zurich. Moreover, the exploration of the monolithic nature of reinforced concrete and its elastic qualities coupled with the stiffness of double curved geometry allowed the construction of thin shells which produced a radically different conception of architectural form as seen in the work of Eduardo Torroja and Félix Candela.

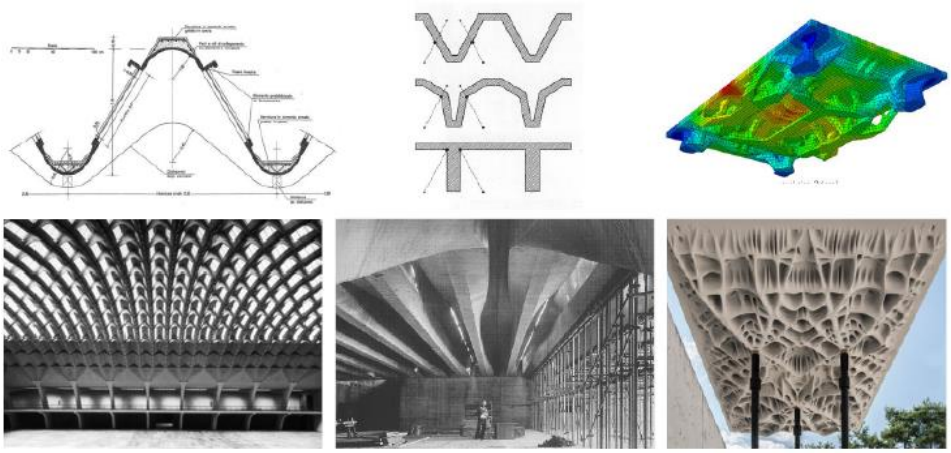

Figure 1.3 The plasticity of concrete allowed thickness variation for structural optimization at Turin exhibition hall by Luigi Nervi 1949 [36], the Sydney Opera house by Jørn Utzon [30] and the topologically optimized ceiling of the DFAB House 2018[37].

Certainly, the structural approach of design marked a significant step to re-engage material in the design process rather than just an applied technology [33]. Driven by the capacities of new materials and techniques, the structural approach stands as a model of form, force and material relationship in which material and geometry are articulated in response to structural diagram of forces [36]. The integral formation and materialization approach led to the creation of efficient yet expressive structures with unprecedented performative and aesthetic values. Further, the new materials and techniques established new tectonics, which became defining aspects of architecture since the end of 19th century.

### 1.2.3 Behavioral role of materials

Making reemerged recently as a powerful framework of design in architecture where material capacities and its formation process are employed a design tool. This approach is not without precedents, thinking by making, material and experimentation has always underlaid the craft practice and a dimension of certain specialized forms of architectural design, such as medieval stone masonry. But since the 19th century, mechanical production marginalized the making craft [38] and the master-builder model was replaced by the master-thinker, which relegated the craft of making and manual labor to a secondary technical role as subordinate to the intellectual practice of design, the new craft of drawing[27].

The dominant architectural tendency to undervalue materialization as technical execution of the architect concept recalls the historical human tendency to value intellectual knowledge over the know-how including materials, tools and technology in general [31,39]. 'To those engaged in materials production and fabrication, it may be disconcerting to realize that for a fair fraction of human history their activities have been viewed with suspicion and downright distaste by social thinkers and the general public[40]'. However, with the ever-increasing pace of technological change, there are a number of strands of thought within cognitive science that 'ascribes to technology a new dignity as a genuine tool of the mind' [41]. Moreover, tools, process and physical experiences are now considered as conceptual means that give shape to the form of thoughts [42,43].

These frameworks reverse the hylomorphic model where it is not the mind that imposes its forms on material objects, but rather the latter that give shape to the forms of thought[44]. Central to this position, natural sciences introduce an alternative concept of form, the morphogenetic model, which considers matter and energy as active agents in genesis of form. Within this model, natural formation are regarded as complex systems where form emerges through the interaction of intrinsic material capacities and extrinsic forces, such emergent systems are said to be self-organized [3]. With reference to these frameworks of thought, materials, processes and making are now widely investigated as thinking tools in architectural design [45,46].

Despite that making approaches and active materiality came to the fore of the architectural research at the end of the last century thanks to the advance of CAM technology, we can still trace such practices in the work of avant-garde architects as well as masters in other design disciplines. For instance, 'process art' and 'anti-object' movements of art in the 1960's considered forms as the results of the interaction of the artist's process and the properties of the material being processed. While in industrial design, the processing of traditional materials with new techniques led to the development of new design methods. For instance, in chairs design the techniques of wood steam bending by Michael Thonet, plywood bending by Charles Eames, and metal welding by Jena Prouvé yielded to new design and production methods.

Previous studies [29,47] in architecture education, refer to the work of Josef Albers at the Bauhaus and Frei Otto at Stuttgart University as radical academic ventures in material exploration. Josef Albers conducted material studies in the late 1920's where he focused on material techniques and their inner qualities and structures as means of morphological studies [48,49]. In his foundation course, Albers focused on material capacities and their formation processes without using tools, neither a methodology of experimentation nor a criterion of evaluation, but to explore material formations.

In engineering, an active role of material in design emerged with the use of physical models to define optimized structures. Since the 17th century, material self-formation behavior was employed to determine the most efficient form of pure compression structures (hanging chain of Robert Hook). The implication of materials as physical means to optimize structural forms was largely used in engineering until the 1970's when manual or computer methods of structural analysis were judged inadequate or inefficient [50].

Physical models would thus become a privileged method in architecture to determine the form of a structure, termed 'form-finding' method. The hanging model of Antonio Gaudi, the fabric models of Heinz Isler, and the soap-film models of Frei Otto are well-known examples of form-finding approaches in design. The developments of graphic statics methods of structural analysis and the concept of catenary arches between the 17th and 19th centuries enabled Gaudi to integrate the structural and architectural design at large scale applications. Catenary analog modeling was later developed by Frei Otto, Heinz Isler and Sergio Musmeci using hanging nets and clothes for the calculation and design of grid sells, concrete shells and bridges.

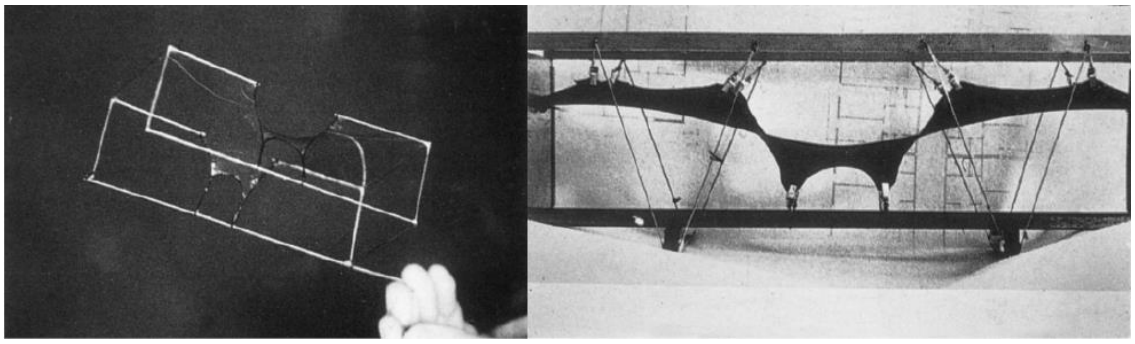

Figure 1.4 Soap film and membrane model studies of the Basento Bridge. by Sergio Musmeci, in Potenza 1976

Frei Otto approach of experimentation was derived by the principle of 'minimum energy' in nature to obtain the maximum performance with the minimum energy. Optimization for Otto was a means to conceive structures that uses the minimum amount of energy and material. Hence, he was focusing on focusing more on the processes of design that contain an optimization from the beginning, like soap bubbles [51]. Between the 1960's and 1980's, Otto conducted a series of experiments with various material systems, ranging from soap bubbles to sand in order to study their inherent capacity to physically compute form as an equilibrium

state of system-intrinsic material behavior and extrinsic forces [29]. In [52], Frei Otto defined the constituent elements of the making process: the material capacities, the formation process, the human will to form, the tools constraints, the design problem, and the evaluation criteria. Within this process, the form it-self, its qualities, and performance emerge from the manipulation of the parameters. Moreover, in the same reference, Otto studied self-forming processes and their emergent structures in a wide range of natural systems.

Two issues are important to note in the framework of form finding. First, the role of the material is analogous, meaning it merely represents the forces to compute the form in the design process [35]. In such a way, the materials used in the experiments are later replaced by a 'real' material in construction like for instance replacing the hanging chains in the catenary model by bricks in the construction phase. Consequently, the active role of materials is limited only to the design phase. Secondly, the advent of computational form finding methods limited the role of physical models where the structural forces are computed numerically rather than physically, except in some cases[53]. In such a way, the physical self-formation behavior is replaced by virtual forces and materials have no roles in the generation of forms but rather the forces. In such, form finding techniques are restricted to the relationship between structure and geometry without incorporating the expression of material properties, organization and behavior[54]. Although form-finding approaches limited the role of materials in representing forces, it brought the discussion on materials and materiality back to the fore in architectural research and practice.

### 1.2.4 New materiality: the integrated role of materials in form making

The discussions on architectural materiality have been growing during the last decades [9,55–58], notably due to the synthesis of computational design tools and the physical world of materials by cutting-edge fabrication technologies [29]. The capacity of computational design in modeling material properties, behavior and geometrical logic coupled with the power of digital fabrication promotes a new understanding of materiality at the interface between the digital and the physical. The fusion of data and material, which decisively failed to develop in the early digital age [59], is being realized in today's architectural approaches such as *New materiality* [32], *Material based-design* [54], *Material computation* [60], and *Digital materiality* [59], among others [61]. Within these approaches, the capacity of materiality in design is being widely reassessed to respond to the challenges and opportunities that confront architectural design within the context of current ecological and technological developments [62]. The emergent material approaches operate through multidisciplinary frameworks that articulate architectural notions in accordance with a coordinated arsenal of concepts from other domains, such as active matter concepts in philosophy [32,58], morphogenetic and self-organizations theories in natural sciences [63,64], constructive models in cognitive sciences [65], allographic and autographic practices in art [26], craft and digital crafting [66], and finally on architects' authority in architectural history [15,26].

In reference to the *machinic phylum* and *morphogenetic space* concepts of Gilles Deleuze [67] as well as thermodynamics and geology sciences, the philosopher Manuel De Landa challenges the 'hylomorphic model' as a paradigm of the genesis of form with the concept of *New materiality*. He describes *New Materiality* as 'the idea that matter has morphogenetic capacities of its own and does not need to be commanded into generating form' [32].

> *'We may now be in a position to think about the origin of form and structure, not as something imposed from the outside on an inert matter, not as a hierarchical command from above as in an assembly line, but as something that may come from within the materials, a form that we tease out of those materials as we allow them to have their say in the structures we create.'* Manuel De Landa [40].

Rather than considering form or design as pure thought, imposed upon homogenized materiality, Delanda suggests the opposite, to treat materials as 'active participants in the genesis of form,' indicating the existence of a heterogeneous materiality with variable properties[31].

In architectural terms, Neil Leach discusses new materialism as a philosophical framework that provides the means to shift from the representational logic of the hylomorphic model, which characterized architectural thinking in the 20$^{th}$ century, toward the form genesis logic of the morphogenetic model. He argues that the morphological approach in architecture necessitates unfolding morphological complexity and performative capacity from material constituents without differentiating between formation and materialization processes [68].

Upon a similar argumentation but with reference to self-organization logic in nature, Neri Oxman questions the historical hierarchical design process' form-structure-material' against the 'nature way' of form genesis. As an alternative she proposes inverting the process bottom-up starting from material in *Material based-design* approach. Her work at the Mediated Matter Group at MIT's Media Lab emphasizes a nonhierarchical association between form, structure and material [54]. Driven by biological principles, novel biomaterials, and robotic fabrication her research agenda explores the variation of material properties through a heterogeneous materiality as a function of environmental performance.

## 1.3 Towards sand tectonics in architecture

Sand self-formation behavior under gravitational forces drew the interest of some architects to study its potentials as an architectural material system. This section introduces a critical appraisal of previous studies[7] which examined the potentials of sand self-organization behaviour (SSB) in architecture. The study examines the methods of material distribution, their parameters, technical processes, and the geometrical characteristics of the emergent forms with an emphasis on the function of SSB being a design and/or a fabrication mean. The contributions and limitations of the previous work is studied in three chronological groups: (i) the work of Jean-Marie Delarue[8] and Frei otto, (ii) the 35 Degree project in 2009-2011, and (iii) the robotic distribution projects in the last decade. At the end of this section the overall limitations of previous work are identified, and the objectives of this research are defined.

### 1.3.1 The work of Jean-Marie Delarue and Frei Otto

The main references of studying SSB in architecture are limited to the work of Jean-Marie Delarue at GSA laboratory at ENSA Paris-Malaquais, and the work of Frei Otto at Institute for Lightweight Structures at Stuttgart University. Although the two works studied the morphology of sand self-formation, their aims and methods were different as outlined below and discussed afterwards:

- **In terms of methods**, Jean-Marie Delarue studied the sand morphologies from a geometrical perspective while the experiments of Frei otto were based on forces and time-based simulations.
- **In terms of objectives**, Delarue used sand as a medium to represent the geometrical characteristics of surfaces of constant slope while Otto used sand as form finding tool to represent structural forces and urban growth.

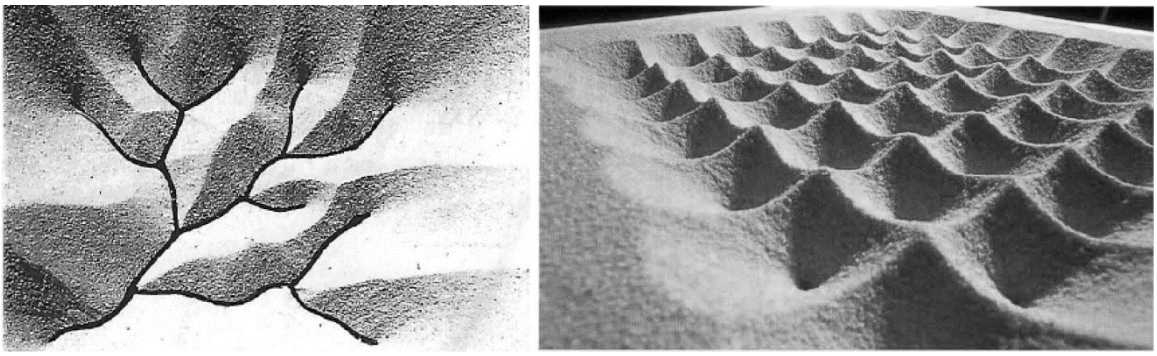

Figure 1.5 Sand morphological studies by Jean-Marie Delarue (left) [69] and Frei Otto (right) [51].

[7] Research into loose granulates as an architectural material system in their own right is relatively unexplored [73]. To our knowledge, there are few researches who examined the SSB in terms of architectural systems.

[8] Professor at Paris Malaquais school of architecture (ENSA Paris Malaquais) and member of the GSA laboratory.

**Jean-Marie Delarue's geometrical methods**

Jean-Marie Delarue explored the emergent morphologies of sand piles and studied the geometrical characteristics of surfaces of constant slope in his academic manuscript '*Surfaces d'égale pente, morphogénèse et applications constructifs*' [69] and his e-learning video lectures [70]. Based on physical methods of sand formation, Delarue studied the following aspects of sand piles:

1. **The morphological parameters of sand formation** and their effect on the emergent forms were explored. Despite its exploratory nature, the study offers insight into some parameters of sand formation, which can be summarized into three major groups:
    - Border : curvature (concave-convex) and shape (rectilinear-curvilinear)
    - Base: planarity (planar-nonplanar) and curvature (concave-convex)
    - Perforations: shape (point-line-curve) and distribution (regular-irregular)

    Moreover, the introduction of obstacles in the formation process, the tilting effect, and the formation of mathematical shapes (ex: the cardioid) were explored. Furthermore, applications for the design of inclined roofs and topographic modeling were proposed.

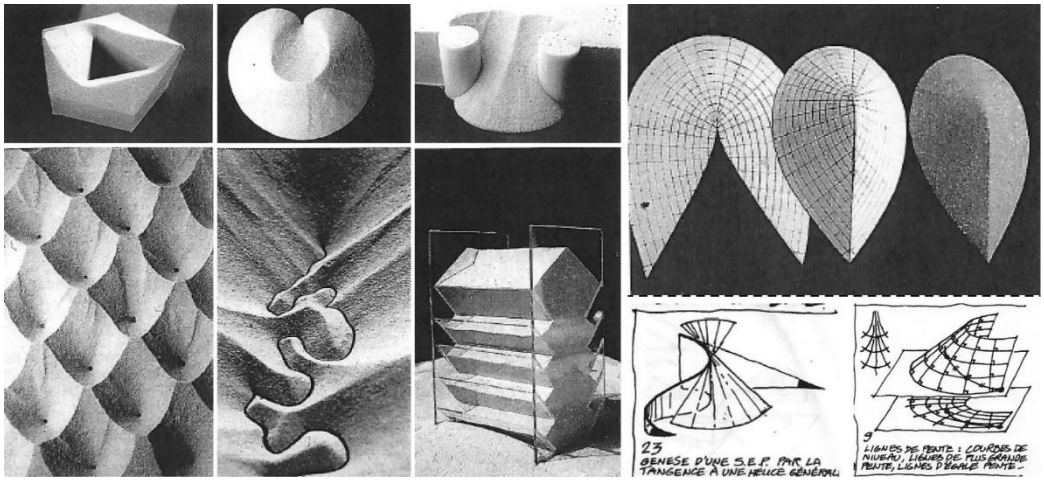

Figure 1.6 Morphological explorations and geometrical analysis of sand piles by Jean-Marie Delarue[69]

2. **The geometrical characteristics of sand piles** being surfaces of constant slope (SCS), ruled, and developable were identified. Also, methods of representation of SCS with constructive geometry were defined (see § 2.3.2).

The morphological parameters defined by Delarue informs the design system developed in this research, which extends the study of the parameters and their effect on the emergent forms (see § 5.1.1). Also, the geometrical methods of constructing the SCS are the basis of the parametric modeling methods developed in this work.

**Frei otto's form-finding methods**

*''Any granular material falling from a fixed point forms a cone on the surface below and a funnel within the granulate mass with the same angle of inclination, the natural angle of repose, 35 Degree''* Frei Otto, Finding Form, 1992 [52].

Frei Otto pointed to the morphological potentials of SSB and the diversity of forms it can generate in [53]. However, the morphological aspects of sand forms were not the focus of his study, but the self-formation process. In his experiments with sand[9], Otto employed the SSB as a form-finding tool to represent forces and time-based processes, including (i) the identification of the cutting pattern of a convertible roof, (ii) the simulation of sequential territorial occupation, and (iii) the calculation of structural loads. In the three experiments, a perforated sandbox apparatus was used.

In the experiment of the convertible membrane, sand was used to determine the intersection lines of the folding membrane. A sandbox corresponding to the membrane boundary was used with holes at different heights to simulate the suspension points. The emergent pattern of intersecting cones[10] retuned cells with curved edges (Weighted Voronoi pattern, see § 5.2.3), which determined the intersection lines of the membrane parts (Figure 1.7) [52].

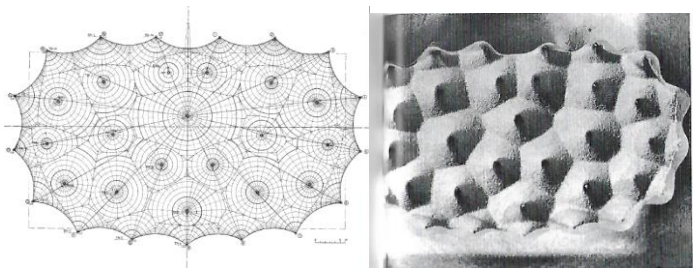

Figure 1.7 The convertible membrane experiment, Frei Otto. The valley lines of a bunched cloth can be determined experimentally using dry sand [52,71]

While in his studies on random occupation and territorial expansion (Figure 1.8), Otto used the sand to visualize the sequential process of urban occupation. The advantage of using the sand flow apparatus is its ability to rapidly determine the expansion of growing territories through the expansion of the mass of sand that flows over time. Like in the convertible roof experiment, small tubes of different heights are introduced into each hole to simulate the time lag in the occupation. The taller the tube is, the later the occupation associated with it initiates. Another method to simulate the different rates of expansion by the variations of the sizes of the hole was proposed by Otto. In this experiment, like in the convertible roof, Otto noted the difference between the ordinary and the weighted Voronoi patterns. In the weighted, the boundaries are no longer linear bisectors but curves that point to the higher hole, representing either a lower

[9] Frei Otto used sand in his experiments much less than other materials such as soap-bubbles, or even wool-thread.

[10] The resulting pattern is a Weighted Voronoi diagram due to the differentiation of the holes heights.

suspension point in the convertible roof or a slower-growing occupier in the territorial expansion experiment[71].

Figure 1.8 The territorial expansion experiment, Frei Otto. Representation of a territorial occupation progression using sand deposition method at different rates.[71]

Finally, in the structural experiment, the objective was to determine the loadbearing capacity of columns and walls in an evenly loaded plane. To simulate a support condition, a plane is perforated with holes and slots to represent columns and walls, while the loads are simulated by the volume of sand that is poured over the plane, which forms a rubble heap with a constant inclination. The loadbearing capacity is then calculated using the weight of sand and the transmission distance to the holes (Figure 1.9).

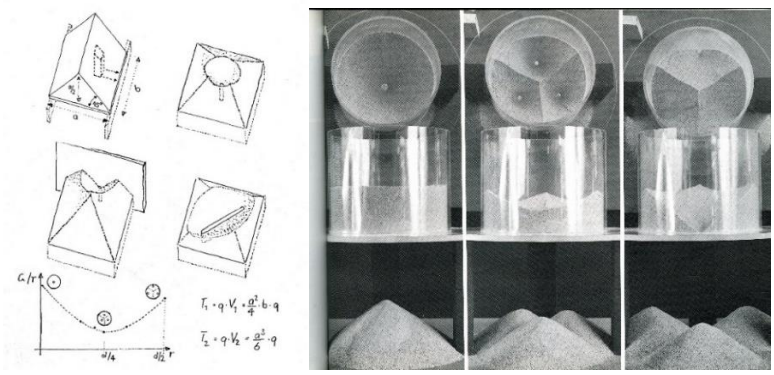

Figure 1.10 the loadbearing experiment, Frei Otto.

Based on the work of Frei Otto, Achim Menges and Michal Hensel conducted a teaching project in 2005 at the Architectural Association school. The project examined the process of sand self-formation for applications in design. Initial experiments focused on the geometrical rules of sand pouring, subtraction, and their emergent formations (Figure 1.11). The research defined some variables of the material system and identified their impact on pattern formation. The variables included the angle of the base surface as well as the amount of sand, pouring speed, and funnel size and configuration [72].

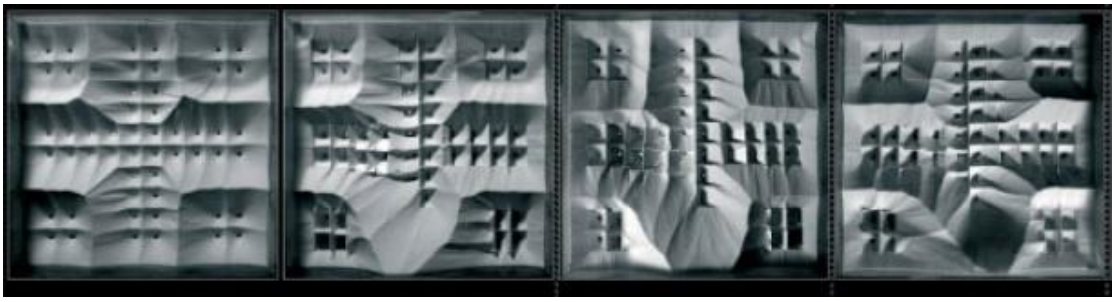

Figure 1.11 Sand formations experiments by Achim Menges and Michal Hensel [65]

To conclude, the above studies established the SSB as a design tool in architecture, highlighted its morphological potentials, defined some parameters of sand formation and their effect on the emergent forms, and associated its emergent morphologies to constant angle geometry. Though, the previous studies have the following limitations:

1. The sand formation processes were limited to the deposition and subtraction methods.
2. The parameters that underpin the emergent formations are not fully examined.
3. The SSB was used only as a design tool but the hardening of the sand morphologies was not addressed which limits the morphological potentials of sand to the design level.
4. The studies were limited to physical distribution no digital modeling was examined.

### 1.3.2 The 35 Degree project

The sand tectonics proposed in this work was established by the 35 Degree project, a master research conducted by a team of four architects, Behdad Shahi, Jiah Lee, Peter Wag, and the author of this dissertation between 2009 and 2011 [73]. The research was conducted at the design studio[11] of Yusuke Obuchi and Robert-Stuart Smith at the design research laboratory (DRL) master program at the Architectural Association school of architecture in London.

The project established the sand tectonic system a material-based tectonic system based on sand self-organization and salt crystallization. It extended the SSB potentials from design to fabrication by means of solidifying the emergent forms with a saline solution that dissolves if in contact with water. The project consisted of three complementary systems:

- **Material system:** a new method of hardening sand with sodium thiosulphate sat was proposed. Two methods of hardening were proposed by means of mixing and spraying. The decomposition of the material with water inspired the research to develop an architectural material system of distribution, solidification, and dissolution. A time-based

[11] 'Proto-Tectonics' , the brief of the design studio, questioned the relationship between architecture and production. It aimed at altering the comprehension of architecture as a production of signature and iconic building to become part of the value of the products being produced. The issue of time in terms of architecture's life-span and life-cycle was central in examining the models of production and consumption in architecture and their engagement with socio-cultural determinants, economic and environmental fluctuations, in addition to material systems. Physical and digital experimentations were conducted to employ materialization as active agent in the development of proto-design systems that are scenario- and time-based.

architectural scenario of production, consumption, and reproduction was then proposed which reorganizes sand naturally available on a desert site and redistributes them back to the environment at the end of the building life-cycle.

Figure 1.12 The fabrication process proposed by the 35 Degree project [73].

- **Fabrication system :** a fabrication technique of sand panels and blocks was proposed. It consisted of three phases: first sand is distributed in perforated boxes. second, the emergent surfaces are solidified by means of spraying and assembled. Finally, a mixture of sand and salt is poured between the panels returning a solid monolithic bloc of sand.

Figure 1.13 Physical model 50x50x2cm [73]

- **Design System**: the experiments of Frei Otto with sand (see §1.3.1) inspired the research to develop a material formation method based on releasing sand from circular holes at the bottom of a sandbox. A parametric technique of modeling conical surfaces was proposed using Boolean method of intersection. Some parameters of the design system were identified, their effect of the emergent sand surface was defined, and a design strategy of nesting conical forms was developed.

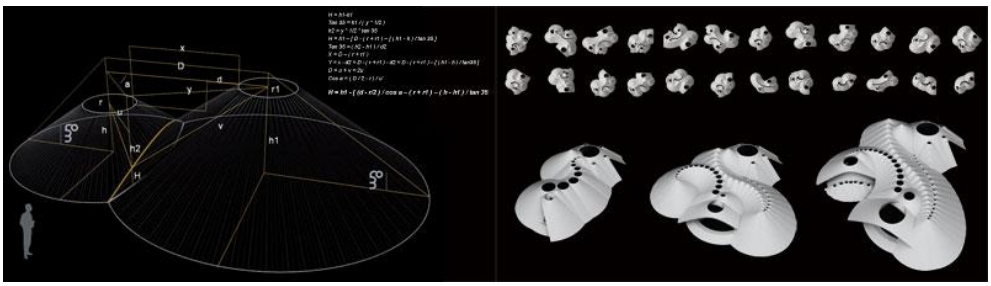

Figure 1.14 Geometrical analysis and design explorations of the conical design system [73]

A large number of digital and physical prototypes were produced along with a design proposal for a temporary eco-resort project at the Red Sea in Egypt where sand is naturally available on site. The project is introduced briefly in [73] and detailed in the thesis book in [1].

The main contribution of the 35 Degree project is the extension of the role of sand self-organization behaviour from design to fabrication by means of the saline solution. Also, the research identified the design parameters and developed complex articulations of sand forms. While the limited scope of the master research could not fully explore the potentials of the proposed material system, the results of the experimental research established the fundamentals of sand tectonics and unfolded the morphological and functional opportunities of the integrated material, design, and fabrication systems. The project showed that sand tectonics is a promising field of research, which called for further investigations in term of material, design and fabrication systems as following:

1. The mechanical behavior of the solidified material was not questioned
2. The material fabrication methods proved to be insightful, but had certain limitations in term of workability and strength due to the type of salt and its preparation method
3. The sand formation method was limited to the subtraction technique from circular holes, which restricted the design possibilities to conical surfaces.
4. The modeling method was based on the Boolean operation of intersecting cones and the geometry of surfaces of constant slope was not studied
5. The robotic methods of sand distribution were not investigated.

### 1.3.3 Robotic formation of sand

In the last decade, there has been an increasing interest in developing architectural systems based on robotic sand forming. The high degree of control provided by robots provided a means to explore the precise distribution of sand that are otherwise hard to achieve. At ETH Zurich, Gramazio Kohler Research conducted a teaching project to study the robotic deposition of sand for the fabrication of non-standard formworks. A feedback process of shaping that combines the material properties and the control of a robotic arm equipped with sensors was developed. Parameters such as speed, height and path of the material deposition were studied, and different formal configurations were developed. The sand patterns achieved rigidity by spraying latex and used as formwork for concrete casting [66].

Figure 1.15 Robotic sand forming techniques. (a) deposition, (b) subtraction, and (c) displacement [66].

Machinic deposition of sand was investigated for developing new additive manufacturing techniques in educational projects conducted by Marta Malé-Alemany at the AA and IAAC [74]. In these projects, sand was used as a scaffolding system to shape other materials. Using a

digitally controlled multiple deposition head, sand was piled up following generative patterns and a liquid binder was deposited on top of sand formations. After hardening, the sand is removed to reveal the solidified structures (Figure 1.16).

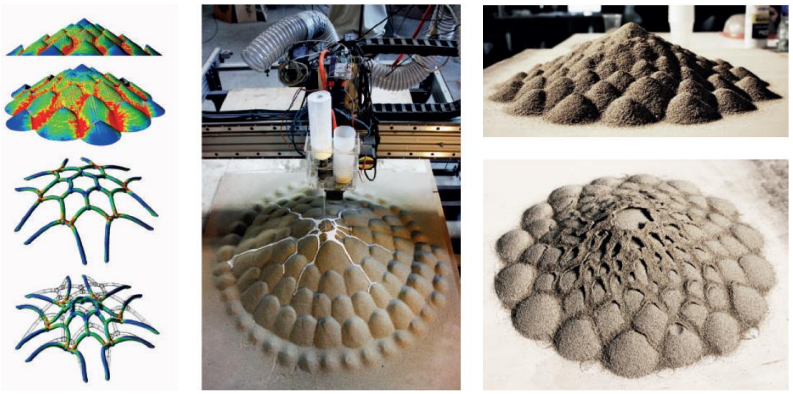

Figure 1.16 Digitally controlled deposition of sand and a binder. Binder flow simulation and structural deformation simulation (left), machinic deposition of sand and binder (middle), results (right)[1].

Now, robotic sand forming is of interest to a large number of research studies, which examines the morphological exploration of robotic forming at the Norman Foster Foundation Atelier [75], UCL, and the IAAC [76], and real-time interactive landscape modeling at the MIT [77–79], the Sci-Arc [80], and Tellart [81].

### 1.3.4 Discussion of the use of sand self-formation in architecture

The above review outlined the key ideas and methods of using SSB in some architectural studies relevant to the current work and defined their advantages and limitations. To conclude, this subsection gives an overall summary of the SSB application in architecture and determines the framework of research of this thesis. First, the major advantages and shortcomings of the previous work are given. Subsequently, the objectives of this thesis are defined, and the methodological framework of this research is introduced.

Overall, the previous work highlighted the capacity of SSB in developing a material-based design system in architecture. In term of sand distribution methods, ‘deposition’ and ‘subtraction’ are the most studied techniques, followed by some experiments with the ‘displacing’ and ‘tilting’ techniques. Some parameters of the design system were identified and their effect on the emergent morphologies were studied. In addition, the geometrical principles of sand piles were analyzed. Finally, the machinic control of sand was investigated and some applications of SSB as formworks were proposed. Through these studies an understanding of the sand tectonics principles is founded.

However, up to now, the relationship between the system parameters and the morphology is not fully examined yet, the relationship between the geometry of surface of constant slope that underpins the emergent forms, and the design system was not systematically studied, and little attention has been paid to digital modeling of the emergent sand forms. Above all, there are few studies that have investigated the solidification of the loose sand pattern. Finally, most of

the previous art has only been carried out in short-term studies, which do not necessarily provide a systematic study of the topic. Hence, to date, no systematic research is conducted on the topic of SSB employment in architecture. This indicates a need for a comprehensive study that correlates material behavior, geometry, digital design, and physical making to employ the sand morphological and structural capacities in architectural design and fabrication.

### 1.3.5 Research objectives and methodological framework

In regard to the above study, and the overall objective of this research to develop the sand tectonic system proposed by the 35 Degree project, the following objectives are defined:

1. Improvement of the methods of making of Hyposand to enhance its workability
2. Characterization of the microstructure and the key mechanical properties of Hyposand.
3. Development of manual and robotic methods of sand formation, analyze their geometrical principles, and identify their parameters and morphological possibilities.
4. Development of parametric tools to model the sand forms and to operate the making process from design to production
5. Production of physical and digital prototypes to examine the developed methods

To develop the sand tectonics, it is essential to address formation, fabrication, modeling, and the material itself simultaneously as inseparable design dimensions. To meet this objective, an organizational framework is constructed based on three comprehensive axes (Figure 1.17):

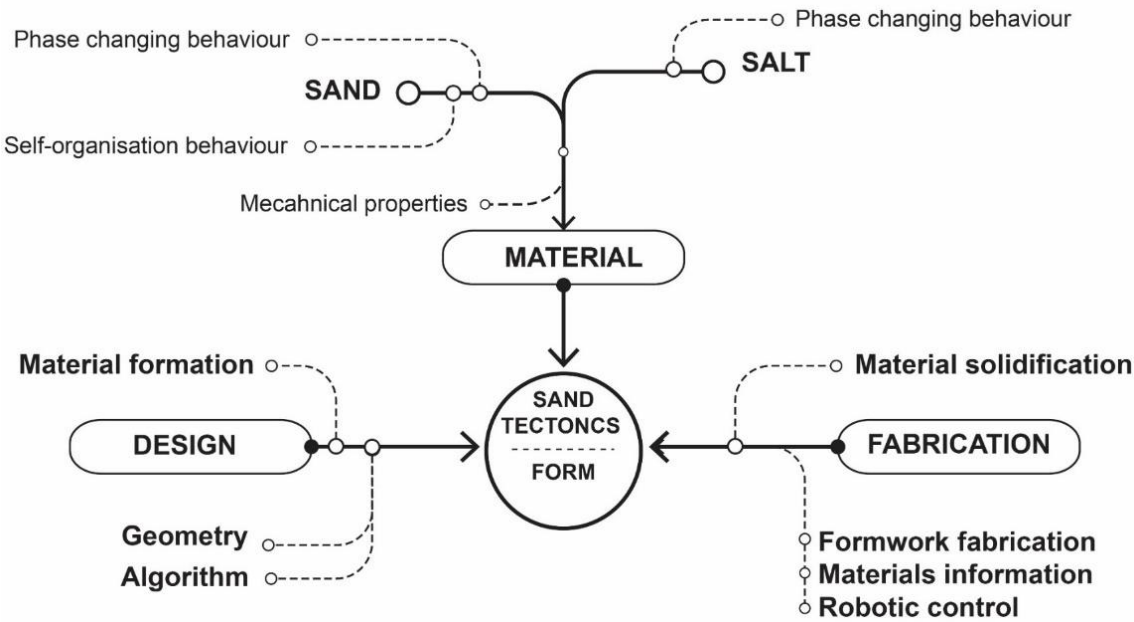


Figure 1.17 The methodological framework of the sand tectonics

1. The **material system** identifies the material itself, its methods of fabrication and its mechanical characteristics in chapters 2, 3 and 4.
2. The **design system** develops physical methods of material formation and their digital modeling techniques in chapter 5
3. The **fabrication system** extends the formation methods to the materialization phase by defining the physical workflow of making in chapter 0

# Chapter 2

Materials fundamentals:

Characteristics and behaviors of sand and salt

# 2 Materials fundamentals: characteristics and behaviors of sand and salt

The chapter introduces some fundamental characteristics of sand and salt essential to developing the proposed ST. As a material based architectural research, the objective of this chapter is to outline some inherent properties and behaviors of the materials to unfold their morphogenetic, mechanical, and ecological capacities. The understanding of the materials capacities is essential to integrate them into the architectural process as design drivers. Accordingly, the material study in this chapter is not conceived as a mere technical study but rather as being the source of an exploratory architectural design system.

The material fundamentals are presented in five axes, the first three define the sand characteristics, behaviors, and solidification methods, and the fifth identifies the salt crystallization behavior.

- **§ 2.1** outlines specific characteristics of sand grains that might affect the mechanical properties of Hyposand studied in chapter 4.
- **§ 2.2** introduces the phase changing behavior of sand and its formation processes
- **§ 2.3** studies the self-organization behavior of sand and its implementations
- **§ 2.4** reviews the available methods of sand solidification in the literature
- **§ 2.5** studies the properties and crystallization behavior of the sodium thiosulfate salt

The theoretical study in this chapter informs the development of the material system in chapter 3 and the mechanical characterization of Hyposand in chapter 4.

## 2.1 The physical characteristics of sand grains

Sand is a natural aggregate substance composed of finely divided rock and mineral accretion[12]. The particles owe their characteristics to their formation processes and weathering agents. Since sand is composed of loose grains, it is essential to study the physical characteristics of the grains to better understand their effect on the mechanical properties of the hardened sand. As Hyposand is a new material, the study refers to the common knowledge in concrete construction to determine the grain characteristics essential to study. The type, size, and shape are the three characteristics of grains outlined in this chapter. Their identification and effects on the Hyposand strength are examined in chapter 4. The data in this subsection are fundamental knowledge in geology and engineering sciences obtained from [82,84,85] and relevant ASTM[13] standards. The study focuses on two main types of sand used in this research, the silica, and the carbonate sand.

[12] Attempts to define sand ,a part of being a size term, and to classify sand types are discussed in [82–84].This discussion goes beyond the scope of this work.

[13] ASTM (American Society for Testing and Materials)

### 2.1.1 Types of sand

The term 'type' refers to the source of sand and its mineral composition (e.g., desert silica). The types of sand are highly variable depending on the type of parent rock(s). A criterion is proposed in [83] to recognize the various types of sand. It distinguishes two main classes of sand based on the formation processes and various subtypes based on the formation agents:

A. **Clastic sand** is formed by disintegration from parent rocks by weathering agents like friction, wind, or water. The most common type of clastic sand is silica, which disintegrates from granite or sandstone. The hardness of quartz and its high resistance to weathering makes it the most common type of sand in the inland continental.
B. **Non-clastic sand types** are formed by the precipitation of chemical solutions or biogenic fragments. An example of non-clastic sand is oolitic sand, which is the product of carbonate precipitation in warm marine and arid coastal environments.

The type of sand can be distinguished[14] by the color and texture of the grains. The color of the grain could indicate its mineral composition. For instance, silica sand tends to be white or translucent gray (depending on the purity of the quartz), but it usually appears in its familiar reddish yellow or orange tones in desert and beach environments due to the oxidation of the hematite on the surface of the grains. While bright white grains might be carbonate or gypsum sand. The texture of sand grain being either rough or smooth can indicate the grain source and formation process. For instance, quartz and gypsum grains of desert areas tend to have an opaque frosted surface due to the wind and friction effects, along with the chemical precipitation on the grains' surface. In contrast, beach, and fluvial sand such as carbonate and biogenic have a shiny, polished appearance due to water currents (Figure 2.1).

Figure 2.1 Visual assessment of sand type. From left to right: desert silica, coastal carbonate, desert gypsum, and beach biogenic (a mixture of organic and silica). [86]

The effect of mineral composition and surface texture on concrete strength and workability is discussed in [84,87]. A smooth surface can improve workability, yet a rougher surface increases the total surface area and enhances the bonding with concrete. Also, the roughness increases the friction between the particles and, therefore, the slope of a dry sand pile.

[14] Chemical analysis methods are essential to determine the mineral compositions of sand. However, in this work, the types of the collected sands are assumed but not identified due to the limitations and scope of the research.

### 2.1.2 Grain size

Sand is distinguished from other aggregates by size, being finer than gravel and coarser than silt on the Wentworth scale with a range of grain size between 0.062mm (very fine) and 2mm (very coarse). The grain size distribution (grading) is determined quantitatively by analyzing the results of a sieve analysis test [88]. The calculations define an index for the proportions of fine and coarse sand (Fineness Modulus), measure the average particle size (median, mode, and mean), and define how well or poorly graded the sample is, as detailed in chapter 4. Various studies have assessed the effect of gradation on concrete workability, hydration, void ratio, and strength [84,89]. Well graded aggregate reduces the voids ratio in the concrete mixture to improve its density and strength when hardened.

### 2.1.3 Grain shape

Two geometrical parameters are used to describe the shape of sand grains, (i) sphericity measures how closely the particle approaches a spherical or elongated shape, and (ii) roundness describes the sharpness of the edges and corners being sharp or round. Residual sand at riverbeds, lakes, oceans, and crushed industrial sand tend to produce flaky particles of low sphericity. On the other hand, spherical well-rounded grains result from many cycles of wind or water transport in coastal, beach, and desert environments (Figure 2.2).

The sphericity and roundness of grains are defined by x-ray computed tomography scanning (CT) and image analysis methods[90]. Grain shape has an essential influence on concrete workability and strength as well as the behavior of dry sand. Higher concrete strengths usually result from more angular grains, but the workability increases with rounded grains. While in a dry mass of sand, rounded grains roll over each other more easily than sharp grains, which return a less steep angle of repose.

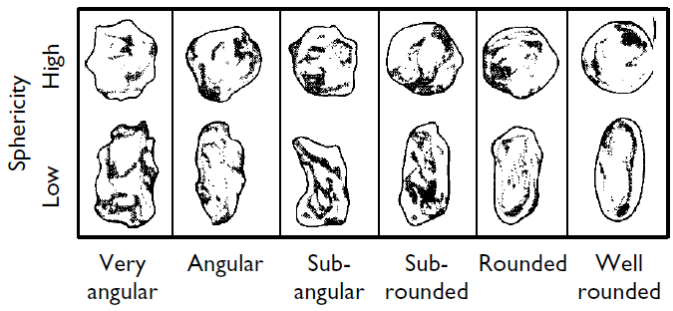


Figure 2.2 Visual assessment of grain shape. Based on morphological observations of sphericity and roundness. [84]

The effect of particle characteristics on the workability and mechanical properties of concrete is discussed in [4,5]. The standard specifications of sand for concrete structures [91] indicate that well-graded, sharp, and rough silica sand grains increase concrete workability and strength. These specifications meet the characteristics of river and pit sand (industrial crushed sand). However, the roundness of desert sand and the chloride content of beach sand eliminate their usage in concrete construction.

To evaluate the effect of the grain characteristics on Hyposand in chapter 4, four types of sand, which highly differ in composition, particle size, shape, color, and texture are studied including: (1) desert silica (2) coastal carbonate (3) beach biogenic, and (4) manufactured silica sand.

### 2.1.4 Environmental advantages of desert sand

Sand is an ‘abundant’ natural material, accessible for local resourcing on a large geographical scale. The word sand is commonly used to express infinity. In the paradox, sand is now a rare material. The ‘abundant’ material is a non-renewable resource over human timescale, and by now it has become the most widely consumed natural resource after fresh water [92]. The demand for sand is increasing rapidly along with the ever-increasing construction industry. Marine sand (river, lake, and ocean), and pit sand, which are the most adequate type of sand for construction, have been excessively exploited all over the world. Moreover, resources for marine sand are limited in many regions, especially for those in desert areas. For instance, Dubai imports construction sand from Australia after all its suitable marine sand supplies were consumed for an artificial set of sand islands. The growing demand for sharp rough sand for construction cannot be met sustainably, which induced serious environmental impacts [93].

However, Desert sand is an abundant type of sand that is less exploited in construction due to the fineness and roundness of its grains, which do not bond well with concrete. Recent researches explored the feasibility of using desert sand in concrete construction and in the brick industry due to its abundance and low cost in comparison to marine and pit sand.

The untapped resources of desert sand drew the interest of this research to explore how to activate its potential as a local building material in desert areas. Moreover, the research explores beach and carbonate sand, which have limited use in construction. In the light of the environmental challenges, the building sector is facing, sand is no longer disregarded as a mere aggregate for concrete but increasingly understood as one of the most promising building materials for the future.

## 2.2 Sand phase changing behavior

This section examines the formability of sand and its inherent morphological capacities of form generation. The relationship between the forms of sand and their formation processes under different conditions are studied. First, sand phase changing behavior (SPB) is defined, then formation processes of wet and dry sand are outlined. Finally, sand self-organization behavior (SSB) under gravitational forces is detailed, and its employment in nature and art is highlighted.

The understanding of the morphological capacities of sand prompts new insights into its formal potentials, which is essential to develop the sand tectonics. As the research uses sand in its dry and wet conditions, it is necessary to construct an initial understanding of sand physics in its both conditions to inform the distribution of dry sand in § 5.1.1, and the making of wet sand with the saline solution in § 3.2 and in § 3.4. A number of textbooks provide simplified introductions of sand physics including the work of Jacques Duran [94,95], Philippe Claudin [96,97], and Philip Ball [98,99]. Moreover, the publications of CRAterre laboratory in Grenoble [100,101] address the topic with demonstrative videos in [102]. Any further sources will be cited *in situ*.

### 2.2.1 Sand phase changing behavior

The term ‘Sand Phase changing Behavior’ (SPB) refers to the reversibly of the structure of sand between fluid-like and solid-like states at certain conditions. For instance, the process of pouring sand into a pile is considered as a simple example of a fluid-to-solid phase transition of an aggregate system [103]. Dry sand can flow like a liquid, yet when stable it acts like a solid that can support load. By adding water, the sand turns almost like a solid, then acts like a liquid when there is much more liquid than sand. The mechanism behind the often-quick transition between fluid and solid behaviors is largely due to the condition of the voids in between the grains. The proportions of water and air to the solid grains define the phase of sand in a range of intermediate stages from dry to wet (Figure 2.3).

Since sand is not typically a solid or a liquid but exhibits a ‘unique’ form of matter [104], it is necessary here to clarify what is meant by the terms solid and liquid states. The solid-state of sand is a stable state of equilibrium between internal and external forces. It occurs when the conditions of the space between the grains prevent mobility. In contrast, the liquid state is when the space becomes large enough to allow for mobility [105]. An everyday example is a vacuum-packed coffee, it is rigid like solid due to the compaction effect but by opening the pack the material dilates and flows easily. The fact that the sand is an amorphous system that switches reversibly between flow and rigidity offers distinct formation and deformation advantages and leads to unique emergent behaviors. By altering the forces and processes by which sand is worked, the material itself changes its characteristics.

### 2.2.2 Formation processes of wet sand

The introduction of a liquid in sand induces the cohesion between the grains due to the capillary tension. The inter-grain cohesion alters some behaviors of sand including angle of repose [106], friction [107], compaction [108], and self-organization [109,110]. The cohesion introduces as well new aspects such as capillary, clustering and dilatancy [94]. The objective of the study is to define the effect of introducing liquid on the formability of wet sand. The acquired data is essential to develop new methods of processing sand with the saline solution (see § 3.2 and § 3.1.4).

Based on the water content, four states of wet sand are distinguished in physics [108], and in earth construction [100] (Figure 2.3.). The formation aspects of each state and their application in architecture are examined in [100]. Altering the way sand and water are mixed give rise to new materials' forms and characteristics (Figure 2.4). For instance, (i) trickling sand on a bed of water develop stalagmite forms induced by the capillary forces, (ii) injecting water in sand develop local clustering of grains due to the permeability of sand, (iii) releasing sand from a hole in a box of compressed humid sand leaves a stable cavity behind due to the chain of forces effect [52,100], and (iv) deposition of sand beds and ripples by water currents and the rolling effect.

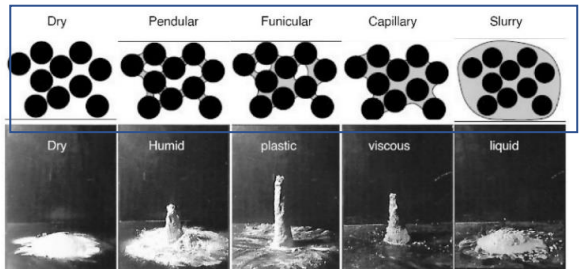


Figure 2.3 states of wet sand in physics (Top) [108], and their formation in earth construction (bottom) [100]

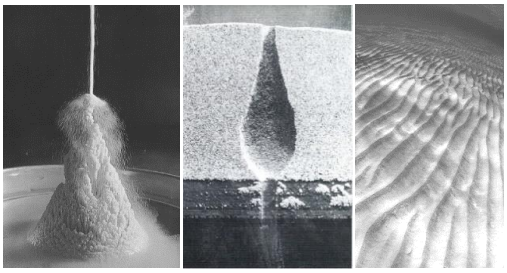

Figure 2.4 forms of wet sand. (a) stalagmite [100], (b) cave [52], and (c) aqueous ripples

Methods of using wet sand formation in architecture include (i) agglomeration of viscous sand bonded with salt in vernacular construction in Siwa oasis, Egypt [111], (ii) compaction of humid sand for the fabrication of disposable formwork for concrete casting in the Philips Pavilion by Le Corbusier[112], (iii) compaction and reinforcement of humid sand layers in the reinforced sand technique [100], (iv) accumulation of sand in aquatic environments induced by water currents and artificial barriers for the creation of underwater structures and protection of coastlines[113].

Figure 2.5 Applications of wet sand in architecture. (a) conglomeration of sand and salt in Siwa oasis in Egypt [111](b) sand formwork for concrete casting in Phillips pavilion by Le Corbusier [112] (c) reinforced sand tower, CRAterre laboratory (d) accumulation of sand by wave forces, Growing Islands project by Self-Assembly lab[113]

### 2.2.3 Formation processes of dry sand

Dry sand exhibits a rich spectrum of morphologies based on the forces that act in it, how they are introduced, and the conditions in which sand is processed (Figure 2.6). For instance, wind forces and saltation processes induce the forms of dunes and ripples [98], which was recently explored as an architectural system [114–116]. Upon random tapping of a shallow layer of sand on a plate, the grains self-organize into irregular landscape of heaps, a phenomenon known as the volcanic effect [100]. However, under controlled frequencies and conditions (plate form, excitation points, and air presence) sand exhibits regular forms known as acoustic patterns[15] [117] such as Chladni figures [118,119], Faraday oscillations [120,121], and Hans Jenny cymatics [122]. Recent studies examined physical methods to move grains and objects with precision in 2D [123] and 3D [124] spaces. Sand behaviour under vibration was examined in architecture as a means of generating self-formation patterns by Frei Otto [52] and at the AA school of architecture [114,125,126].

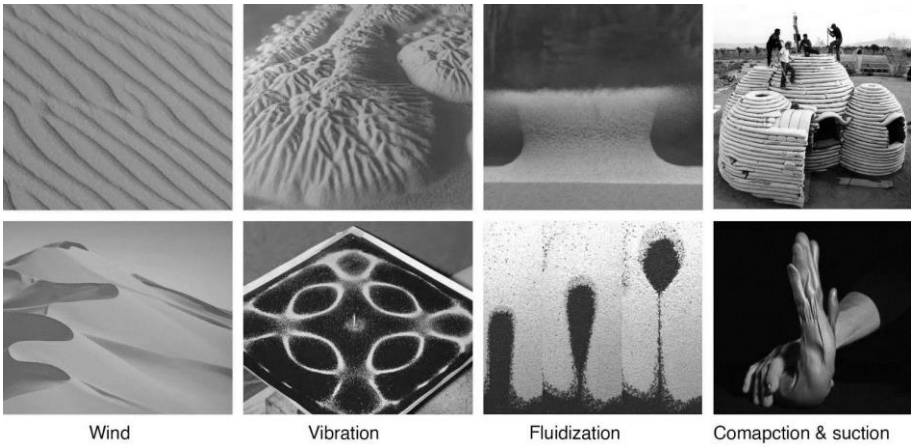


Figure 2.6 Forms of dry sand under different formation forces.

Injecting air through sand decompacts the stable mass and turns it into a dynamic fluidized bed like a boiling liquid. The fluidized state of sand triggers the formation of bubbles on the surface, droplets within the mass[127], and splashes when a rigid body is dropped on the surface[128]. Finally, packing sand in a membrane either by compression or vacuum [101,129] returns the material solid but with a certain degree of formability.

Dry and wet sand have many aspects in common. In terms of workability, both can be poured and fill the shape of a container. Moreover, emergent patterns such as ripples and dunes occur in both desert and aqueous environments despite the difference of acting forces (wind vs. water currents) and transport mechanisms (saltation vs. rolling).

[15] The vibration forces generate air currents on the plate surface which cause the displacement of the grains from the higher frequencies areas to accumulate over the nodal areas where minimum frequencies occur.

## 2.3 Sand self-organization behavior

Under the influence of gravity, sand self-organization behavior (SSB) generates constant slope piles on the horizontal plane. The SSB is central to the material system developed in this work as it informs both the design and fabrication methods. This subsection constructs the essential knowledge of the SSB and its emergent forms. First, the factors affecting the angle of repose are highlighted. Then, the morphological aspects of the emergent forms are outlined. Finally, the employment of the SSB in architecture is reviewed to identify the current state-of-the-art.

**The angle of repose of sand**

Pouring sand on a horizontal plane generates a pile with a constant slope. The pile is a state of equilibrium between its own weight and the internal friction resistance. Within the process of formation, the pile evolves through successive phases of accumulation of the material. As soon as the slope becomes too steep, an avalanche is triggered, which reorganizes the grains at a stable slope. The angle between the surface of the stable pile and the horizontal plane is termed the angle of repose (AR). It is defined as the steepest slope at which an aggregate material can be piled without collapsing. For the same type of sand and pouring conditions, the AR is constant regardless of the size or form of the pie.

A common value of the AR of sand is 35°. However, it varies between 30° and 40° depending on the following factors. (i) particles characteristics where the AR increases with the particles fineness, angularity, and roughness [130]) (Figure 2.7), (ii) moisture content, which increases the cohesion and therefore the AR [101], (iii) height of pouring where the AR increases when the pouring height decreases due to the impact of falling particles and the occurrence of avalanches[131], and (iv) vibration, which causes the pile to slip and thus reduces the AR. Three common methods of measuring the AR are detailed in [130]. In this research the AR for each sample of sand is measured to calibrate the digital and physical models.

Figure 2.7. The AR of different materials. (Left) the slope of glass marbles (white) is flatter than that of rounded gravels of the same size (red), which is smaller than that of angular gravels (black). (Right) the AR of dry sand is almost the same regardless of the grain size[101].

### 2.3.1 Morphological aspects of the sand pile

The simplest form of a pile is the cone, which can be produced by pouring sand from a fixed point. Releasing sand from a hole at the base of a sandbox produces a cone at the bottom and a funnel at the top with 'almost' the same AR. A given organization of holes generates a complex aggregation of cones and funnels, which are matching positive and negative forms. The emergent form is a landscape of conical valleys separated by sharp linear ridges. However, curved ridges can be produced by cones with different heights where the ridges curve towards the higher cone (Figure 2.8 d) [52]. The form of the pile is analogous to the diagram of forces defining it. It emerges from the process of self-formation determined by the forces of friction and gravity. By opening the holes, the grain falls towards the closest point on the nearest hole. The falling path is the line of steepest slope, which is the minimum distance between the grains and the hole. The falling process is characterized by the least-energy principle in nature as described by Frei otto in [52].

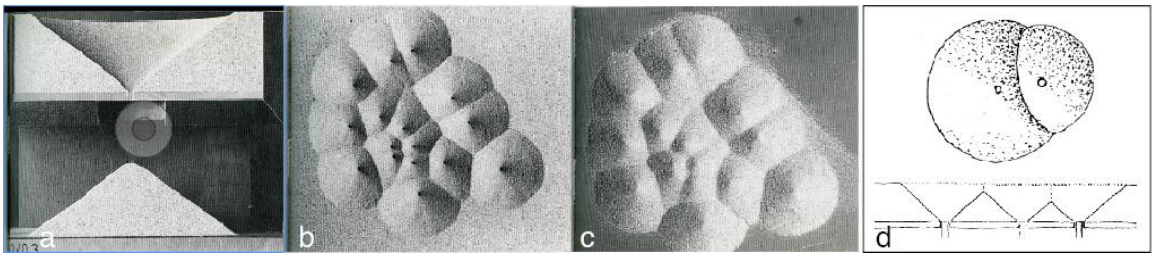


Figure 2.8 Sand piles formation. (a) sandbox, (b, c) aggregation of funnels and cones, (d) curved ridge[52]

An important feature of the SSB lies in being a minimum inventory-maximum diversity system[16]. As shown above, the pile formation is based on the simple rule of constant slope. However, the simple rule gives rise to a wide variety of morphologies by changing (i) the boundary conditions (organization of the holes, their heights, shapes, the form of the base…) and (ii) the distribution method (deposition or subtraction from a box). Frei Otto[52] (Figure 2.8), Jean-Marie Delarue [69] (Figure 2.9), and CRAterre laboratory[17] [101] conducted experiments on the morphology of sand piles under different conditions.

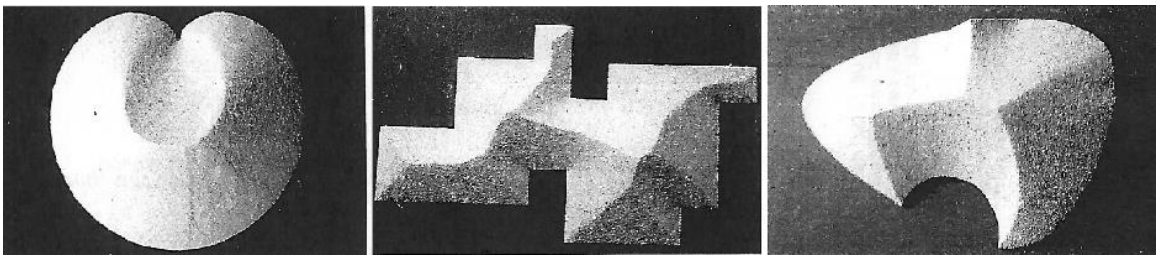

Figure 2.9 morphological and geometrical studies of sand piles by Jean-Marie Delarue[59]

[16] The principle of minimum inventory-maximum diversity is a characteristic of formation processes in nature governed by conservation of resources and least-energy responses. In design it refers to a system that achieves a wide variety of effects from a small variety of parts.

[17] Research Laboratory at Grenoble school of architecture, France (ENSA Grenoble)

### 2.3.2 Geometrical principles of sand pile

Even though the sand slope is constant, its emergent forms exhibit a rich morphological variation, which necessitates the examination of its underlying order, the geometry of surface of constant slope (SCS). The objective is to analyze the sand physical formation methods and to construct the digital modeling techniques in this work. The fundamental principles of SCS being ruled and developable are studied in this subsection based on the literature[18]. While § 5.2 analyses the hyperbolic conic sections, the Voronoi patterns, and the medial axis features of sand piles through feedback experiments between the digital and physical models. Therefore, the geometry informs and correlates the design and modeling methods in this work to decode and encode the order in the almost infinite range of morphological possibilities.

A general surface of constant slope *S* is the tangent surface of a curve *r* of constant slope (Figure 2.10). The tangent planes of *S* form a constant angle with the horizontal plane. The surface is ruled and developable as the tangent plane intersects *S* in a line, which is the generatrix of the ruled surface. On *S*, the rulings are the curves of steepest descent and they intersect the curves of constant height (contour lines) of *S* at a right angle. The contour lines form a family of offset curves whose common evolute is the top view of *r* [132]. The developable helicoid is a surface that is tangent to a helix which is a constant slope curve known as the cuspidal edge or edge of regression of the surface. The SCS are to surfaces what the helices are to curves [133].

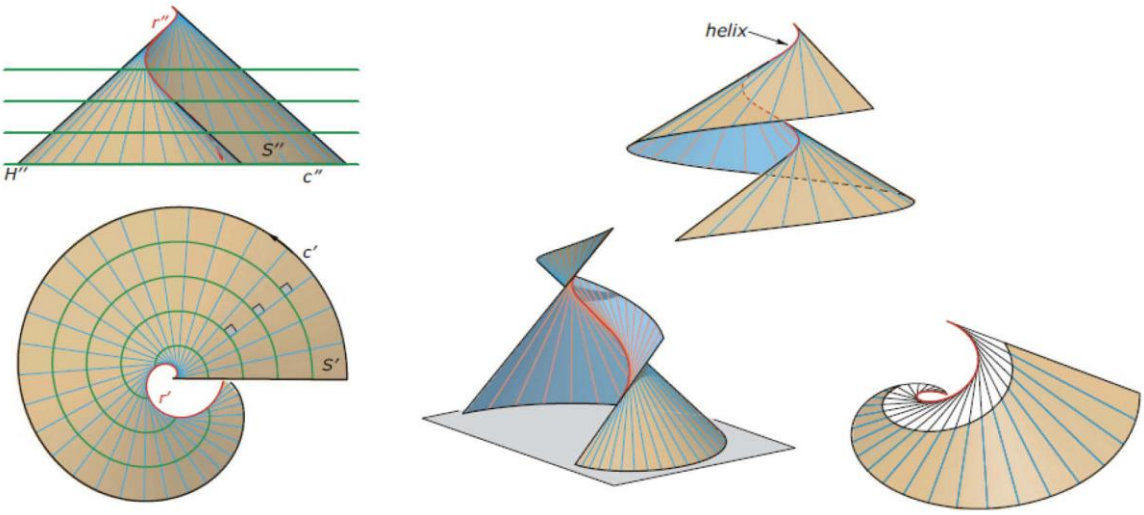


Figure 2.10 General surface of constant slope [132].

[18] The fundamental knowledge of SCS in this work is mainly acquired from the discussion with Jean-Marie Delarue at the GSA his educational publications and videos [69,70], in addition to the 'Architectural Geometry' book [132] among other references of descriptive geometry.

Figure 2.11 study the characteristics of SCS surfaces on a hollow sand pile. Given the surface *S* Θ constant angle of slope, *M* point on the surface boundary (the intersection curve between the surface and the horizontal plane), *V* tangent vector of the boundary curve at M, H point on the ridge of the surface and *H'* is the vertical projection of *H* on the horizontal plane.

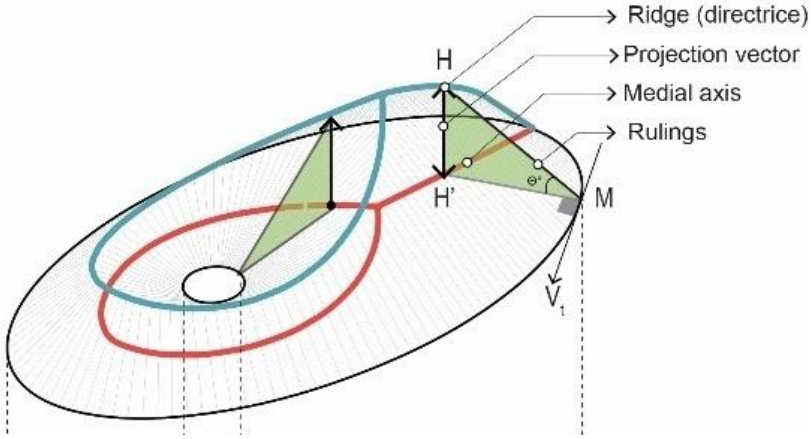


Figure 2.11 Geometrical analysis of a hollow sand pile.

The surface of SCS is ruled as the tangent plane intersects *S* in the line *MH*, which is the generatrix (rulings) of *S,* while the boundary curve is the directrix of the surface. The rulings of *S* are its curves of steepest descent. The surface is then a portion of developable surface as the tangent planes are constant along the rulings. The rulings *MH* of the surface are normal to the boundary curve and subsequently to the contour curves. Finally, the relationship between the ridge curve, its vertical projection (the medial axis), and the boundary can be defined by trigonometric functions with the input of slope and any two of *M*,*H*, and *H'*.

From the characteristics of SCS introduced above, three methods for the generation of SCS are identified: (i) by the movement of a plane of constant slope, (ii) as the envelope of all cones generated by the movement of a right circular cone along a directrix curve, and (iii) as the envelope of the tangents of a curve of constant slope.

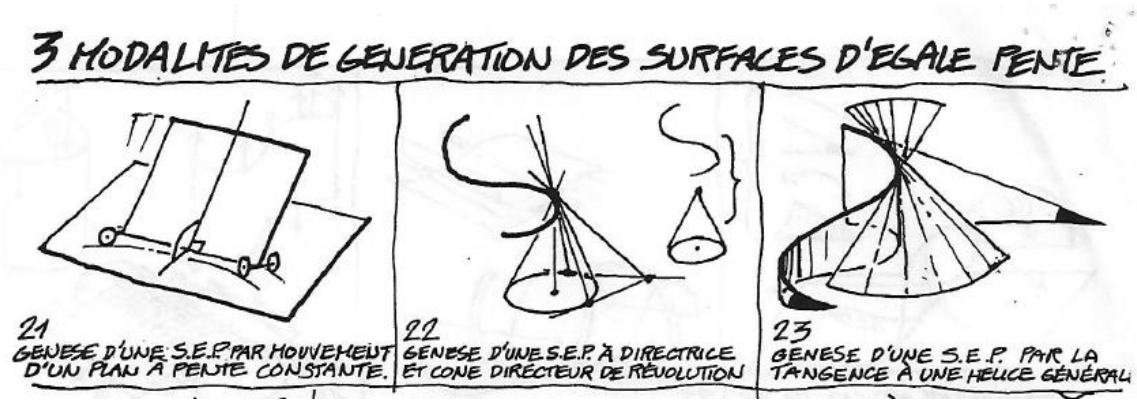


Figure 2.12 Methods of generation of surfaces of constant slope [69,70]

### 2.3.3 Sand self-organization in nature and art

This subsection highlights the implementations of sand self-organization behaviour (SSB) in nature and art as they employ formation processes at different scales that are relevant to this study. The objective is to construct a broader background of the sand distribution methods and the morphological aspects of the emergent forms.

The formation of sand piles based on SSB is of major importance in certain industries such as geoengineering, mining and construction [94]. In nature, it occurs in forms of sand dunes, mounds, and mountains. While in the living nature, strategies of building based on SSB are reported in the trap of the antlion insect [95] and in the breeding pits of specific fish species[134–136] (Figure 2.13). Formation methods such as digging, throwing, deposition, and displacement are used in these natural constructions. Moreover, the Voronoi pattern in Figure 2.13-c emerges from the collective behaviour of the school of fish.

Figure 2.13 Building strategies based on SSB in nature. (a)The trap of the antlion [95], (b) the spawning pits of pufferfish [134], and (c) the breeding territories of Tilapia fish [135,136]

In the fields of artistic study, the process of sand under gravitational forces is explored as a bearer of meaning. Static [137], cyclic [138–140], pendular [141,142], and mobile [143] sand processing methods are investigated on different scales. Lara Almarcegui, Willner Olsson and Jean Bernard Métais employ large scale sand deposition in Land Art installations (Figure 2.14).

Figure 2.14 ‘Temps Imparti’, installation by Jean-Bernard Métais, 1999-2001. The electronically controlled cyclic flow of sand generated continuously changing patterns over the two years duration of the artwork [144].

## 2.4 Sand solidification methods

The previous subsection highlights two distinct potentials of sand formation, its castability when wet and its self-formation when dry. The latter is of little value since the forms are just as easily lost when dry. However, by turning the loose sand into a durable solid, it becomes a construction material rather than being a mere design tool. By a combination of shaping and solidifying of sand, the design system greatly expands the morphological capacities of sand towards structural applications.

It is important here to note that the solidification process is not a mere technical question, but it has the following cross-functional role: (i) formative as it largely affects the formation process and define its potentials and limits, (ii) structural to meet sufficient strength for construction, and (iii) ecological to attain a minimum impact of construction on the environment. Above all, the solidification process should meet the phase changing behavior of sand, i.e., to exhibit reversible behavior between liquid and solid states to be able to be mixed, sprayed, solidified, and reused like sand. In light of these considerations, this subsection highlights certain solidification methods that might meet the above cross-functional criteria. First, a traditional method of solidification with salt is introduced, followed by new ecological methods, then binding technologies in foundries are highlighted.

In the vernacular construction technique in Siwa, an oasis of the western Egyptian desert, sand is solidified by sodium chloride (NaCl) salt, which is available in the nearby salty lakes. Salt blocks, lake mud rich with salt, and sand are mixed to produce a mortar known as ‘Karshif’. The crystallization of salt inside the sand mortar gives rise to a sort of monolithic conglomerate with compressive strength between 0.58 and 2.34 Mpa [111] (Figure 2.15).

Figure 2.15 Salt architecture in Siwa, Egypt. (a) salt lakes (b) houses with sand and salt mortar (c) salt bricks

Nowadays, numerous studies have developed new ecological methods of aggregate binding such as natural pozzolanic binders[100] and bio-cementation [145–148]. Inspired by the natural cementation methods of calcium deposition, bio-cementation techniques are now investigated for binding sand. The cementation process involves the use of a type of bacteria into the mixture that induces the production of calcite through a chemical reaction, binding the grains together in a few days [149]. Bio-cementation has been investigated in soil stabilization [150], solidification of sand for bricks and sandstones [145,149,151,152], sealing concrete cracks, development of self-healing concrete [153], improving the mechanical properties of mortar and concrete [154]. Available results in the literature reported that the compressive strength of bio-

sandstone ranges from 1 to 2 MPa after 7 days while 16.58 MPa is also reported [145]. Despite the promising applications of bio-cementation in different disciplines, the available assessment in construction's literature reported two main challenges: the excessive production of ammonia that affect the environment and the problem of mass production as the process of bacteria production is time and cost consuming [150,155].

In foundries, sand casting is a well-established technique for the fabrication of molds and cores using a range of bonding composites. An example of a fast binder at room temperature is sodium silicate solution, which when mixed with sand, then exposed to carbon dioxide gas, returns solid sand with a compressive strength of around 2MPa [156]. This binding method is examined for the fabrication of sand bricks in architecture, but an epoxy resin is applied, which increases the compressive strength up to 20MPa [157].

Sand-3D printing technology has recently emerged as an additive manufacturing technique, bringing new fabrication methods. In binder jetting technique, a thin layer of sand is first spread then a liquid binder is sprayed, which solidifies the particles and forms a 3D object by the stacking of layers. The 3D sand printers are commercially available, providing advantages in terms of scale (up to 4 x 2 x 1 m) and resolution (600 DPI voxel and 0.3mm layer thickness). Architectural applications of such technology include the fabrication of highly detailed freeform architecture components [158] and stay-in-place sand formworks filled with concrete [159]. Despite the advantages of sand 3D printing in architecture, its structural and ecological performances are still in question. Structurally, 3D printed parts are too weak to operate as a building material due to their limited strength in compression (8-12 Mpa) and bending (3-9 Mpa) [159]. Ecologically, it heavily relies on phenolic resin, polyurethane and Furan [160,161], which are highly toxic, flammable binders with low environmental compatibility such as [162,163]. Recently, a new method has been proposed by Enrico Dini [146], which uses less harmful binders (sodium chloride solution and magnesium oxides powder) yet giving high strength 50 MPa in compression and 5 MPa in tension [164]. Finally, sand sintering technologies, that apply heat to weld together the sand particles, are now examined in architecture on small scale prototypes using laser beam [165] and solar radiation [166] as means of heat sources.

Among the above methods, Siwa oasis introduces an interesting method of solidification, salt crystallization. The interest lies in the reversible phase changing behavior of salt from liquid to solid, which when coupled with the phase changing behavior of sand, gives rise to a reversible construction material. Among different types of crystals and hydrate salts [167] that were experimented during the master research, sodium thiosulfate was found as an appropriate material for cementing sand thanks to its low transition temperature, its strength when solid, its low environmental impact, its availability on the market, and its low-cost. The following section deepens the understanding of the salt properties to better inform the making methods in this work.

## 2.5 Sodium thiosulfate pentahydrate salt

This section studies the Sodium thiosulfate salt, the binding agent introduced by the 35 Degree project for cementing sand (see § 1.3.2). First, the salt is defined, then its phase changing behavior is detailed, next its supercooling, reversible and thermal behaviors are highlighted.

The sodium thiosulfate pentahydrate (STP) $Na_2S_2O_3{\bullet}5H_2O$ is a phase changing hydrate salt that is soluble in water with a melting point of 48°C and boiling point of 100°C. It is characterized by a phase changing behavior (PCB) that turns between solid and liquid states in response to thermal cycles of heating and cooling. An everyday product that employs STP is the reusable heating pad (hand warmer), which provides instant heat[19]. The salt is available in the market in two forms as shown in Figure 2.16: (i) white powder (sodium thiosulfate $Na_2S_2O_3$, anhydrous form), and (ii) colorless crystals (sodium thiosulfate pentahydrate $Na_2S_2O_3{\bullet}5H_2O$, hydrate form). A major difference between the two forms is that the powder ST, used in the 35 Degree project, requires water and heating for melting. While the crystal STP, used in this research, requires only heat which elimantes the use of water in the preparation phase. The commercial name of the STP is 'hypo' from which is adopted the term 'Hyposand' to describe the mixture of sand and salt in this work.

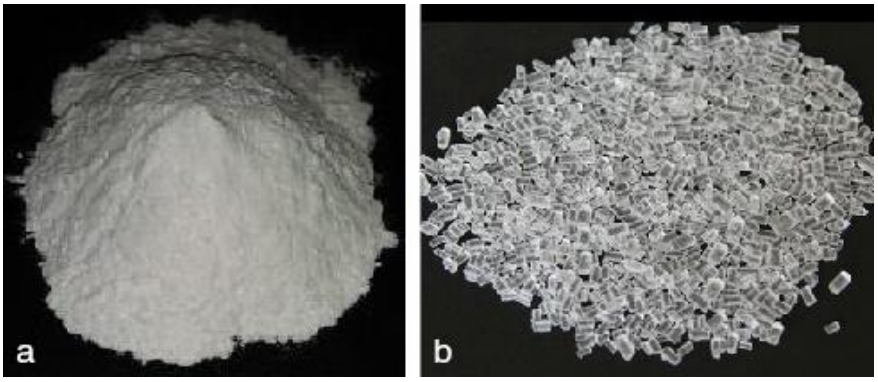


Figure 2.16 Forms of sodium thiosulfate salt. (a) sodium thiosulfate anhydrous, white powder (b) sodium thiosulfate pentahydrate, translucent crystals.

The STP is a safe substance where no physical, environmental, or health hazards have been classified for this compound according to the European Chemicals Agency (ECHA) and the U.S. Environmental Protection Agency (EPA). The STP is produced on the industrial level as a by-product of sodium sulfide manufacturing. It is available in the market at chemical vendors. A bag of 25 kg costs around €125 in France, €20 in Egypt, and €3 in China. On an industrial scale, 1-ton costs €200 in China. STP is used in medical products, water treatment and photographic processing. In construction its use is presently limited to thermal applications for heat storage in solar panels [168], for the reduction of thermal conductivity in PCM bricks, concrete, and glazing [169] and for stabilizing indoor temperatures [170].

[19] Typically, a small plastic pack filled with STP in its liquid phase. By flexing a small metal disk in the pack, the salt crystallizes instantly and produces heat. By immersing the pack in hot water, the STP melts and returns to its liquid state for a reusing phase.

### 2.5.1 The phase changing behavior of the ST salt

The STP compound ($Na_2S_2O_3$•$5H_2O$) contains 65% Na2S2O3 and 35% water by weight [171]. The water molecules make part of the crystal structure of the salt and they define its transition to lower hydrates[20]. When the STP is heated up to its melting point (48 °C), the associated water molecules melt into an aqueous solution in which the salt crystals dissolve completely. Along with heating, the water content evaporates 'partially', which increases the saturation of the salt creating a supersaturated saline solution. By cooling the solution at room temperature below its melting point, it turns into the supercooled liquid phase that if not disturbed crystallizes gradually. The rate of crystallization rises remarkably as well as the released heat if the supercooled solution is disturbed with a nucleation agent like a seed crystal, dust, or sand as in the case of this research [172,173].

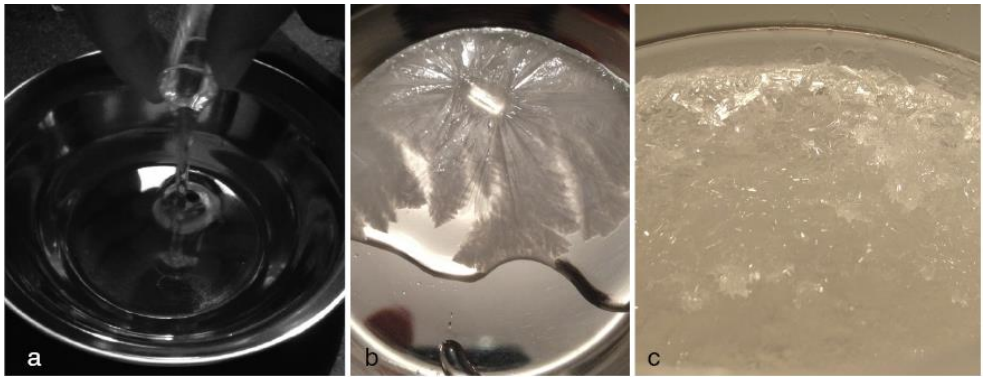


Figure 2.17 Crystallization process of STP. (a) melted, (b) nucleation with a crystal seed, and (c) crystalized

Figure 2.18 shows the PCB of STP in two graphs. In the heating and cooling curves (left), time in hours is plotted against temperature in C°. The arrows point to the melting, nucleation, and crystallization points. In the phase changing diagram (right), saturation in water by percentage is plotted against temperature in C°. The arrows point to the transition of STP into lower hydrates upon heating and their resulting concentration percentage [167].

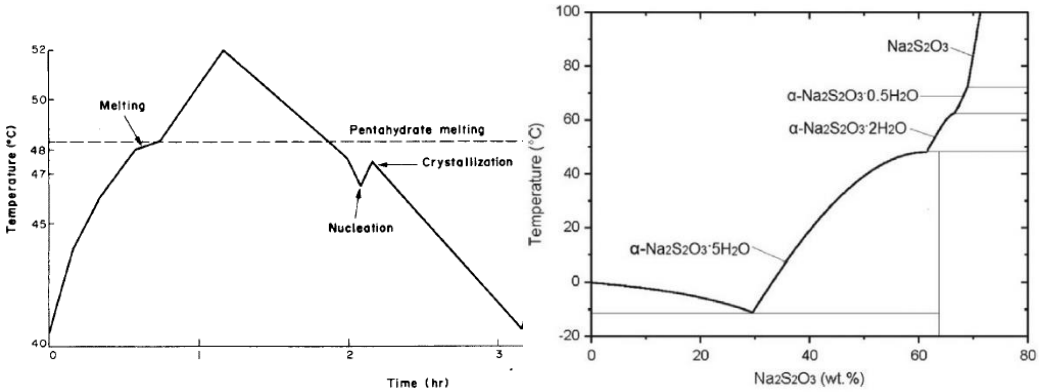


Figure 2.18 Phase changing behavior of STP. Heating and cooling curves (left), and the phase diagram(right) [167].

[20] The associated water molecules to the crystal structure of the STP play a major role in its transition to lower hydrates during heating and cooling processes. Upon heating, the water evaporates gradually from the pentahydrate compound forming lower hydrates and when the water totally evaporates, it leaves the anhydrous salt.

### 2.5.2 Characteristics of the ST salt

After outlining the phase changing behavior of the STP in the previous subsection[21], it is essential here to highlight certain characteristics of the salt to study their effect on the Hyposand workability, its life cycle in chapter 3, and its strength and thermal conductivity in chapter 4.

1. **The supercooling phase and the storage of the salt in its liquid state:** supercooling refers to the liquid phase of the STP when it is cooled below its freezing point without crystallization. This phase occurs if the saturated solution is not disturbed with a nucleation agent and thus does not crystallize. It is reported that the STP can be stored in its liquid phase up to ten years in vacuum containers[22] [173]. This feature is of interest for this research to use the salt in sites where no heating sources are available to melt the crystals.
2. **The solubility and the recyclability of the salt:** the STP is soluble in water, and when exposed to humidity it absorbs water molecules and dissolves. This characteristic defines the salt lifecycle and opens potentials for the salt recyclability.
3. **The semi-congruent property and the recyclability of salt:** semi-congruent refers to the semi-reversibility feature of the PCB, which allows upon re-melting a crystalized sample to restore the salt but in lower hydrates forms and not in its original composition of pentahydrate. Hence, the salt can be restored but with less strength and concentration [174]. However, this undesired property can be eliminated by adding stabilising additives [175].
4. **The thermal behavior of salt and heat storage ability:** the STP is a heat storage material as it absorbs heat when melted, store it when supercooled, the release the gained heat when crystalized[23]. The STP stores five times more heat than water and ten times more than masonry and rocks. The thermal conductivity of the STP is 0.57 W/m°K at a temperature range of 10 to 50 °C [112]

The application of the STP in construction is mainly based on its PCB and latent heat capacity. It is used in solar panels and for heat storage in bricks, concrete and glazing [169,170,176].

---

[21] The STP has a very complex PCB as it is capable of changing into five forms of lower hydrates in solid, liquid, or mixed phases based on the temperature and number of heating/cooling cycles. The properties of each form of STP highly affect the strength of bonding [117] which necessitated a more detailed study in this research to deepen the understanding of the behavior of salt (Appendix A).

[22] The supercooled phase can also be improved by certain additives such as urea and chloroform among other materials. This method is widely used in the solar panels industry which employs STP in its supercooled phase [106].

[23] By heating the STP, it melts at 48°C and goes into an endothermic process where it absorbs large amounts of heat without getting hotter, and the temperature keeps constant at 48°C for a while until complete melting is achieved (superheated property). Once the STP is fully melted, it performs as a sensible heat storage material. The exothermic process occurs when the supersaturated STP cools below its freezing point to form a supercooled liquid that upon nucleation solidifies and releases its stored latent heat.

# Part II

# SAND TECTONICS

Chapter 3

# Material system:
# Hyposand fabrication methods

# 3 Material system: Hyposand fabrication methods

Part I of this manuscript discusses how new formation possibilities may arise by altering the technique by which the materials are worked (chapter 1). It also examines how introducing a liquid in sand brings forth new formation possibilities informed by the amount of liquid and how it is introduced in the sand (chapter 2). Based on the literature in Part I, the previous work in the 35 Degree project, and the physical experimentation conducted in this work, this chapter develops the know-how of the Hyposand making techniques and identifies its aspects of workability. The objective of this chapter is to develop the material system of the proposed sand tectonics.

This chapter defines the fabrication methods of Hyposand by means of mixing sand and the saline solution of sodium thiosulfate pentahydrate salt. The chapter discusses how the amount of salt in the mixture and the way the sand and salt are mixed bring forth new formation possibilities. Mixing-casting, shaping-spraying, and pouring-shaping are among the different processes used in this work. The order of the processes returns different formation possibilities as will be discussed.

First, the process of material preparation is outlined. Secondly, the mixing and spraying methods of making are detailed. Then, the essential considerations to ensure the quality of making are outlined. Next, different experimental methods of making that are thought in this work are highlighted. Finally, the workability aspects of Hyposand and the saline solution are discussed.

Figure 3.1 Sand grains and salt crystals

To better understand the structural possibilities of Hyposand, the following chapter examines its mechanical characteristics. While the morphological potentials of Hyposand as an architectural material system are examined in chapter 5 and employed in many prototypes in chapter 6.

## 3.1 Materials preparation method

Hyposand is an accessible material that relies on limited resources being sand, sodium thiosulfate pentahydrate salt, and heating energy to melt the salt. To improve the workability of Hyposand, it is necessary to define the type of sand and salt being used, the method of salt preparation and the spraying tool.

**Sand type and the quality of production**

It is important to distinguish between two types of sand used in the fabrication process:

- **Casting sand:** to attain a castable mixture of Hyposand, which returns high strength when solid, fine to medium (0.125-0.5 mm), well graded, and rounded sand is used conforming the results of the material characterization campaign in chapter 4.
- **Formation sand:** to achieve a flowable (self-formation) mass of sand, which returns clear patterns, sharp ridges and smooth surfaces when set, the used sand has to be clean, dry, fine (0.125-0.225 mm on Wentworth scale), poorly graded, and rounded.

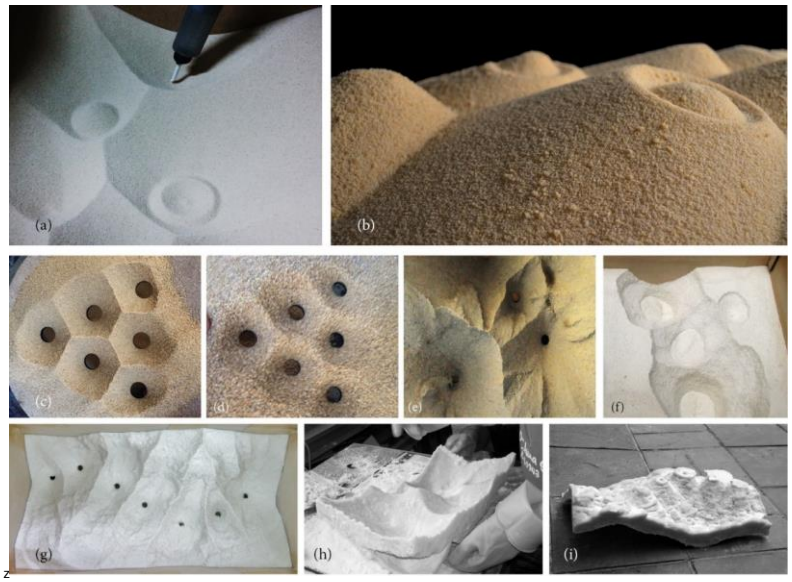


Figure 3.2 Effects of sand characteristics on the emergent patterns. Dry, clean, fine, poorly graded, and rounded grains return sharp ridges and clear surfaces in formation (a) and when solidified (b).

**Salt type, preparation, and spraying tool**

To overcome the limitations of the saline solution in the 35 Degree project, the crystal form of salt is used instead of the powder form to exclude the use of water in the preparation phase. Moreover, the salt is prepared using a kettle instead of a heating top to heat it up to its boiling point (100°C) which avoid the decomposition of the salt and the reduction of its strength if overheated. The salt is prepared by heating it up to its boiling point (100°C) until the whole crystals are melted into a colorless supersaturated solution. A spraying gun is used instead of manual sprayers which returns more even surfaces, sharper sand, patterns, and more resistant panels.

## 3.2 Mixing method of making

Mixing is a blending-shaping process, where formation possibilities depend on the proportions of the materials. To avoid deviations in the properties of Hyposand it was necessary to standardize the manual mixing technique through the following procedures. After the preparation of the materials, the hot saline solution (80°C to 100°C) is poured into a mixing container, then sand is added gradually while steering until no lamps of sand, excessive saline solution, or air content can be detected and the mixture appears to be uniform[24].

The quantity of salt in the mixture determines its consistency and workability and accordingly its formation and applications possibilities. Three states of hydrated Hyposand and their formation possibilities are distinguished based on the salt content in percentage[25] by weight:

a. **Plastic-moldable (50%):** the mixture is malleable, and it can be molded and compacted to take the shape of a simple container (Figure 3.3a). Vibrating the plastic states cause liquefaction and return more homogeneous mixture.
b. **Viscous- castable (55%):** the mixture can flow under its own weight and can fill the shape of a relatively complex container. By casting the viscous mixture in between two sand panels it bonds with them and returns a monolithic block (Figure 3.3b). Vibration causes dilatancy and segregation where the salt rises to the surface.
c. **Liquid-pourable** (60%): the material flows like a liquid and can be poured. By pouring the material in a flexible formwork it can be shaped while hardening, which gives rise to a new process of formation (Figure 3.3c) (see the tube casting technique in § 6.6).

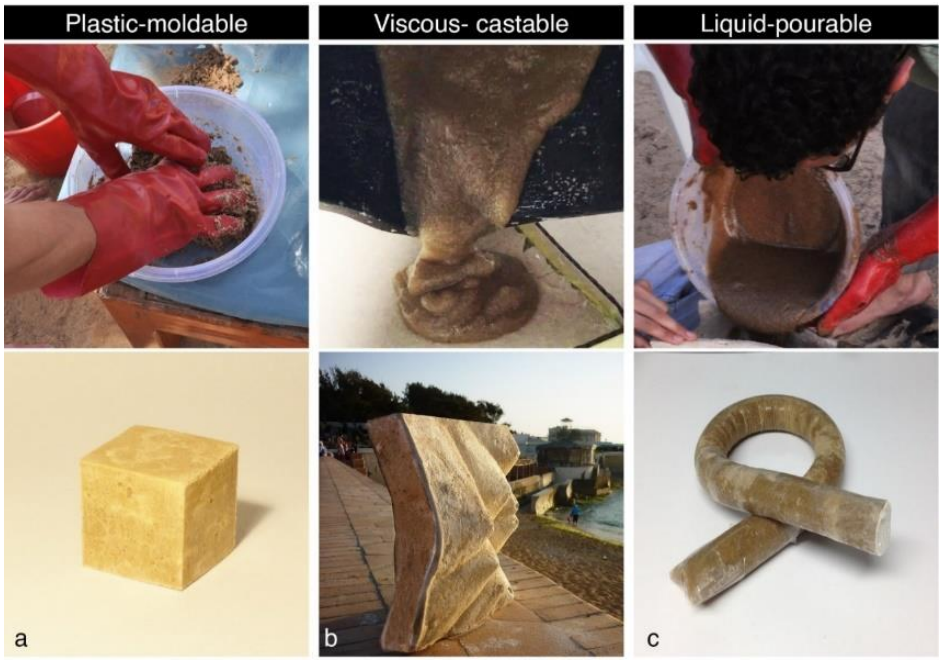


Figure 3.3 The mixing technique of making. Three hydrated states of Hyposand and their respective formation possibilities are distinguished based on the proportion of the saline solution in the mixture.

[24] A mechanical mixer might return a more homogeneous and standard material which is not available for this research

[25] The effect of sand to salt proportion on the material compressive strength is discussed in chapter 4,§ 00.

## 3.3 Spraying method of making

Spraying is a shaping-solidification process where the saline solution is applied on dry sand piles to harden. The objective is to turn the emergent sharp patterns and forms of sand into solid panels assembled and used as formwork for casting Hyposand or other materials such as concrete. The spraying process is first introduced followed by a discussion of its advantages and constraints.

Figure 3.4 A thin crust of sand solidified by spraying

It is important here to note that the solidification process is not a mere technical question, but it has the following cross-functional role:

1. **Formative** as it largely affects the formation process and define its potentials and limits
2. **Structural** to meet sufficient strength for handing the sand panels
3. **Ecological** to attain a minimum impact of construction on the environment
4. **Reversible** to meet the phase changing behavior of sand

**Spraying process**

In the light of the above considerations, the following process of spraying is sought. Spraying is an additive manufacturing method based on the accumulation of sand layers sprayed with the saline solution. After the preparation of the sand and salt the typical process is as follow:

1- the sand is formed either with or without a formwork.

2- the saline solution is sprayed[26] while hot over the surface and binds the exposed sand grains instantly. The grainy yellow surface of dry sand turns into a soft white texture, which indicates the saturation and hardening of the first layer.

3- a thin layer of sand is spread over the solid layer.

4- steps 3 and 4 are repeated until the required thickness is achieved.

5- the solidified layer of sand is then demolded

[26] As there is no special sprayer for the process, the research had to find a suitable equivalent in the market. The sprayer had to meet two conditions, rigid enough to sustain a 100°C solution, and demountable to clean it from the salt that quickly crystalizes inside and blocks the nozzle.

A process of 5 layers turns a 20x20cm surface into a solid panel of around 1 cm thickness in 10 minutes. Figure 3.5 illustrates the process of spraying a 50x 50cm panel, which thickness had to be increased to 2 cm to better withstand the charges.

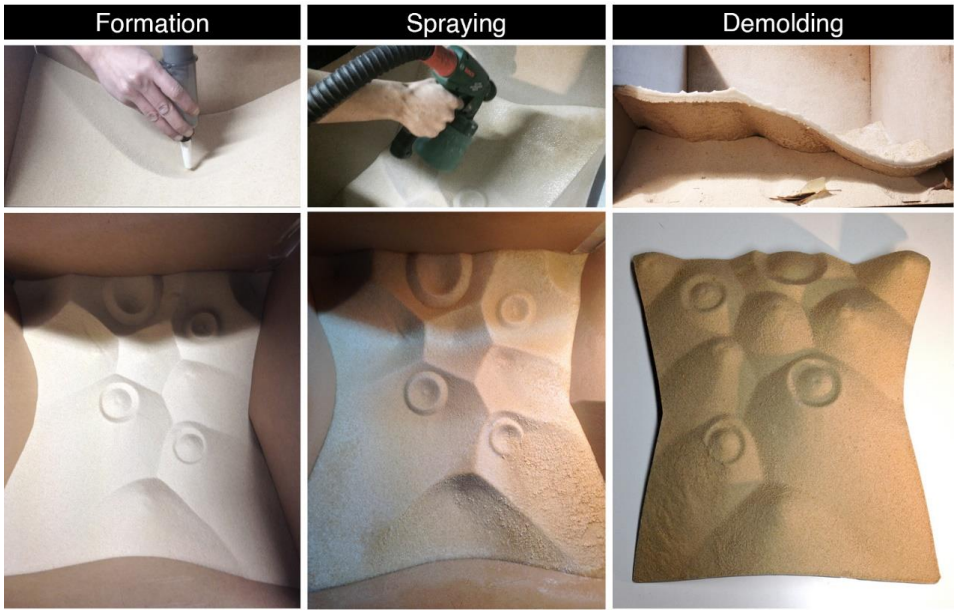


Figure 3.5 process of the spraying method. 50x50x2 cm panel

**Spraying protocol**

Spraying is the most critical process of making in this research as the dry patterns of sand can be easily deformed or lost if the saline solution is not properly applied. To overcome this technical challenge a precise protocol of spraying (phases, distances, and patterns) and specifications of the sprayer are developed and discussed below.

1. **Application phases**: as the first layer of and is the most critical to sustain the shape it is essential to apply the process on three phases:
   a. The general phase is applied far from the surface (around 1m) to shower the whole surface with a mist of salt. This phase ensures an Initial adherence between the sand grains, which creates a thin crust of sand. After few seconds of spraying, a clear white layer of salt is composed over the sand surface indicating the initial crystallization of the surface.
   b. The local phase is focused spraying on parts of the surface from a close distance (around 20 cm). To avoid pushing the grains with the air and liquid pressure of the sprayed salt, it is also important to spray in a normal direction to the surface.
   c. The layering phase applies the local method several times while spreading an even thin layer of sand over the surface. The number of times depends on the required thickness of the sand panel.

Among the available patterns of spraying that the nozzle can afford it is found that the linear flat patterns return more even distribution than conical and circular patterns.

The design capacities of the spraying technique are shown in Figure 3.6, including preserving the sharpness of the patterns (a-d) and the rise of specific morphological qualities such as ribbing and translucency (c, e). In terms of workability, the strength of the panel allows its handling for transporting, stacking, cutting, drilling, assembly, and casting (f).

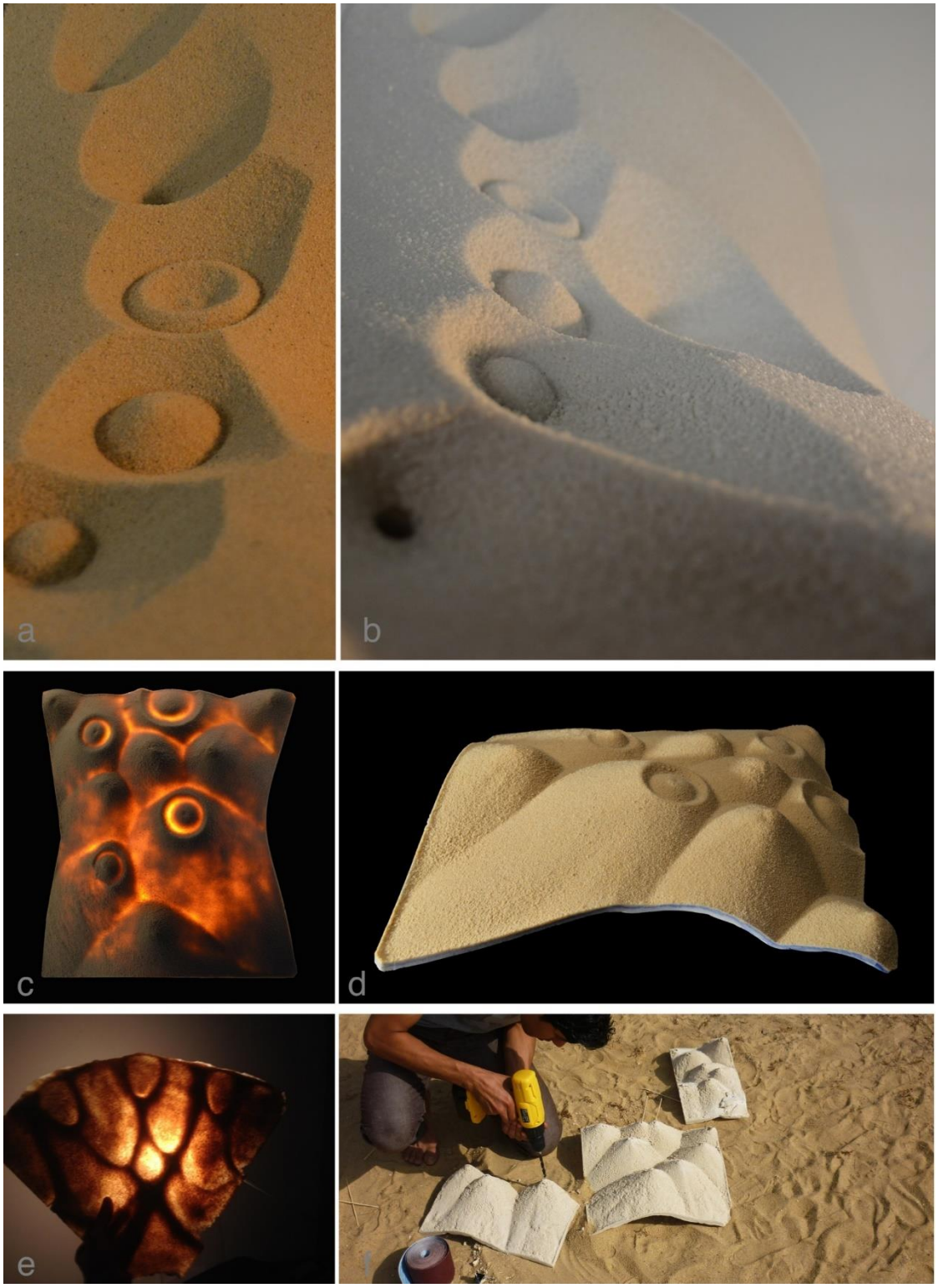


Figure 3.6 Spraying method of making. The precise patterns of loose sand (a) are preserved when solidified (b). A 50x50cm solid panel (d) with a 2 cm thickness border (g). A designed layering of sand allows the development of material translucency (c, e). The resulting panels are strong enough to be worked, drilled transported and casted (h).

## 3.4 New methods of making

Altering the way a liquid is introduced into sand give rise to new material form and characteristics as discussed in the literature (see § 2.2.2). This subsection explores new methods of making with sand and salt to reveal the morphological capacities of the materials. Some making experiments that were conducted along the research are highlighted. The first three methods explore ways of mixing sand and salt. While the other four explore different formation possibilities of sand, Hyposand, and the saline solution. The advantages of each method are briefly introduced below with its drawbacks and visuals (Figure 3.7).

1. **Steaming**: to preserve the sharpness of the sand patterns at maximum quality and to avoid its destruction if it is not properly sprayed, a solidification technique by steaming the saline solution over sand is thought. A water based steam cleaner composed of a boiling container and a pressure nozzle is used. First, the sand pattern is produced in a box then closed with a cover. Second, the steam cleaner is filled with the saline solution and heated. Thirdly, the steam is introduced in the closed box and the sand surface is subjected to the steam for few minutes. However, the experiment did not return a solid surface. This might be due to the phase changing behavior of the STP salt that when it transforms to vapor it transits to lower hydrates that do not crystalizes when cooled (see § 2.5.1).
2. **Capillary action:** trickling sand on a bed of salt (equipped with a vertical transparent sheet) produces stalagmite forms on the sheet surface. After a short rise, the instant hardness of the salt prevents the capillary action and stops the growth. In another experiment to experiment the capillary process, a disk filled with dry sand is introduced into a bed of salt. The salt flows into the sand up to the height of the salt bed and returns a solid disk of sand.
3. **Injecting** salt in sand develop local clustering of grains due to the permeability of sand [73].
4. **Vacuum:** shaping dry sand in a vacuum container then solidification by injection.
5. **Printing** with Hyposand is thought to explore the possibility of 3D printing in this research. The experiment raised two main challenges. The first is the fast hardening of the Hyposand agglomerate in the printing device. To prevent the device clogs, a portion of clay is added to the mixture, but it reduced the strength, delayed the hardening time, and evoked cracks on the surface when solidified.
6. **Extruding** Hyposand is thought to take advantage from the viscosity of the material and its instant hardening. Extruding a mortar of Hyposand by a rotational robotic formwork produce torsional vertical structure. The structure hardens instantly while forming but it developed gaps due to the delay in hydration between the deposited layers.
7. **Fabric hardening**: since salt is a sprayable bonding material, it is thought to harden pretensioned Lycra fabric by spraying the salt over the fabric. The process hardens the surface and maintain the pretensioned surface after removing the tensile support.

Figure 3.7 Experiments of other making techniques. **Mixing sand and salt** by: Steaming sand patterns with the saline solution, Capillary action, and injecting salt into sand. **Formation of dry sand** in vacuum container then injection. **Formation of Hyposand** by printing and extruding. **Solidification of pretensioned fabric** by spraying the saline solution.

## 3.5 Aspects of Hyposand

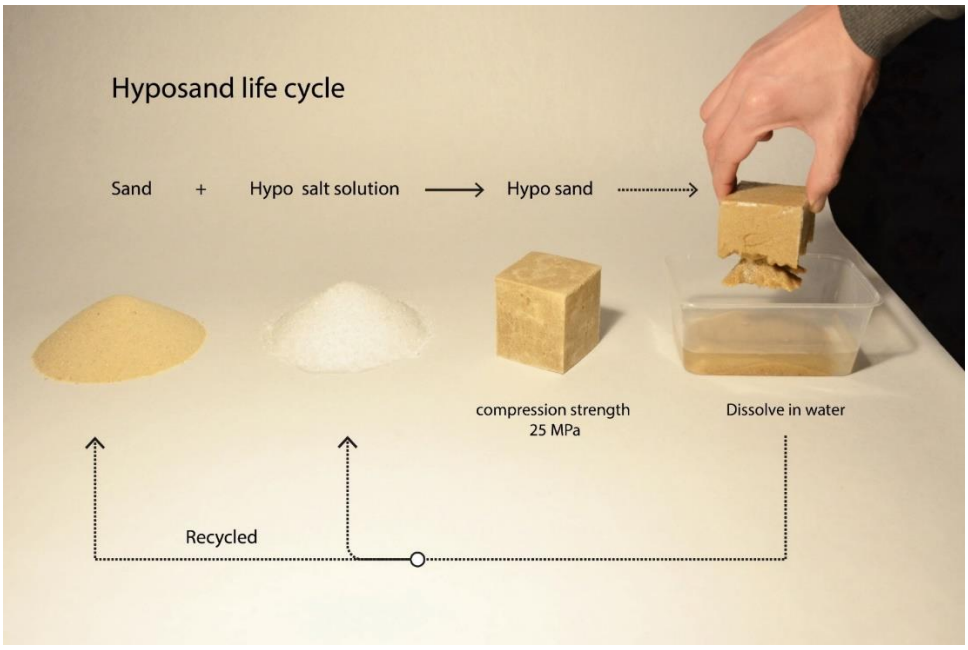


Figure 3.8 Hyposand life cycle. The material dissolves in water, which allows the recovery of sand and the semi-recycling of salt.

- **Fabrication resources**: the fabrication of the Hyposand material relies on limited resources being sand, STP salt and heating energy to melt the salt. No water being needed for the process, and it solidifies at room temperature in relatively short time without need for burning or additives.
- **Type of sand**: any type of sand can be used to fabricate Hyposand including oolitic and desert sands desert sand, which have nowadays limited use in construction industry (see § 2.1.4) even though they are widely available, especially in the Middle East and desert areas.
- **Accessibility**: Hyposand is an accessible material since the sand and salt are available at low-cost (see § 2.52.5) and the fabrication method is straightforward at low-tech.
- **Workability**: Hyposand is a castable and a sprayable material, and its workability time is relatively short depending on the volume of the material and the ambient temperature.
- **Hardening time**: Hyposand solidifies relatively fast at room temperature. Such timing is proportionally related to: (i) the temperature of the saline solution: the crystallization rate increases inversely with temperature, i.e. at 60°C or below it crystallizes faster than at higher temperatures. (ii) the volume of the specimen, for instance, a 10 cm cube dries in 3 hours while larger volumes take a longer time to solidify. The fast hardening of the material enables rapid production of sand structures and opens possibilities for material extrusion and printing.
- **Hardening conditions**: Hyposand solidifies with air contact but also in vacuum containers, i.e. without presence of air. This feature motivated the research to develop

the tube casting technique where Hyosand is casted in plastic tubes that are shaped then the Hyposand solidifies inside the tubes (see § 6.6)

- **Reusability:** a recent research on Hyposand [27] [177] shows the possibilities of reusing the material by means of heating. By subjecting samples of solid Hyposand to heat, the salt dissolves and release the sand grains giving a workable paste that can be reshaped. The research shows that the compressive strength of the material remains constant up to three cycles of reusing.
- **Recyclability**: Hyposand can be decomposed into sand and salt by immersion in water using a method that is not discussed in this work. However, it is important to note that the recovered salt exhibit lower crystallization strength due to the semi-reversible property of the STP (see § 2.5).
- **Decomposition in water**: Hyposand is not stable if in contact with water, it erodes if washed or immersed in water and it degrades with humidity. The decomposition of Hyposand limits its application to temporary structures in arid climates and to recyclable formworks.
- **Waterproofing**: water insulation of Hyposand is thought in this work to extend the material lifespan and to broaden its usage in other climates than arid areas. To overcome the instability of Hyposand if in contact with water small scale experiments are conducted using natural and artificial water repellant materials including: (1) linseed oil, (2) casein, (3) Sikagard®-701 W[28], (4) Bostick® HYDROFUGE[29], and Aqua-Bloc®. Three application methods of the insulation materials are thought in accordance with the fabrication techniques in this work: (i) external application by means of a brush on the surface of molded Hyposand, (ii) mixing with the saline solution, and (iii) spraying on the solidified sand panels. The tests are conducted following the standard methods of application of the insulators on stone and concrete. The first three materials are applied on the surface. Upon the tests, it is noted that the applied insulators infiltrate the surface of Hyposand but do not provide water insulation. The Bostick® HYDROFUGE is mixed with the saline solution before adding the sand but as well did not provide insulation. Finally, the Aqua-Bloc® is sprayed on the external surface and retuned a water repellent surface. However, the performance of the protective coat reduces overtime

[27] A master research conducted by Thomas Magnaval at ENSA Paris Malaquais, under supervision of Professor Robert Leroy in 2018.(https://seminairemateriaux.wordpress.com/2018/01/06/le-sable-et-le-sel-comme-nouveau-materiau-de-coffrage/)

[28] Water repellent impregnation for absorbent materials including natural and reconstituted stone substrates (produced by Sika company – product name: Sikagard 701W)

[29] https://www.bostik.com/fr/france/products/HYDROFUGE_liquide_Bostik

## 3.6 Aspects of the STP saline solution

The following aspects of the saline solution construct a better understanding of the material system and its workability. They are drawn from the observations and experimentations during the research and supported by the study of the salt properties introduced in the previous chapter.

- **Fast hardening:** the saline solution crystalizes relatively fast[30] at room temperature. The crystallization rate increases inversely with (i) the solution temperature (it hardens instantly below 20°C), (ii) the solution volume (droplets and shallow beds of salt increase instantly and a 10 cm cube in 5 minutes), and (iii) by introducing a nucleation agent (a crystal seed for instance). Moreover, it increases proportionally with the ambient temperature (it hardens faster at high temperatures). Finally, adding certain quantities of water to the solution reduces the crystallization rate.

- **Storable in liquid state:** the saline solution can be stored in its liquid state up to 2 years if stored in a vacuum container at room temperature. This allows to use the salt where no heating resources are available (offsite preparation – remote sites). Liquid state storage is possible due to the supercooling property of the salt (see chapter 2).

- **Semi-recyclable and semi-reusable**: melting the solidified salt (second cycle of heating) returns a viscous yellowish solution. Upon cooling, the solution crystallizes at lower rate and solidifies in form of white opaque flakes of salt (Figure 3.9 g). The degradation of the salt qualities is due to its semi-reversible characteristic, which forms lower hydrates that are less concentrated with weaker crystalline bonds. The solution cannot be sprayed due to its viscosity, but if mixed with sand it returns a solid material with less strength.

- **Crystal forms:** when solidified, the salt exhibit different crystal forms (Figure 3.9 a-d) based on the type of its lower hydrate, the temperature at cooling and the volume of the solution.

[30] The instant crystallization most often blocks the nozzles of the sprayers but hot water deblock it easily.

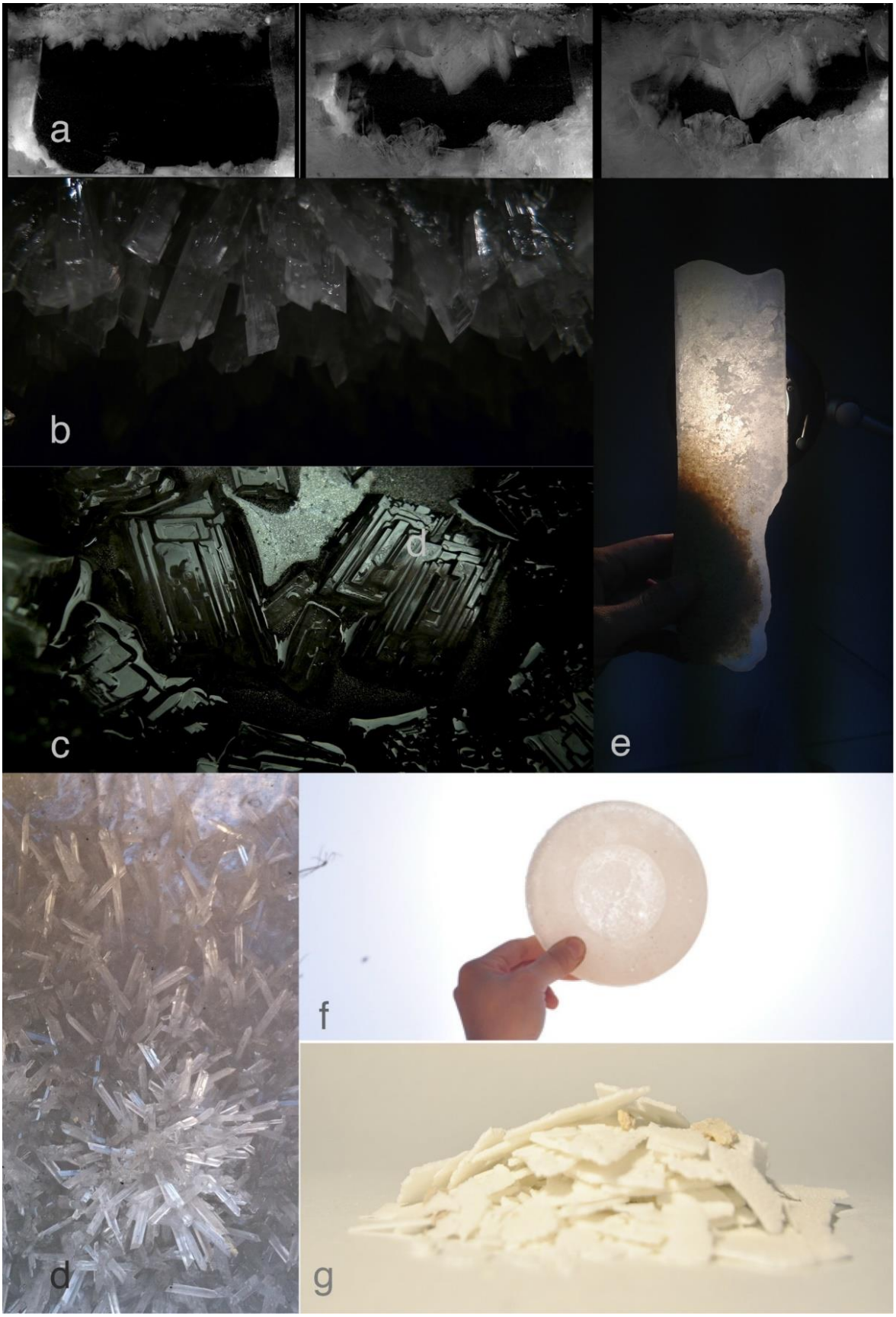


Figure 3.9 Forms of crystalized STP salt. Crystallization process (a) [73], crystals forms (b [73],c [73] and d), translucency (e, f), and recycled flakes (g).

# Chapter 4

Material characterization campaign

# 4 Material characterization campaign

This chapter identifies the mechanical properties of Hyposand through an experimental campaign. The objective is to understand how the mechanical properties of Hyposand are affected by the material microstructure, properties, and the mixing method. Furthermore, information on the effects of exposure to humidity and the thermal conductivity of the material are studied. Finally, an initial comparison of Hyposand with other classes of materials is given. The understanding of the mechanical properties of Hyposand help in defining the optimum materials, methods, and conditions of making to improve the material workability and strength. Moreover, the results give an insight on the possible applications of the material and its condition of use.

## 4.1 Structure of the experimental work

The material tests presented in this chapter are listed below and summarized in Table 4.2.

1. **Visual assessment** to distinguish the four types of sand being used in the tests
2. **Sieve analysis** to assess the particle size distribution of the four types of sand
3. **Grain size statistics** to numerically analyze the results of the sieve test
4. **X-ray tomography** to determine the sand grain shape and the mixture porosity
5. **compression tests** to assess how the compressive strength is affected by:
    1) types of sand
    2) grain size distribution
    3) grain shape
    4) mixture porosity
    5) proportion of sand and salt
    6) melting temperature of salt
    7) temperature of salt at mixing
    8) setting time
    9) addition of gravel
    10) standard deviation

Based on the results of the compression tests, the best mixture in strength is subjected to:

6. **Flexural test** to determine the effect of humidity on the strength of the mixture.
7. **Thermal conductivity** of the material is thought.

| | Test | Variable |
|---|---|---|
| 1 | **Visual assesment** | Type of sand |
| 2 | **Seive analysis** | |
| 3 | **Grain size statistics** | |
| 4 | **Tomography analysis** | |
| 5 | **Compression test** | Type of sand |
| | | Proportion of sand and salt |
| | | Melting temperature of salt |
| | | Temperature of salt at mixing |
| | | Setting time |
| | | Addition of gravel |
| 6 | **Flexural test** | Humidity |
| 7 | **Thermal conductivity test** | Temperature |

Table 4.1 List of tests presented in this chapter and their variables

In each test, the materials and methods are first introduced followed by a discussion of the results. Due to the novelty of the material no standard tests methods are available. To overcome this problem, the testing procedure is referring to ASTM[31] standards, when applicable, as will be detailed in each subsection. Parts of this chapter are published in a journal article [178] co-authored by the author of this thesis. The parts cited from the article are typed in *italic* type charchteres.

## 4.2 Standard method of specimens preparation

The following describes the standard methods of specimen preparation used in this chapter, herinafter referred to as the Standard method. It descirbes the materias, procedure and conditions of preparation. The concerned test are: the tomography, compression, flexuaral and thermal tests. In ach test one or more variable are measured while other factors are constant following the data described in Table 4.2. However, in some tests the preparation methods are adapted to meet the test objective as will be detailed at the begining of each test description.

| **Standard materials and methods** | |
|---|---|
| Type of sand | yellow |
| Salt to sand proportion | 1/2 |
| Salt melting temperature | 100 °C |
| Salt mixing temperature | 80 °C |
| Granularity of sand | fine to medium |
| Proportion of gravel | 0% |
| Setting time | 3 days |

Table 4.3 Standard materials and conditions followed in the tests

1. The used materials are yellow quartz sand and sodium thiosulphate pentahydrate salt.
2. The materials are prepared according to the standard method of preparation described in § 3.1. Dry clean yellow sand is seived using seives numbers 30 and 16 to return fine to medium grains (0.125 to 0.6 mm). The salt is melted by heating to its boiling point (100°C).
3. The Hyposand mixture is prepared following the solidification by mixing technique detailed in § 3.2. First the hot salne solution (80°C) is poured into a mixing container then sand is added gradually while steering until the mixture appears to be uniform.
4. The mixture is then casted into standard test moulds with a lubricated inlay. The casting process is performed in layers, and each layer is tamped to extract the air from the mould. The moulds are afterwards placed in a dry place in the ambient temperature. One day after casting, the specimens are demolded and stored in the laboratory until the test date. On the test day, the samples are weighted and then tests are applied.

[31] (ASTM) American Society for Testing and Materials, an international organization that develops standards of materials tests.

## 4.3 Specifications of sand types

The Hyposand characterization campaign is using two materials, sand, and sodium thiosulfate pentahydrate salt. The same type of salt is used along the tests and its characteristics are detailed in chapter 2. However, as shown in chapter two the strength of aggregate mixtures is affected by the sand grain type, size, and shape [28]. Accordingly, this chapter made the tests using four types of sand that have different characteristics to define their effect on the material strength.

*The four types of sand named yellow, white, brown, and red are collected from Alexandria in Egypt and used for all the experimental campaigns presented here, except the flexural test and thermal tests. The types of sand are chosen due to their availability on site and for their differences in characteristics (type, size, and shape). The identification of grain size and shape for each type of sand is based on two steps: the first step is a visual assessment presented in this section, the second is a standard sieve analysis (*§ 4.4*) and x-ray tomography test (*§ 4.6*). The visual assessment is based on macro photography (Canon MP-E 65mm 1-5× lens) as shown in* Table 4.4*, and microscopic observation (10, 40 and 100x lenses).*

*The yellow sand is a quartz desert fine sand with a yellowish patina* [179]*. Locally known as 'sahrawy' (desert in Arabic), it is used for plastering in construction due to its fineness. The white sand is oolitic carbonate fine sand washed from the degradation of oolitic coastal ridges* [180]*. This type is not used in construction as an aggregate, but soft stones of the same material are extracted from the limestone quarries in the region and widely used in local construction. The brown sand is shore sand composed of seashell fragments mixed with quartz grains. This sand is locally known as 'shatt' (shore in Arabic) and it is not used in construction.*

*The results of the visual assessment are shown in Table 4.4 where the assumption of the grain size referred to Wentworth scale* [181] *and the assessment of grain shape referred to Powers' chart for describing sphericity and roundness* [182,183]*. It is important to note that the verbal terms of evaluation in the chart of Power are remapped in this work to differentiate the three types of sand* [178]*.*

| Type | Yellow | White | Brown | Red |
|---|---|---|---|---|
| **Composition** | Silica | Calcium carbonate | Shells and silica | Silica |
| **Formation** | Weathering | Accumulation | Mixture | Weathering |
| **Source** | Quartz rocks | CaCo3 | Quartz/Caco3 | Quartz rocks |
| **Fineness** | Fine | Fine to coarse | Coarse | Coarse |
| **Roundness** | Sharp to rounded | Rounded | Sharp to rounded | Sharp to rounded |
| **Sphericity** | High sphericity | High sphericity | Low sphericity | High sphericity |
| **Macro photos** | 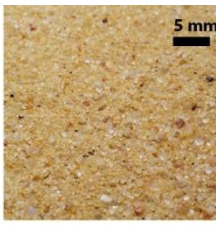 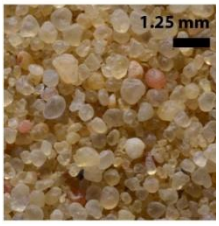  | 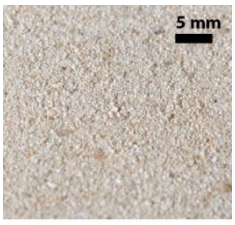  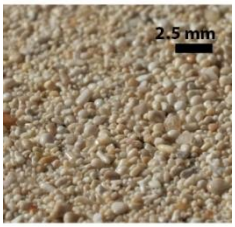  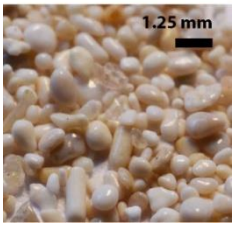  | 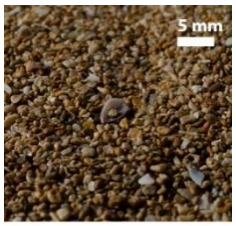 | |
| **Microscopic photos** | | 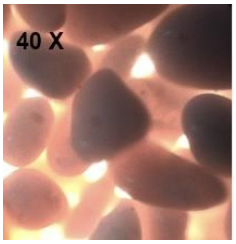  | 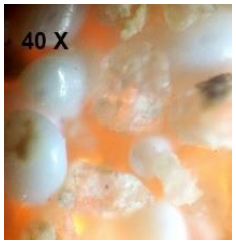  | |

Table 4.4: Results of the visual assessment of the four types of sand, and macro photos (with 3 zoom factors), and microscpic photo (40 x) for three types of sand.

## 4.4 Grain size analysis: sieve test

The sieve analysis (gradation test) determines the grain size distribution of sand according to the ASTM C136 standard test[32]. First, the materials and methods being used are introduced. Secondly, the results are presented in tabular form and plotted graphically in the cumulative curve[33] and the histogram graphs[34]. Finally, the Fineness modulus[35] of the samples is calculated.

### 4.4.1 Materials and methods

- **Material sampling:** the test is carried out on the four types of sand introduced in the previous section: yellow, white, red and brown sand
- **Apparatus:** the analysis test uses a digital balance of 0.1g accuracy to weight the samples, a set of six brass sieves of ASTM numbers 8,16,30,50,100,200, a solid pan, and a cover. The sieve specifications meet the requirements of ASTM E11 – 16[36].
- **Procedure of the test:** for each type of sand, a 1kg dry sample finer than 4.75 mm (pass through sieve No. 4) is prepared. The sieves are nested vertically in ascending order of aperture size. The largest size sieve (No. 8, aperture 2.36 mm) is at the top, and the smallest sieve (No. 200, aperture 0.075 mm) is at the bottom. The solid pan is set under sieve No.200.The sand is poured at the top sieve and covered with a lid. The set of sieves is shaken by hand in a circular horizontal motion for about five minutes.
- **Calculation method of the seive nalysis:** on the completion of the sieving operation, the total weight of sand (WT) and the weight of the fraction retained (R) on each sieve are recorded. To define the complete gradation of the sample, the following values are calculated:
    - Percentage of Weight Retained ($\%R_i$) = ($R_i$ /WT) x 100
    - Cumulative Weight Retained ($\sum R_i$) = ($R_i + R_{i-1}$)
    - Percentage of Cumulative Weight Retained ($\sum \%Ri$) = ($\sum$ Ri / WT) x 100
    - Cumulative Weight passed ($\sum Pi$) = (WT-$\sum Ri$)
    - Percentage of Cumulative Weight passed ($\sum \%$ Pi) = ($\sum Pi$/ WT) x 100
- **Calculation method of the Fineness modulus**: based on the sieve analysis results, the fineness modulus is defined mathematically as the sum of the cumulative percentages retained on the sieves divided by 100 ((FM) = $\sum$ %MR / 100). Lower FM indicates fine sand and higher FM indicates coarser sand

[32] ASTM C136 Standard Test Method for Sieve Analysis of Fine and Coarse Aggregates.

[33] The cumulative curve represents the grain size versus the cumulative percentage of the weight passed from the sieves.

[34] The Histogram is a bar graph of the percentage of remained grains on each sieve.

[35] The Fineness modulus is an empirical index of fineness of an aggregate.

[36] Standard Specification for Woven Wire Test Sieve Cloth and Test Sieves.

### 4.4.2 Results and discussion

The results of the seive analysis are noted in Table 4.5 and plotted in the cumulative curve (Figure 4.1) and the histogram graph (Figure 4.2).

| | | YELLOW | | | | WHITE | | | |
|---|---|---|---|---|---|---|---|---|---|
| | | Retained | | | Passed | Retained | | | Passed |
| Seive | | ($M_R$) | ($\sum M_R$) | ($\sum\%M_R$) | ($\%M_P$) | ($M_R$) | ($\sum M_R$) | ($\sum\%M_R$) | ($\%M_P$) |
| No | Apparture size (mm) | Mass retained (g) | Cumulative retained (g) | Cumulative % retained | % of mass passed | Mass retained (g) | Cumulative retained (g) | Cumulative % retained | % of mass passed |
| Pan | Solid | 35.0 | 1000.1 | 100.0 | 0.0 | 5.0 | 1010.0 | 100.0 | 0.0 |
| 200 | 0.075 | 95.0 | 965.1 | 96.5 | 3.5 | 5.0 | 1005.0 | 99.5 | 0.5 |
| 100 | 0.15 | 325.0 | 870.1 | 87.0 | 13.0 | 355.0 | 1000.0 | 99.0 | 1.0 |
| 50 | 0.3 | 230.0 | 545.1 | 54.5 | 45.5 | 530.0 | 645.0 | 63.9 | 36.1 |
| 30 | 0.6 | 315.0 | 315.1 | 31.5 | 68.5 | 105.0 | 115.0 | 11.4 | 88.6 |
| 16 | 1.18 | 0.1 | 0.1 | 0.0 | 100.0 | 5.0 | 10.0 | 1.0 | 99.0 |
| 8 | 2.36 | 0.0 | 0.0 | 0.0 | 100.0 | 5.0 | 5.0 | 0.5 | 99.5 |
| | Total | 1000.1 | | | | 1010.0 | | 275.2 | |

| | | RED | | | | Brown | | | |
|---|---|---|---|---|---|---|---|---|---|
| | | Retained | | | Passed | Retained | | | Passed |
| Seive | | ($M_R$) | ($\sum M_R$) | ($\sum\%M_R$) | ($\%M_P$) | ($M_R$) | ($\sum M_R$) | ($\sum\%M_R$) | ($\%M_P$) |
| No | Apparture size (mm) | Mass retained (g) | Cumulative retained (g) | Cumulative % retained | % of mass passed | Mass retained (g) | Cumulative retained (g) | Cumulative % retained | % of mass passed |
| Pan | Solid | 5 | 1030.0 | 100.0 | 0.0 | 1 | 1002.0 | 100.0 | 0.0 |
| 200 | 0.075 | 15 | 1025.0 | 99.5 | 0.5 | 1 | 1001.0 | 99.9 | 0.1 |
| 100 | 0.15 | 155 | 1010.0 | 98.1 | 1.9 | 15 | 1000.0 | 99.8 | 0.2 |
| 50 | 0.3 | 265 | 855.0 | 83.0 | 17.0 | 70 | 985.0 | 98.3 | 1.7 |
| 30 | 0.6 | 320 | 590.0 | 57.3 | 42.7 | 660 | 915.0 | 91.3 | 8.7 |
| 16 | 1.18 | 170 | 270.0 | 26.2 | 73.8 | 250 | 255.0 | 25.4 | 74.6 |
| 8 | 2.36 | 100 | 100.0 | 9.7 | 90.3 | 5 | 5.0 | 0.5 | 99.5 |
| | Total | 1030 | | 373.8 | | 1002 | | 415.3 | |

Table 4.5 Measurement and results of the sieve analysis test

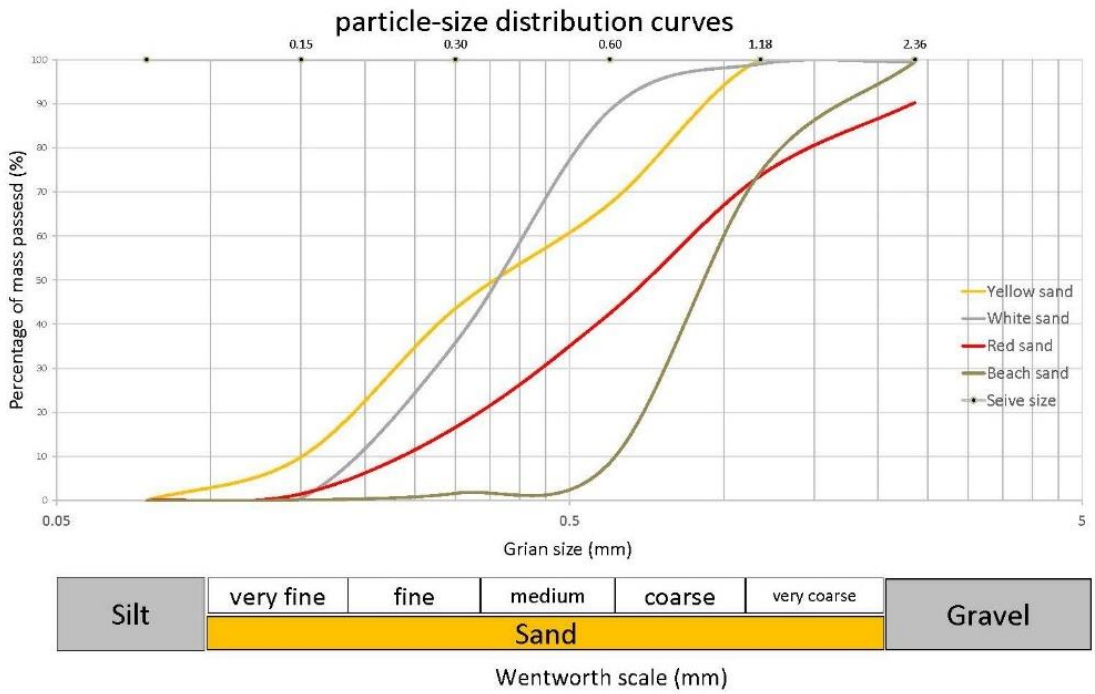


Figure 4.1 he cumulative curve of grain size distribution.

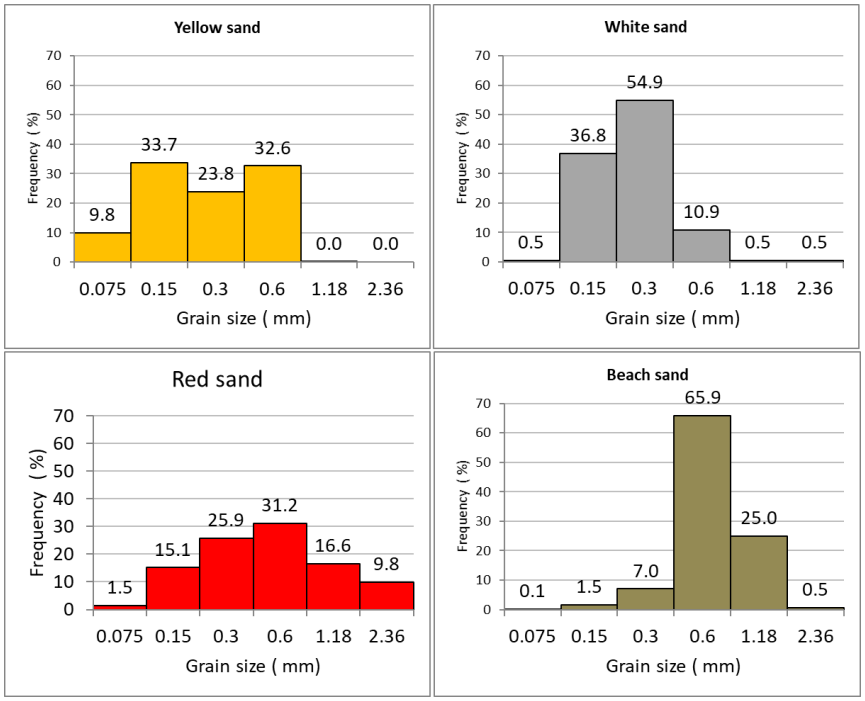


Figure 4.2 The Histogram graph shows the percentage of remained grains on each sieve in columns

In the cumulative graph (Figure 4.1) the sieves sizes are plotted at the top in mm and at the bottom is the Wentworth scale of grain size classification (silt, sand and gravel). The grain size is plotted in mm on the X-axis (semi-log scale) versus the cumulative percentage of the weight passed on the Y axis (arithmetic scale).

Through visual analysis of the gradation curves in Figure 4.1 and the histogram in Figure 4.2 the following gradation characteristics can be derived:

- **The positions of the curves on the graph** indicate the fineness or coarseness of the sample. Left handed curves indicate fine sand while right handed curves point to coarse sand. As seen in the cumulative graph, the yellow and white curves are to the left means that they are finer than the red (medium) and much finer than the brown sample (coarse). This is also seen in the histogram as the columns of the yellow and white samples are mostly to the left (fine) the brown is to the right (coarse) while the columns of the red are represented on all the scales (medium).
- **The gradual and steepness** of the curves indicate how well or poorly-graded the samples are. More the curve is gradual more it is well graded and vice versa for the steep curves. The red curve is the most gradual one (well graded) in comparison to the brown and white curves that are the steepest curves (poorly-graded). In this view, the yellow is considered as a moderate graded sample. Also, the flat parts in the white and yellow curves indicate the missing of some grain sizes. This analysis is also confirmed through the reading of histogram where the columns of the red samples are well represented all along

the grain size scale with little differences in heights (well-graded). The Brown and white are missing some columns on the grain size scale and represented on a narrow scale with big differences in heights (poorly-graded). Finally, the red columns have a bit larger representation of the grain size than the Brown and the white but the differences in heights is less important (moderate-graded)

- **The location of the start and the end** of the curve in respect to Wentworth scale of the grain size indicates the presence or lack of silt or gravel. A slight presence of gravel is found in the brown and red samples.

The Fineness modulus (FM) indices of the sand samples are represented on the linear scale in Figure 4.3. The intervals from 1 to 6 (below the line) are the order of the sieves accompanied with their corresponding apparatus in mm (above the line). The FM of each type of sand is marked below the red line. On the scale the Yellow sand shows an FM index of 2.70 means that its average value is in between the 2nd sieve and 3rd sieve and its grain's average size is in between 0.15mm to 0.3mm. Upon the FM values, the yellow is considered as the finer type of sand (2.7), and it is slightly finer than the white (2.75) and much finer than the red sand (3.74) while the brown is almost two times coarser than the Yellow one.

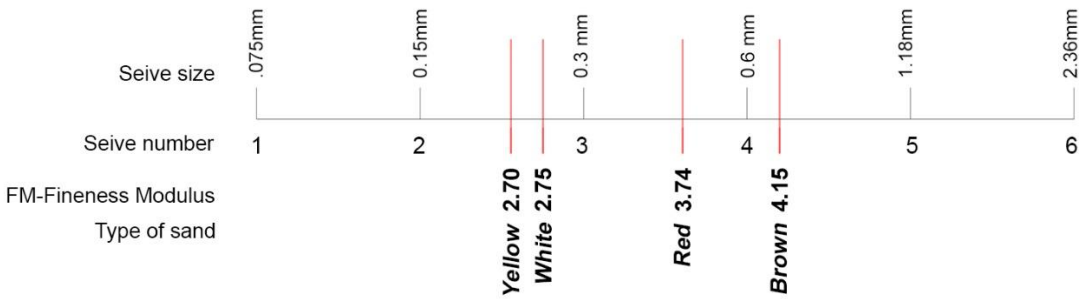


Figure 4.3 The scale of the Fineness Modulus

The sieve analysis test identifies the grain size distribution of the four samples of sand. The visual analysis of the gradation curves and the histogram define the fineness of the samples (fine, medium, coarse), their gradation (well, moderate or poorly-graded) and the presence of silt or gravel. While the fineness modulus defined the finnenes index of of each type of sand. These results of the seive analysis are summarised in Table 4.6.

| Type of sand | Fineness | Gradation | Silt or Gravel | Finenes modulus |
|---|---|---|---|---|
| **Yellow** | Fine | Moderate-sorted | No | 2.70 |
| **White** | Fine | Poorly-sorted | No | 2.75 |
| **Red** | Medium | Well-sorted | Few gravel | 3.74 |
| **Brown** | Coarse | Poorly-sorted | Few gravel | 4.15 |

Table 4.6: The verbal description of the sieve analysis results

## 4.5 Grain size analysis: statistical methods

The previous section assesed the grain size distribution qualitatively through the visual analysis of the accumulative curves. However, a quantitative method of analysis is essential to better understand the grain size distribution and to compare its values to the compression strength. Based on the results of the seive analysis, this section analyses and measure the folowing parameters of grain size distribution: mean, median, mode, sorting, skewness and kurtosis. Four statistical methods of measurment are used. First the parameters and methods are resented in § 4.5.1 followed by the results in § 4.5.2.

### 4.5.1 Parameters and methods

#### 4.5.1.1 Parameters of grain size distribution

The following six parameters of the grain size distribution are measured in this section:

1. **Median** is the grain size where half of the grains by weight are finer, and half are coarser.
2. **Mode** is the most frequent grain size in the sample.
3. **Mean** is the average grain size.
4. **Sorting** measures the grain-size variation of a sample. It evaluate how well sorted (nonuniform, poorly graded) or poorly sorted (uniform, well graded) the sample of sand is.
5. **Frequency curves** illustrates the percentage of distribution of grain sizes on a phi scale
6. **Skewness** measure the symmetry of the frequency curve around the mean value. Figure 4.4 shows the three skewennes descriptions of curves (i) symmetrical, (ii) negatively assymetrical (coarser), and (iii) positively symemtrical (finer).
7. **Kurtosis** measure the flatness of of the frequency curve. Figure 4.4 shows the three types of curves: (i) the flat curve (platykurtic) is better sorted in the tails than in the central portion, (ii) the medium curve (Misokurtic) is where the sorting in the tails equal to the sorting in the central portion, and (iii) the peaked curve (leptokurtic) is the excessively peaked curve that is better sorted in the central part than in the tails.

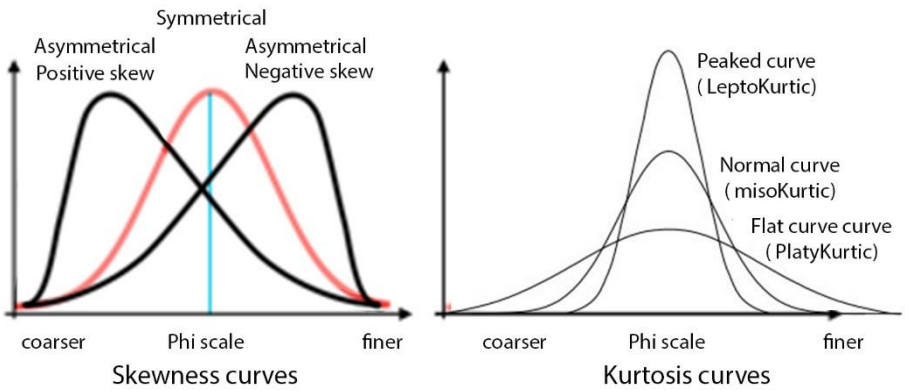


Figure 4.4 Skewness and Kurtosis descriptions of frequency curves (after [184])

#### 4.5.1.2 Calculation methods of grain size distribution

Based on the results of the sieve analysis, this section presents four methods[37] to measure the grain size parameters: **(i) Wentworth scale** defines the percentage of gravel, sand, and clay in each sample, **(ii) USCS system** (Unified Soil Classification System) defines the sorting of the samples, **(iii) Trask method** defines the size statistics, sorting and skewness, and **(iv) Folk and Ward method** defines the mean, sorting, skewness, and Kurtosis. Firstly, the description of each method is introduced, followed by its formulas of caculation and its evaluation criteria. Finally the results of the analysis are presented in Table 4.10. and discussed in § 4.5.2.

1. **Wentworth scale** classifies the grains finneness and types according to their size in mm. The cumulative curve in Figure 4.1 shows the Wentworth scale at the bottom of the cumulative curve to define the grade of each sample verbally. However, in this subsection, the percentage of each grade is calculated through the *Gradistat* Excel package [185].
2. **The USCS[38] system** (in mm) is a standard method according to the ASTM (D 2487-06)[39]. It defines the sorting of a soil sample by calculating the coefficient of uniformity (Cu) and the coefficient of curvature (Cu) in mm [186].
   - **(Cu) The Coefficient of uniformity** is a crude shape parameter defined as Cu= D60/D10. If Cu is equal to 1, it indicates a well-sorted soil (theoretical uniform soil where all grains have the same size). A well-sorted sample has a Cu value close to 1 while poorly sorted sand has Cu values far of 1.
   - **(Cc) The coefficient of curvature** is a shape parameter that complements Cu, and it is defined as Cc= $(D30)^2$/ (D10xD60).

For sand to be classified as poorly sorted the following criteria must be met: Cu ≥ 6 and 1 < Cc < 3, If not, the sand is classified well sorted (uniform). The formulas and evaluation criteria[40] of the USCS method are shown in Table 4.7.

| **Method: USCS** | **USCS** | |
|---|---|---|
| **Parameter** | **Cu** | **Cc** |
| **Formula** | D60/D10 | $(D30)^2$/ (D10xD60) |
| **Evaluation** | 1 < Cc < 3 (poorly sorted) | Cu ≥ 6 (poorly sorted) |
| | smaller values >> well sorted<br>larger values >> poor sorted | Smaller values >> Poorly sorted<br>Larger values >> Well sorted |

Table 4.7: Formulas and evaluation of the USCS method (after [186])

[37] The concepts of the methods were originally defined by Wentworth (1922 ), Trask (1930) and by Folk and Ward (1957).

[38] Unified Soil Classification System

[39] Standard Practice for Classification of Soils for Engineering Purposes (Unified Soil Classification System)

[40] ASTM D2487-06, Standard Practice for Classification of Soils for Engineering Purposes (Unified Soil Classification System), ASTM International, West Conshohocken, PA, 2006, www.astm.org

3. **The Trask method** (in mm) defines the measurement of central tendency (mode, median and mean) [187] as well as the sample sorting and skewness based on the sieve analysis results and the D sizes[41] in mm. To evaluate the central tendency, it is considered that lower values indicate fine sand while higher values point to coarse sand. The formulas and evaluation of the method are shown in Table 4.8.
   - **(MDt) The median** It is considered as the $D_{50}$ on the grain size distribution curve. $MDt=D_{50}$
   - **(MOt) The mode** is the largest column of the histogram and also as the sieve number that retains the largest weight of sand.
   - **(MNt) Mean** is the average grain size calculated as the average of the 25$^{th}$ and 75$^{th}$ percentiles. $MNt=(D_{25}+D_{75})/ 2$.
   - **(SOt)Sorting coefficient.** The Trask's sorting coefficient provides a measure of the uniformity of the sample where it is equal to one if the sample is uniform (entirely composed of the same grain size). The wider the value of SOt is, the poorly sorted the sample is while if it is close to 1 it is considered as well sorted[188]. It is defined as $SOt= (D75/D25)^{1/2}$
   - **(SKt) Skewness** is indicated by the difference of the Mean from the Median, which if close to 0 it is near symmetrical and more it departs from the zero it is more asymmetrical. Skewness is defined as: Skt= (D25xD75)/(D50).

| Parameter | median | mode | mean | Sorting | Skewness |
|---|---|---|---|---|---|
| **Formula** | $D_{50}$ | | $(D_{25}+D_{75}) / 2$ | $(D75/D25)^{1/2}$ | (D25xD75)/(D50). |
| **Evaluation** | a low value indicates fine sand higher value indicates coarse sand | | | 1.0 – 2.5 well sorted<br>2.5 - 4.5 normally sorted<br>> 4.5 poorly sorted<br>If close to 1 is well sorted<br>If far from 1is poorly sorted | If close to 0 is symmetrical and far from 0 is asymmetrical |

Table 4.8: Formulas and evaluation of Trask method (after [187])

4. **Folk and Ward method** (1957) is more accurate and satisfactory than the Trask method as it includes a wider range of the curve in the calculations [188]. It is a logarithmic graphical method used in sedimentary petrology that defines the Mean, Sorting, Skewness and Kurtosis in phi scale[42]. The parameters are calculated using the

[41] The 'D-size' is a measurement unit used in the USCS, Trask and Folk methods. It corresponds to an equivalent percent passing on the grain size distribution curve. It could be determined by visually reading the gradation curves. For instance, D10 is the grain size that corresponds to 10% of the sample passing by weight. The D-size is expressed in mm or Phi depending on the method of calculation.

[42] The readings of the D values from the cumulative curve in mm are converted to phi scale (Φ) value using the equation ; Θ = _Log2D.

Gradistat software, which is based on Folk and Ward (1957) graphical method of calculation. Table 4.9 shows the calculation formulas and the evaluation criteria while the results are shown in Table 4.10. The method defines the following parameters:

- **Mean (Mf):** unlike the Trask method that considers the mean as the average of the 25th and 75th percentiles, Folk and Ward method is more spread over the sample. It calculates the average of the both ends of the curves as well as the middle, which is more reliable in case of skewed (asymmetrical) samples. Larger the median value is smaller the grain size is and vice versa, this due to the phi scale used in calculations.
- **Sorting(SOf):** is a measure of how well or poor the sample is sorted. Smaller the value is (close to 0.35) poorly sorted the sample is and vice versa.
- **Skewness(SKf):** is a measure of the curves symmetry of the average (Mean). Symmetrical curves have a skewness of SKf =0.00: those with a large proportion of fine material are positively skewed (SKf>0): those with a large proportion of coarse material are negatively skewed (SKf <0).
- **kurtosis(Kf)**: is a measure of peakedness or flatness of curves and calculated using the same percentages of sorting. For normal curves Kf= 1.00 (Mesokurtic), Peak curves have Kf >1.00 (Leptokurtic), and flat curves have Kf <1.00 (Platkurtic).

| Parameter | Mean (Mf) | Sorting (Sof) | Skewness (Skf) | Kurtosis (Kf) |
|---|---|---|---|---|
| Formula | $\frac{\phi_{16}+\phi_{50}+\phi_{84}}{3}$ | $\frac{\phi_{84}-\phi_{16}}{4}+\frac{\phi_{95}-\phi_{5}}{6.6}$ | $\frac{\phi_{16}+\phi_{84}-2\phi_{50}}{2(\phi_{84}-\phi_{16})}+\frac{\phi_{5}+\phi_{95}-2\phi_{50}}{2(\phi_{95}-\phi_{5})}$ | $\frac{\phi_{95}-\phi_{5}}{2.44(\phi_{75}-\phi_{25})}$ |
| Evaluation | Smaller the value coarser is the sand and vice versa | smaller the value, well sorted<br>Larger the value is poorly sorted | closer to 0 is symmetrical, positive values are fine skewed,negative values are coarse skewed | closer to 1 is normal, smaller than 1 is flat, larger than 1 is peaked |

| | |
|---|---|
| Very well sorted | < 0.35 |
| Well sorted | 0.35 – 0.50 |
| Moderately well sorted | 0.50 – 0.70 |
| Moderately sorted | 0.70 – 1.00 |
| Poorly sorted | 1.00 – 2.00 |
| Very poorly sorted | 2.00 – 4.00 |
| Extremely poorly sorted | > 4.00 |

| | |
|---|---|
| Very fine skewed | $^{+}0.3$ to $^{+}1.0$ |
| Fine skewed | $^{+}0.1$ to $^{+}0.3$ |
| Symmetrical | $^{+}0.1$ to $^{-}0.1$ |
| Coarse skewed | $^{-}0.1$ to $^{-}0.3$ |
| Very coarse skewed | $^{-}0.3$ to $^{-}1.0$ |

| | |
|---|---|
| Very platykurtic | < 0.67 |
| Platykurtic | 0.67 – 0.90 |
| Mesokurtic | 0.90 – 1.11 |
| Leptokurtic | 1.11 – 1.50 |
| Very leptokurtic | 1.50 – 3.00 |
| Extremely leptokurtic | > 3.00 |

Table 4.9: Folk and Ward statistical measures and evaluation criteria (after [185])

### 4.5.2 Results and discussion

Table 4.10 shows the results of the grain size statistics of the four methods. The results of each method is accompagnied by the verbal description[43] of the evaluation at the bottom of the Table.

**Results of grain statistics analysis**

| Method | Parameters | Type of sand | | | |
|---|---|---|---|---|---|
| | | Yellow | White | Red | Brown |
| Wentworth classification scale | MUD | 0.00% | 0.00% | 0.00% | 0.00% |
| | V FINE SAND | 7.30% | 0.40% | 1.10% | 0.10% |
| | FINE SAND | 27.40% | 26.20% | 11.50% | 1.10% |
| | MEDIUM SAND | 26.40% | 48.20% | 23.00% | 5.50% |
| | COARSE SAND | 30.90% | 21.80% | 30.40% | 51.60% |
| | SAND | 100.00% | 99.40% | 86.30% | 93.50% |
| | GRAVEL | 0.00% | 0.60% | 13.70% | 6.50% |
| Indices (mm) | D10 | 0.14 | 0.19 | 0.23 | 0.61 |
| | D25 | 0.20 | 0.26 | 0.39 | 0.72 |
| | D30 | 0.23 | 0.28 | 0.44 | 0.78 |
| | D50 | 0.34 | 0.37 | 0.70 | 0.90 |
| | D60 | 0.47 | 0.41 | 0.88 | 1.00 |
| | D75 | 0.70 | 0.49 | 1.30 | 1.20 |
| USCS (mm) | Cu | 3.36 | 2.16 | 3.83 | 1.64 |
| | Cc | 0.80 | 1.01 | 0.96 | 1.00 |
| | | poorly sorted | moderatly well sorted | poorly sorted | well sorted |
| Trask (mm) | Median | 0.34 | 0.37 | 0.70 | 0.90 |
| | Mode | 0.15 | 0.3 | 0.6 | 0.6 |
| | Mean | 0.45 | 0.375 | 0.845 | 0.96 |
| | Fine / coarse | fine sand | fine sand | coarse Sand | coarse Sand |
| | Sorting | 1.87 | 1.37 | 1.83 | 1.29 |
| | | poorly sorted | moderatly well sorted | poorly sorted | well sorted |
| | Skewness | 0.41 | 0.34 | 0.72 | 0.96 |
| | | symmetric | symmetric | asymmetric | asymmetric |
| Folk and Ward (phi) | Mean | 1.420 | 1.530 | 0.471 | 0.440 |
| | | medium Sand | medium Sand | coarse Sand | coarse Sand |
| | Sorting | 1.082 | 0.744 | 1.135 | 0.661 |
| | | Poorly sorted | Moderatly well sorted | Poorly sorted | Well |
| | Skewness | 0.00 | 0.02 | 0.12 | -0.11 |
| | | symmetrical | symmetrical | fine Skewed | coarse Skewed |
| | Kurtosis | 0.765 | 0.966 | 0.743 | 1.259 |
| | | Platykurtic | Mesokurtic | Platykurtic | Leptokurtic |

Table 4.10: Results of grain size statistics

The results of grain size statistics are plotted in Figure 4.5 to Figure 4.9 to visualise and compare the characteristics of each sample of sand.

43

#### 4.5.2.1 Percentage of grain size on Wentworth scale

Figure 4.5 shows the percentage of presence of grains (y axis) in each class of wentworth scale of grain size (x axis). From the graph it can be noted that the yellow and red sand are well distributed on a wide range of sizes but the red is coarser than the yellow as it shift to the right. It is noted that the white is well sorted with finer sand while the brown is more sorted on the coarse size to the right of the graph with the presence of gravel for both the brown and red.

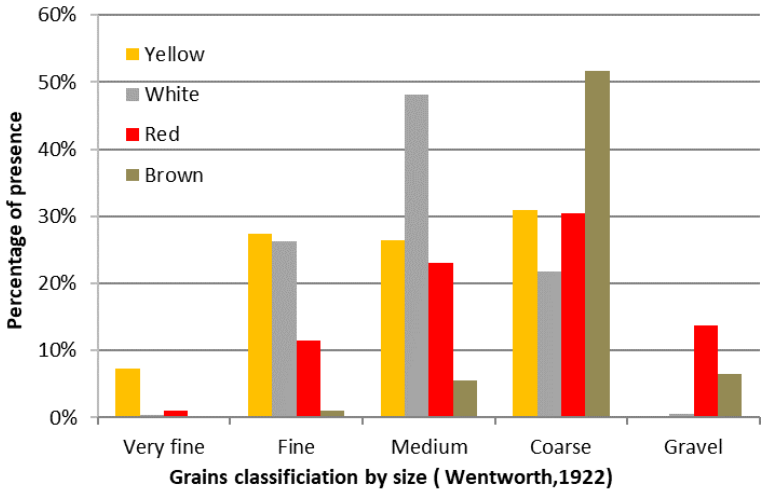


Figure 4.5 Percentage of grain size on Wentworth scale

#### 4.5.2.2 Frequency curves in phi scale (skewness and kurtosis analysis)

Figure 4.6 shows the frequency curves where the brown curve is the sharpest and negatively skewed (coarse) means that it has a narrow grain size that is well sorted in the middle (coarse) more than in the tails. While the white is 'normal' and symmetrical showing that its mass is moderately well sorted over its different sizes. Both the red and yellow are flat, wide with a right tendency means that they are well graded with medium and fine sizes (poorly sorted).

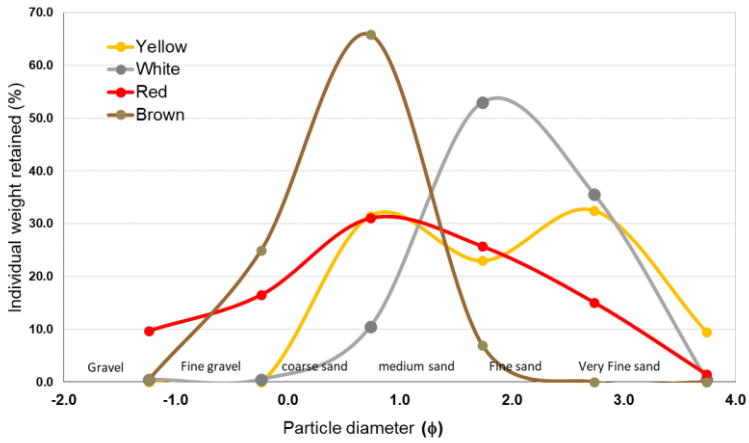


Figure 4.6 Frequency curves on Wentworth scale (Φ)

#### 4.5.2.3 Skewness vs. kurtosis

Figure 4.7 shows that the white sand is at the center, which indicates that it is symmetrical (Skewness close to 0) and evenly sorted (Kurtosis close to 1) sample. While the brown and red are on two opposite sides, as the red is a fine skewed flat curve, while the brown curve is sharp and coarse skewed.

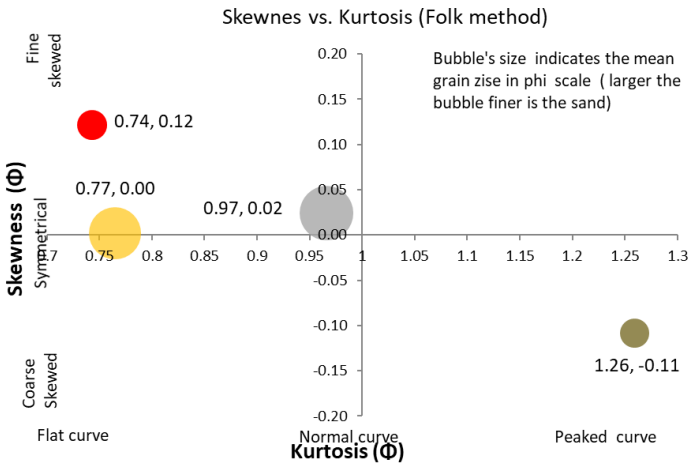


Figure 4.7 Skewness vs kurtosis (Folk method)

#### 4.5.2.4 Sorting vs skewness and kurtosis

The difference between the red and brown samples is confirmed in Figure 4.8 that shows that the red is poorly sorted than the brown. In the same graph, the white sand is again occupying the middle of the graph as it is better sorted than the red and yellow but less sorted than the brown. In Figure 4.9, the white sample is clearly showing its median among another sample as it is at the center showing a medium value of skewness that is slightly ‘ fine skewed’.

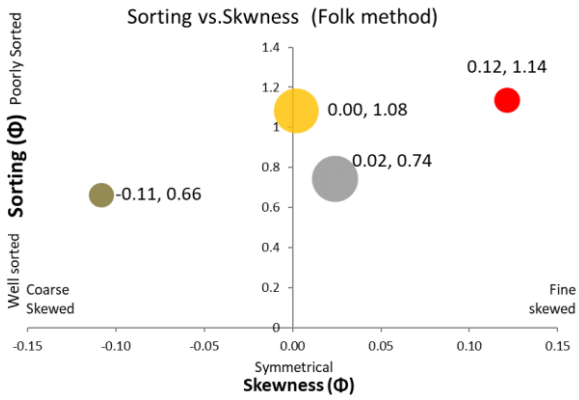


Figure 4.8 Sorting vs skewness

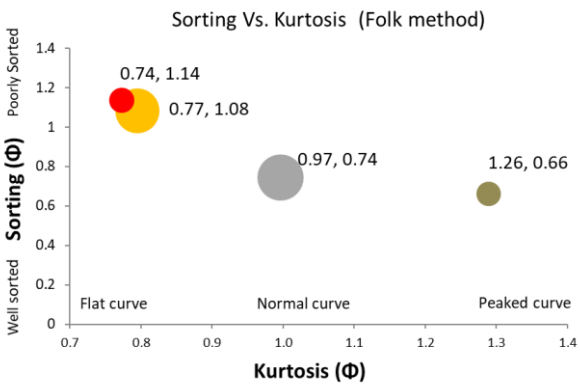


Figure 4.9 sorting vs kurtosis

The sorting vs skewness and kurtosis study shows that the yellow and white are both fine sand, but the yellow is less sorted (better grade) than the yellow as its grains extends over a wider range of sizes. This could be seen in the frequency curves in Figure 4.6 where the white curve is narrower and higher than the yellow. Also, the skewness of the white curve is positive asymmetrical while the yellow is symmetrical. This means that the white has a finer mass of

grains than the yellow. This is also confirmed by the results of Wentworth scale in Figure 4.5 that shows that the white has finer grains in percentage than the yellow. Following up the sorting analysis with the coarse samples: red and brown: the difference between both curves shows that the brown is better sorted than the red. This indicates the red is better graded than the brown as its grains extends on a wider range of sizes. However, the brown is coarser as the skewness of its curve is negative (skew to the left) while the red is skewed positively to the right (fine skewed).

#### 4.5.2.5 Fineness: Median, Mode and Mean results in Folk and ward method

The results of the median, mode and mean in Table 4.10 show that the white sand is the finer type of sand (Mean=1.53 ϕ) followed by the yellow (Mean=1.42 ϕ). While the red and brown are coarse sand with mean values of 0.47 and 0.44 ϕ respectively[44]. Table 4.11 summarizes the verbal descriptions of the four types of sand as obtained from the grain size statistics analysis.

| Parameters | Type of sand | | | |
|---|---|---|---|---|
| | Yellow | White | Red | Brown |
| Fineness | fine sand | fine sand | medium sand | coarse sand |
| Sorting | poorly sorted | moderatly well sorted | poorly sorted | well sorted |
| Skewness | symmetrical | symmetrical | fine Skewed | coarse Skewed |
| Kurtosis | Flat | Normal | Flat | Sharp |

Table 4.11 The verbal description of grain size distribution

[44] due to the use of phi scale the larger the value the finer is the sand

## 4.6 Grains shape analysis: tomography scan

The X-ray computed tomography (CT) scan aims at identifying the porosity and the grain shape (roundness and circularity) of the solidified sand samples. The results are correlated to their corresponding compression strength in § 4.7.3.2 to evaluate the effect of the grain shape and porosity on the material strength.

### 4.6.1 Materials and methods

**Materials and preparation of specimens**: the materials and the methods of samples preparation in this test follows the standard method introduced in § 4.7.1. However, the red sand is not studied here but the yellow, white, and brown. For each type of sand, three cylindrical specimens (10 mm width and 20 mm height) are prepared making nine specimens in total.

**Scanning aperture**: for scanning the specimens, the test uses a built-to-specification x-ray Tomograph scanner (Figure 4.10) at laboratory 3SR (Grenoble).

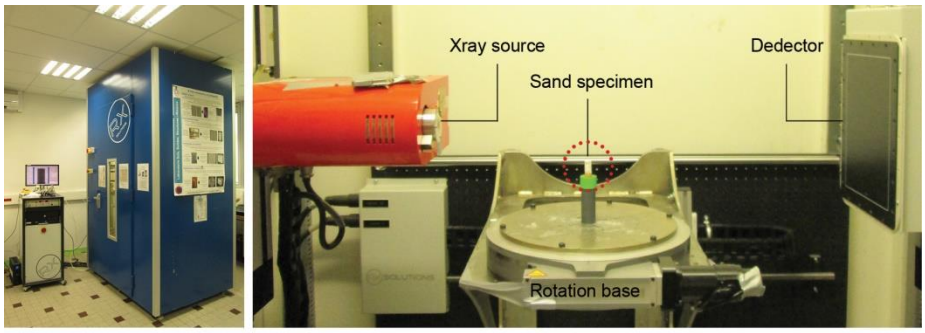


A- Scanner isolated cabin B- x-ray scanner appartures

Figure 4.10 The x-ray tomograph scanner at laboratory 3SR in Grenoble. Scanner chamber (left) inner view of the scanner parts and the specimen (right)

#### 4.6.1.1 Scanning method

The X-ray tomography scanner is placed in an isolated chamber as shown in Figure 4.10 and it is composed of three main parts, the X-ray source that emits the photons, the rotary stage for placing and rotating the sample and the detector that acquires the image. Each sample is placed on the stage and rotated 360 degrees while scanned to acquire the 3d image. The x-ray source emits the photons in the direction of the specimen where the sand grains and the salt as being solids reduce the x-ray transmission to the detector more than the void areas making them appear darker than the void in a grey scale range. To produce the 3D field of x-ray, the rotation stage rotates the sample from 0 to 360° at regularly spaced intervals. At each angular station, eight radiographies are acquired and averaged to produce 1500 projections in total taking up to 2 hours. For each level of the specimen, the scanner produces three projections (Y, XZ and YZ planes) as shown in Figure 4.11. After then, the scanner transfers the slices (images) to the ‘DigiCT’ software to reconstruct the slices into a 3D field of x-ray projections. This ‘DigiCT’ software exports the 3D images in the form of a ‘stack’ of 1500 slices for each specimen to analyse them with the ‘ImageJ’ software.

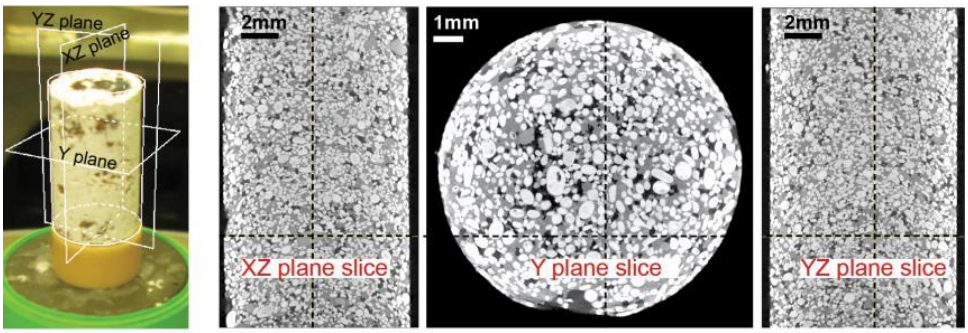


C- Sand specimen with slices planes

D- x-ray grayscale image of slice 1022 / sample 1 of white sand sand

Figure 4.11 sand specimen (left) and the x-ray images (left)

**Images analysis software**: The scanned images are analysed using 'ImageJ' software, which is a Java based open source software and programming platform based on Fiji project[45] and developed by [90]. This software is mainly used in Biological and medical sectors for microscopic image analysis but also used in geophysics and material science for particles analysis.

#### 4.6.1.2 Images analysis method

'ImageJ' software stacks the acquired 1500 images for each sample to construct a 3D field of the X-ray projections. The acquired images provide a large amount of data that can be analysed through a set of plugins to extract the required information. In this work, the analysis focuses on developing specific information of the sample properties including: the proportion of sand to salt to void, the number of grains and the grain shape (circularity and roundness). This information is used in the analysis of the compression results to understand the effect of the grain shape of each type of sand on the corresponding compression strength. The images are an attenuation of grey scale values (from 0 to 255) that represents different material's densities in the samples where white (value 255) stands for absolute voids parts and black (value 0) represents the entirely solid and dense parts. In this part of the test, the process of analysis focuses on tuning the grey values to distinguish between the sand, the salt and the voids to retrieve the data of each part for analysis. This process consists of four main parts: setup, binarisation, watershed and particle analysis, which are illustrated in Figure 4.12 and detailed below.

[45] http://fiji.sc/

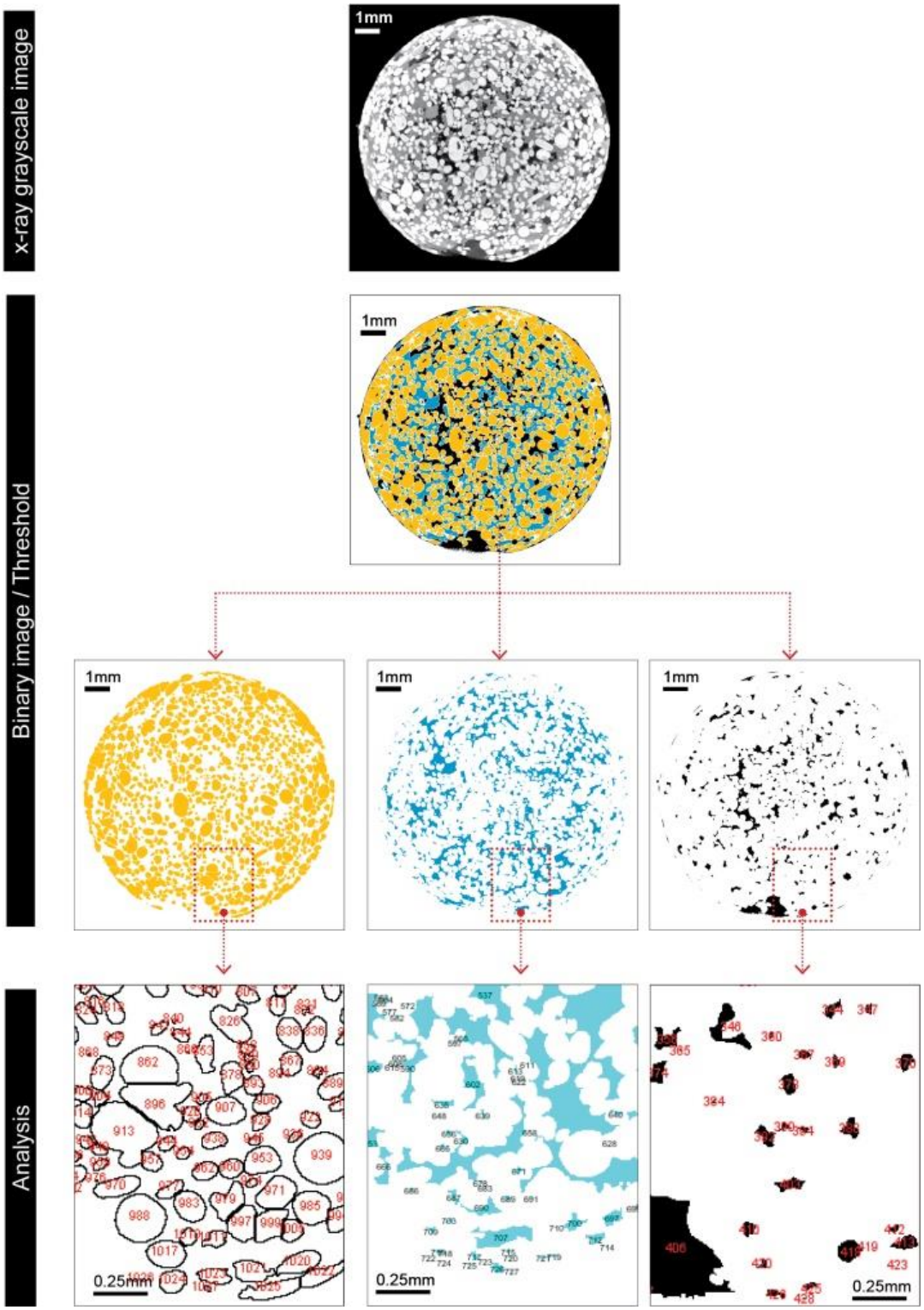


Figure 4.12 Analysis process of one slide of Hyposand

1. **Setup**: First the scale of the images is adjusted to meet the actual size of the samples. The scanner uses pixels for 2D and voxels for 3D measurements while the dimensions of the specimens are in mm. In this test, the width of the specimen is 10 mm, which is represented in the image by 800 pixels. Hence the image is scaled to 80pixel/mm to return the analysis results measurements in mm.

2. **Binarisation and threshold**: Binarisation is the method of turning the images into binary black and white images where all pixels of each component (sand or salt or void) contain one value, and all other pixels contain another value. This enables the software to precisely distinguish between the three components under study. The separation process called '**Threshold**' is essential to separate the greyscale range of each component. The threshold range respects the greyscale values between 0 (black) and 255(White). For instance, in the white sand specimen, the threshold range of sand is (150-255), the salt is (40-150), while the void is (1-40). From this process, an image for each component, sand salt and voids are extracted from each slice. The threshold values change slightly between the samples and considerably in between different types of sand due to the density of sand grains. Hence, a separate threshold values are set for each type of sand to get to the possible optimum separation of materials. **Edge problem**: the materials (sand, salt and voids) at the edges of the specimens are brighter than the similar material at the core of the specimen (Figure 4.13-A). This difference in brightness causes a problem in the threshold (B) that can not detect individual particles on edge. This is can be the cause of problem during the scan process, but it is solved by eliminating the particles that touch the edge.

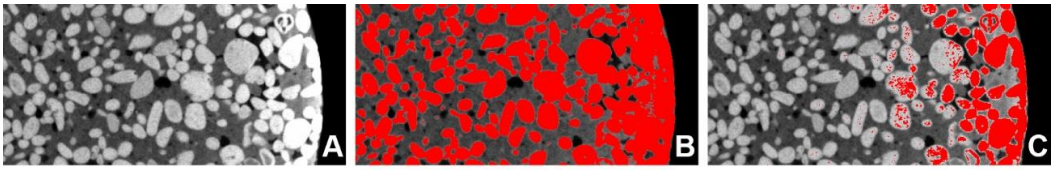


Figure 4.13: The brightness of the edges (a) cause problems of separation with high (b) and low thresholds

3. **Watershed**: Often in the solid sand samples, many grains are tangent, which looks like a connected black area in the binary image (Figure 4.14).

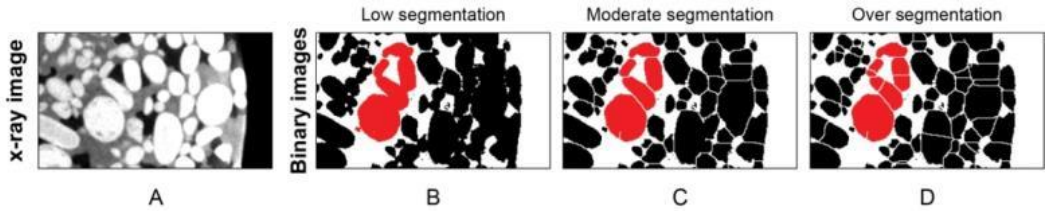


Figure 4.14 Problem of segmentation

To separate the grains at their edges a separation (segmentation) methods and algorithms are used. 'ImageJ' software affords the 'Watershed' plugin[46], which is a method to separate the binary image based on the greyscale of the original image. In this work, the segmentation method is used only for the sand grains, but the salt and voids do not need separation as they are a continuous field without segmentation. The quality of the watershed is crucial as it may lead to an over-segmentation of the input image, i.e. if the watershed value is high it can split a single grain into several particles and if it's too low it may combine a number of particles in one, which does not correspond to the physical reality of grains. In this test it is noted that the edges of the samples are poorly scanned and reconstructed with a very low greyscale in contrast with the core of the samples. Hence, the particles on edge are ignored to avoid the over segmentation of the grains. The methods of segmentation are studied in many publications that develop more sophisticated algorithms to avoid the problem of over segmentation. For more precise work, it is recommended to use an advanced commercial code like Visilog. This helps to respect the real grain's geometry to much more extent.

4. **Particle analysis process:** The particle counting method in the ImageJ software analyses automatically the black and white images to calculate the circularity and roundness of the sand grains as well as the area of sand, salt, and the pores in between. The particle counting method calculates the circularity and roundness based on Riley's formulas [1,2] as following:
    A. **Circularity** is a function of area and perimeter (circularity = 4π*area/perimeter^2)). The circularity index (0-1) defines how circular the grain shape is. 1 indicates a perfect circle and 0 indicates an increasingly elongated polygon.
    B. **Roundness** is a function of the area and the length of the major axis (roundness= 4*area/ (π*major axis^2)). The roundness index (0-1) describes the angularity or roundness of the grain edges. 1 indicates smooth edge and 0 indicates sharp edges
    C. **Porosity and proportion of sand and salt (%):** The area of voids, sand and salt, are measured in $mm^2$ and calculated as a percentage of the total area of the slice (circle of 1mm diameter).This is measured based on the grey value and the defined threshold for each material.

The indexes of circularity and roundness and their corresponding verbal terms (circular vs. elongated, rounded vs. angular or sharp) are based on Krumbein & Sloss index [183,189]. The verbal terms in Krumbein & Sloss index were remapped in this work to differentiate the three types of sand. It is important to note that in this work two methods of grain shape assessment

[46] http://imagej.net/Classic_Watershed

were used; the first was visual § 4 based on Powers' visual chart [182] while in this section the assessment was numerical based on the index of Krumbein & Sloss [189]. Also, in this section, the term 'circularity' was used and not 'sphericity' to indicate the shape of the grain as the software analyses 2D and not 3D images. This should not be confused with the term 'sphericity' used in § 4.3 that visually assessed the grain sphericity based on Powers' visual chart as mentioned above.

#### 4.6.1.3 Experimental work : the strucutre of the analysis process

Despite the considerable number of images available from the CT scan[47], only three slices from each specimen are analyzed due to the limitations[48] of the numerical tool. By analysisng 3 slices (top, middle and bottom) from each of the 9 specimens, a total of 27 slides is considered for analysis (Figure 4.15). The study returns close results for each type of sand, which allowed to distinguish the difference in the grain shape between the three types of sand. However, an automatic method of analysis is recommended in future work to return more accurate results.

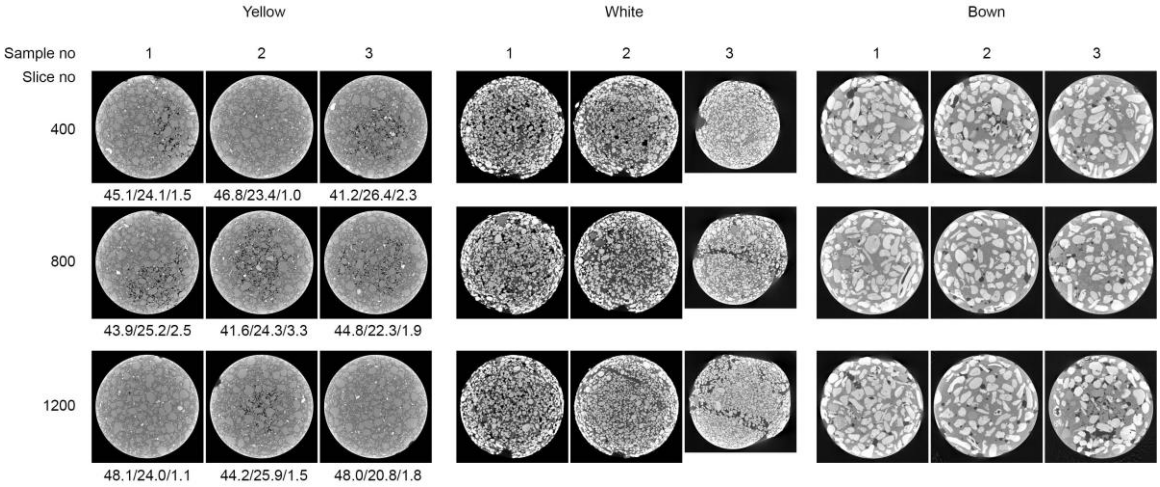


Figure 4.15 The 27 slides used in the Tomography analysis

Each type of sand is represented by its first letter Yellow (Y), White (W) and brown (B), these colours are also used to represents each type of sand in the graphs.The slices are tagged following this method [type of sand/specimen number/slice number] for instance, the slice no 400 in the first sample of yellow sand is tagged as [Y.1.400].

[47] Three samples of each of the three type of sand are scanned giving 1500 images for each sample which returns 13.500 slices in total.

[48] The limitations of manual threshold and segmentation processes as discussed in the analysis method.

### 4.6.2 Results and discussion

The results of the tomography analysis are discussed here in two groups: (i) particle shape (circularity and roundness) and (ii) proportions of sand, salt, and porosity. A comparative analyses is given at the end of this subsection to correlate the results of porosity with the grain size and shape. These results are then compared to the corresponding compression strength in § 4.7.3.2.

The results are reported in In Table 4.12 where the areas of sand, salt, and voids (porosity) are given in percentage, followed by the index of circularity and roundness. The averages of the results are summarized in Table 4.13.

| | Sample No. | Slice No. | Area (%) | | | Circularity | Roundness |
|---|---|---|---|---|---|---|---|
| | | | Sand | Salt | Void | | |
| Yellow Sand | 1 | Y.1.400 | 54.07 | 32.17 | 2.46 | 0.60 | 0.63 |
| | | Y.1.800 | 43.97 | 31.24 | 2.55 | 0.59 | 0.64 |
| | | Y.1.1200 | 48.16 | 30.04 | 2.36 | 0.59 | 0.56 |
| | 2 | Y.2.400 | 46.82 | 25.41 | 2.36 | 0.61 | 0.63 |
| | | Y.2.800 | 41.47 | 30.33 | 3.36 | 0.59 | 0.68 |
| | | Y.2.1200 | 44.27 | 31.95 | 1.57 | 0.60 | 0.67 |
| | 3 | Y.3.400 | 41.20 | 32.43 | 2.34 | 0.59 | 0.67 |
| | | Y.3.800 | 44.85 | 29.40 | 1.95 | 0.59 | 0.64 |
| | | Y.3.1200 | 48.09 | 28.82 | 3.25 | 0.62 | 0.69 |
| | Average | | 45.88 | 30.20 | 2.47 | 0.60 | 0.65 |

| | Sample No. | Slice No. | Area (%) | | | Circularity | Roundness |
|---|---|---|---|---|---|---|---|
| | | | Sand | Salt | Void | | |
| White sand | 1 | W.1.400 | 43.60 | 37.51 | 1.52 | 0.79 | 0.68 |
| | | W.1.800 | 43.40 | 37.82 | 1.35 | 0.78 | 0.73 |
| | | W.1.1200 | 42.30 | 37.15 | 1.12 | 0.78 | 0.76 |
| | 2 | W.2.400 | 43.84 | 38.52 | 1.05 | 0.78 | 0.64 |
| | | W.2.800 | 41.75 | 40.04 | 1.27 | 0.79 | 0.69 |
| | | W.2.1200 | 46.38 | 39.02 | 1.57 | 0.78 | 0.72 |
| | 3 | W.3.400 | 0.00 | 0.00 | 0.00 | 0.00 | 0.00 |
| | | W.3.800 | 0.00 | 0.00 | 0.00 | 0.00 | 0.00 |
| | | W.3.1200 | 0.00 | 0.00 | 0.00 | 0.00 | 0.00 |
| | Average | | 43.5 | 38.3 | 1.3 | 0.8 | 0.7 |

| | Sample No. | Slice No. | Area (%) | | | Circularity | Roundness |
|---|---|---|---|---|---|---|---|
| | | | Sand | Salt | Void | | |
| Brown Sand | 1 | B.1.400 | 43.10 | 37.98 | 2.84 | 0.61 | 0.52 |
| | | B.1.800 | 44.39 | 39.11 | 3.20 | 0.61 | 0.57 |
| | | B.1.1200 | 43.77 | 35.73 | 3.26 | 0.60 | 0.61 |
| | 2 | B.2.400 | 39.91 | 41.12 | 3.68 | 0.59 | 0.57 |
| | | B.2.800 | 39.68 | 46.11 | 2.80 | 0.60 | 0.63 |
| | | B.2.1200 | 38.24 | 46.05 | 3.70 | 0.59 | 0.67 |
| | 3 | B.3.400 | 35.36 | 46.60 | 3.70 | 0.61 | 0.55 |
| | | B.3.800 | 37.73 | 49.01 | 3.20 | 0.62 | 0.61 |
| | | B.3.1200 | 36.24 | 42.80 | 4.35 | 0.60 | 0.64 |
| | Average | | 39.8 | 42.7 | 3.4 | 0.60 | 0.60 |

Table 4.12 Results of the tomography analysis.

| Type of sand | Circularity Index (0-1) | Roundness Index (0-1) | Area (%) Porosity | Area (1:1) Sand : Salt |
|---|---|---|---|---|
| Yellow | 0.62 | 0.65 | 2.47 | 1 : 0.6 |
| White | 0.78 | 0.70 | 1.3 | 1 : 0.9 |
| Brown | 0.60 | 0.60 | 3.4 | 1 : 1.1 |

Table 4.13 Summary of the results of the tomography scan analysis

#### 4.6.2.1 Grain shape analysis (circularity and roundness of sand grains)

The results of roundness and circularity in Table 4.13 and Figure 4.17 show that the grains of white sand are the most rounded (0.7) and circular (0.78) followed by the yellow which was less circular (0.62) and less rounded (0.65) and finally the brown sand was the least circular and rounded having the value of 0.6 for both roundness and circularity.

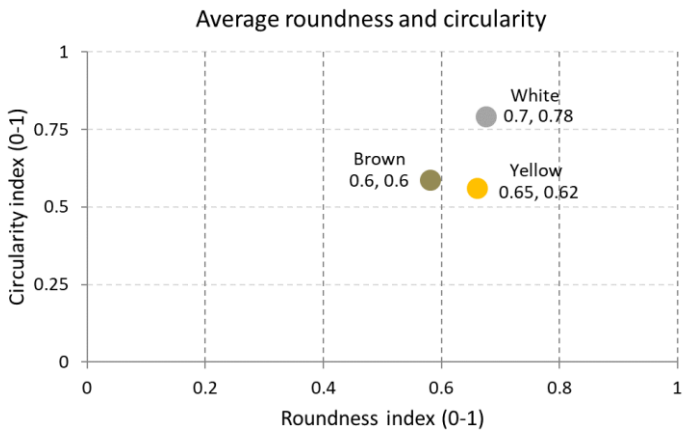


Figure 4.16 Average roundness and circularity

To better undestand the average of grain shape the distribution of grains shape of one slice from each type of sand is plotted on a scatter graph in Figure 4.17. The points represent the roundness and circularity index of the individual grains, while the circle shows the average shape index. The graph shows that the grains of white sand are massed at the top right of the graph showing very circular and well-rounded shapes, while the yellow sample has more grains that are diagonally scattered from sub angular to well rounded. Finally, the brown sand has the fewer amount of grains, which shapes are distributed linearly from angular to well rounded.

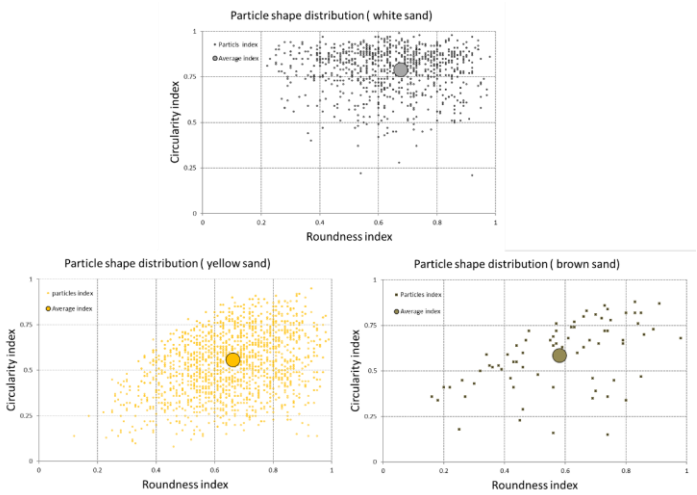


Figure 4.17 Average roundness and circularity (top left), Particle shape distribution for each type of sand Porosity analysis: proportions of sand, salt, and voids.

Figure 4.17 shows the analysis of one slide of each type of sand. At the top row are the original greyscale images while the bottom rows show the analysis and separation of the materials: the sand grains are illustrated in yellow, the salt in blue and the pores in black. The proportions of the materials and voids are plotted in Figure 4.19.

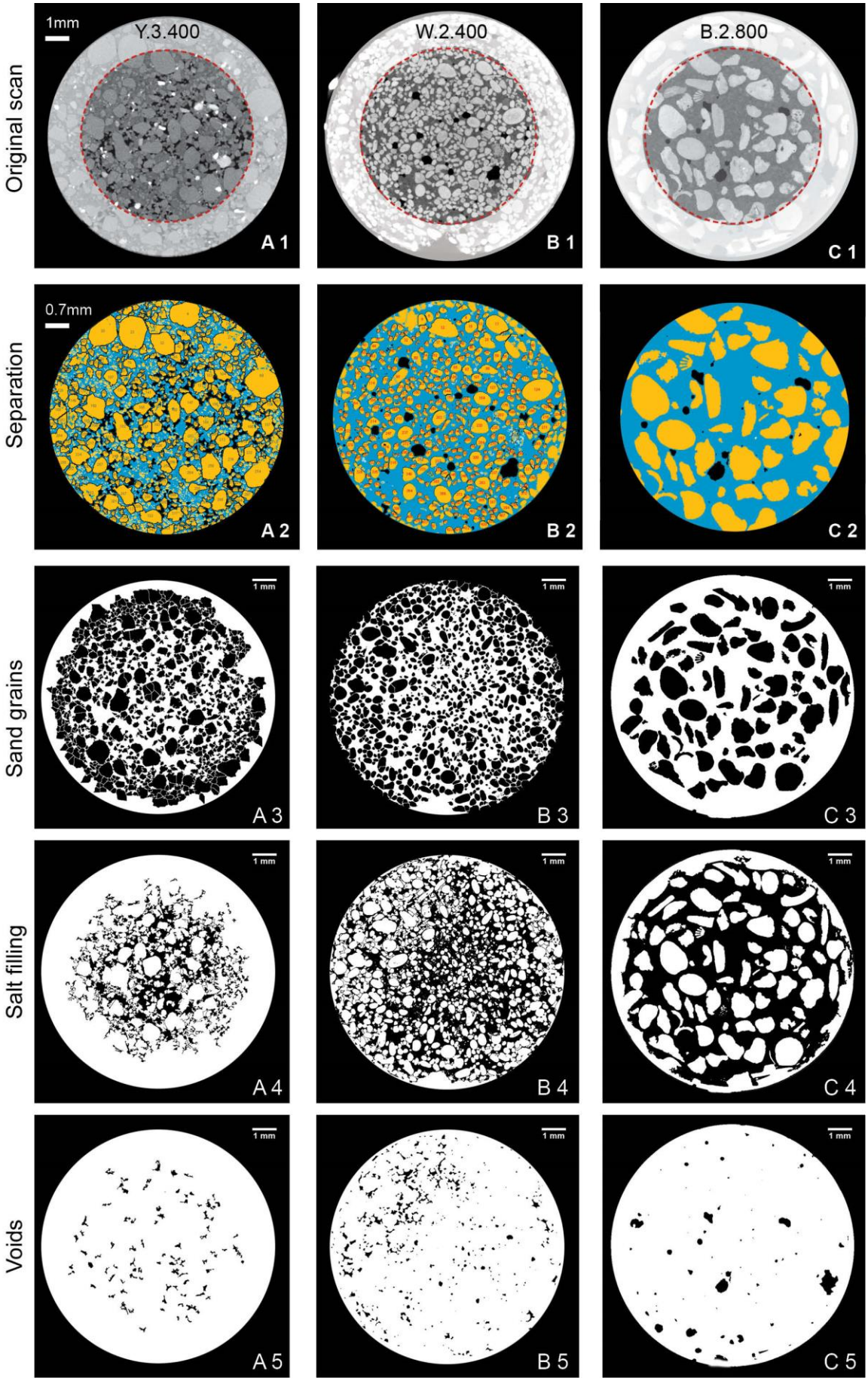


Figure 4.18 The analysis of one slide of each type of sand.

**Sand distribution**: on the level of the area and count of sand grains, it is remarked that the brown has the less area of sand because its grains are larger but fewer and well sorted, which causes large areas of salt and voids in between. The sizes of the white grains are almost standard, but they are smaller, which increases the area of sand in comparison to the brown, and they are also rounded, which enables the salt to permeate easily. The yellow stands for the higher in sand ratio due to its well sorted characteristic that fills the gaps between the grains with smaller grains, which as much as helps in creating a dense mass of sand in the sample but it prevents the salt from penetrating all the voids as seen in the core of the slice that is much porous than the other types.

**Sat distribution**: the salt is well distributed all over the slices, but its pattern differentiates largely between the types of sand. The area of salt is smaller in the yellow and wider in the brown while the white presents the most homogeneous distribution that is neither too large nor too small. This homogeneity is due to the roundness of the white grains that enables the salt to permeate smoothly in between the grains and consequently impregnates and bonds the grain giving the higher strength in compression. In contrast, the angular (less rounded) grains of the yellow prevent the good penetration of salt. Also, the good sorting of the yellow grains fills the gaps with smaller grains that contribute to the prevention of salt penetration. In the case of the brown sand the large size of the grain and its well sorting creates large voids that are easier for the salt to penetrates giving a well-impregnated specimen but with large salt areas that might broke easily

**Porosity**:

In the yellow slide, the pores have irregular shapes, and they are relatively small but their number is important, and they are diffused all over the slide especially in the core. The white sample is the least porous where the voids are fewer and having circular shapes. The brown is the most porous, despite it has fewer voids in the count but the pores are larger in the area.

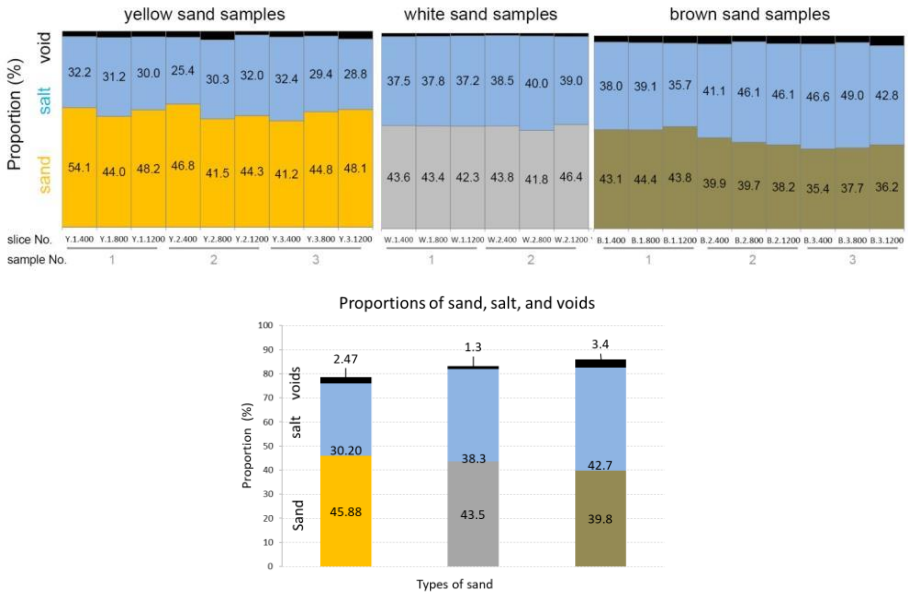


Figure 4.19 The proportions of materials in each slide (left) and their averages (right)

The average of proportions of sand, salt, and voids in each type is presented in Figure 4.19. The graph indicates that the yellow has a higher proportion of sand in comparison to the brown that has more salt than sand, while in the white the proportions of sand and salt are closer than the yellow. In terms of porosity, white sand returns the most solid and homogeneous substance with a porosity of 1.3 %, followed by the yellow (2.47%) and finally the brown that is the most porous (3.4%).

#### 4.6.2.2 Comparative analysis of porosity vs. grain shape and size

This subsection aims at correlating the results of porosity to the grain shape from 4.6.2.1, and grain size from § 4.7.2.

**Porosity vs. grain shape**

In Figure 4.20 porosity shows an inverse linear relationship to grain shape (roundness and circularity), i.e., more the grains are rounded less porous is the material and consequently harder.

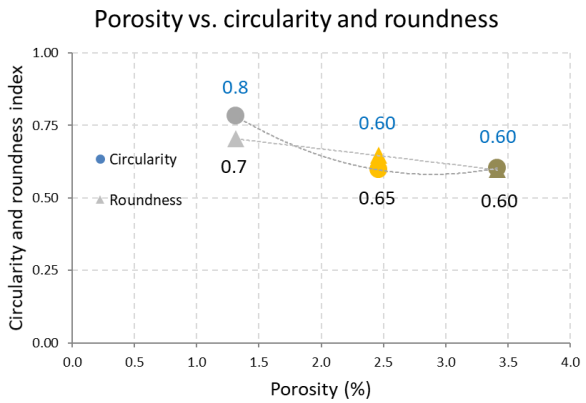


Figure 4.20 Porosity vs. grain shape (circularity and roundness)

**Porosity vs. grain size**

Figure 4.21 shows that porosity increases with larger grain size herein the brown, which is the coarser type of sand used in this work while it decreases with finer sand, i.e. the white and the yellow. The results of the grain size are related to the results of sorting in Figure 4.22, which shows that the poorly sorted brown sand is more porous while the well sorted yellow sand is less porous. The results of the relation between size, sorting and porosity are confirmed visually by the images of the analyzed slices in Figure 4.18. For instance, the brown sand is coarse and poorly sorted, this character creates large voids in between the grains that are hardly filled with salt due to the sharpness of the grains that prevent the salt from permeating smoothly in between the grains, which cause large pores and consequently a low strength material.

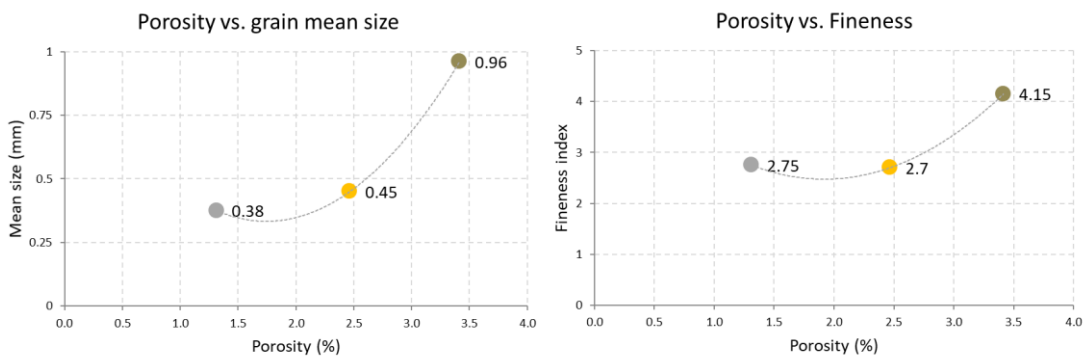


Figure 4.21 Porosity vs grain mean size (left), and fineness modulus (right)

**Porosity vs. grain size distribution (sorting, skeweness and kurtosis)**

In contrast to the brown sand, the yellow is finer and well sorted, this features decrease the voids that are filled with smaller grains. Despite that the white sand is poorly sorted, but it is fineness and its roundness play a vital role in allowing the salt to flow smoothly in between the grains bonding them together and giving the higher strength among other types of sand. These results meet the

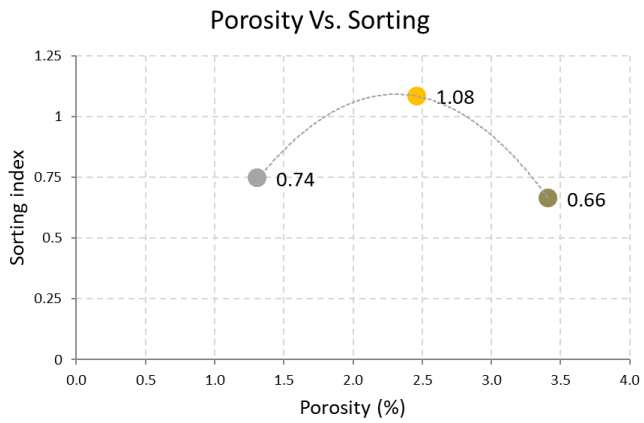


Figure 4.22 Porosity vs sorting

The correlation of sorting with skewness and kurtosis provides a good understanding of the porosity of the sample. It is well known that the porosity has a linear relation with sorting, i.e., a 'well-sorted' sample like the brown is more porous than a 'poorly sorted' sample like the yellow. This could be seen clearly in the x-ray analysis of the sand sample in Figure 4.18 that shows that the yellow is less porous than the brown as the variety of the sizes of the grains creates a well-packed sample. While the lack of smaller grains in the brown sample leaves pores in between the large grains. The relation between sorting and porosity defines the easiness of diffusion of salt in between the grains in the mixing process and consequently the strength of material after solidification.

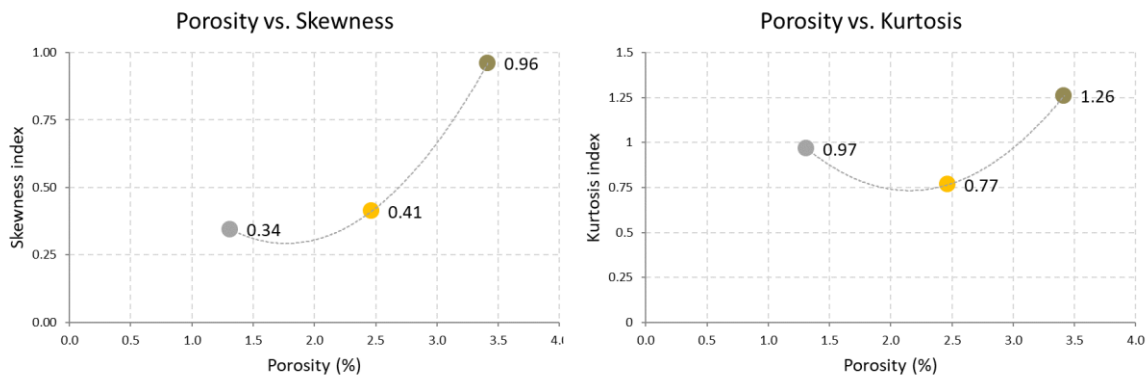


Figure 4.23 Porosity vs. skewness (left) and kurtosis (right)

## 4.7 Compression tests

This section presents the compression tests of Hyposand. The test aims at determining the optimum materials and methods which returns the maximum strength of Hyposand. The effect of the following factors on the copressive strength are assessed :

1. Sand types
2. Sand granularity
3. Sand and salt proportions
4. salt temperature at mixing
5. salt temperature at preparation
6. setting time
7. addition of gravel
8. standard deviation

Table 4.14 The factors which influence on the compressive strength are assessed

### 4.7.1 Materials and methods

- **Specimens preparation**: The specimens are prepared according to the standard method introduced in § 4.2, but for each test one factor is changed according to the list in the above Table 4.15. The sand and salt are mixed according to the method introduced in § 4.2. After the material preparation and mixing, the mixture is casted into steel cubic test moulds of 7x7x7 cm with lubricated inlay. The casting process is performed in three layers, each layer is tamped with a rounded end steel rod for 25 times to extract the air from the mould. The moulds are afterwards left in a dry place in the ambient temperature. One day after casting, the specimens are demolded and stored in the laboratory until the test date. On the test day, the samples are weighted and then tests are applied.

- **Testing machine**: a uniaxial manual compression machine of 2000 KN capacity is used.
- **Weather conditions**: the test were performed in Alexandria, Egypt during August where the average temperature is 32°C and the average humidity is 80%.
- **Tests standards procedures:** When applicable, the testing procedure is foreseen referring the ASTM standards for cement mortar C109 / C109M [49] and concrete C39 / C39M[50]. To assess the mechanical properties of this new material, around 200 specimens are tested.

Figure 4.24 The compression test machine

[49] ASTM Standard Test Method for Compressive Strength of Hydraulic Cement Mortars

[50] ASTM Standard Test Method for Compressive Strength of Cylindrical Concrete Specimens

### 4.7.2 Results and discussion

#### 4.7.2.1 Sand types

The test identifies the compressive strength of four types of sand: yellow, white, red, and brown. These four types of sand are chosen as they show a wide range of differences in their grains type, size, and shape. The data acquired from this test are essential to assess the effect of the grains size and shape on the strength of Hyposand as will discussed in § 4.7.3.

The results are noted in Table 4.16 and plotted in Figure 4.25. Within the same conditions the highest average strength is achieved by the white sand (σ = 30.9 MPa) followed by the yellow (σ = 25.8 Mpa), then the red (σ = 20.1 Mpa), and lastly the brown (σ = 19 Mpa). The results show that the average strength of the Hyposand varies from 19 MPa to 30.9 MPa with a difference of 5 MPa (25%).

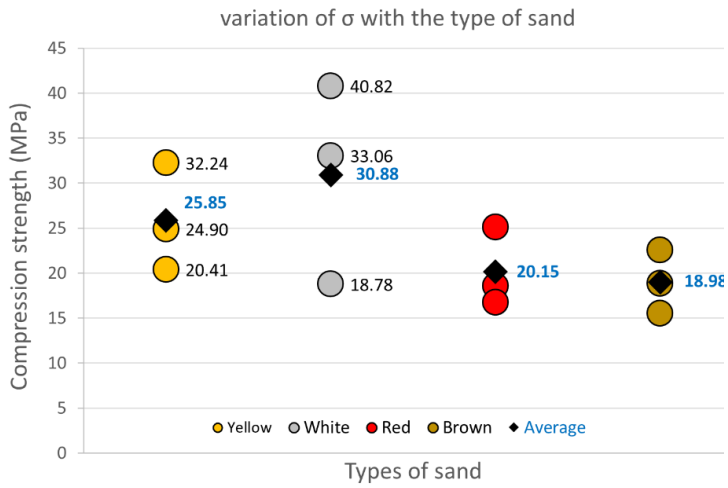


Figure 4.25 Compressive strength of the four types of sand

| Type of sand | σ (MPa) | Average of σ (MPa) |
|---|---|---|
| Yellow | 32.24 | 25.85 |
| | 24.90 | |
| | 20.41 | |
| White | 33.06 | 30.88 |
| | 18.78 | |
| | 40.82 | |
| Red | 25.13 | 20.15 |
| | 18.59 | |
| | 16.73 | |
| Brown | 22.56 | 18.98 |
| | 15.51 | |
| | 18.87 | |

Table 4.16 Results of Compressive strength of the four types of sand

The result indicates that the highest types of sand in compression are the white then the yellow. The results raises the question of the reasons behind the high values of the white samples in comparison to the low values of the brown.

To better understand the above resuts of the compression test it was essential to first measure the grain size distribution in § 4.5.2, the grain shape in § 4.6.2.1 , and the Hyposand posoity 0 in § 4.6.2.2 then compare the results to the compression strength in § 4.7.3.1

#### 4.7.2.2 Sand granularity within the same type of sand

The test aims at identifying the effect of the grain size on the compressive strength of the Hyposand. Three grades of granularity of yellow sand are tested: fine, medium and coarse. The sand is seived and sorted in respect to the Wentworth scale of grain size in mm as following: fine (0.125 to 0.25 mm), medium (0.25 to 0.5 mm) and coarse (0.5 to 1 mm). The results are plotted in Figure 4.26.

The results show that medium sand return the highest average of compressive strength (23.49 MPa), followed by the fine (22.11 MPa), then the coarse sand (19.33 MPa). In comparison to the results of the same type of sand but with a well graded fine to medium sample in the previous test, it is clear that a well-graded sample of sand is more resistant than a uniform sample. This is confirmed by the study of the relation between sorting and strength in § 4.7.3.2, which shows that a well-graded sand is less porous and consequently more resistant. Grading of sand is important from the point of view of packing theory. A well graded sample of sand packs well and reduces the porosity of the Hyposand mixture and consequently increases the material strength.

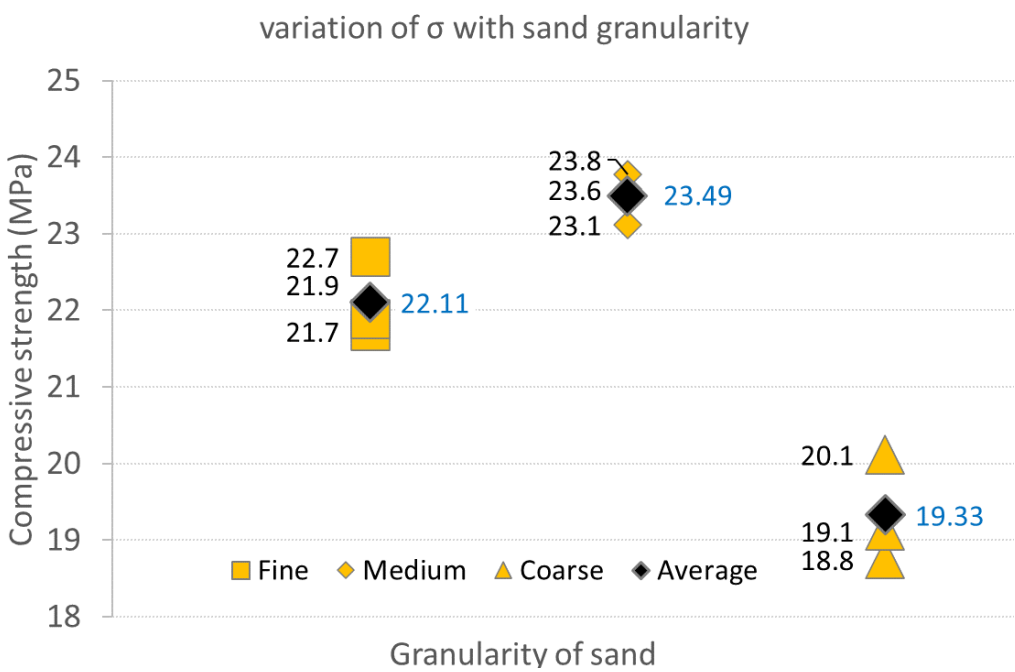


Figure 4.26 Compressive strength vs. Granularity of sand

### 4.7.2.3 Sand and salt proportions

§ 3.2 discussed the effect of the proportion of sand and salt on the workability of the material. In this test the effect of proportions on the compressive strength of the material is examined. The objective is to define the optimum proportion which returns the maximum strength. Three proportions of salt to sand are tested: 0.25, 0.33 and 0.5 salt to 1 sand in weight (kg).The test is applied using yellow and white sand as they show the best strengths in compression from the previous subsection. The results are noted in Table 4.17 and plotted in Figure 4.27.

The results show that the strength rises in a linear trend with the increase of salt proportion. The 0.5 proportion gives the best average strength value (25.85MPa), which is almost the double of the 0.25 proportion (11.84 MPa). Based on the results of the test, the best proportion for the maximum strength is 0.5 salt to 1 sand.

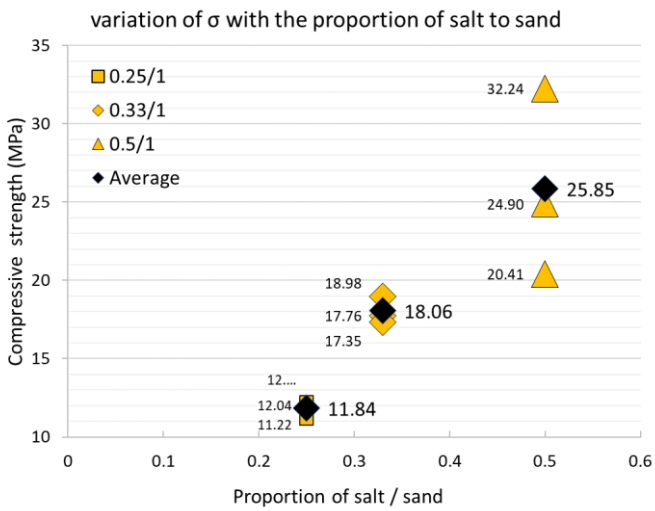


Figure 4.27 Compressive strength vs. proportion of salt to sand

| Salt / Sand proportion | σ (MPa) | Average of σ (MPa) |
|---|---|---|
| 0.25/1 | 12.04 | 11.84 |
| | 12.24 | |
| | 11.22 | |
| 0.33/1 | 18.98 | 18.06 |
| | 17.76 | |
| | 17.35 | |
| 0.5/1 | 32.24 | 25.85 |
| | 24.90 | |
| | 20.41 | |

Table 4.17 Results of compressive strength vs. proportion of salt to sand.

To test the limits of the salt proportion another test is carried to verify the compression strength if the percentage of salt exceeds the 50%. 0.6 salt to 1 sand is then tested, but along the curing of the samples, it was observed that the salt segregates from the sand and create a liquid layer on the top of the sample (Figure 4.28), which is not applicable for the testing machine as it easily cracks. The relationship between the proportions of sand and salt and the Hyposand strength, consistency and workability is essential to study in future work.

Figure 4.28 The segregation of salt on the top of the specimen.

#### 4.7.2.4 Salt temperature at mixing

The test aims at identifying the effect of salt temperature at the mixing stage on the strength of the material. Two temperatures are tested, at 80°C, which is the standard temperature used along the research and at 35°C the room temperature at the lab at the time of the test. Within the same conditions, the 80°C samples show the higher average strength of 25.85 MPa than the 35°C samples (12.79 MPa). This indicates that the strength is higher when using the hot salt than the warm salt. The study of the salt behavior in subsection  shows that the properties of the melted salt changes while cooling. The main observation is that the salt is used in this test at 35°C, which is below it melting point (48°C) and where the salt is in the supercooling phase. At this phase, the salt crystallises instantly if disturbed with a nucleation agent, herein the sand. Consequently, the salt solidifies at a very high rate when mixed with sand where it crystallises while mixing and clogs in the mixture before getting in between all the grains creating weak bonds and pores. Also, when the salt is cooled below its melting point, it is more viscous, which difficult the penetration of the saline solution into the grains of sand. Hence when applying the salt to the sand below its melting point, it starts to crystallise while mixing and can't get in-between all the grains leaving voids, which increase the porosity of the sample and subsequently decreases its strength (Figure 4.29).

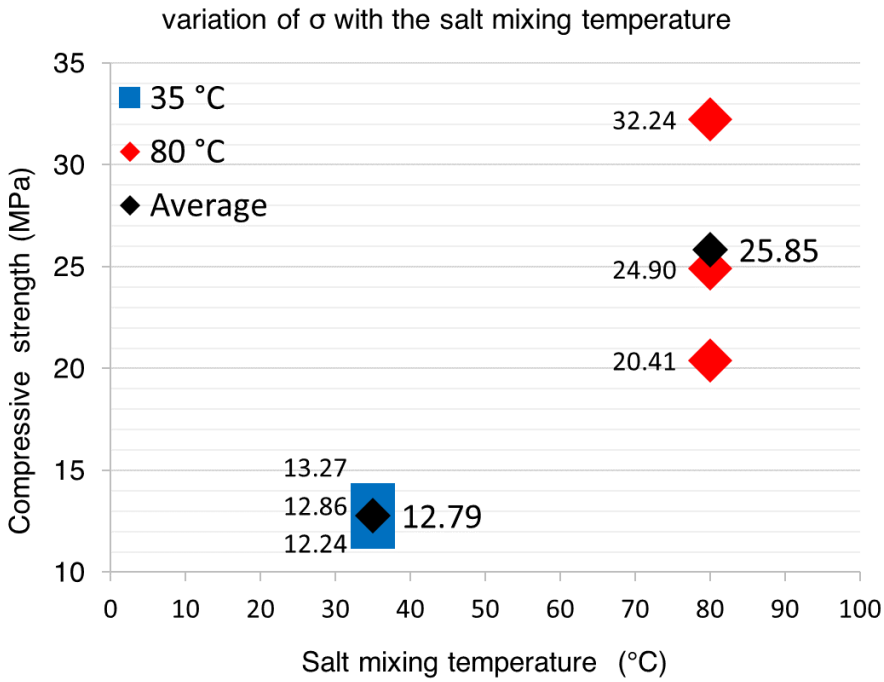


Figure 4.29 Compressive strength vs. salt mixing temperature

| Salt mixing temperature (°C) | σ (MPa) | Average of σ (MPa) |
|---|---|---|
| 80 | 32.24 | 25.85 |
| | 24.90 | |
| | 20.41 | |
| 35 | 13.27 | 12.79 |
| | 12.24 | |
| | 12.86 | |

Table 4.18 Compressive strength vs. salt mixing temperature

#### 4.7.2.5 Salt melting temperature

The test aims at verifying the effect of the melting temperature of salt during its preparation on the compressive strength of the Hyposand. Along the research, it is observed that heating the salt up to its boiling point at 100°C increases the strength of the material as well as its workability as it takes longer duration to crystalise. To verify this observation, the test examines the strength of the material at two heating temperature, 48°C (melting point) and 100°C (boiling point). The results are noted Table 4.19 and plotted in Figure 4.30.

The results show that the average strength at100°C is higher (25.85 MPa) than at 48°C (11.48 MPa). The initial analysis of the results is that boiling the salt over its melting point increases the saturation of the saline solution as the contained water within the crystals evaporates during the boiling process. This, in turn, increases the strength of the liquid salt in bonding the sand grains giving a higher strength material. This is confirmed by the study of the salt behavior in § 2.5 which shows that the sodium thiosulfate pentahydrate decomposes by heating to lower hydrates that when cooled contains fewer water molecules and consequently is more saturated and harder in crystallisation.

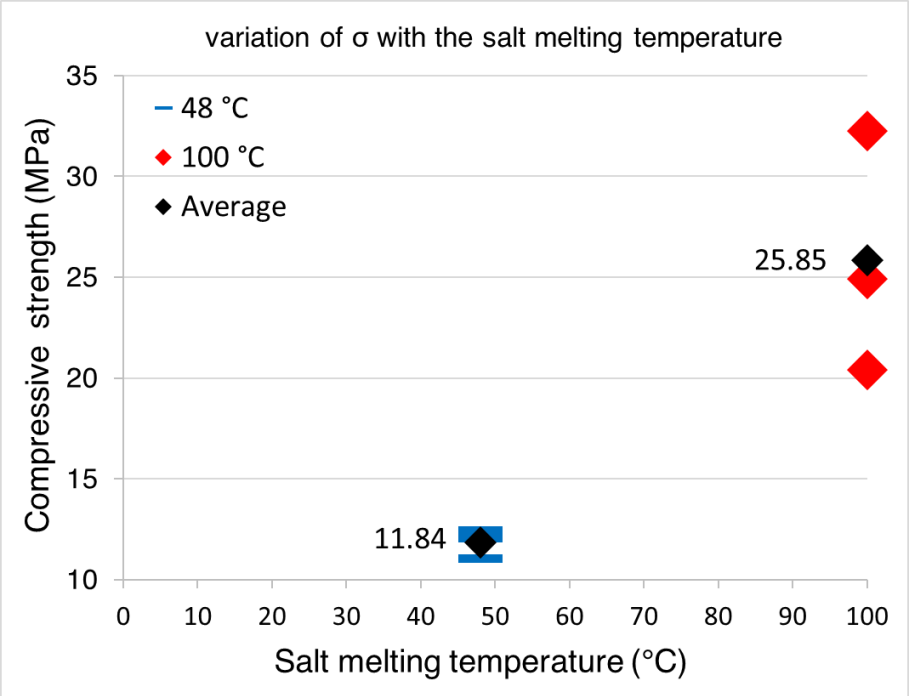


Figure 4.30 Variation of compressive strength with the salt melting temperature

| Salt melting temperature (°C) | σ (MPa) | Average of σ (MPa) |
|---|---|---|
| 100 | 32.24 | 25.85 |
| | 24.90 | |
| | 20.41 | |
| 48 | 12.04 | 11.84 |
| | 12.45 | |
| | 11.02 | |

Table 4.19 Results of the variation of σ vs. the salt melting temperature

#### 4.7.2.6 Setting time

This test identifies the effect of setting time of the Hyposand on its comrpessive strength. Five ages are assesed: 3 hours and 1, 3, 7 and 28 days using 6 samples for each age. The results are plotted in Figure 4.31.

The results shows that Hyposand achieves the highest strength at the age of 3 days (25.8 MPa). In comparison to the 3 days strength, it is deduced that the material gets to 91% of its strength in between the age of three hours and one day (23.6 MPa). Then it decreases to 76% at the age of 7days (11.5 MPa) then to 49% at the age of 28 days (12.7 MPa). The decrease of Hyposand strength can be analysed in the light of the charachterestics of the salt discussed in § 2.5, and the weather conditions at the time of the test in Alexandria (32°C of average temperature and 80% of average humidity). The crystallised salt repels its water content in hot, dry environments and gets harder. While in humid conditions it absorbs water from the environment, which breaks the salt bonds and degrades the solidified sand. Based on the weather data and the behavior of salt, it is well noted that after the third day the humidity affects the samples and breaks some of the solidification bonds, which decreases the strength. Furthur, It is noted from the results that the strength gets to 90% of the maximum value after three hours, which is due to the high rate of crystallisation of the salt. To conclude, the test of setting time shows the high rate of the material solidification in three hours and the effect of humidity on the strength of the material that decreases after the third day.

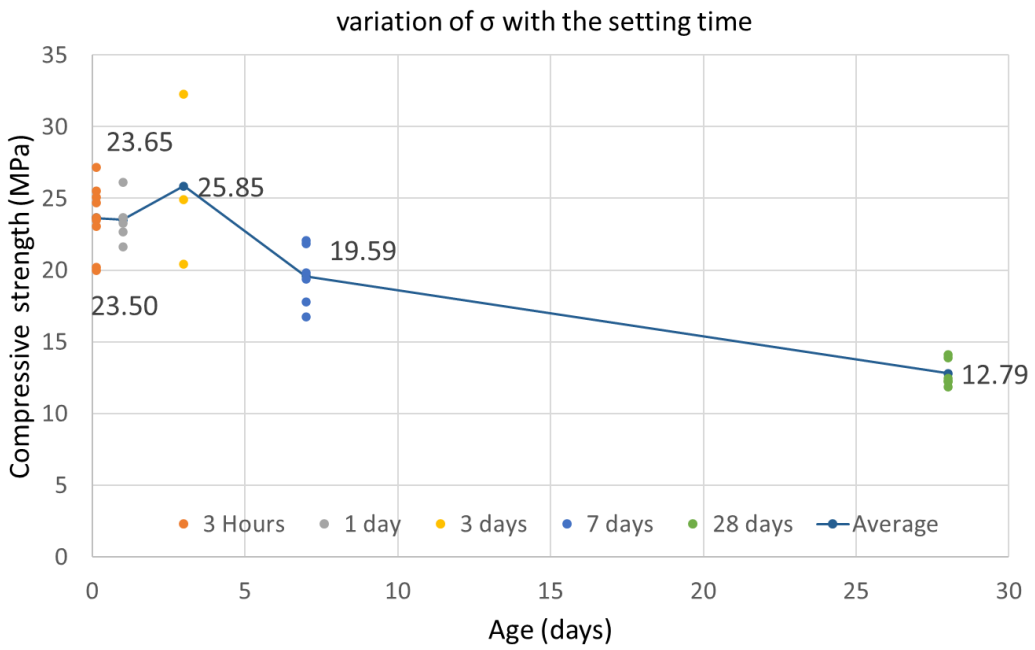


Figure 4.31 Compressive strength vs. setting time

### 4.7.2.7 Addition of gravel

The test aims at identifying the strength of the Hyposand with the addition of gravel into the mixture. The sizes and terms of the gravel used in this work are identified according to the Wentworth scale as: very fine, fine and medium pebbles (grain size between 2.38 and 13.4 mm). The gravel passes from the ASTM sieve no: 1/2" and retains on sieve no: 8. The coarse aggregate has an irregular shape, sharp edges with a coarse texture derived from crushed stones. The test follows the standard method described in § 4.2 but gravel is used (sizes between 13.4 and 2.83 mm). Two proportions of gravel to yellow sand by weight are tested: 30% and 50 %. Also the proportion of 30% is tested with the white sand. The results are noted in Table 4.20. and plotted in Figure 4.33. The results are compared to the standard strength of Hyposand (§ 4.7.2).

Figure 4.32 Detail of a broken specimen of the mixture of Hyposand and gravel

The results show that the addition of gravel by 30% decreases the strength of both the white and the yellow by 18% and 14% respectively. While with the proportion of 50% the strength of the yellow sand falls by 36% of its original strength without gravel. It is clear from the results that the strength decreases remarkably by the addition of gravel. The results are in accordance with the results of both the compression test of sand types in § 3.6.2 and sand granularity in § 3.6.6, which confirm that the Hyposand shows better strength with finer material. Indeed, the addition of gravel creates a better-graded mixture, but the main reason behind the decrease of strength is that the salt cannot bond Hyposand with the gravel.

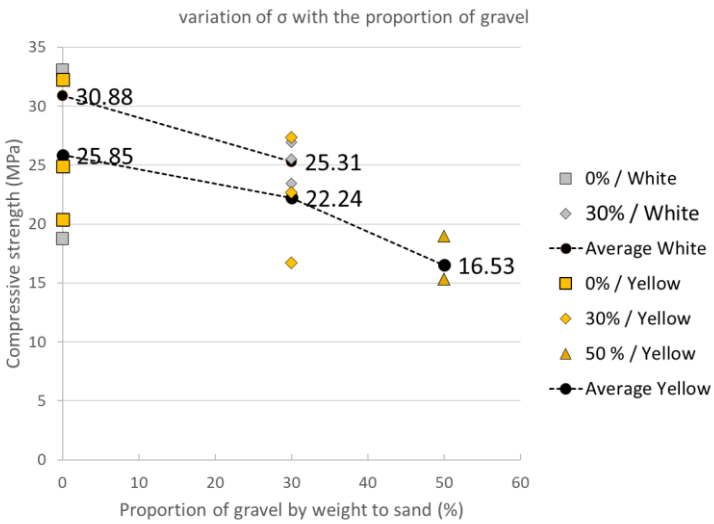


Figure 4.33 Compressive strength vs. Proportion of gravel in the Hyposand material

| Sand type | Gravel proportion | σ (MPa) | Average of σ (MPa) |
|---|---|---|---|
| Yellow | 0% | 32.24 | 25.85 |
| | | 24.90 | |
| | | 20.41 | |
| | 30% | 22.65 | 22.24 |
| | | 16.73 | |
| | | 27.35 | |
| | 50% | 18.98 | 16.53 |
| | | 15.31 | |
| | | 15.31 | |
| White | 0% | 33.06 | 30.88 |
| | | 18.78 | |
| | | 40.82 | |
| | 30% | 23.47 | 25.31 |
| | | 26.94 | |
| | | 25.51 | |

Table 4.20 Fixed and variable parameters of the test and Compressive strength of three different proportion of gravel (0,30,50%) with yellow and white sand

### 4.7.2.8 Standard deviation

To examine the dispersion of the values of the compressive strength, a standard deviation test is applied on 9 samples of yellow sand. The samples are prepared according to the standard method described in § 4.2. The standard deviation (σ) was calculated as the root mean square deviation of the nine compressive strength values $\sigma = \sqrt{\frac{\sum(x-\mu^{2})}{n-1}}$

The results of the standard deviation test are reported in Figure 4.34. The results showed an average value of 25.01 MPa with a minimum and maximum values of 22.45 and 27.14 MPa, respectively. The results showed a limited dispersion of 1.53 for standard deviation, which indicated the stability of the process. While considering the limited resources during the test that limited the possible number of specimens to only nine, it is recommended to run further tests, with a larger number of specimens to return more reliable results in terms of dispersion.

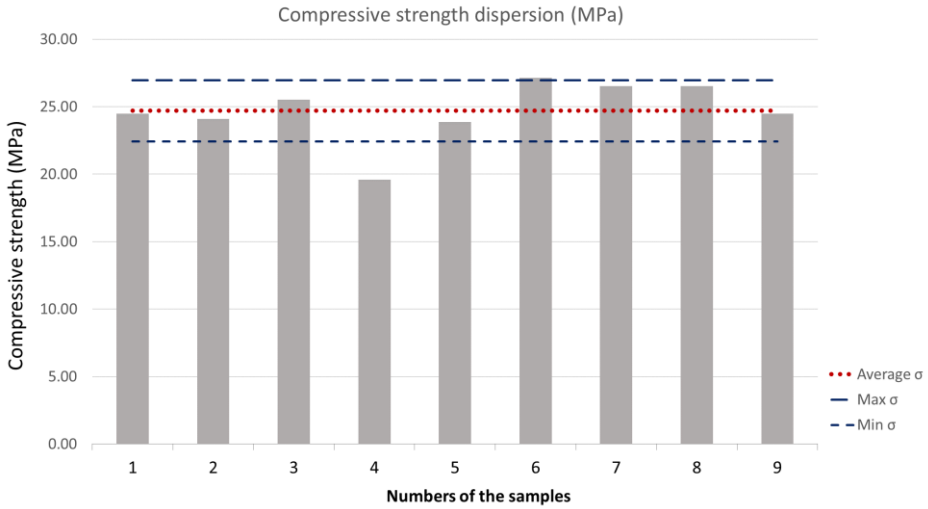


Figure 4.34 Compressive strength dispersion (MPa)

### 4.7.3 Comparison of the compression results to the grain size and shape

To better understand the results of the compression tests, they are discussed in this subsection in comparison with the results of the grain size, grain shape, porosity, and proportion of sand and salt. The study aims at identifying the effect of grain size and shape as well as the porosity on the material compressive strength.

#### 4.7.3.1 Compressive strength vs grain size

This subsection aims at identifying the effect of grain size on the compressive strength results in § 4.7.2. The four types of sand showed a remarkable difference in their average strength (Figure 4.35 left). The results are compared to the Fineness modulus of the sand types in Figure 4.35 right. The comparison indicates that the strength increases linearly with the grain fineness.

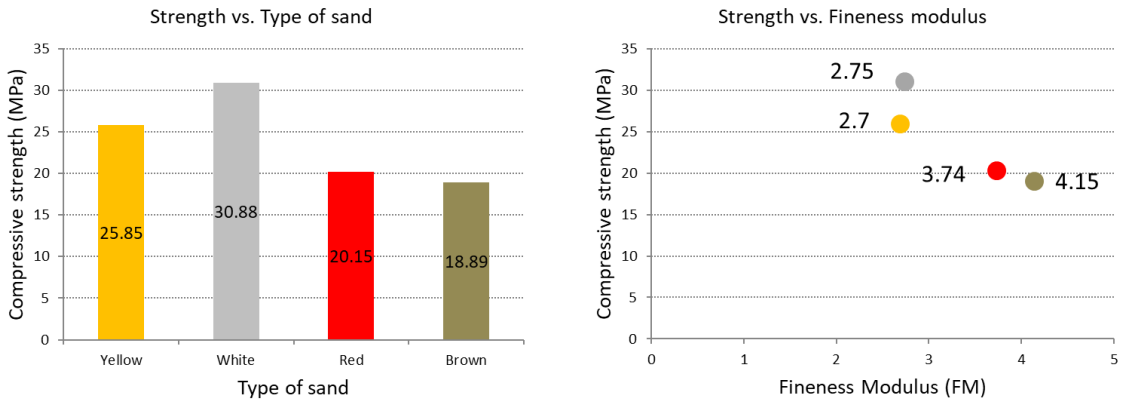


Figure 4.35 Compressive strength of each type of sand (left) and compressive strength vs. Fineness modulus (right)

The above finding is confirmed in Figure 4.36 (left) which shows that the compressive strength increases linearly with the mean size, i.e., finer the sand is more resistant the material is. In addition, sorting is not linearly related to strength as seen in Figure 4.36 (right): however, it affects the porosity and consequently the strength.

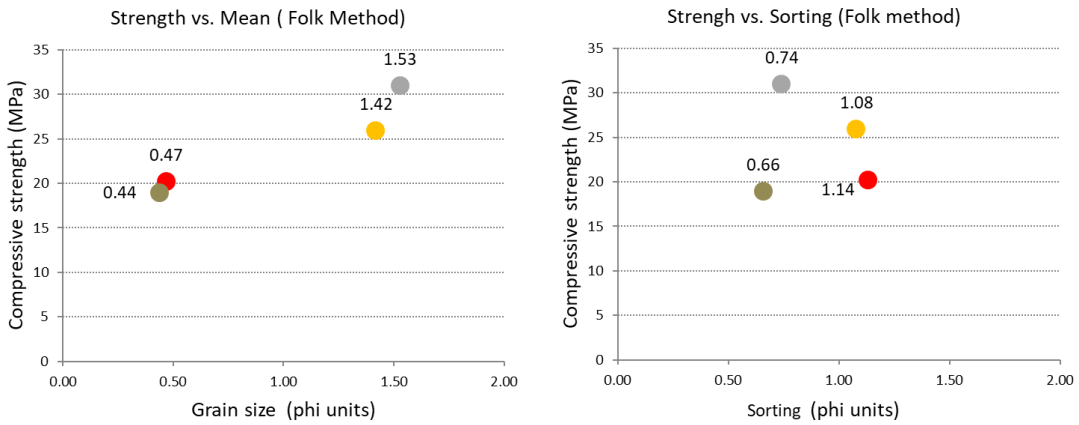


Figure 4.36 Compressive strength vs. Mean size (left) and vs. porosity (right)

The linear relation of strength and skewness is interesting as symmetrical samples (yellow and white) show more resistance than the asymmetrical samples (brown and red). Finally, the

Kurtosis vs strength graph shows that the normal curves (white) of distribution is better than the flat and the sharp (yellow, red, and brown) curves (see Figure 4.6 for curves)

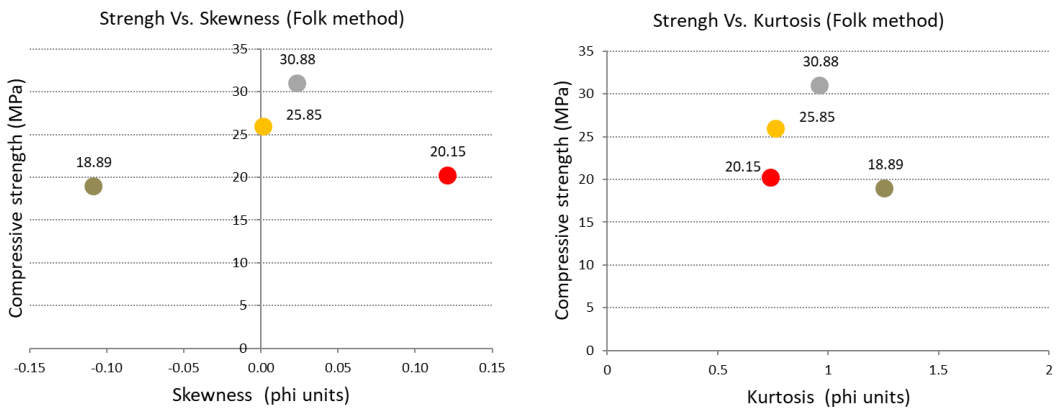


Figure 4.37 Compressive strength vs. Skewness (left) and vs. Kurtosis (right)

### 4.7.3.2 Compressive strength vs grain shape and porosity

This subsection details the analysis results of the . and compares it to the material stiffness in compression followed by a discussion of the effect of grain shape and size on the material porosity and strength. The analysis results are presented in graphical and visual forms as following: (i) Porosity vs Compressive strength and (ii) Porosity and grain shape vs Compression strength. Figure 4.38 shows that the average compressive strength decreases with the increase of porosity. The bubble graph in Figure 4.39 concludes these results where the roundness index is plotted horizontally, and the average compressive strength is plotted vertically while the porosity is presented by the area of the bubbles.

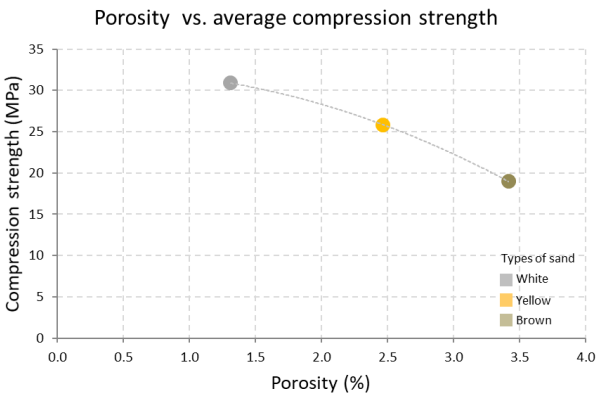


Figure 4.38 compressive strength vs. porosity

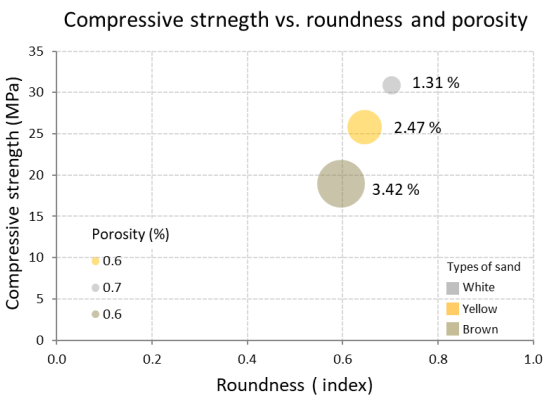


Figure 4.39 compressive strength vs. roundness and porosity

### 4.7.3.3 Compressive strength vs proportions of sand and salt

The corresponding compressive strength of each type of sand is linearly plotted in Figure 4.40 overlapping the proportion of materials in each type. The results indicate that the lowest strength is achieved when there is much more salt than sand as in the brown type. It is important to note that these results of correlating proportions to strength in this analysis could not be compared to the proportions used in material preparation as the first is area proportion while the second is weight based proportions.

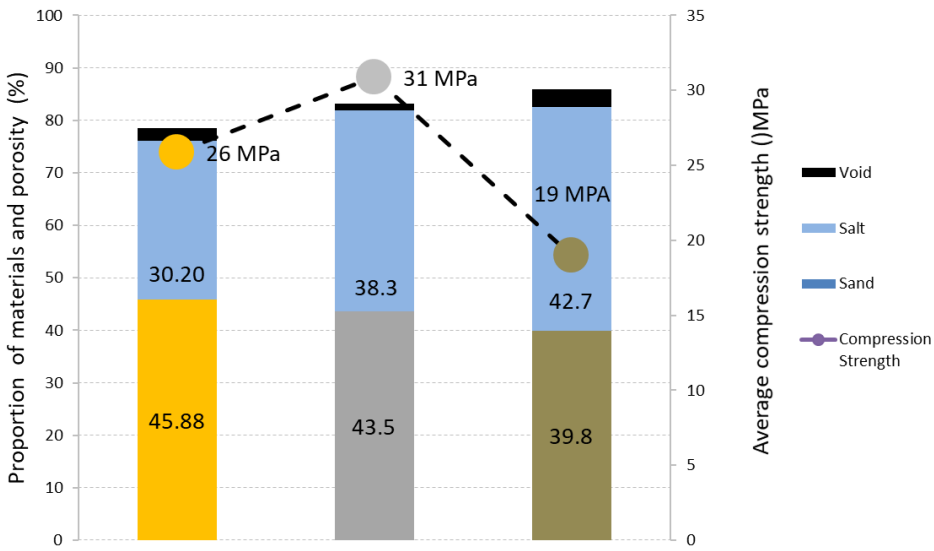


Figure 4.40 Average of proportion of materials in the three types of sand

.

## 4.8 Flexural test

The section studies the effect of humidity on the flexural and compressive strengths of Hyposand. The test is performed on two sets of specimens at two different relative humidity conditions.

### 4.8.1 Materials and Methods

The test was performed at Navier laboratory (Ecole des Ponts ParisTech, IFSTTAR and CNRS) in Paris. It was not possible to use the same yellow sand of Alexandria, a similar sand type found in Paris was used, i.e. a manufactured yellow silica fine sand (0.1 to 0.6 mm fineness). After the preparation of the mixture following the standard method described in § 4.7.1, six specimens (40x40x1600 mm) were prepared in two sets, A (S1, S2 and S3) and B (S4, S5 and S6). One day after casting, both sets were demolded and transferred immediately into a “dry box” (humidity 33±1 %). On the second day, the set B was transferred to a “humid box”[51] (humidity 50±5%)[52] while set A remained in the dry box (Figure 4.42). Figure 4.41 shows the humidity conditions during the curing which increased 15 % in the third day. On the fourth day, both sets of specimens are removed from the boxes and subjected to the tests according to the ASTM C348[53] standards. A uniaxial electromechanical testing machine[54] is used. The six prisms are tested in flexure following the three points flexural test method. Afterthen, the broken parts are tested in compression.

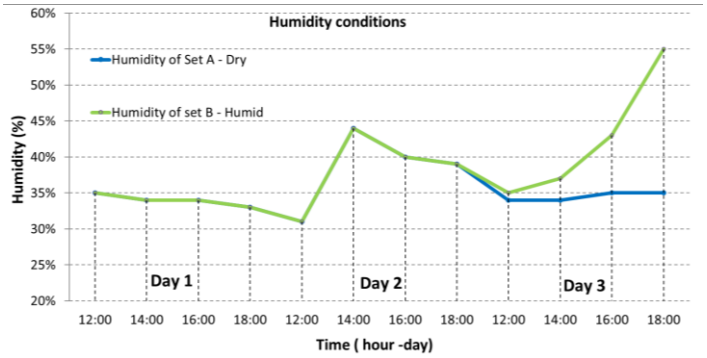


Figure 4.41 Humidity conditions for the flexural test

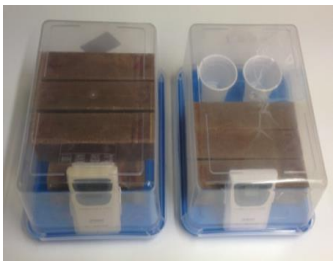

Figure 4.42 Set A in the dry box (left) and set B in the humid (right).

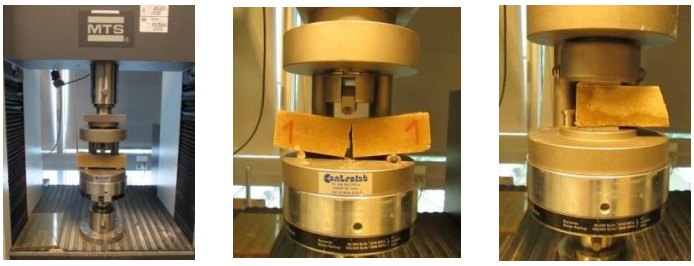


Figure 4.43 Three-point flexural test (left, middle), the compression test on the broken sample (right)

[51] To create two different humidity conditions, the humid box is supplied with 150 grams of water in two cups.

[52] A digital sensor is used to read the temperature and humidity data

[53] Standard Test Method for Flexural Strength of Hydraulic-Cement Mortars

[54] Machine model: MTS Excced

### 4.8.2 Results and discussion

*The results of both flexural and compression tests are reported in Figure 4.44 and Table 4.21. The curves vary both in terms of maximum stress and strain as well as in terms of dispersion. With the increase in humidity, the maximum flexural stress that the specimens can withstand decreased from a maximum of 9.73 MPa to a minimum of 4.28 MPa. Within the same humidity curing conditions, set 'A' presented an average tensile strength of 8.10 MPa with a standard deviation of 1.48, while set B presented a maximum of 4.78 MPa with a lower standard deviation of 0.62. However, if we consider the standard deviation of the elastic modulus, rather than the maximum value of the stress, it can be noted that the set B results were more dispersed. On the other hand, compression tests curves were less dispersed that flexural ones, highlighting the extreme sensitivity of flexural tests. Regarding the humidity, the decrease in strength was evident also for the compression tests going from a medium value of 40–25 MPa. The reduction was similar for both tests, 37% for compression and 41% for flexural tests. Humidity conditions also affected the standard deviation, for compression tests, it passes from 2.31 to 0.9 with the increase of humidity.*

*Another interesting fact that can be deduced from the curves was the ductility of the material. Hyposand presented a relatively low elastic modulus (in the range 0.2–2 GPa) and a deformation at the peak flexural resistance between 0.5% and 1%.*

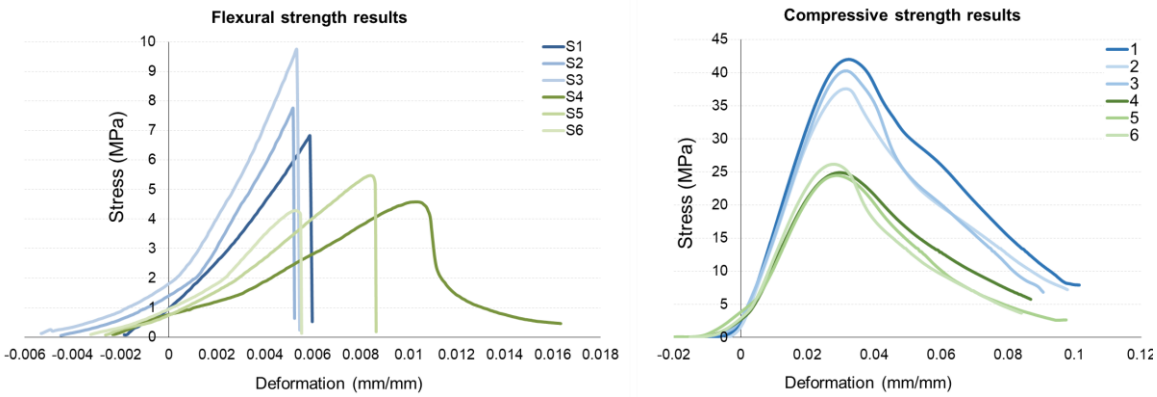


Figure 4.44 Comparison between the results of the three-point flexural test (left) and compression test on the broken specimen (right).

| Sample | Curing condition | | | | | | Readings | | | | | | |
|---|---|---|---|---|---|---|---|---|---|---|---|---|---|
| | Day 1 | | Day 2 | | Day 3 | | Flexure | | | Compression | | | |
| | T °C | H % | T °C | H % | T °C | H % | strength (MPa) | Average | max. Force (N) | strength (MPa) | Average | max. Force (N) | Module (MPa) |
| 1 | 29 | 34 | 29 | 38 | 29 | 35 | 6.82 | 8.10 | 3206.00 | 42.20 | 40.03 | 67198.93 | 1616.92 |
| 2 | | | | | | | 7.75 | | 3552.90 | 37.60 | | 60104.04 | 1490.82 |
| 3 | | | | | | | 9.73 | | 4151.90 | 40.30 | | 64428.98 | 1517.52 |
| 4 | | | | | 29 | 50 | 4.58 | 4.78 | 1999.90 | 24.90 | 25.20 | 39853.37 | 1096.59 |
| 5 | | | | | | | 5.47 | | 2507.50 | 24.50 | | 39142.38 | 1064.00 |
| 6 | | | | | | | 4.28 | | 1964.90 | 26.20 | | 41864.33 | 1199.48 |

Table 4.21 Results of the flexural and compression tests

## 4.9 Thermal conductivity test

This section aims at defining the thermal conductivity of Hyposand to understand its thermal performance, which is crucial to estimate its possible applications in construction. The results are compared to other construction materials, as will be shown in the following subsection. Thermal conductivity, also known as Lambda (λ), is the measure of how easily heat flows through a specific type of material. The lower λ is, the slower heat will move across material and have better thermal performance in construction. It is measured in Watts per Meter Kelvin (W/m.k).

### 4.9.1 Materials and Methods

Following the standard making method described in § 4.2, a 50x50x3cm specimen plate of Hyposand is prepared in the GSA laboratory in Paris using the same industrial sand used in the flexural test. One day after hardening, the sample is sent to the mechanical test laboratory at the University of Venice IUAV where the test is performed seven days after hardening. The test is performed according to the UNI EN ISO 8302-8303 standard using a single-specimen apparatus. The sample is subjected to unidirectional and uniform density of heat flow-rate at steady-state conditions in the apparatus. The sample is exposed to cycles of heating and cooling within the temperature range of 6 to 40°C

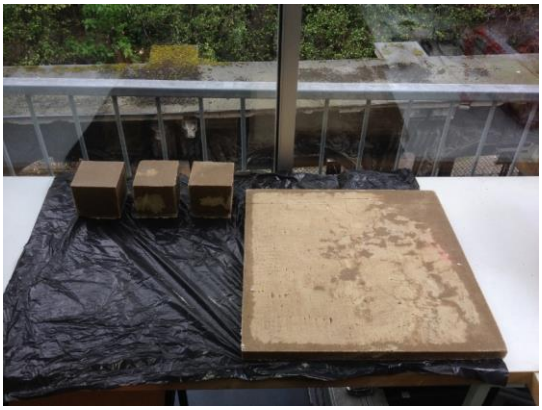

Figure 4.45 The Hyposand specimen of the thermal conductivity test (50x50x3cm).

### 4.9.2 Results and discussion

The results are reported in Figure 4.46, showing the values of thermal conductivity (λ) plotted against the Mean temperature. The results indicate that the λ of Hyposand range between 0.45 and 0.7 W/(m.k) with an average of 0.58 W/(m.k). From the graph, it can be noted that the trends of the curves are similar. The values of λ rise gradually, then show a peak of around 0.7 W/(m.k) at the range of 25 to 35 °C, then decrease by around 0.5 W/(m.k).

| Temperature (C) | λ (w/m.k) | Sample no | Delta T |
|---|---|---|---|
| 12.7 | 0.453 | 1 | 10 |
| 23.7 | 0.6349 | 1 | 9.7 |
| 22.3 | 0.5474 | 2 | 11.7 |
| 31.5 | 0.6329 | 2 | 10.1 |
| 40.1 | 0.5891 | 2 | 10.9 |
| 13.4 | 0.5021 | 3 | 7.4 |
| 25.2 | 0.6614 | 3 | 7.2 |
| 33.8 | 0.6404 | 3 | 7.2 |
| 15.9 | 0.5577 | 4 | 4.8 |
| 26.5 | 0.6913 | 4 | 4.6 |
| 35.4 | 0.6407 | 4 | 4.7 |
| 14 | 0.4731 | 5 | 10 |
| 22.9 | 0.6985 | 5 | 9.2 |
| 27.8 | 0.6901 | 5 | 9.3 |
| 32.3 | 0.662 | 5 | 9.7 |
| 36.2 | 0.6331 | 5 | 9.7 |
| 6.3 | 0.4394 | 6 | 8.1 |
| 9.8 | 0.4638 | 6 | 8 |
| 13.6 | 0.496 | 6 | 8 |
| 17.7 | 0.548 | 6 | 7.9 |
| 22.9 | 0.6843 | 6 | 7.6 |

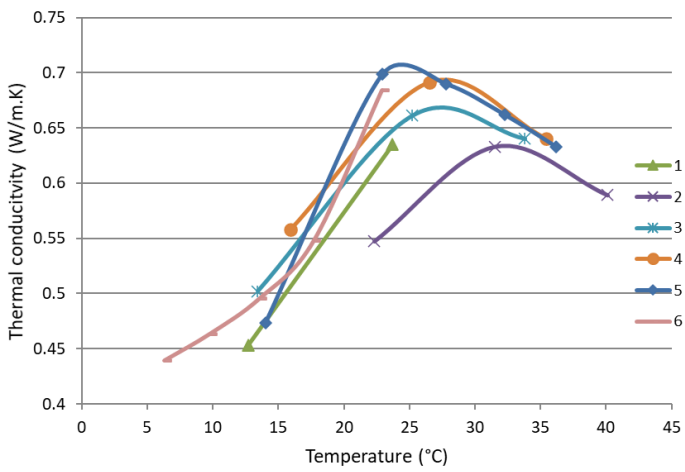


Figure 4.46 Results of the thermal conductivity test

To better understand the peak of the λ of Hyposand at the range of 25 to 35 °C, it is essential to study the λ of the sodium thiosulfate pentahydrate salt (STP) and its melting point. The STP thermal conductivity is studied in [167], and the obtained values are plotted in Figure 4.47.

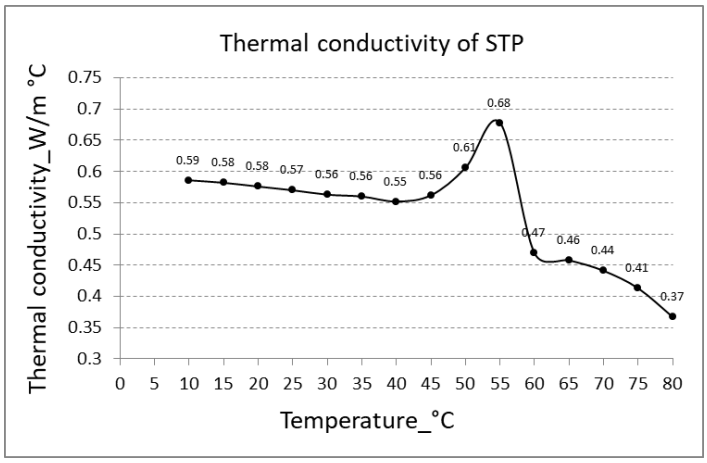


Figure 4.47 Thermal conductivity of the sodium thiosulfate pentahydrate salt (after [167])

The graph shows that the λ of the STP peaks at the range of 45 to 55°C, where the melting point of the STP (48°C) is. Hence, the λ of the STP peaks at its melting point, at which it transits from pentahydrate to lower hydrates. It is important to note that the transition of the STP to lower hydrates due to cycles of heating and cooling decrease its melting point up to 30°C, as discussed in § 2.5.1. The STP thermal behavior might explain the peak of λ of Hyposand in this test performed in this work. Most probably, the exposure of the sample to cycles of heating and cooling during the test caused the melting of the salt and, consequently, the decrease of its melting point up to 30. Thus, the λ of Hyposand peaks around its new melting point at the range of 25 to 35 °C. Methods to control the instability of λ of the STP by additive materials are proposed in [170,190], where STP is used for thermal storage in construction and the industry of solar panels.

## 4.10 Comparison of Hyposand with other materials

In this section an initial comparison between Hyposand and other classes of materials is given using Ashby plots. The comparison provides and preliminary understanding of the properties of Hyposand in regard to other materials. A detailed comparison with existing construction materials will be performed in the future after further studies, especially on ageing.

### 4.10.1 Method of comparison

Ashby plots collect and display two properties of classes of materials on the vertical and horizontal axis of a scatter graph. The charts map the areas of property space occupied by each material class. The plots are used in structural and mechanical engineering for material selection in the conceptual design phase. Background and data sources can be found in the book "Materials Selection in Mechanical Design" [191] by M.F. Ashby.

The following six plots are presented in this section with a brief commentary about its use.

3. Strength vs. Density
4. Young's modulus vs. Density
5. Thermal conductivity
6. Relative cost vs. strength
7. Approximate cost per unit volume
8. Approximate cost per unit mass

To plot the properties of Hyposand, Ashby graphs are first collected from [191], then the minimum and maximum values of Hyposand properties, retrieved from the results in this chapter, are plotted. Finally, the intersection area of the range of the two properties are marked in yellow to represent the area of properties of Hyposand and other construction materials are highlighted in gray as shown in the figure below.

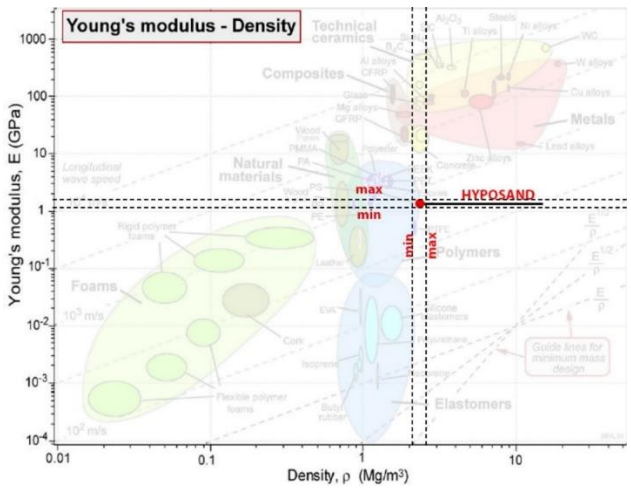


Figure 4.48 The method of plotting the properties of Hyposand on Ashby plots (after [191]).

### 4.10.2 Results and discussion

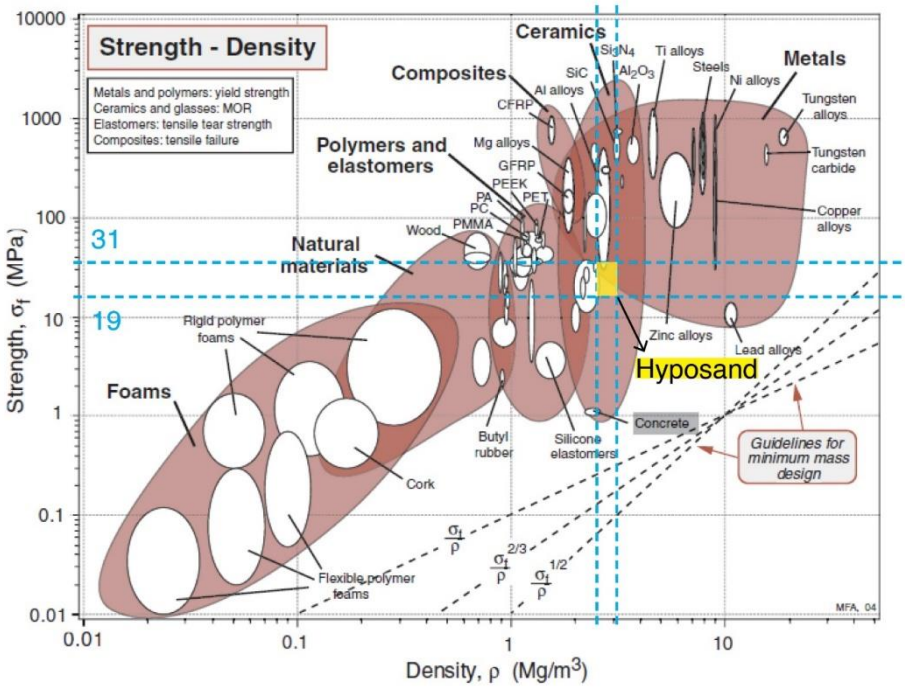


Figure 4.49 Strength vs. Density of Hyposand (after [191]).

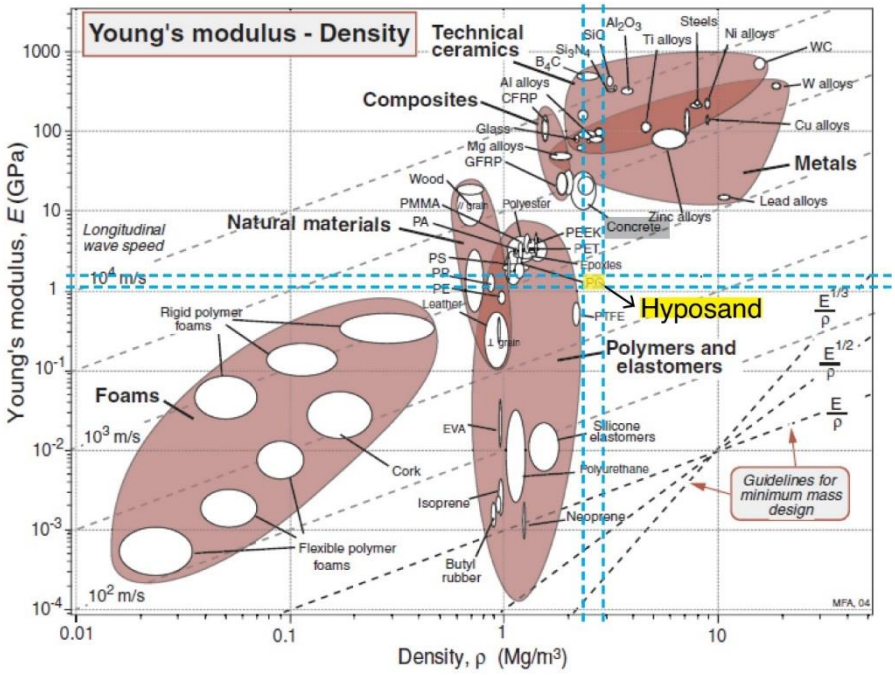


Figure 4.50 Young's modulus vs density. of Hyposand (after [191]).

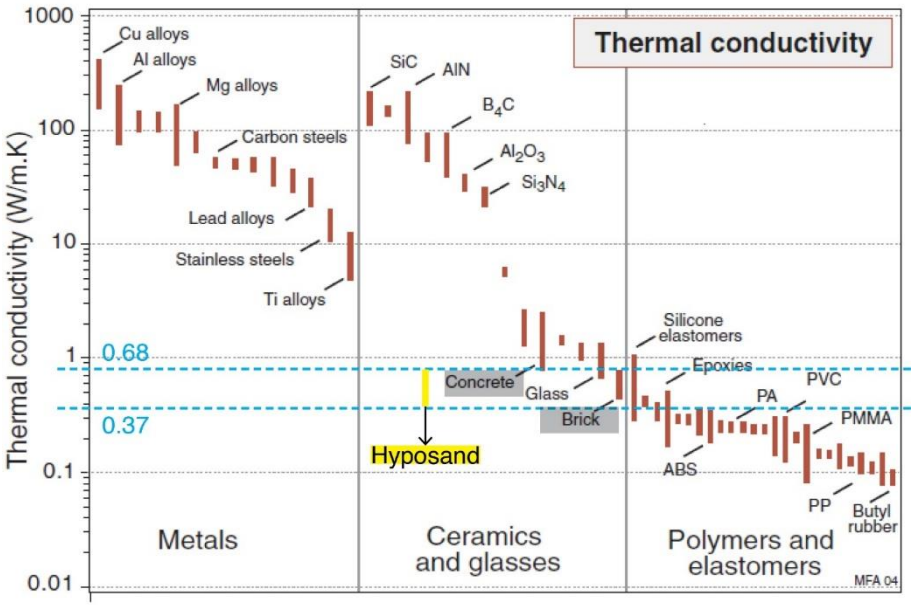


Figure 4.51 Thermal conductivity of Hyposand (after [191]).

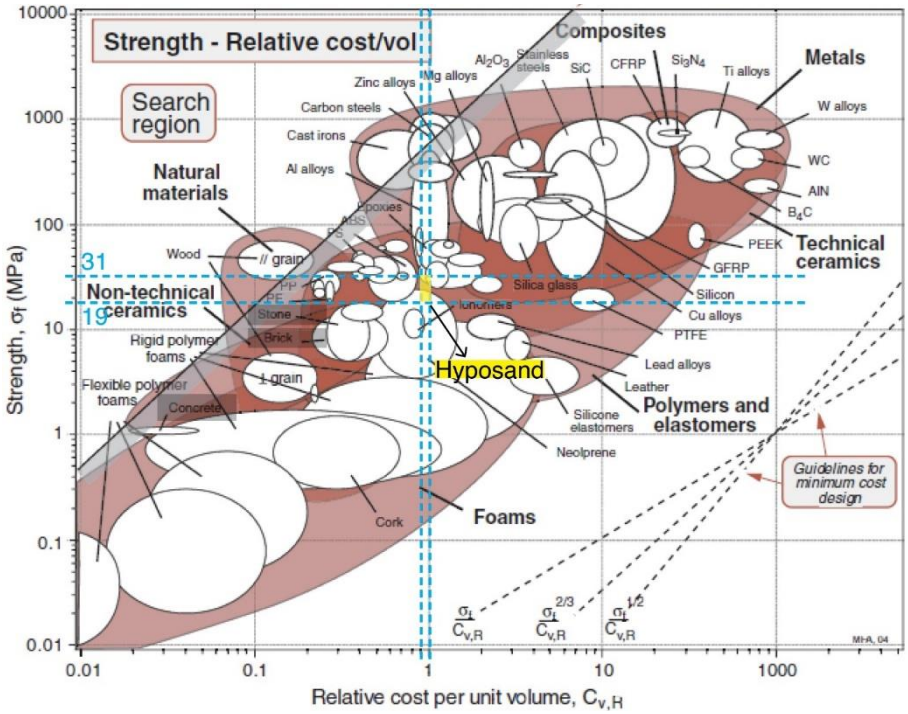


Figure 4.52. Strength vs. relative cost of Hyposand (after [191]).

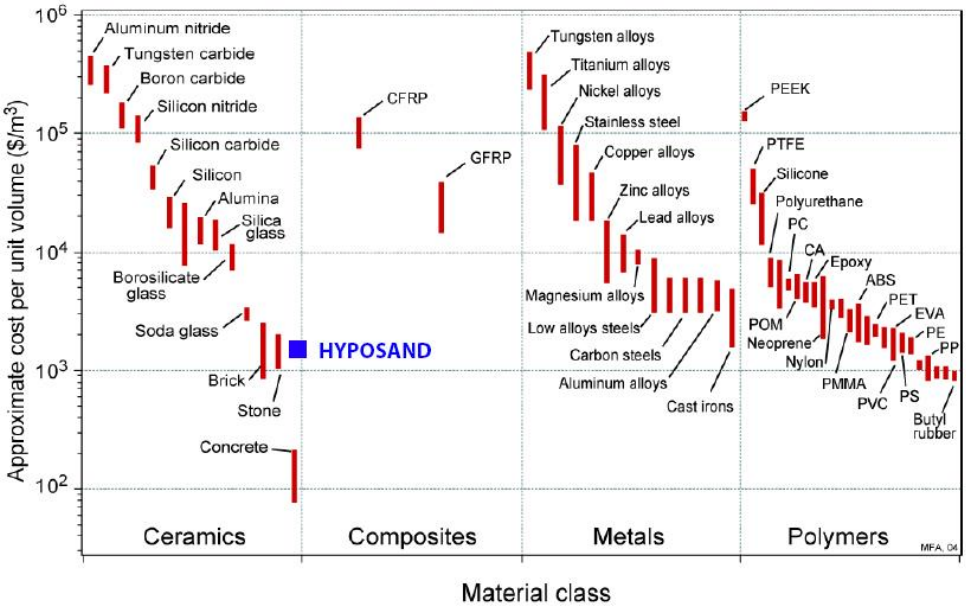


Figure 4.53 Approximate cost per unit volume of Hyposand (after [191]).

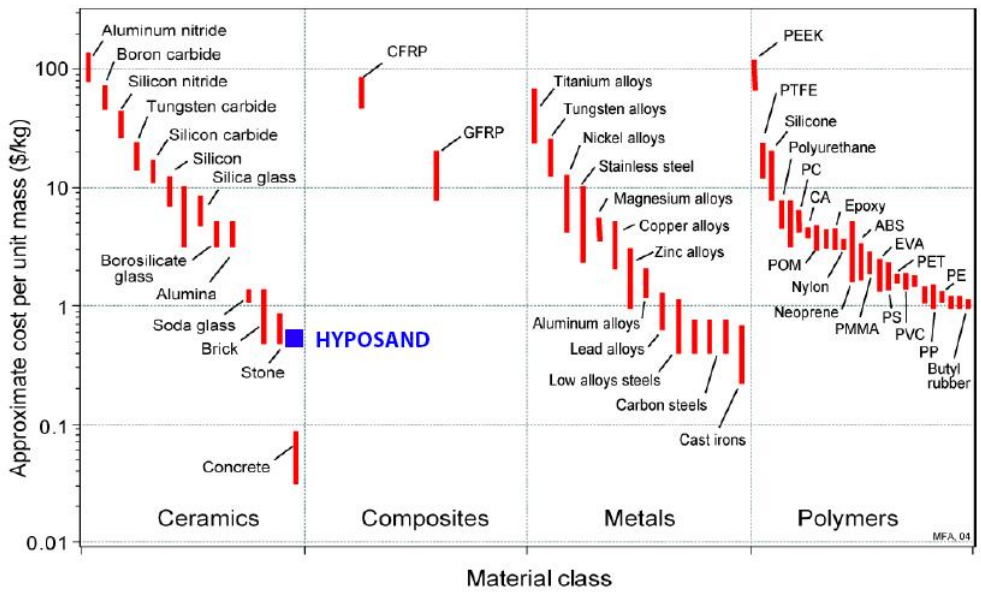


Figure 4.54 Approximate cost per unit mass (after [191]).

# Chapter 5

Making system

design and fabrication methods

# 5 Making system: design and fabrication methods

This chapter constructs the making system of the sand tectonics by developing the design and fabrication methods and associating them in a coherent digital-physical workflow. The design system defines the physical and digital methods of sand formation, while the fabrication system identifies the fabrication processes and constraints. The making methods defined in this chapter are examined and applied through digital and physical prototyping in the following chapter.

The overall objective of this chapter is to define the formation and manufacturing methods allowed by the material logic to unfold its morphogenetic possibilities without forcing external ideas. A methodology of research by design is set to tease out formation processes from the materials capacities rather than constructing predefined forms. The purpose is to systemize the processes and to establish order in the almost infinite range of morphological possibilities. To develop the making system, an empirical methodology is employed through physical and digital experiments. A Feedback between the physical and digital experiments is central to this work to integrate material behaviour, geometry, code, design, and fabrication constraints in a coherent making system. The chapter is structured in six subsections as following:

§ 5.1 **Design system:** defines the physical methods, parameters, and tools of sand formation.
§ 5.2 **Geometry**: analyses the geometrical principles of sand piles to inform the algorithms.
§ 5.3 **Modeling methods:** develops parametric methods of form generation and robotic control
§ 5.4 **Fabrication system**: defines the fabrication process and constraints.
§ 5.5 **The physical-digital workflow** associates the design and fabrication processes
§ 5.6 **The framework of methods** integrates the developed methods in a toolbox of making

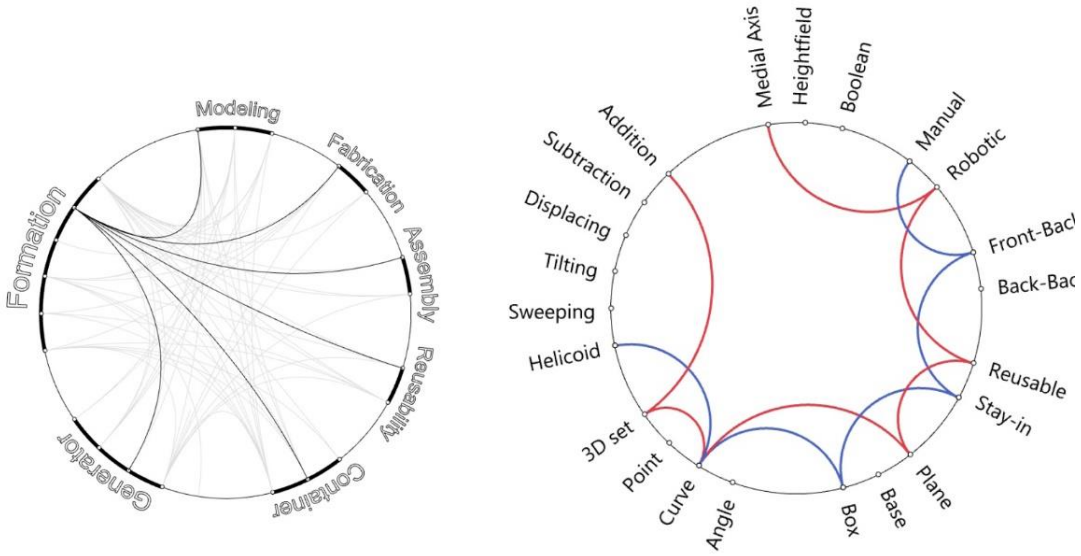


Figure 5.1 Diagram of the framework of making methods. And abstract diagram (left), and a representation of helicoid making methods in blue, and robotic deposition in red (right)

## 5.1 Design system: material formation methods

The design system addresses the main question of the research: what the sand wants to be? [55] The main driver behind the question is the morphological capacity of sand, which arises from its formability and its formation processes. The study speculates the form of the material and the means by which it can be instrumentalized as a design tool. It explores the interplay between sand formability, representing the material agency, and its formation process that stands for the architect's authorship.

**The formability of sand**, as discussed in chapter 2, relies on: (i) its phase changing behavior (SPB) from liquid to solid, and (ii) its self-organization behavior (SSB) that generates constant angle surfaces under gravitational forces. While **the formation process**, as will be discussed in this chapter, refers to (i) the external forces acting on the material, and (ii) the boundary conditions in which sand is formed. The design of the physical context of formation is of great importance in the design system as it is the means by which the architect negotiates with the material. The design research tends to cede the designer's authorship in favor of the material agency to examine the formation methods that can be teased out from the material logic without 'forcing' external ideas. The architectural creative is nevertheless maintained in the setting of formations methods and their interchanges. The creative will of the architect unfolds even more fully through the variations of the highly diverse parameters of the boundary conditions.

To address the research question, a theoretical and an experimental study are conducted. The theoretical study aims at developing an in-depth understanding of the material capacity and its architectural formation possibilities. It reviewed the prior art that implemented sand behavior in architectural design in chapter 1 and studied the material behavior and the geometrical principles of surface of constant slope in chapter 2. While the experimental research in this section defines the formation methods based on the observations and analyses of iterative physical and digital experiments of material formation. The section defines the formation methods, their parameters, and tools. The study provides the morphological typologies that are necessary for the geometrical analysis, the generation algorithms, and the fabrication process which will be discussed in the following sections. Finally, the formation methods are examined in the last chapter through prototyping.

[55] The question is evoked based on Louis Khans's quote "… *you must ask brick what it wants or what it can do* …" Louis.I.Kahn, 1991[14]. Chapter 1 discusses the interpretations of Khans's conversation with a brick which is most often quoted to support materiality approaches of design.

### 5.1.1 Formation parameters

The design system of ST is defined by a constant and two groups of variables for form generation as listed below and detailed in the following subsections:

1. **The constant** is the slope of sand and its value is considered constant along the research, 35°, the sand natural angle of repose.

2. **The variables** are the inputs of the system defined by the architect including:
   A. **The formation method** is the process of sand distribution (ex: deposition)
   B. **The boundary condition** is the context in which sand is formed, which includes:
      i. **The border**: the container where sand is formed (ex: box)
      ii. **The generators**: the elements that trigger the process (ex: points of deposition)
      The previous examples of variables return the following method: deposition in a box from points.

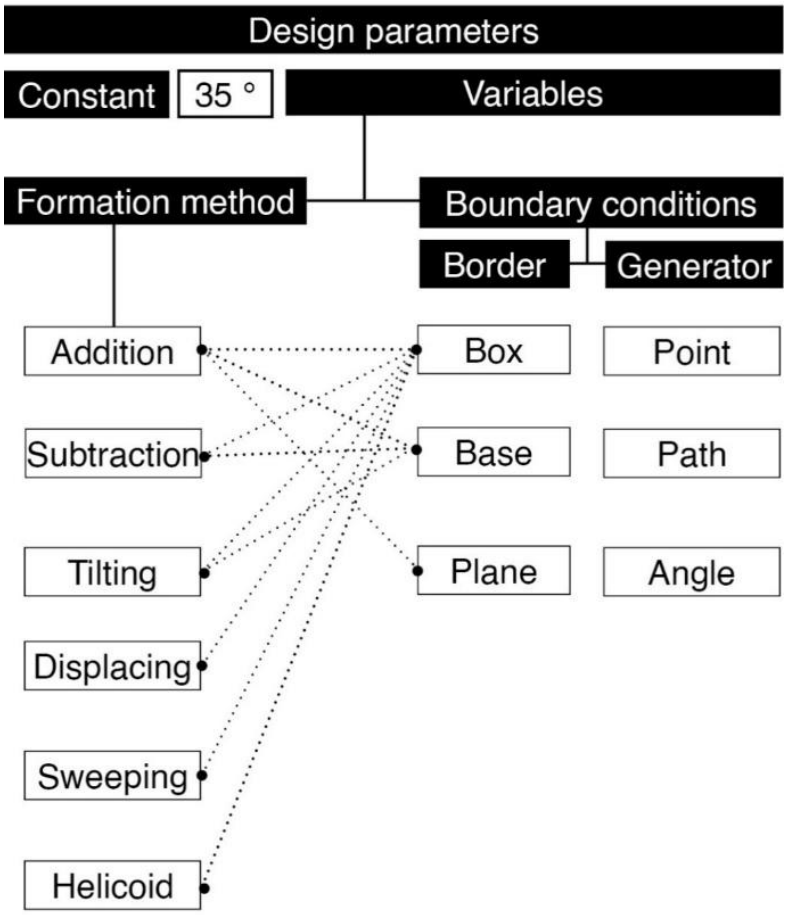


Figure 5.2 Diagram of the ST design parameters

#### 5.1.1.1 Formation methods

This work is not meant to be limited to one formation method, but rather to provide an interchanged set of methods that exhibit the morphological capacities of sand and their architectural possibilities. Following the above objective, and in respect to the design approach described above in § 5.1, the research defined six formations methods of dry sand based on the following actions.

1. ***Pouring*** sand on a plane to accumulate aggregated piles (additive process - § 6.1)
2. ***Releasing*** sand from a mass to shape engraved forms (subtractive process- § 6.1)
3. ***Tilting*** a mass of sand to relax the slope of certain faces § 6.26.1).
4. ***Displacing*** sand in a mass to shape engraved patterns (§ 6.3)
5. ***Sweeping*** sand surface to shape it according to a predefined profile (§ 6.4)
6. ***Helicoid***: releasing sand from a designed container to create helicoid surface (§ 6.5)

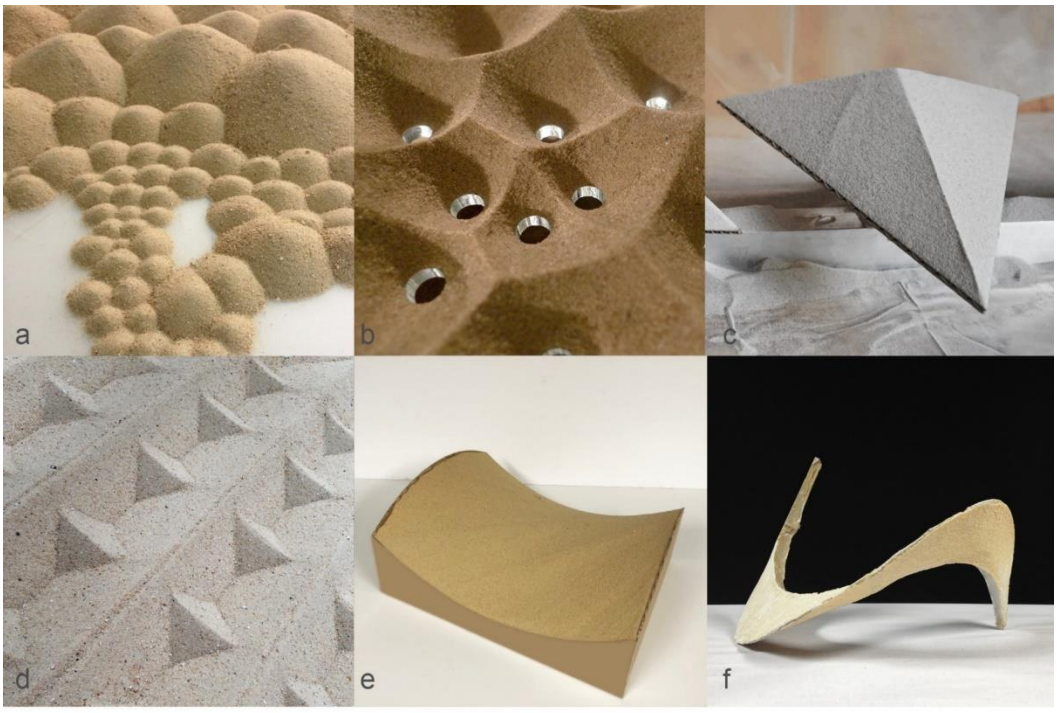


Figure 5.3 Sand formation methods. (a) Addition, (b) Subtraction [73], (c) Tilting, (d) Displacing, (e) Sweeping, and (f) Helicoid

Each method returns distinct morphological aspects that emerge from the interplay between the material behavior and its unique process of material distribution. Since the formation methods are considered as actions, then different actions can be coordinated to act sequentially on the same model. For example, sweeping then subtraction followed by addition as shown in Figure 5.4-d. The sequential process is enabled by the formability of sand, which allows iterative modifications of the form. The integration of formation methods extends the morphological capacities of the design system and enables hybrid formations, yet the trace of each action can be observed in the model.

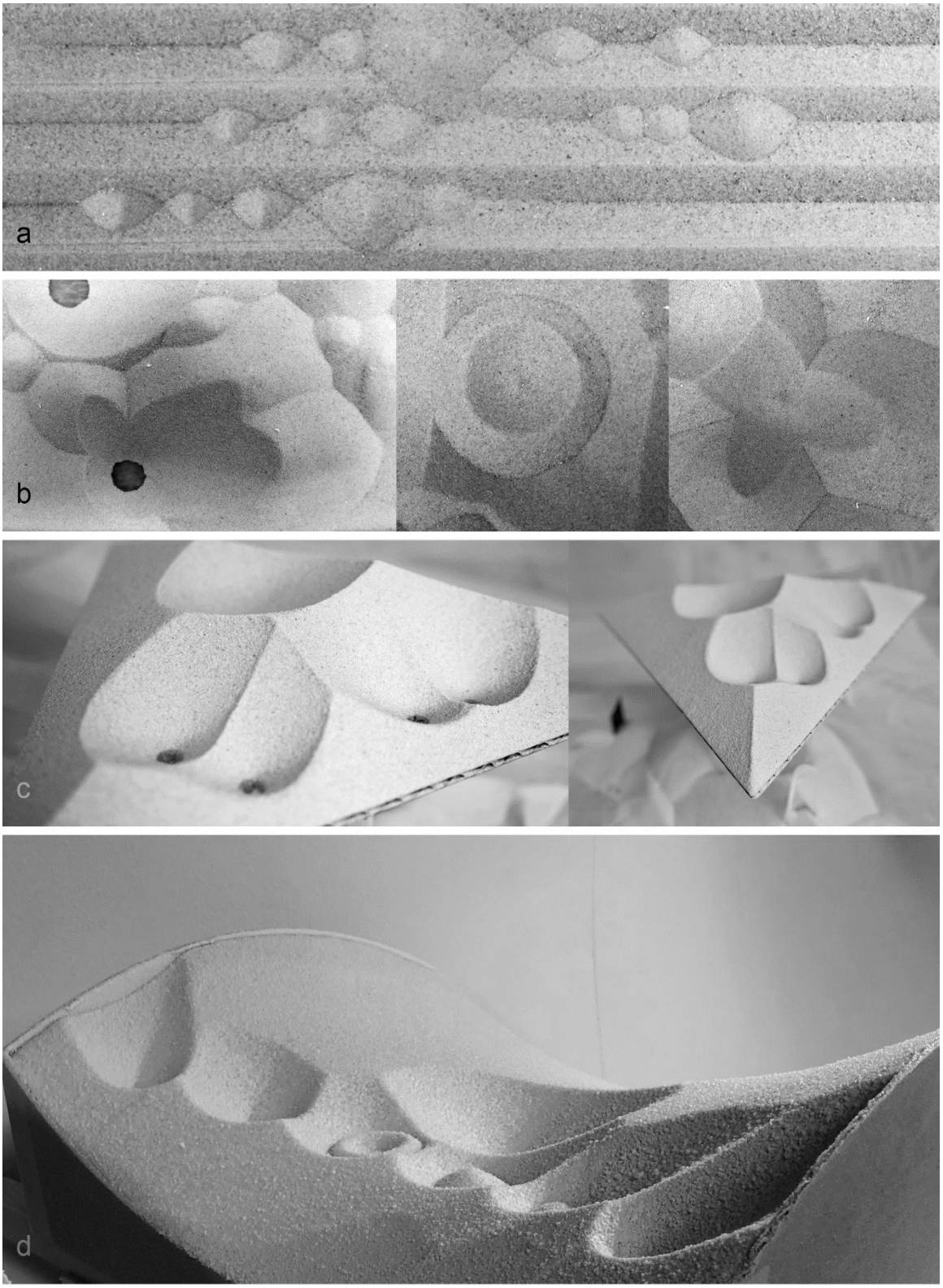


Figure 5.4 Mixed formation methods: displacement then addition (a), addition and subtraction (b), addition, subtraction then tilting (c), and sweeping followed by subtraction then addition(c)

#### 5.1.1.2 Boundary conditions

Each formation method has a distinct morphological effect that depends on the physical context where sand is formed, herein, the boundary conditions. This subsection defines two groups of boundary conditions (the border, and the generators), and identifies their types.

**A. The border** is the container where sand is formed, such as a box, a raised base, or a plane. The border is an essential constraint to fabricate it physically and to parametrize it digitally to generate the sand surface. The forms of sand emerge from the interplay between the formation methods and the border type. Each combination between the two constraints defines a different typology of sand formation (ex: pouring in a box or tilting a pile). The possible interchanges between the formation methods and the containers types are illustrated in Figure 5.5. In the same figure, the letter 'G' indicates the conditions that might be affected by the generators.

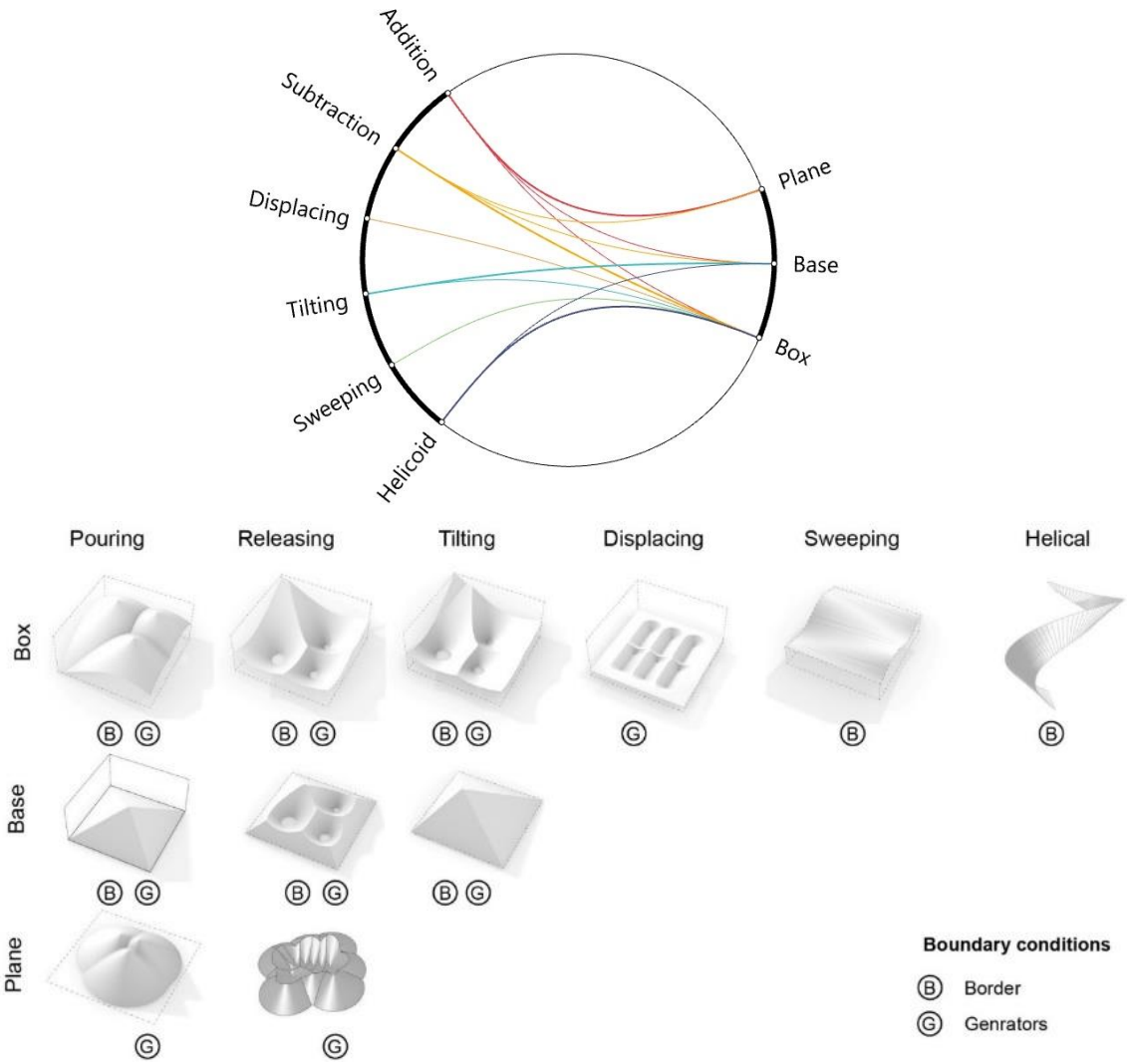


Figure 5.5 The interrelation between the formation methods, types of container, and boundary conditions.

B. **The generators** are the elements that trigger the formation process, such as the points or paths of sand deposition, angles of tilting, or the shape of the displacement tools. The types of generators are grouped in four sets and illustrated in Figure 5.6 in an abstract shape[56] of a hollowed non-standard container:

   a. **Open or closed curves** (ex: releasing hole or deposition path)
   b. **Curvature:** rectilinear or curved
   c. **Direction:** concave or convex
   d. **The angle condition of the corners**: acute, right or reflex.

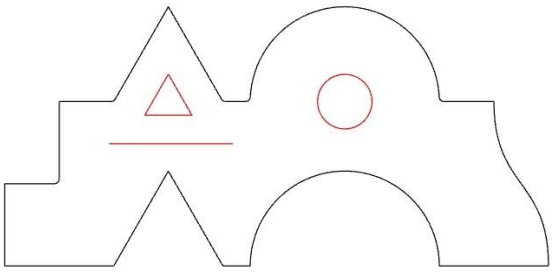

Figure 5.6 An abstract shape that represents the different typologies of generators in a hollowed non-standard container.

If the formation methods are limited to six actions, the boundary condition is the architect tool to unfold almost infinite formation possibilities. Since the boundary conditions are assigned as points and curves, then their shape, height, and distributions in the container are the parameters of the design system. The variability of the system parameters allows the exploration of unlimited configurations not only in the virtual space of a computer but also in the materialization process allowed by sand formability. The effect of the variability of boundary conditions on the emergent formations is discussed in the following chapter in accordance with each formation method. It is essential to parametrize the variables to communicate them as inputs in the surface generation algorithms in § 5.3. The design inputs are parametrized according to the following logic:

a. Since the formation methods are actions, they are then represented by vectors to inform the direction of slope of sand.
b. The boundary conditions whether the border or the generators are assigned as points or curves, which might represent for instance the shapes of container, holes, deposition path, or shape of displacement tool or sweeping edge.

The definition of the range in which these parameters can be operated upon, and yet remain coherent with the material, fabrication, and construction constraints, is the critical task of the design system.

[56] The shape is used in this work to assess the capacity of the developed algorithms in modeling different curves typologies as will be detailed in § 5.3.

### 5.1.2 Formation tools

In this research, the toolset used to enact the formation process includes:

**1- Sandbox**, with a solid or perforated base used in the subtraction method of formation.

**2- Vacuum machine** for sand subtraction method.

**3- Six-axes robotic arm** to perform addition, subtraction, displacing and tilting methods of formation.

The advantage of the vacuum machine, in comparison to the perforated sandbox, lays in its capacity of processing on almost any path shape. This advantage returns a practical design tool without consuming time and materials for the fabrication of customized perforated bases. Moreover, it can be mounted on the robotic arm.

Figure 5.7 A vacuum machine is used for removing sand in the subtraction method of formation

**The robotic arm**

A six-axes industrial robot, ABB-IRB-1600, at ENSA Paris-Malaquais is used for the robotic sand formation experiments conducted in this thesis. To operate different formations methods the robot is equipped with a tool-holder on which four simple end-effectors are mounted (Figure 5.8).

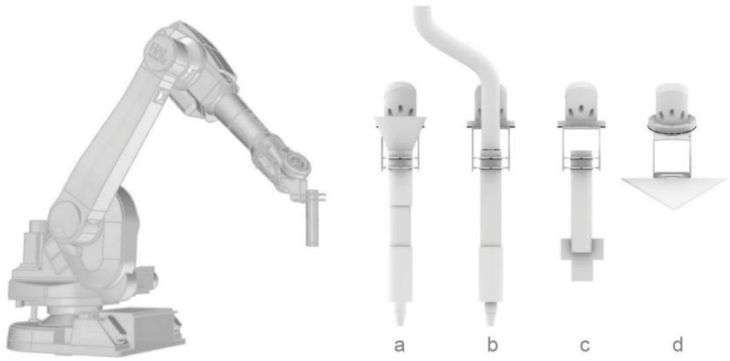


Figure 5.9 The six-axes robotic arm and the mountable end-effectors, (a) pouring funnel, (b) subtraction vacuum machine, (c) displacement plate, and (d) tilting base.

The engagement of robot in the materialization process allows the synthesis of design and materialization processes. Since the robot operates directly from the input data of boundary conditions (planes, points, and curves), a direct link between design and material is established. The robot is then considered as a physical means of design exploration. Such advantage evoked two research interests in robotic sand forming:

1. Extending the formation processes by coupling the multi-functionality of the robot and the formality of sand. This is possible by mounting simple custom tools on the robot arm to process deposition, releasing, displacing, and tilting formation methods (see chapter 6).
2. Negotiating the precision of the robot and the 'almost' accurate constant slope of sand to realize unique material expressions that are otherwise hard to achieve (Figure 5.10).

Figure 5.10 Robotic patterns generated by displacement, addition and tilting methods

To examine the interplay between the machinic and natural logics of precision it is necessary to:

A. Set up the robotic control code to assign the design parameters into attributes, simulate the trajectories, and generates the control commands for physical execution (see § 5.4).
B. Define the relationship between the robotic parameters such as trajectory, speed, and wait time and the parameters of the emergent sand forms such as height and width foreach distribution method (see § 6.1.3 for example for the deposition method of distribution).

## 5.2 Geometry of sand piles

Although the slope of the sand is constant, the emergent sand formations in this work range widely from simple to complex aggregations of solid and hollowed piles, and from flat to ruled and doubly ruled surfaces. Such variation is evoked by the formation methods and the boundary conditions as introduced in the previous section and will be detailed in the final chapter. The variety of such structures necessitates the examination of their underlying order and its parametrization to inform the modeling technique in the following section.

In contrary to the formal approach of design, which assigns materials to predefined geometries, this section analyses the geometry of the material, which results from material behavior and processes. The objective is to communicate the material behavior, the design system, and the modeling techniques by the material geometry to construct the design system of sand tectonics. Through a feedback loop of observation of physical models, examination of geometrical principles, and assessment of digital models, this section defines four fundamental concepts of material geometry: slope, conic sections, Voronoi diagrams and medial axis. These concepts support the physical and digital constructability of sand piles in this research as will be detailed.

### 5.2.1 Constant slope

Sand piles are surfaces of constant slope (SCS) for which the angle of repose $\theta$ is constant at all points in respect to a horizontal plane. In this research, a constant value of $\theta$ is used, 35°, which is a common value of the angle of repose of sand (see § 2.3). Through trigonometric functions, the tangent of $\theta$ defines the relationship between the height $h$ of the ridge at point $r$ and the length $d$ between point $m$ on the medial axis and point $b$ on the boundary (Tan 35°=$h/d$=0.7002).The length of the ruling $s$ can thus be driven from $\theta$ and either $d$ or $h$ (Figure 5.11). Since the slope is constant and the medial axis is the central axis of the boundary and at the same time it is the vertical projection of the ridge, then the boundary and ridge curves can be derived from each other's by the information of the medial axis and the slope. The trigonometric relationship between the curves of the pile is the base of the modeling technique as will be introduced in the algorithm in § 5.3.

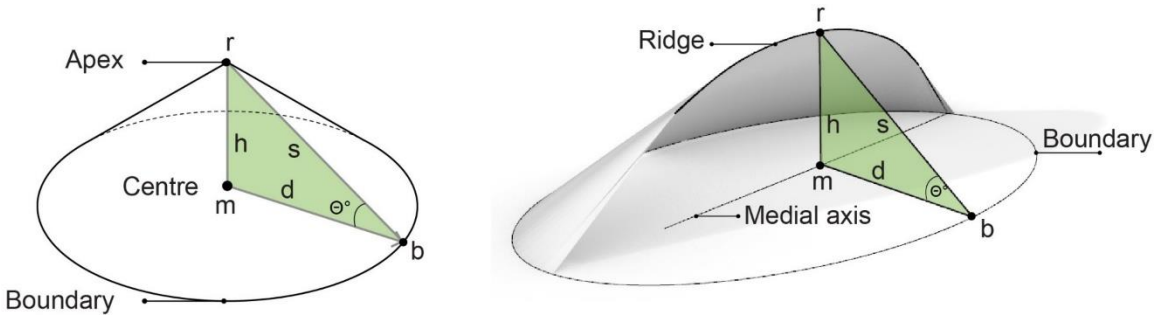


Figure 5.11 Trigonometric relationships between the ridge, boundary, and medial axis curves of a sand pile.

### 5.2.2 Conic sections

The study of conic sections is of major importance for the addition and subtraction methods of formation to articulate the relationship between the cones distributions and their emergent ridges. Releasing sand from multiple holes generates a landscape of intersected cones where the holes are separated by sloped surfaces and sharp ridges. Since the shape of the ridges varies depending on the organization and height of the holes it is necessary to define the geometrical principles of the emergent formation. The ridges are conic sections that lies on the intersection plane between the cones. The type of conic section depends on the height and position of the intersected cones. In this research three conic sections are identified bellow and illustrated in Figure 5.12.

A- **Circular** if the two cones are on opposite bases and they share the same axes. Physically it occurs when sand is subtracted from the apex of a cone or added on the apex of a funnel.

B- **Elliptical** if the two cones are on opposite bases but they do not share the same axes. Physically it occurs if sand is subtracted or added on the surface of a cone or a funnel.

C- **Hyperbolic** if the two cones have coplanar but acentric bases. Physically, it arises from the intersection of two adjacent cones or funnels, which is the dominant case in this work.

It is important to distinguish between two types of hyperbolic sections that occurs due to the effect of the cones heights.

C1- **Right hyperbolic** if the two cones have the same height. The projection of the right hyperbola returns a straight line that divides the border into two identical cells.

C2- **Inclined hyperbolic** if the two cones have different heights. The vertical projection of the inclined hyperbola is a hyperbolic curve that divide the border into two cells with different areas. The curvature of the hyperbola increases proportionally with the difference between the heights of the two cones and the curvature points toward the higher cone Figure 5.13.

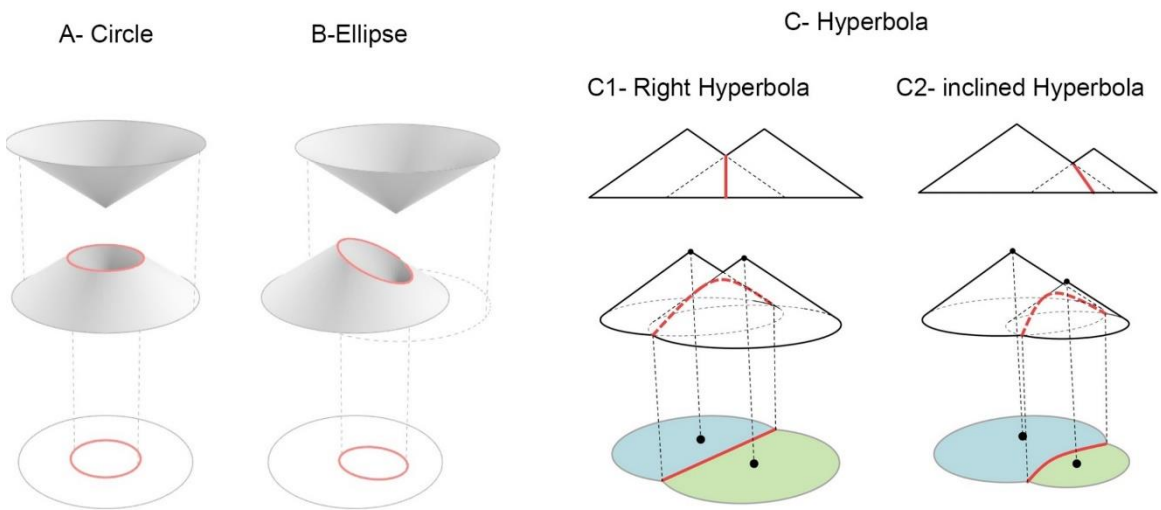


Figure 5.12 Types of conic sections that occur in sand formation and their relevant conditions of cones.

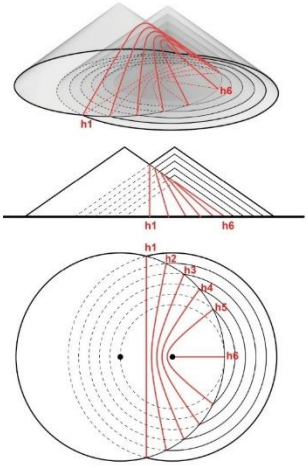


Figure 5.13 The curvature of the hyperbola increases proportionally with the difference of the heights of the cones. The curves point towards the smaller cone.

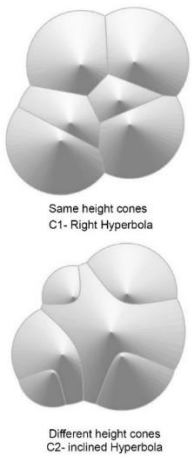


Figure 5.14 The intersection of cones with the same height returns straight lines (ordinary Voronoi), while in case of different heights the intersections are hyperbolics (Weighted Voronoi)

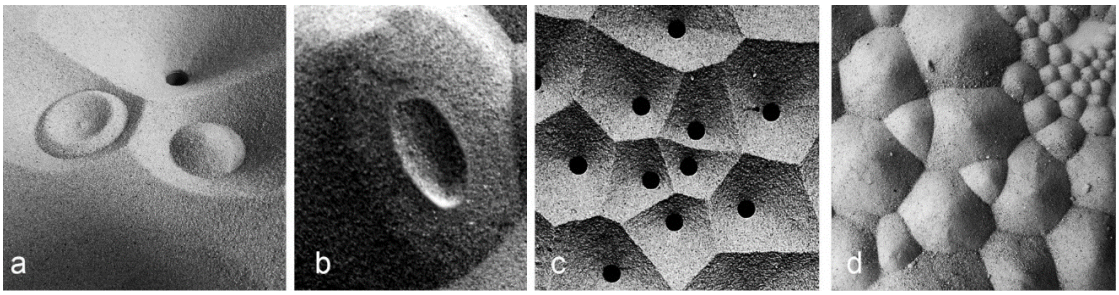


Figure 5.15 Conic sections in sand models. Circle (a), ellipse (b), right and inclined hyperbola (c [73] & d)

Physically, it is noted that sand grains flow in a linear path (the steepest slope - rulings) to their closest hole. The gradual collective behavior provokes a landscape of valleys separated by ridges, where the latter define the boundary of the region of influence of ach hole. The surface is then divided into regions based on a distance function, which is the definition of a geometrical method of surface tessellation termed Voronoi diagram as will be detailed in the following section.

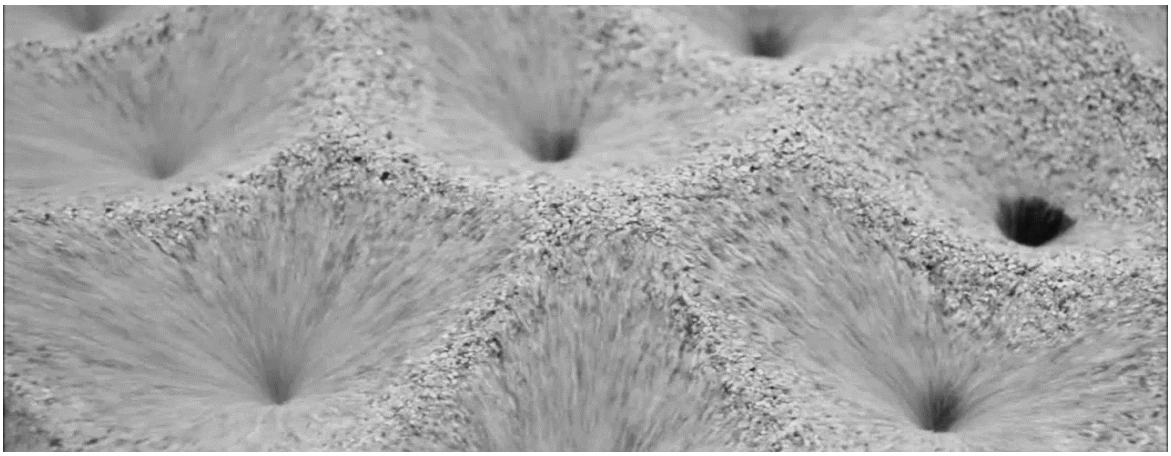

Figure 5.16 Sand falls in a linear path towards the closest hole, which define the boundary of influence of each hole.

### 5.2.3 Voronoi diagrams

In this research, Voronoi diagrams plays a key role in the analysis and construction of surfaces of constant slope. Their importance for this works lies in being the projection of conic intersections, a method of points clustering in the Heightfield algorithm (§ 5.3.2), and a method of defining the medial axis in the Medial axis algorithm (§ 5.3.3). Understanding the structure of Voronoi diagrams allows to define the relation between sand self-organization behavior, its formation and modeling methods. This section defines first the elements and structure of the simple (generalized) Voronoi diagram, then presents its second type the Additively weighted. Next, a geometrical method of constructing both the simple and the weighted is introduced. Finally, the challenge of computing the Additively weighted Voronoi diagram in this research is presented.

Voronoi diagrams are mathematical methods of surface tessellation based on the distance and weight of a set of points on a surface. In two-dimensions space, Voronoi diagram tessellates a plane into convex regions based on the Euclidean distance between **generator points (**also called **sites**) and **field points** on the surface. Each region encloses all the points on the surface that are closer to its associated generator than to any other generator [192]. The generator points are predefined points of influence enclosed at the centers of the cells. Each point has a range of influence based on their locations. **The Voronoi cells** are convex polygons, which boundaries consists of straight edges and vertices. **The edges** of the cells are bisectors of the Delaunay triangulation lines, which join the generator points. Every point on a Voronoi edge is equidistance from at least two generators. **The vertex** of the cells is the intersection of at least three edges, and so it is equidistant from at least three generators. Let $S$ be a two-dimensional Euclidean space in $R^2$ that includes a set of generating sites $\{S_1, \ldots\ldots S_n\}$, and a set of field points $P = \{P_1, \ldots\ldots P_n\}, n \geq 2$. $S$ is tessellated by the set of sites into clusters in which any point is closer to its generator than to any other generator point. The Euclidean distance $d_E$ between a site $S_1 = (S_x, S_y)$ and a field point $P_\mathrm{i} = (P_x, P_y)$ in $S$ is defined by the following distance function [193,194].

$$d_E(S_1, P_\mathrm{i}) = \|S_1 - P_\mathrm{i}\| = \sqrt{(S_x - P_x)^2 + \left(S_y - P_y\right)^2} \text{ (Equation 5.1)}$$

**The Weighted Voronoi diagram** is a variant of the simple Voronoi, which uses some combination of distance and a weight associated with each site. Five types of weighted Voronoi are reported [193,194]. This research is interested in the **additively weighted Voronoi** type (also known as the hyperbolic Dirichlet tessellation) as it returns hyperbolas as boundaries for the cells (in case of different weights) and line segments (in case of equal weights), which meets the patterns generated by the sand. In the additively weighted Voronoi diagram, the positive weight is subtracted from the distance between the points and the sites [193,194]. The distance from a point $p$ to site $s_i$ with assigned weight $w_i$ is

$$d_E(S_1, P_\mathrm{i}) = \|S_1 - P_\mathrm{i}\| - w_i = \sqrt{(S_x - P_x)^2 + \left(S_y - P_y\right)^2} - w_i \text{ (Equation 5.2)}$$

Figure 5.17 compares simple and Additively weighted Voronoi diagrams using an applet of Wolfram demonstration[57]. A random set of six sites is given with associated weights. The ordinary Voronoi diagram (left) returns polygonal regions in respect to locations, and the Additive weighted Voronoi (right) returns hyperbolic regions in respect to locations and weights.

| Voronoi Diagram | Simple | Additively Weighted |
|---|---|---|
| metric | $d_E(S_1, P_i) = \|S_1 - P_i\|$ | $d_E(S_1, P_i) = \|S_1 - P_i\| - w_i$ |
| Region segments | Linear | hyperbolic |

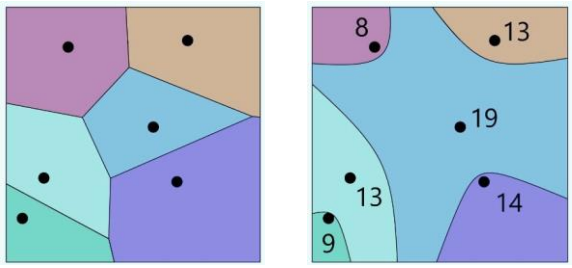


Figure 5.17 Comparison of ordinary and Additively weighted Voronoi diagrams [193,194].

The Voronoi diagrams can be also be obtained from the orthogonal projection of the lower envelope of intersecting cones [195], a technique used in computer graphics to compute discrete Voronoi diagrams [196]. To illustrate the lower envelope method, the following example is given based on [195]. In a set of six weighted points, a circular cone is drawn from each point with a height corresponding to the weight of the point. The weights are uniform in case A, and random in case B. The orthogonal projection of the lower envelope of intersecting cones in case A, returns simple Voronoi diagram with polygonal regions. But the different weights in case B returns Additively Weighted Voronoi diagram with hyperbolic regions. The lower envelope corresponds to the analysis of intersecting cones in the previous section (see Figure 5.14).

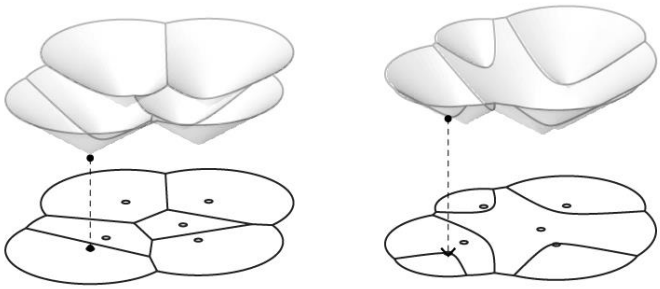

Figure 5.18 the lower envelope of intersecting cones is a geometrical method to define Voronoi diagrams

There Voronoi diagram is an interdisciplinary concept that can be found in many different kinds of natural structures [99] as well as a mathematical method of clustering data in many disciplines[135]. The reported algorithms [135,197] to calculate standard and weighted Voronoi diagrams from points clouds can be generally divided in two phases: the first clusters the points in respect to their Euclidean distances and weights, while the second phase defines the curves

[57] https://demonstrations.wolfram.com/WeightedVoronoiDiagrams/

of the closed regions (the cells). Grasshopper provides a component to calculate the simple Voronoi diagram from 2D points, but, until now, no methods for calculating weighted Voronoi from 3D points is available in Grasshopper. Another limitation of the grasshopper component that it is a closed component, i.e. inaccessible for editing to develop it to higher level of Voronoi. This limitation is challenging for this research as it restricted the possibilities of the design system to only 2d organizations of points without the implementation of weights (herein the height of cones as an organization of 3D points).

To overcome this challenge, the research developed a custom component in Grasshopper for clustering 3D points based on the weighted distance function (equation 5.2), which is used in the Heightfield algorithm in § 5.3.2 . While in the Medial axis algorithm in § 5.3.3 , a similar approach is conducted but in Mathematica software. The aim is to apply the two phases of the weighted Voronoi algorithm, the clustering, and the definition of the boundary of the cells (hyperbolic curves). The process and limitations of the Mathematica algorithm are given along with the Medial axis algorithm.

### 5.2.4 Medial Axis

As indicated earlier in §5.2.1, the medial axis is the vertical projection of the ridge of a sand pile and the central axis of its boundary. This subsection defines the medial axis and introduces some methods to construct it from a given boundary, which is an essential phase in the modeling of sand piles as will be detailed in the Medial axis algorithm in § 5.3.3. An evaluation of the methods is given at the end of this subsection to define the optimal means for this research.

The medial axis[58] (*Ma*) is the central axis of a 2D shape. It is defined as the set of all points having more than one closest point on the closed boundary of a shape. The *Ma* has found applications in a number of areas that deal with shapes, e.g. shape analysis in computer graphics and shape recognition in biology [198]. Different computational methods to calculate[59] the *Ma* are discussed in [198,199]. This subsection introduces four methods, which are the most relevant to this work:

a. **Voronoi method**: the boundary curve of the given shape is sampled by a dense discrete set of points to capture the curve correctly. Then, the Voronoi diagram of the points is computed, which returns a Voronoi cell for each point. Since the Voronoi vertices interior to the curve are characterized by having at least two closest points among the sample points, they are then extracted to approximate the *Ma*. Another way

[58] The medial axis is also referred to as ‘topological skeleton’ or ‘descriptors of shape’.

[59] Exact *Ma* computation is possible only for simple shapes, but for free-form shapes approximations methods are widely used.

is by extracting the edges of the Voronoi cells that are interior to the curve but do not intersect with it [200].

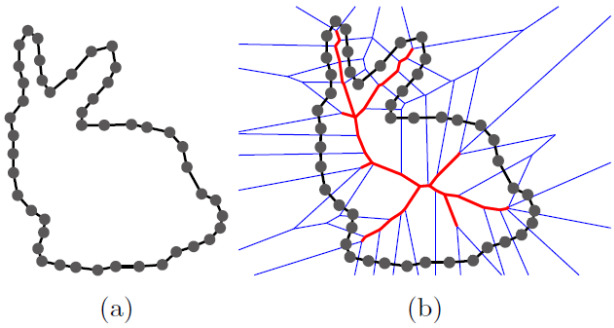


Figure 5.19 Definition of the *Ma* curve by the Voronoi diagram method. (a) Boundary sampling of a 2D shape, (b) The Voronoi cells of the boundary points (in blue) and the extracted *Ma* (in red) [200]

b. **Inscribed circles methods**: the *Ma* is defined as the locus of the centers of the maximal inscribed circles that are contained in a boundary curve and tangent to it in at least two points (Figure 5.20-left) [201].
c. **Conical intersections method:** the *Ma* is derived from the intersection of a set of cones, which apexes lies on the boundary. The boundary curve of a given shape is sampled by a set of points. For each point, a right circular cone is generated, then the cones are intersected by the Boolean union operation. The projection of the intersection curves on the boundary plane yields the medial axis (Figure 5.20-middle) [201].
d. **Offset method:** the *Ma* is defined by the trimmed offsets of the boundary curve (also known as thinning or grassfire method) (Figure 5.20-right) [202].

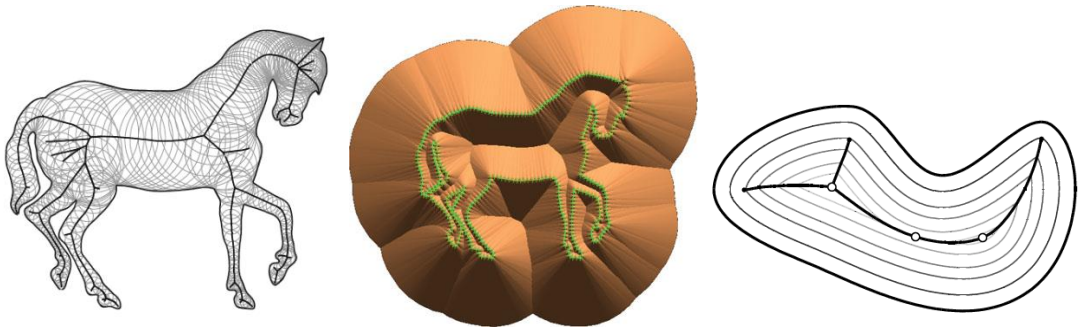

Figure 5.20 Definition of the *Ma* by the inscribed circles (left), the intersecting cones (middle), and the offset of the boundary methods (right) [201]

Physically, the *Ma* can be illustrated by pouring dry sand on a predefined boundary where the projection of the emergent ridge is the *Ma* of the boundary. Similarly, modeling of sand dunes is reported as a technique of visualizing the *Ma* on geographic maps [203] where the projection of the highest point of the ridge is the furthest point from the border [204].

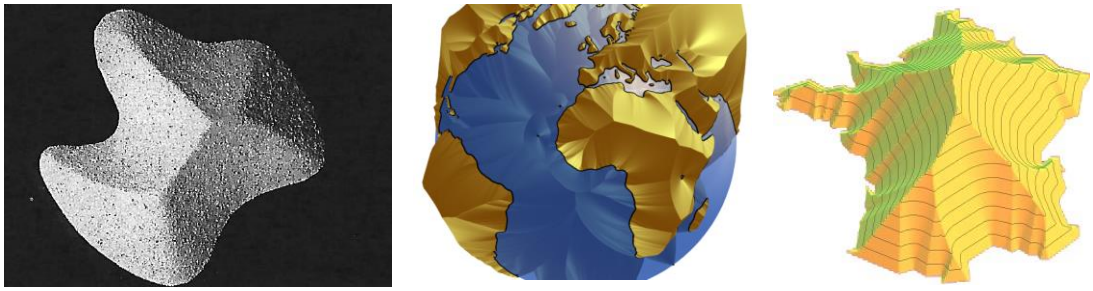

Figure 5.21 Physical illustration of the *Ma* by sand on a free-form base (left) [69], digital illustration by sand dunes on earth's continents (middle) [203], and France map (right) [204].

After the above introduction of the different methods of defining the MA, they are evaluated here against their applicability within the Rhino and Grasshopper (GH) environment of modeling used in this work. Among the four methods, Voronoi tessellation stands as the most efficient tool as a 2D Voronoi tessellation is a built-in component in GH and the extraction of the boundaries of the Voronoi cells to define the *Ma* is relatively simple (see § 5.3.4). The challenge of the inscribed circle method lies in the lack of an efficient method in GH for the generation of inscribed circles. While the offset method is limited because it demands trimming of the self-intersecting parts of offset curves, which add a complication to the process especially with free-form convex shapes. Still, the inscribed circle and offset methods can be applied for the reversed process, i.e., defining a boundary curve from a given *Ma* as will be detailed in § 5.3.5. Based on the above evaluation, the research employs the Voronoi method to define the *Ma* from a given boundary (Figure 5.22), and the inscribed circles and the offset methods to define the boundary curve from an input MA.

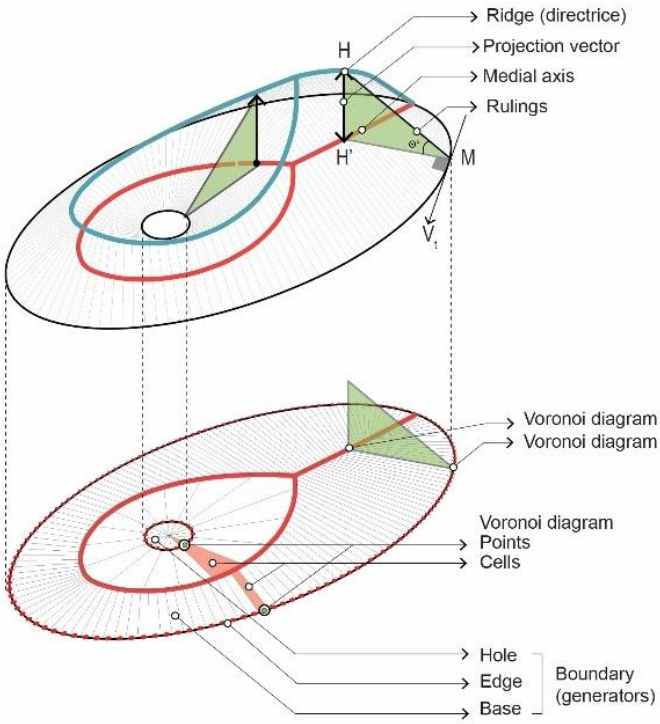


Figure 5.22 Geometrical construction of a hollowed sand pile from a given boundary using the Voronoi method

## 5.3 Modeling methods

The digital workflow of sand tectonics is introduced in this section through a sequence of custom digital tools that parametrically operate the workflow from form generation to fabrication setup. The digital tools are developed within Rhinoceros[60] and Grasshopper[61] CAD environments for form generation, and HAL[62] plugin for robotic control tasks.

The main objective of the digital workflow is to provide an efficient design tool to explore further morphologies that reach beyond the physical limitations[63]. The digital workflow is operated and presented here in four interdependent phases:

1. **Boundary design**: to input the data inferred from material, geometry, design, and fabrication.
2. **Form generation**: to explore the possible morphologies of the sand tectonics
3. **Manufacturing information**: to produce the formwork drawings and materials quantities
4. **Robotic control**: to generate the trajectories of the robotic arm.

The form generation algorithm aims at modeling four distribution methods, pouring, releasing, tilting, and displacing. The sweeping and helicoid methods have different approaches of modelling as will be discussed in their corresponding sections, § 6.4 and § 6.5, respectively. Although sand simulation as a particle system is a well-established technique, the interest of this research lays in the constructive logic of modeling, which associates geometry of constant slope, formation, and making methods.

Three surface generation codes are developed in this work based on the geometrical concepts introduced in § 5.2.

1. **Boolean method** is a straightforward technique of modeling based on conic intersection
2. **Heightfield method** emulates sand surfaces as field of points based on Weighted Voronoi function
3. **Medial axis method** construct sand piles as patches of ruled surfaces based on Voronoi and medial axis concepts.

The algorithms are first introduced then an evaluation of their efficiency in modeling the different distribution methods is given. This is followed by the manufacturing information and robotic control phases of the digital workflow. The efficiency of the algorithms is evaluated based on two principles:

---

[60] Rhinoceros is a 3D CAD software developed by Robert McNeel & Associates (https://www.rhino3d.com/).

[61] Grasshopper is a visual programming environment in Rhinoceros, developed by David Rutten (http://grasshopper3d.com).

[62] Hal is a robot control plugin for Grasshopper developed by HAL Robotics ltd in 2011 (https://hal-robotics.com/)

[63] Such as scale, density, time, and cost.

1. **Adaptability** by means of constructing the digital workflow as a flexible[64] framework that allows manipulating the different formations methods, the variations of boundary conditions while considering the material, fabrication, and assembly constraints.
2. **Productivity** refers to the speed and accuracy of the algorithm to engage with complex geometries and a large set of data while being a playful tool that induces rapid yet accurate iterations.

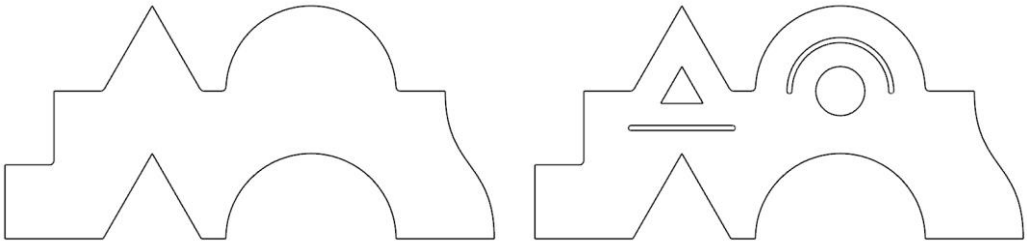

Figure 5.23 The abstract boundary shapes for the assessment of the algorithms. The shape represents different curves typologies of a sloid (left) and hollow pile (right).

The algorithms are introduced as pseudo-codes. i.e., the concepts and operating principles are presented, but the organizational operations are omitted[65]. Moreover, they are presented in their general form but their detailing and customization to meet specific formation tasks are detailed in the final chapter in accordance with the formation techniques.

[64] The objective of flexibility is derived from the logic of sand where a simple rule, the slope, underlines the variability of the emergent morphologies.

[65] such as data tree processes in Grasshopper which organise the flow of data in hierarchical structures of nested lists.

### 5.3.1 Boolean method

The Boolean algorithm is a parametric modeling method of conical surfaces used by the 35 degree project. On a set of intersected cones, the Boolean algorithm conducts Union operation, which trims the shared areas of the cones and creates a single polysurface from the unshared areas. The method is introduced here, and its advantages and limitations are discussed.

#### 5.3.1.1 The parameters and procedure of the Boolean method

Based on the Boolean logic, a simple algorithm is developed to model conical surfaces. The typical procedure is as follows: first, subtraction circles or deposition points are given as inputs from which right circular cones are generated on the same base plane. The height *Hc* and radius *Rc* of the generated cones are defined by the trigonometric functions with respect to the slope of sand *θ* and its height in the box *Hs* (Figure 5.24). Then, Boolean union is applied to the intersected cones to create a conical polysurface. Finally, the polysurface is trimmed with the input border curve, which represents the sides of the box.

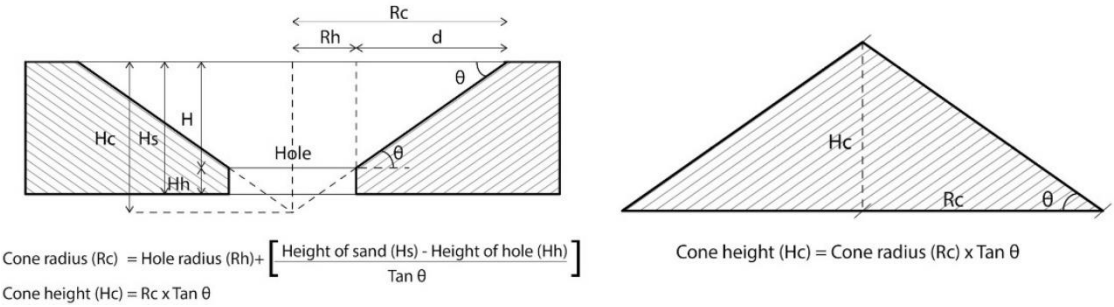


Figure 5.24 The trigonometric functions of the subtraction and addition methods of sand formation

#### 5.3.1.2 Evaluation of the Boolean method

**A- Formation methods**

In terms of sand formation methods, the algorithm allows the modeling of subtraction from a pile, addition in a box, or on a plane (Figure 5.25), as well as a mixed formation method of both addition and subtraction (Figure 5.26). However, the displacing and tilting methods of formation are not possible to model with the Boolean method.

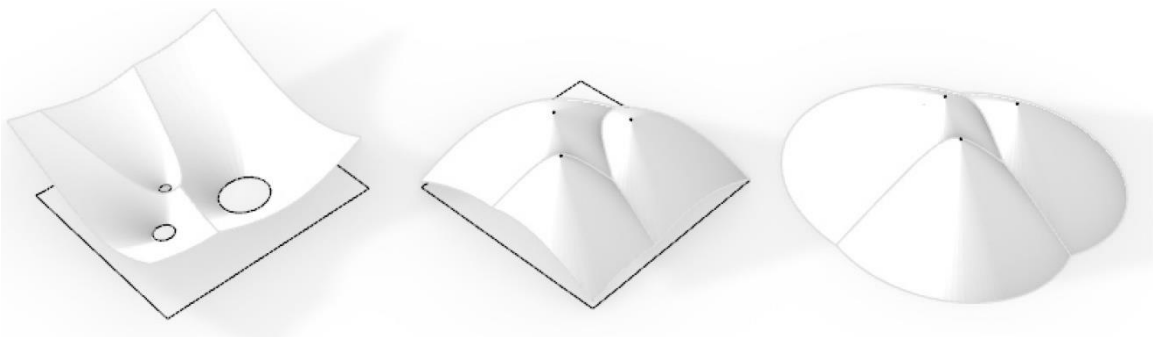

Figure 5.25 Sand formation methods modelled by the Boolean algorithm: subtraction from a box, addition in a box and addition on a plane

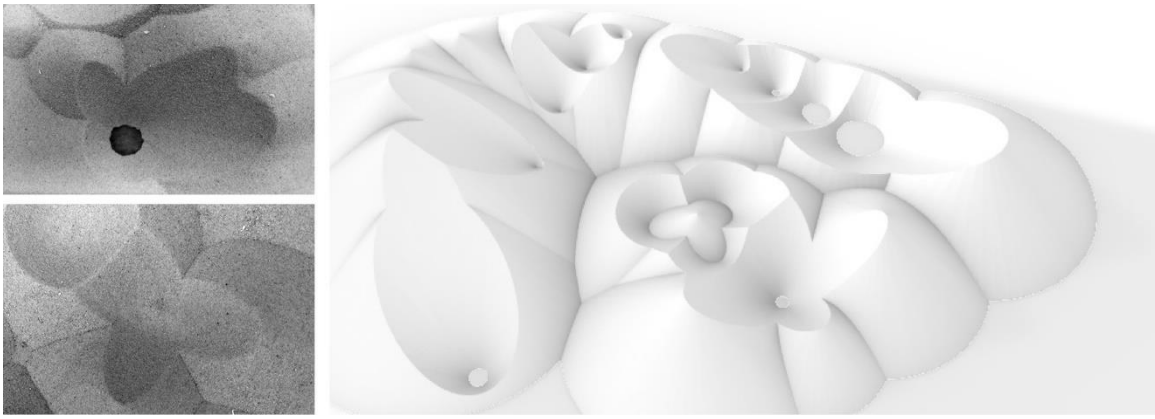

Figure 5.26 physical and digital models of the addition and subtraction mixed method of formation

**B- Boundary conditions**

In terms of boundary conditions, a major advantage of the algorithm is that it allows the modeling of holes and/or points at different heights (Figure 5.27). However, its dependence on the intersection of cones has two major drawbacks: (i) it limits the algorithm to circular holes in subtraction and points in deposition (Figure 5.28). (ii) it increases the calculation time due to the union operation which computationally is not a very efficient method especially with a large number of cones. To overcome these limitations, it is essential to develop other algorithms that are not dependent on intersection operations and can consider other shapes of holes and path-based deposition as will be introduced in the following algorithms.

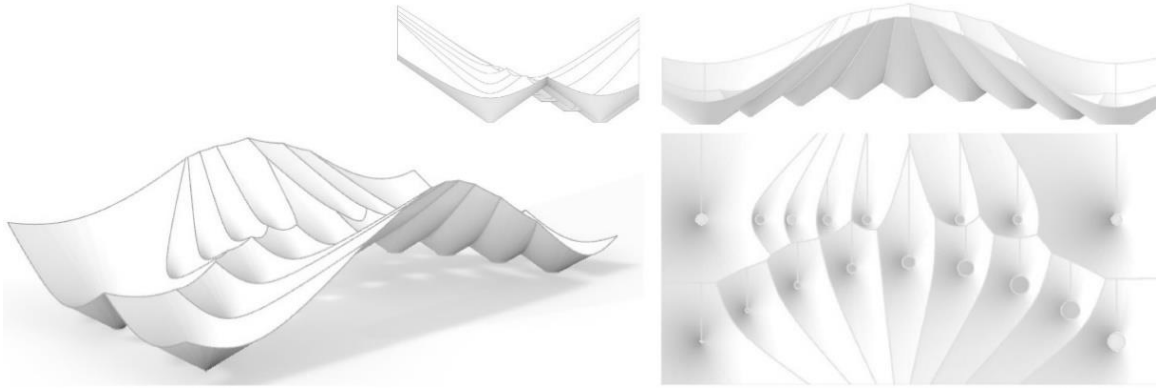

Figure 5.27 The intersection of cones with different radii allows the modeling of holes at different heights

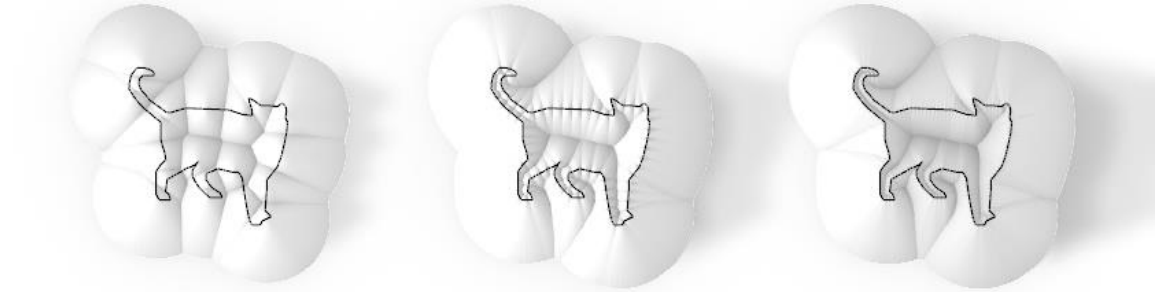

Figure 5.28 The deposition path is processed by sampling the boundary curve which returns patches of cones. The sampling density enhances the resolution of the surface but increases the calculation time.

### 5.3.2 Heightfield method

The Heightfield algorithm (HF) emulates sand surface by a field of points which heights are defined by their distance to their closest boundary and the slope of sand. The procedure of the algorithm is detailed below using a hollow pile as an example. The pile is physically formed by pouring sand on an oval base perforated with circular holes at different heights. The diagram in Figure 5.31 illustrates the workflow (input, process, and output) of the HF algorithm.

#### 5.3.2.1 The parameters and procedure of the HF algorithm

A. **Initialization:** to create an initial field of points a mesh is generated from the input boundary curves then the mesh vertices are extracted as the required points.

B. **Clustering:** to define the range of effect of each boundary, the points are clustered and assigned to their nearest boundary. The shortest distances between each point and each boundary are first calculated, then sorted to define the shortest distance to the closest boundary. The range of effect of the boundary decreases proportionally with its size and inversely with its height (Figure 5.29).

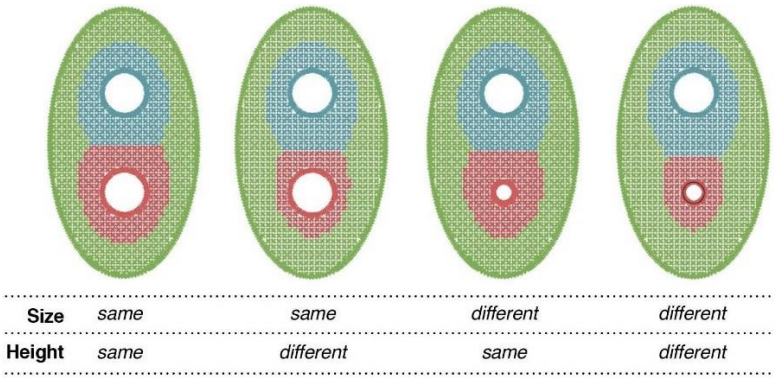


Figure 5.29 Effect of the size and height of the holes on their range of effect.

C. **Displacing:** the points are then displaced with a normal vector, which length $v_L$ is defined by the trigonometry function $v_L = ((d_s * \tan \theta) + h)$ where $d_s$ is the shortest distance to the closest boundary, $\theta$ is the slope of sand, and $h$ is the height of the boundary curve.

D. **Generation:** finally, a 3D mesh is constructed from the displaced points. The accuracy and sharpness of the 3D mesh are informed by the density of the points, which can be controlled by the lengths of the edges of the input 2D mesh (Figure 5.30).

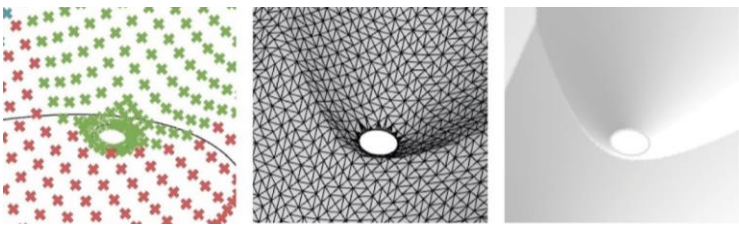

Figure 5.30 The construction of the mesh from the displaced points. The ridge sharpness increases proportionally with the density of points.

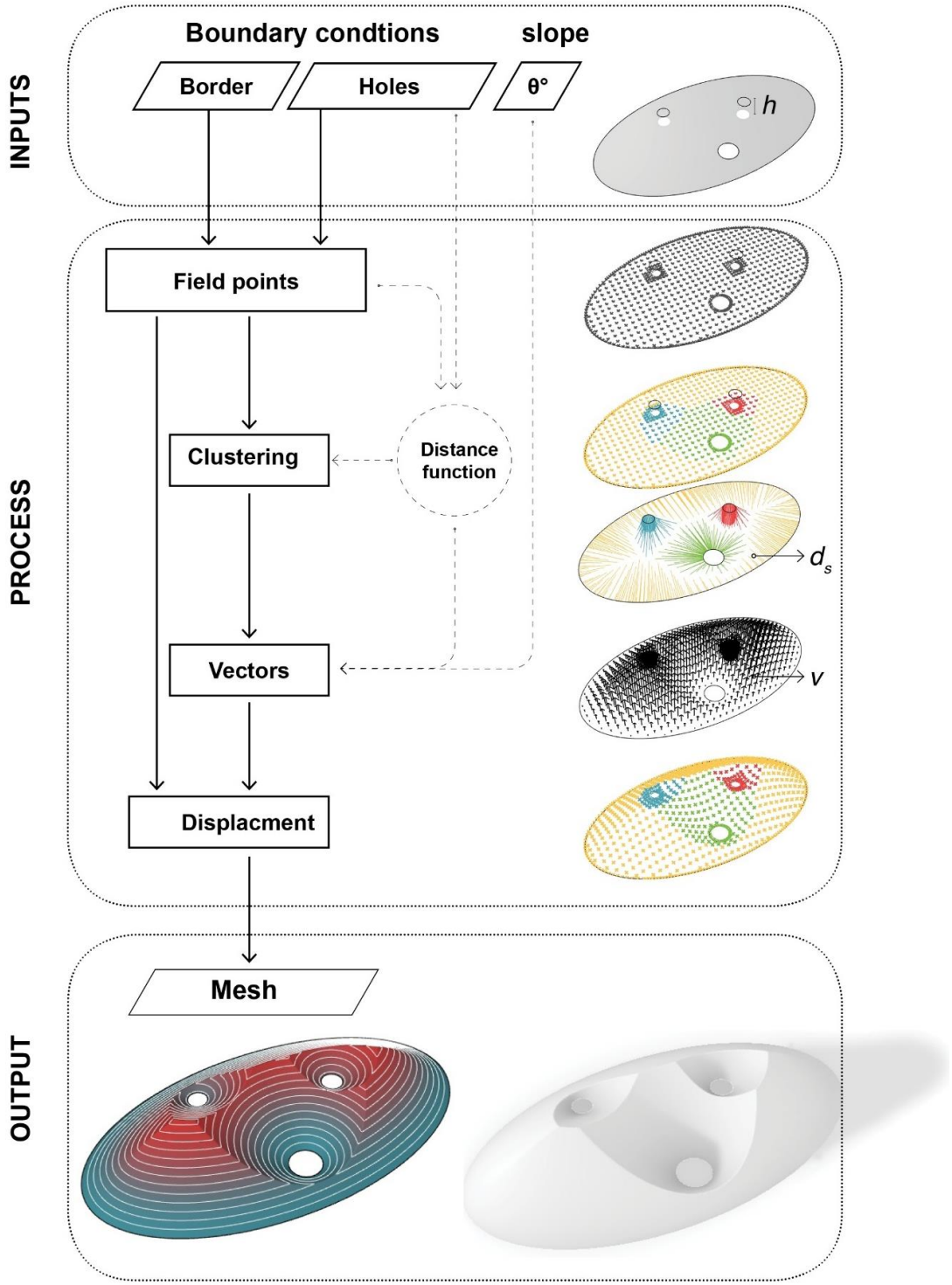


Figure 5.31 Diagram of the Heightfield algorithm showing the key operations

### 5.3.2.2 Evaluation of the Heightfield method

#### A- Formation methods

The HF algorithm is capable of modeling the four formation methods (addition, subtraction, tilting, and displacement) by controlling the conditions of the input parameters (the border, holes, and vector). Some of the possible variations of the conditions and their associated formation methods are shown in Figure 5.32 and discussed below.

1. The border can be considered as an obstacle, i.e., the side of a sandbox as in A, B, and C. In this case the border curve is used in the generation of the field points but not in the clustering process. The border can also be considered as an attractor, i.e., a plane that receives sand on top but releases excessive sand from its border as in D, E, and F. In this case the border curve is considered in the point generation and the clustering processes.
2. The holes can be considered or omitted to represent hollows (B, C, E, F) and solid piles (A, D).
3. The altering of the vector angle between normal, inversed, and tilted allows additive (A, D), subtractive (B, E), and tilted piles (C, F) respectively.

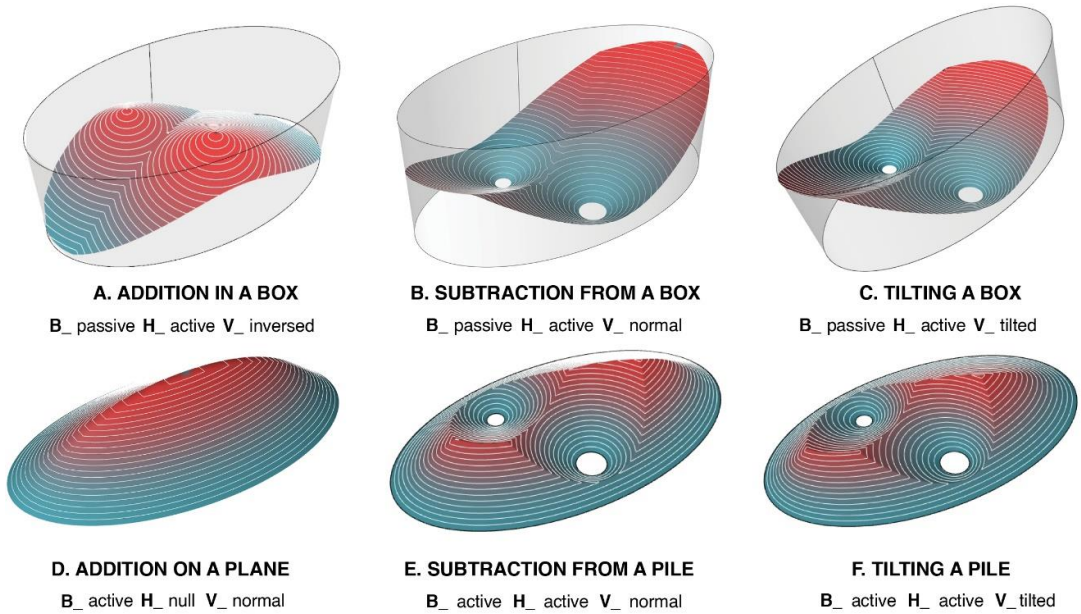


Figure 5.32 The HF algorithm can model three distribution techniques each in two settings by changing the conditions of the border (B) and holes (H) being active or passive, and the vector direction (V) being normal, inverted or tilted.

#### B- Boundary conditions

Since the logic of the HF algorithm is based on modeling the sand surface as a field points, it is not dependent on the shape of holes or border curves. Hence, it is capable of modeling different curves typologies of boundary conditions for either solid or hollow piles as shown in Figure 5.33. Another advantage of the HF algorithm is its capacity to consider holes at different heights due to the weighted distance function that includes the height of the holes (Figure 5.34). The main drawback of the method is the time of calculation, which increases with the density of the points.

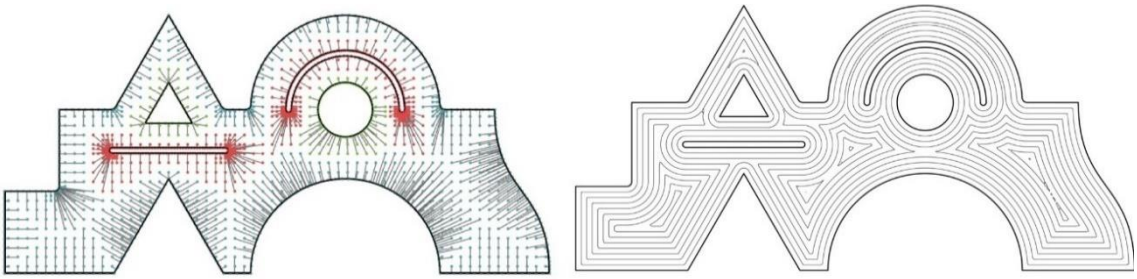

Figure 5.33 Evaluation of the adaptability of HF algorithm in considering different typologies of boundary curves of a solid pile (left) and hollow pile (right). The shortest distances from each field point to its closest boundary and the contour lines of the emergent surface are illustrated.

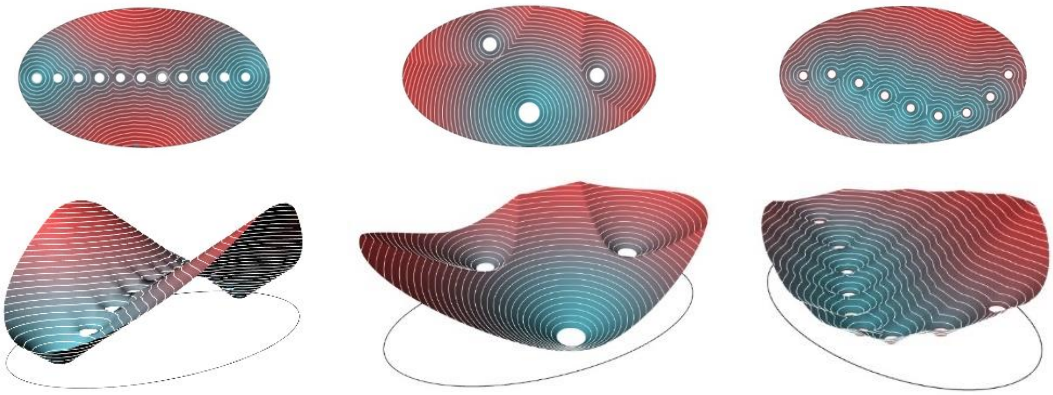

Figure 5.34 The mesh from points logic of the HF algorithm allows the modeling of holes at different heights

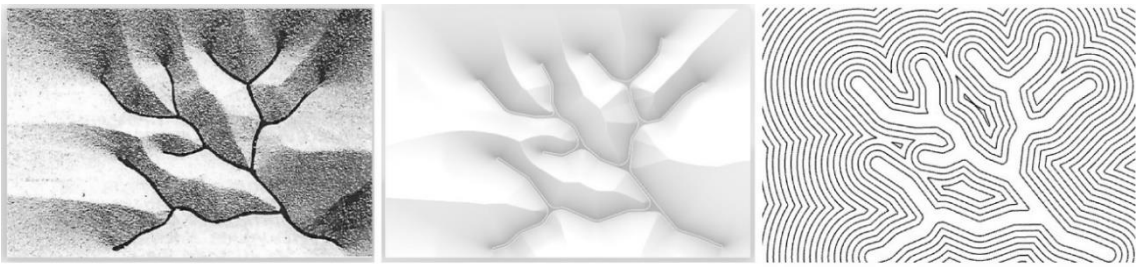

Figure 5.35 The sand physical model of a topographic surface by Jean-Marie De Larue(left) is accurately modeled by the HF algorithm (right) based on the input of a branching set of linear holes.

Figure 5.36 The advantage of the HF method in modeling curved and linear holes at different heights.

### 5.3.3 Medial axis methods

The medial axis algorithm (MA) models sand piles as patches of ruled surfaces. From the information of either the boundary or the ridge of the pile, the algorithm defines the medial axis, construct the rulings of the surface between the boundary and the ridge, and generates the surface of the sand pile. The logic behind the MA algorithm is derived from the geometrical features of the sand pile and its physical formation processes.

Geometrically, the constant slope of sand defines the trigonometric relationship between the boundary *B*, the ridge *R*, and the medial axis *Ma* curves (Figure 5.37). Since the *Ma* is the orthogonal projection of *R* and the center axis of *B*, it allows the determination of *R* and *B* by the information of one of them and the slope $\theta$. Physically, the pile emerges either by pouring sand on a predefined base (boundary) or by the deposition of sand along a predefined path (ridge) as shown in Figure 5.38.

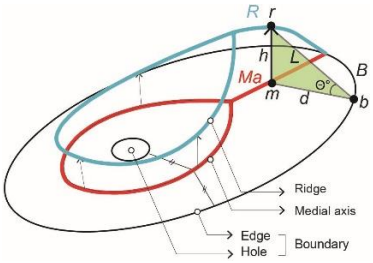


Figure 5.37 The trigonometric relationship between *b*, *r*, and *m* is defined by the slope of sand $\theta$.

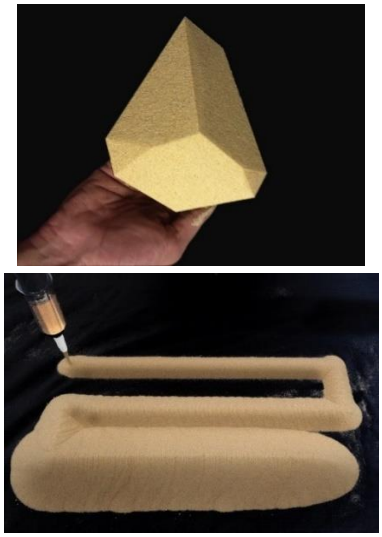

Figure 5.38 Sand deposition methods. Boundary to ridge (left) and ridge to boundary (right).

Based on the physical formation methods of sand and the geometry of the pile, two MA algorithms are developed, they are briefed below and detailed in the following two sections.

1- **From input boundary to output ridge method (B-R)**: physically, sand is poured on a predefined boundary and the ridge emerges with respect to the boundary and the slope. Digitally, the boundary curve is processed to define its medial axis, which points are vertically displaced to generate the ridge curve with respect to the slope.
2- **From input ridge to output boundary method (R-B)**: physically, the sand is deposited from a predefined path on a plane and the boundary of the pile emerges from the path and the slope. Digitally, the ridge is projected to the base plane to define the medial axis, which is then processed to generate the boundary with respect to the slope.

### 5.3.4 Medial axis_ Boundary to ridge method

The boundary to ridge algorithm (B-R) is a modeling method of sand piles based on the input of the boundary curve(s) and the slope of sand. It identifies the ridge of the pile from the medial axis of the boundary and generates the pile as patches of ruled surfaces between the ridge and the boundary. The procedure of the algorithm is detailed below and illustrated in Figure 5.40 using a hollow pile as an example. The pile is physically formed by pouring sand on an oval base perforated with a circular hole.

#### 5.3.4.1 The parameters and procedures of the B-R algorithm

1. **Defining the boundary conditions:** the slope of sand $\theta$ and a predefined boundary curve are given as inputs. The boundary is described by two groups of coplanar curves: the edge (a closed curve, which represents the base or the sides of the box), and the holes (open or closed curves).
2. **Voronoi tessellation**: first, the boundary curves are sampled by a dense discrete set of points $P_b$ with the sampling density determined by each curve length to capture the boundary shape correctly. The sampling points represent the locations from which the sand falls. The $P_b$ are then used as the sites of a Voronoi diagram to generate the Voronoi cells, which represent the region of effect of each $P_b$.
3. **Cells clustering**: the cells are then grouped and associated with their boundary curve to create clusters that represent the region of effect of each boundary curve.

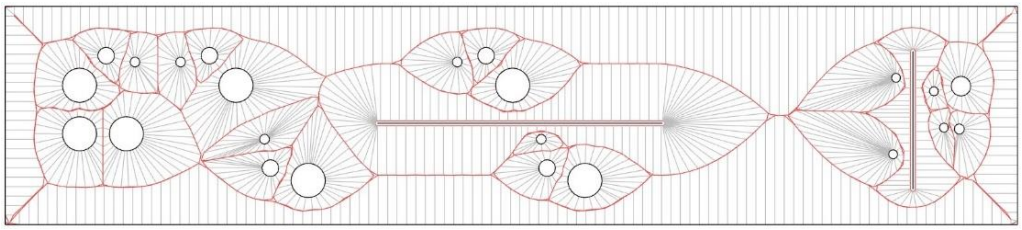

Figure 5.39 Voronoi tessellation of a hollowed pile, holes (black), Voronoi cells (blue) and medial axis /cluster edges (red).

4. **Medial axis extraction**: the edges of the clusters are then extracted and joined to determine the medial axis curve.
5. **Ridge generation**: next, the medial axis is sampled into points $P_m$, which are displaced with a normal vector to define the points of the ridge $P_r$ that are then interpolated to define the ridge curve $R$. The vector length is calculated by the trigonometric relationship between the slope $\theta$ and the distance between $P_m$ and their closest point $P_b$ on the associated boundary.
6. **Surface generation**: the rulings are then constructed by creating lines between $P_m$ and $P_b$, which are the steepest descent lines from the ridge normal to the boundary curves. The rulings are also the falling path of the grains of sand. Finally, a ruled surface is created between the rulings to generate the sand pile surface.

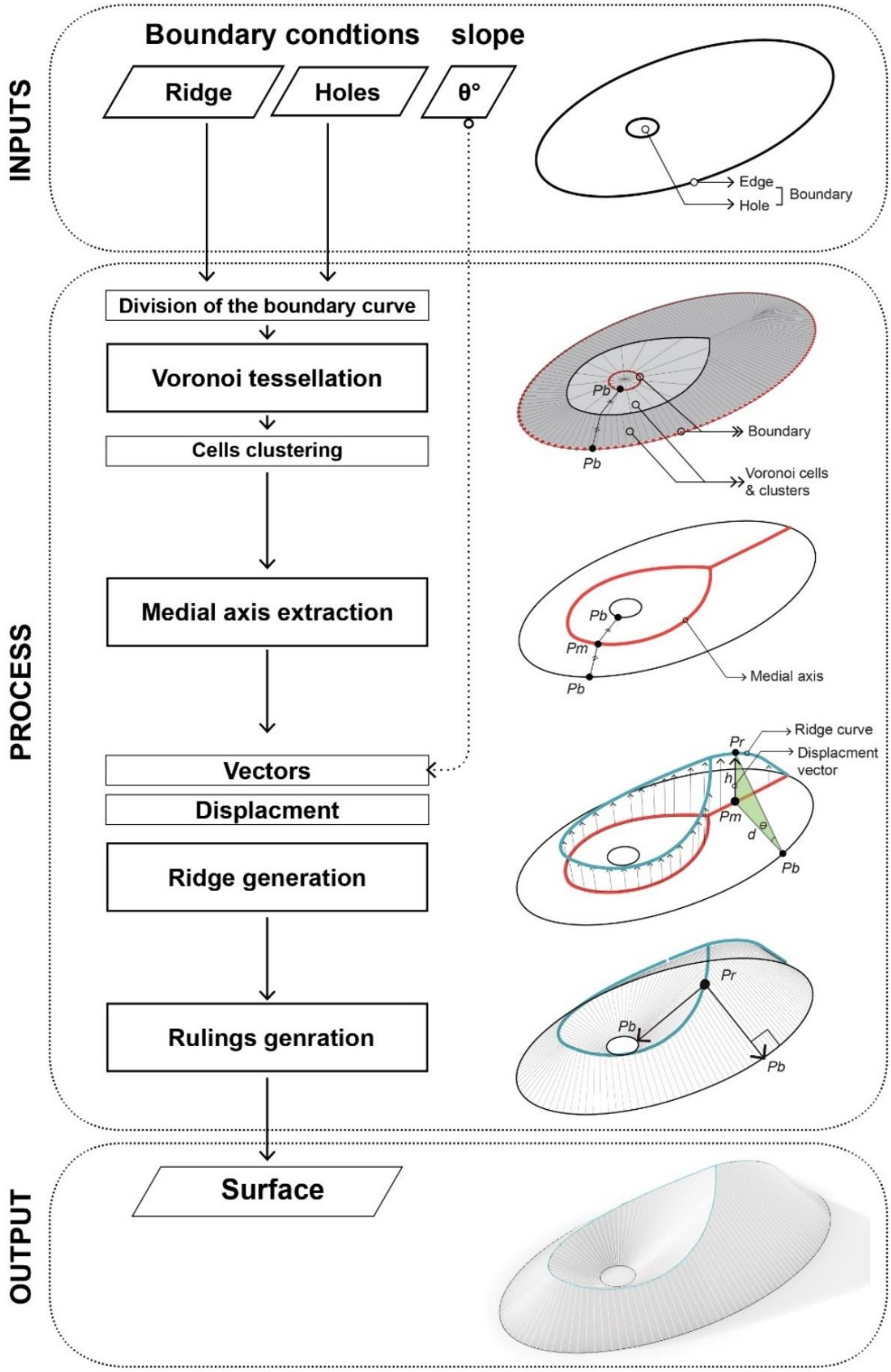


Figure 5.40 Diagram of the Boundary to ridge algorithm showing the key operations

### 5.3.4.2 Evaluation of the boundary to ridge method

#### A- Formation methods

The B-R algorithm is capable of modeling the four formation methods (addition, subtraction, tilting, and displacement) by the manipulation of the inputs (boundary conditions and direction of slope), and the operations of Voronoi tessellation and distance function. Figure 5.41 shows four conditions of the addition and subtraction methods:(A) addition in a box, (B) subtraction from a box, (C) subtraction from a pile, and (D) addition on a solid base. The variations of the inputs and operations, and their resulting techniques are detailed below.

- **Border (*b*)**: in A and B cases, the border is considered as a passive curve to represent the side of a box that prevents sand from falling. While in C and D it is considered as an active curve to represent a base that allows the sand to fall.
- **Holes (*h*)**: in A,B, and C, the holes are considered as active curves to represent the locations from which the sand falls. While in case D of a solid pile, the holes do not exist.
- **Voronoi tessellation (*t*)**: Voronoi diagram is applied on active curves that represents the location from which the sand falls, which are the holes in A and B, border and holes in C, and border in D.
- ***Distance function* (*d*)**: the distance function is measured from the medial axis to the active curves, which are the holes in A and B, the border and holes in C, and the border in D.
- **Vector direction (*v*)**: the points of the medial axis are displaced vertically with an inversed vector in A and a normal vector in B,C, and D. The vector can also be tilted.

To optimize the algorithm for productive design exploration the formation methods and settings are set as a switch list in the input phase to control the variations of the parameters and operations.

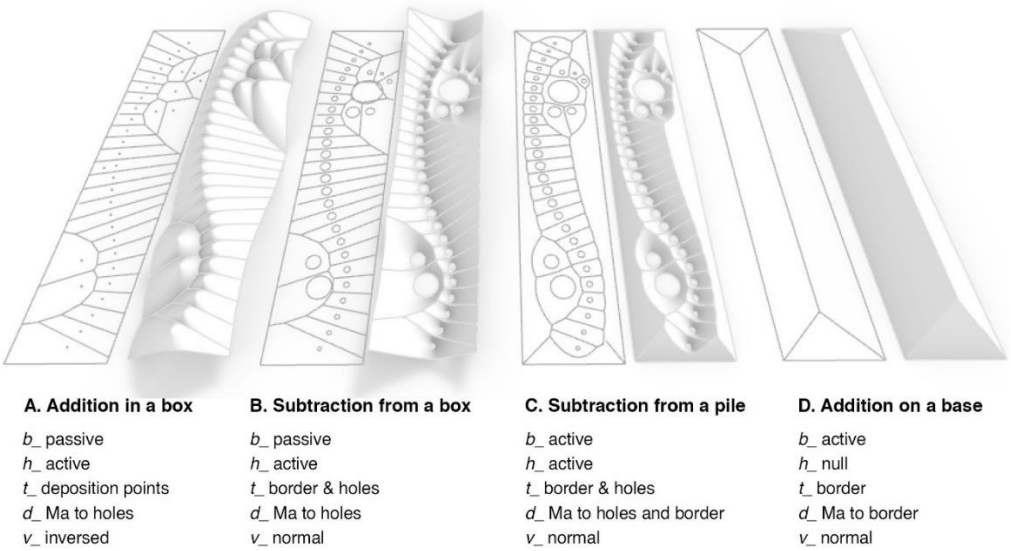


Figure 5.42 The B-R algorithm can model two formation methods in two settings by the variations of the input border (*b*), holes *(h*), and vector direction *(v*), and the operations of Voronoi tessellation (*t)* and distance function (*d*).

### B- Boundary conditions

The B-R algorithm is capable of modeling different curves typologies of boundary conditions for either solid or hollow piles as shown in Figure 5.43. The illustration presents the medial axis in red, and in gray are the rulings, which are normal to the boundary curves.

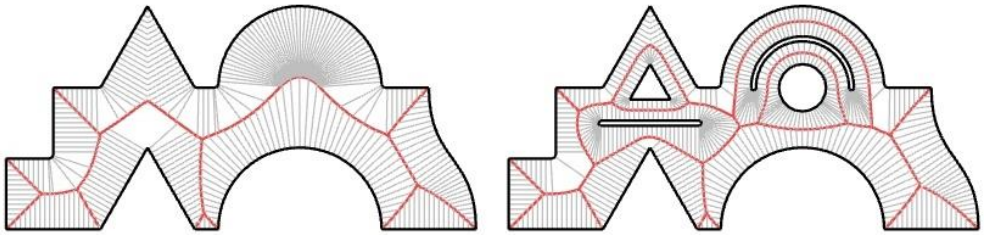

Figure 5.43 Evaluation of the adaptability of B-R algorithm in considering different typologies of boundary curves of a solid pile (left) and hollow pile (right). Are illustrated. The medial axis and rulings are illustrated.

The major drawback of the medial axis algorithm is that it cannot generate a surface from points or curves at different heights. This limitation is a primary consequence of using the Voronoi component in grasshopper, which operate only on 2d points. To overcome this challenge, it is essential to understand the mathematical function of Weighted Voronoi and its available algorithms (see §5.2.3). In brief, the weighted Voronoi operates on the Euclidean distance function of the simple Voronoi but considering the weights (heights). While the reported algorithms [135,197] to calculate standard and weighted Voronoi diagrams from points clouds are generally applied in two phases: the first clusters the points in respect to their Euclidean distances and weights, while the second phase defines the curves of the closed regions (the cells).

$$d_E(S_1, P_i) = \|S_1 - P_i\| - w_i = \sqrt{(S_x - P_x)^2 + (S_y - P_y)^2} - w_i$$

The research developed[66] a code in Mathematica software based on the above study in order to apply the two phases of the weighted Voronoi algorithm. Figure 5.44 shows an example of the developed code, a set of 3D points (black) and a site point (red) are given. The code succeeded at clustering the 3D points and defining the hyperbolic curves (blue) between the points, but it was not possible to find their intersections to define the border of the Weighted Voronoi cell (red).

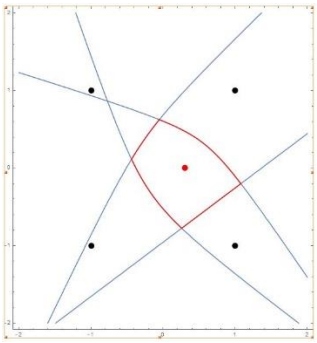

Figure 5.44 Weighted Voronoi method in Mathematica

[66] In collaboration with Ahmed Elshafei (PhD, ENSA Paris-Malaquais) and Mohamed zaghloul (PhD, ETH).

### 5.3.5 Medial axis _ Ridge to border method

The ridge to border algorithm (R-B) models linear deposition of sand on a plane. The algorithm operates on two phases, first it evaluates and optimizes the deposition path to define the ridge, then it determines the medial axis and the border from the ridge and the slope of sand. Finally, it generates the surface from the rulers connecting the ridge and the border. The procedure of the algorithm is detailed below and illustrated in Figure 5.45 using as an example a dune like pile formed by pouring sand from a non-planar curved path on a plane.

#### 5.3.5.1 The parameters and procedure of the R-B algorithm

1. **Ridge optimization**: the slope of the deposition path is first evaluated against the slope of sand $\theta$ by determining the angle $\alpha$ between the curve tangents and their vertical projection. If $\alpha \leq \theta$, the deposition curve is then considered as the ridge, but if $\alpha > \theta$, the curve is relaxed to the maximum slope of sand (the optimization algorithm is detailed in the following paragraph).
2. **Medial axis definition**: after defining the ridge curve, it is then projected vertically on the ground plane to determine the medial axis. The vertical distances *h* between the set of points *Pr* on the ridge and their corresponding projections *Pm* on the medial axis are also determined.
3. **Border generation**: the border is defined from the height of the ridge, the location of the medial axis and the slope by either of the following two methods (i) as the offset of the medial axis at distance d where d = h / tan $\theta$. Or (ii) as the envelope of the tangents of the inscribed circles, which centers are the *Pm* points on the medial axis and their radius r = h / tan $\theta$.
4. **Surface construction**: the rulings of the sand pile are then defined by constructing lines between the set of vertical planes that are normal to the border and their intersection points with the ridge *Pc*. Finally, a series of ruled surfaces are generated between each two successive rulings and joined together to approximate the surface of the pile.

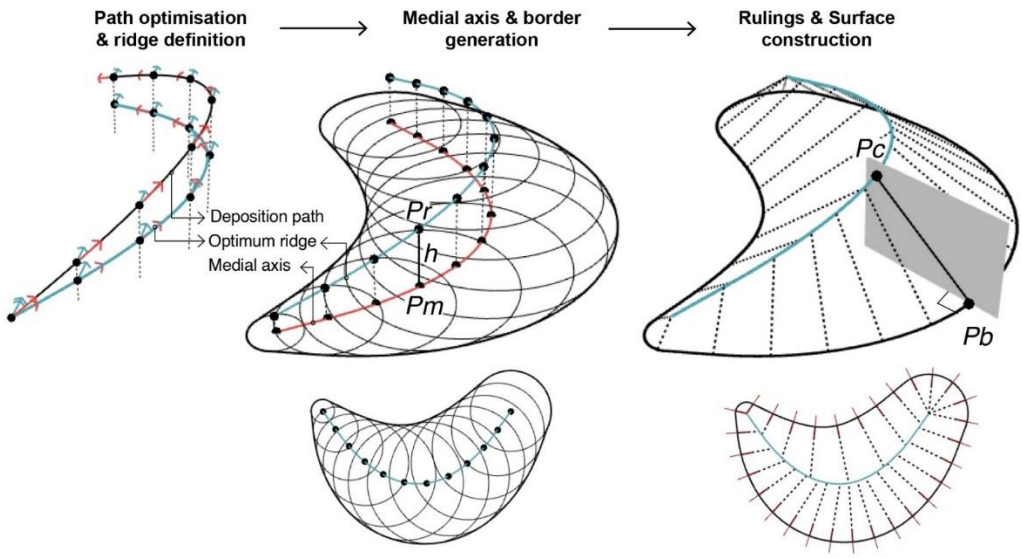


Figure 5.45 Procedure of the R-B algorithm. (1) ridge definition by the relaxation of the deposition curve, (2 & 3 ii) medial axis and border generation, and (4) surface construction from rulings

### 5.3.5.2 Optimization algorithm of the deposition path curve

The optimization algorithm defines the ridge curve from the deposition path. It evaluates the slope of the path curve and if it exceeds the slope of sand it uses an evolutionary solver (Galapagos[67]). The solver searches for the optimum ridge within a domain of curves and returns the ridge, which slope is the closest to the maximum slope of sand. The algorithm operates through the following phases:

1. **Construction of the domain** as vertical lines between division points on the path curve *Pc* and their projection *Ps* on the horizontal plane of the lowest point of the path. The construction lines represent the morphing space between the path and its projection where the optimum curve lies (range to search from).
2. **Construction of the domain curves** as interpolations between points *Pn* on the construction lines. The location of the points are the variable of the algorithm (genome).
3. **The search for the optimum curve** is defined by searching for the curve, which slope returns the minimum difference with the slope of sand (fitness criteria).

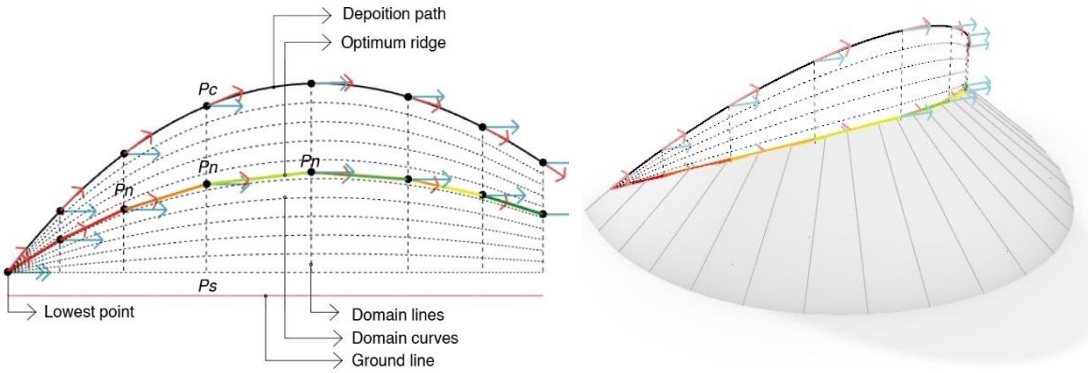


Figure 5.46 Path curve relaxation. The deposition path is relaxed to define the optimum ridge.

### 5.3.5.3 Evaluation of the R-B algorithm in modeling different border conditions

The R-B operates on different curve typologies including linear, curved, open, closed, non-planar, and overlapping curves as shown in Figure 5.47.

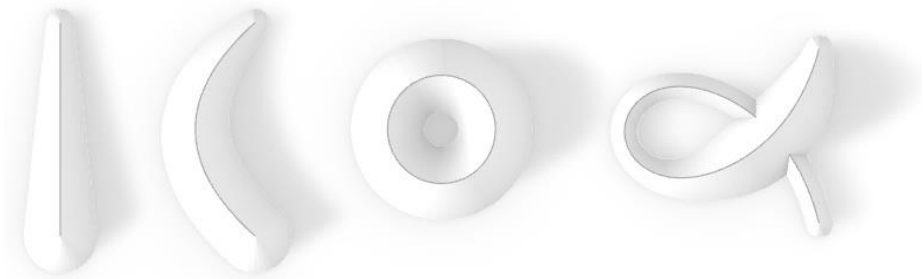

Figure 5.47 The R-B operates on different curve typologies

[67] Galapagos is an evolutionary solver within Grasshopper. It generates a population of candidates by changing an input variable (Genome) and search for the optimum candidate that meets an input criterion (Fitness).

### 5.3.6 Comparative evaluation of the algorithms

The evaluation criteria of the algorithms (adaptability and productivity) are introduced in § 5.3, and the assessment of each of the three algorithms is discussed in their corresponding subsections. Table 5.1 compares the results of evaluations to inform the design techniques in chapter 6.

- The Boolean method is restricted to the addition and subtraction methods. In term of boundary conditions, it is limited to deposition points and circular holes.
- The Heightfield and Medial axis methods allow the modelling of the four formation methods under almost all boundary conditions. However, a major drawback of the Medial axis method is that it can't consider 3D organisation of generators (points and/or curves at different heigths) due to the limitation of the Weighted voronoi tessellation. In future work this limitation must be overcome to allow the design of more complex forms.
- In terms of productivity, the medial axis is the most efficient, followed by the heighfield.

| | | | | **Algorithms** | | | | | |
|---|---|---|---|---|---|---|---|---|---|
| | | | | Boolean | | Heightmap | | Medial Axis | |
| **1. Adaptability** | | | | | | | | | |
| **a. Formation methods** | | | | | | | | | |
| Pouring | | | | ✓ | | ✓ | | ✓ | |
| Releasing | | | | ✓ | | ✓ | | ✓ | |
| Displacing | | | | X | | ✓ | | ✓ | |
| Tilting | | | | X | | ✓ | | ✓ | |
| **b. Boundary conditions** | | | | | | | | | |
| Curves | Open | Closed | | X | ✓ | ✓ | ✓ | ✓ | ✓ |
| Curvature | Linear | curved | | X | X | ✓ | ✓ | ✓ | ✓ |
| Curve direction | Concave | Convex | | X | X | ✓ | ✓ | ✓ | ✓ |
| Angle | acute | right | reflex | X | X | ✓ | ✓ | ✓ | ✓ |
| Non-coplanar holes (different heights) | | | | ✓ | | ✓ | | X | |
| **c. Generated surface types** | | | | | | | | | |
| Conical surfaces | | | | ✓ | | ✓ | | ✓ | |
| Piles surfaces | | | | X | | ✓ | | ✓ | |
| Tangential surfaces | | | | X | | X | | X | |
| **2. Productivity** | | | | | | | | | |
| Complex geometries | | | | low | | medium | | high | |
| Speed of computation | | | | low | | medium | | high | |
| Accuracy of generated surfaces | | | | high | | medium | | medium | |

Table 5.2 Evaluation of the feasibility and performance of the three modelling techniques.

The comparison shows that the medial axis is the most efficient (despite its limitation to 2D inputs) as it engages with most of the formation methods, variabilities of boundary, and complex geometries while retuning convenient accuracy of surfaces in the shortest time. These results suggest the consideration of the medial axis method as the main tool of modelling followed by Heightmap then Boolean methods to overcome the 2D limitation.

Figure 5.48 associates the formation, methods, and boundary conditions to their corresponding modelling methods. The results of the comparative study and the association diagram is crucial to inform the design and fabrication techniques in the following chapter.

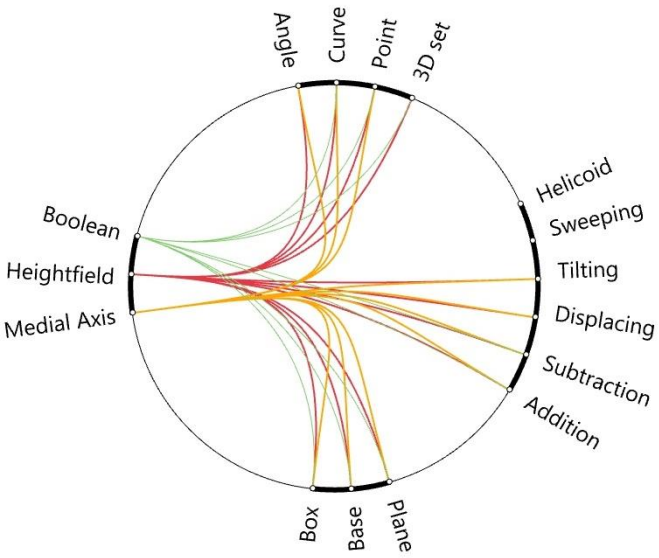


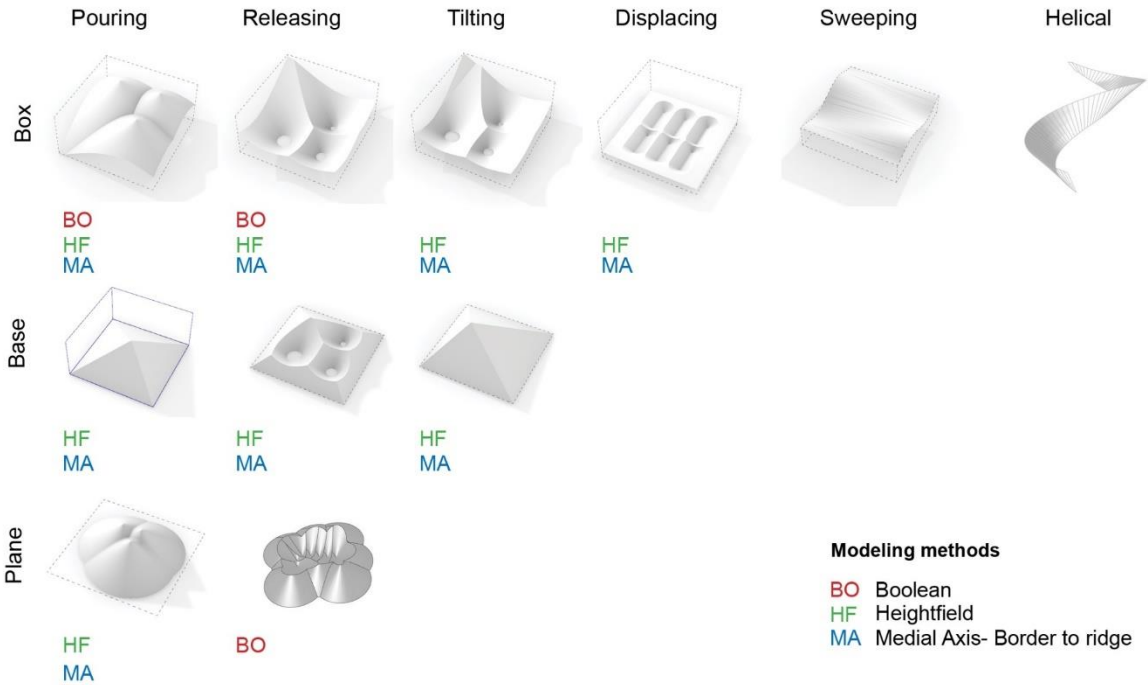


Figure 5.49 The interrelation between the formation methods, types of container, and the modelling methods

### 5.3.7 Robotic control code

Based on the data of a predefined boundary condition (border and generators), the robotic control simulates the robot movement and generates the control commands for physical execution. It operates using HAL robotic control plugin in Rhino / Grasshopper environment.

The engagement of the robot in materialization adds a new dimension to the design process, ‘time’, i.e. the speed of the robot and the flow rate of sand. Moreover, the ‘wait’ duration (the case in which the robot is paused while the material flows) is an added design dimension. The link between time and materiality is significant as formation processes are now considered as time-based and form is now defined by time. To identify the relationship between the speed of robot and the height of sand a study is conducted in § 6.1.3. In brief, since the flow of sand is constant (approximately 33.4 mm/s), the experiments focus on tuning the speed of robot. The effect of speed, slowing, and wait on height of sand are identified (Figure 5.50).

Figure 5.50 Tests of tuning the robot speed and wait duration with the flow of sand and the resulting heights.

The typical process of the robotic control code operates in four stages: 1) assignment of the boundary, 2) generation of the toolpath, 3) simulation of the robot motion, and 4) generation of the control code. First, the boundary is assigned including: (i) Static bodies: the form of the border where sand is shaped (ex: sandbox) and the form end-effector that shapes the sand are assigned as surfaces to avoid collisions. (ii) Targets: the generators (ex: deposition points or path) are assigned as points and /or curves of to define the robot trajectory curves. Moreover, (iii) the speed and wait duration of the robot at each target are defined as a sequence in mm/sec. Second, the generators are sampled into directional planes and organized in the sequence in which they must be processed by the robot to generate the toolpath Then, HAL plugin automatically simulates the robotic motion and finally converts the coordinates of the toolpath (position and orientation of target planes) into robotic control code for physical execution.

## 5.4 Fabrication system: fabrication methods of sand panels

This section introduces the third axis of sand tectonics, the fabrication system which extends the material and design systems to the materialization phase. The main objective is to define methods of making enabled by the material logic and the formation methods, while considering feasible fabrication and assembly constraints. From the outset, the fabrication system is designed as a prefabrication system primarily intended to produce non-standard sand panels and blocks that can be transported and assembled into a larger whole.

To develop the fabrication system, it was essential to break it into separate tasks, conduct technical studies and iterative experiments on each task to improve its workability, then merge the tasks into a coherent procedure. The architectural creative is nevertheless maintained in the flexibility of the fabrication system and the interchanges between its processes: forming, spraying, and casting. The creative unfolds even more fully through the variations of assembly methods and the employment scenarios of the solid panels as will be discussed. Such an understanding of physical production yield to consider fabrication not as a mere execution of form but rather as a design tool.

The fabrication process is first introduced followed by the manufacturing constraints, which inform the design and modeling methods. Then, the digital-physical workflow of making is presented which integrates the design, modeling, and fabrication methods in a comprehensive yet flexible process. As such, this section concludes the making system and accomplish the construction of the sand tectonics framework.

### 5.4.1 Fabrication process

The fabrication process consists of four main tasks: (i) fabrication setup, (ii) sand formation, (iii) panel solidification, and (iv) block casting. The process is detailed below and illustrated in Figure 5.51. The example being used is a sand block (50x50x5cm) fabricated by sandwich casting of two sand panels formed by the subtraction from a box method using a perforated box.

1. **Fabrication setup:** after the two surfaces has been designed in the digital phase, the fabrication process starts by preparing the following necessary information and materials:
    a. **Fabrication data:** the 3D model is first processed to generate the drawings of the formwork, the required quantities of dry sand, saline solution for the formation and solidification phases, and the Hyposand liquid mixture for the molding phase.
    b. **Formwork production**: typically, the formwork is produced in flat sheet materials (cardboard or plywood) using a laser or a CNC machine. In this case, it consists of four sides and a base that is perforated according to the holes of the surface.

c. **Materials preparation**: the sand, alt and Hyposand liquid mixture are then prepared according to the materials preparation and making methods introduced in § 3.1.

2. **Sand formation:** the formwork is then filled with dry sand and the holes at the bottom are opened to release the sand and form the required surface.
3. **Panel solidification:** the emergent patterns of dry sand are then sprayed with the saline solution, which instantly binds the grains on the surface. Then, layers of sand are spread and sprayed until the required thickness is achieved. A process of 5 layers turns the surface into a solid panel of around 1 cm thickness in 10 minutes. The detailed process of spraying is given in § 3.3. Once solid, the panel is demolded. The resulting panel is self-supporting with a satisfactory strength for handling, assembly, and casting.
4. **Block casting:** the two solid sand panels are then assembled, and the Hyposand mixture is poured in between the panels according to the mixing method of making described in § 3.2. The fluidity of the mixture and the heat produced from the crystallization process bind the panels and the mixture into a monolithic solid block in around 3 hours.

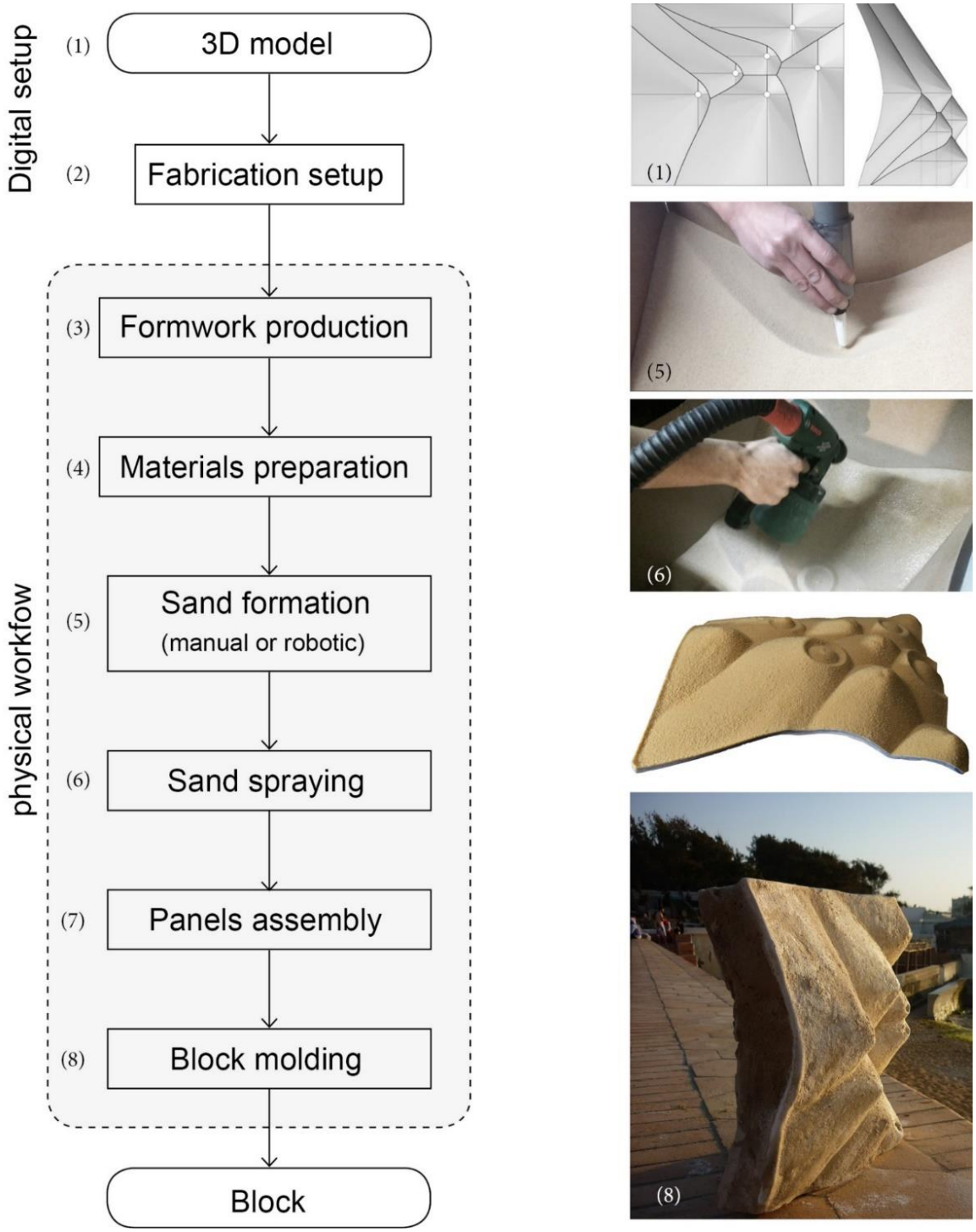


Figure 5.51 Diagram of fabrication process

### 5.4.2 Fabrication constraints

Upon the iterative experimentation and the feedback between physical and digital prototyping along this research, six fabrication constraints are identified in this subsection. To achieve a successful physical production, the fabrication constraints are considered at the early stage of the design process, and in every aspect of the digital workflow. Incorporating these constraints through a feedback loop between fabrication, design, and modeling into the overall framework of ST is a key aspect to achieve feasible, productive, and high quality making process. It is important to note that the fabrication constraints differ upon the fabrication technique as will be discussed in the following chapter, but in general the following are the common constraints:

1. Panel size and shape
2. Assembly technique
3. Edges alignment
4. Casting technique
5. Panels orientation
6. Formwork design

#### 5.4.2.1 Panel size and shape

The size of a sand panel is informed by its possible thickness and practical size of formwork. Firstly, the thickness provides the panel with sufficient resistance of charges under its own weight when handled, assembled, or cast. The maximum thickness achieved by the spraying technique is around 2 cm, restricting the panel size to 50x50 cm which is accepted in this work as it returns a workable panel. However, for smaller panels, the thickness can be reduced up to 3mm for a 10 cm length panel (Figure 5.52).

Figure 5.53 The size of panels is restricted by it thickness and the feasible size of the formwork. A 0.3cm thickness for a 20 cm panel (left), and 20 mm (right)

Secondly, the size of a sand panel is directly proportioned to the possible size of formwork. A large mass of sand increases the charges applied on the formwork, which requires reinforcement especially on the sides where most of the sand charges are applied. For instance, a 50x50 cm panel made by sand subtraction, requires 120 kg of sand (5 standard bags of 25kg) which requires a timber frame and at least 6mm plywood sides. Based on the above, the maximum edge length of panel is restricted in this work to 50 cm.

#### 5.4.2.2 Surface paneling and edges alignment

For large scale fabrication it is necessary to divide the surface into panels with feasible size and shape, then assemble them as a formwork for casting. To assemble two adjacent panels, The 35 Degree project proposed that their edges have to meet with a common profile in order to ensure the continuity of the pattern between the panels [73] (Figure 5.54- top). To overcome the challenge of edges alignment the holes in each panel are mirrored around the profile axis to create the same surface profile on both panels. However, this method has three drawbacks: (i) it limits the organization of holes in the surface to respect the mirroring constraints, (ii) it works only for the addition and subtractive methods of formation, and more importantly (ii) it necessitates the application of holes around the edges of each panel and consequently it is impossible to design large surfaces. To overcome these limitations, a paneling method is proposed along with a customized fabrication method for large scale assemblies (Figure 5.54- bottom).

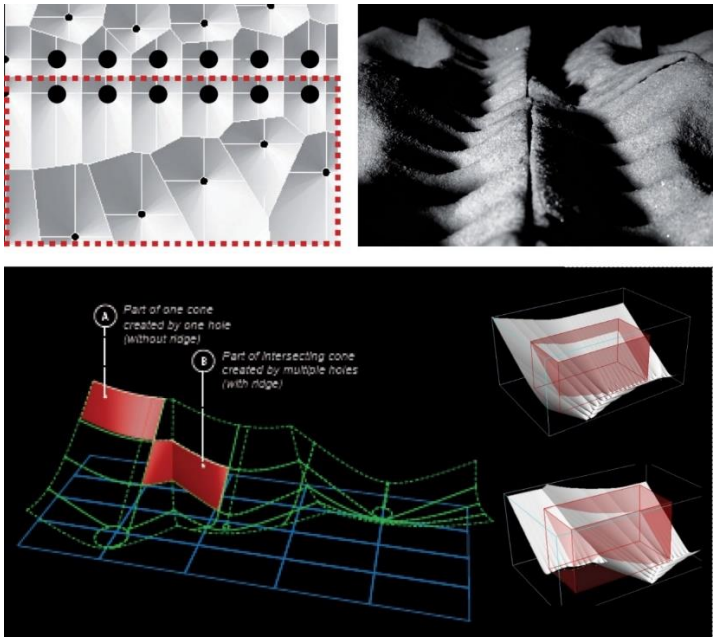


Figure 5.54 method of alignment of the panels edges [73].

#### 5.4.2.3 Panels laying techniques

Assembly refers to joining two or more panels as a formwork for casting Hyposand. Since the maximum size of panels is 50 cm as discussed in the previous paragraph, it is necessary to develop an assembly method for large scale casting. Drawing on this, three assembly techniques are defined below and illustrated in Figure 5.55. **(i) Stacked**: assembly of two panels for blocks smaller than 50 cm. **(ii) Split:** for a block larger than 50 cm, its formwork is constructed from three to four split panels. **(iii) Interlocked:** for large scale casting, the formwork is constructed from a staggered assembly of panels. The staggering arrangement provides the necessary interlocking between the panels such that they form a stable formwork for casting. Moreover, each face of the formwork has a different orientation to avoid vertical or horizontal sliding (Figure 5.55).

to ensure the stability of a casting formwork, the panels should be laid following a staggered pattern to maintain an adequate lap between joints from one panel to the next and to ensure that vertical joints are not positioned above one another. The staggering arrangement provides the necessary interlock between the panels such that they form a stable formwork for casting.

Figure 5.55 Assembly techniques of sand panels for casting monolithic blocks

#### 5.4.2.4 Panels orientation

Panel orientation refers to the side of the panel being used in casting, either the top or bottom side.

The importance of this consideration is that in order to produce a block with a sharp pattern, its face should be the bottom side of the panel as will be explained. In the spraying phase, the saline solution is carefully sprayed over the sand pattern to preserve its sharpness. Then, a sequence of spraying salt and layering sand is applied to thicken the panel. The process results in a solid panel with two sides: (i) the bottom, which have sharp pattern, and (ii) the top layer with fuzzy patterns. Consequently, it is important in the assembly of panels, in case of a reusable formwork, to use the bottom side of the panes as the internal side of the formwork to get a sharp cast. While in the stay-in-formwork, the bottom side should be the exterior side of the formwork. Such detail is of main importance to consider in the modeling and fabrication phases to achieve quality in the result.

Figure 5.56 the top side (left) and bottom side (right) of a sprayed sand panel.

#### 5.4.2.5 Casting techniques

The sand panels are used in this work as formworks for casting either Hyposand or other materials such as concrete. To illustrate the potentials of sand panels in fabrication, this subsection defines two formwork systems and three casting possibilities (Figure 5.57).

Sand panels might be used either as a:

1. **Stay-in-place formwork** for casting Hyposand. Upon casting, the saline solution bonds the fresh mixture with the internal surface of the panels giving a monolithic block.
2. **Reusable formwork** for casting Hyposand or other materials such as concrete. In this case, a separation layer is applied on the panel surface before casting. The advantage of the reusable formwork is that it can be recycled following the methods discussed in § 3.5.

Three casting techniques are possible based on the orientation of the panels (Figure 5.57).

A. **Front to back** returns the least possible thickness with a standard profile along the edges.

**B.** **Back to back** provides larger thickness with favorable differentiated profiles

**C.** **Flat casting** refers to casting on one panel in a box, which returns a block with a flat side.

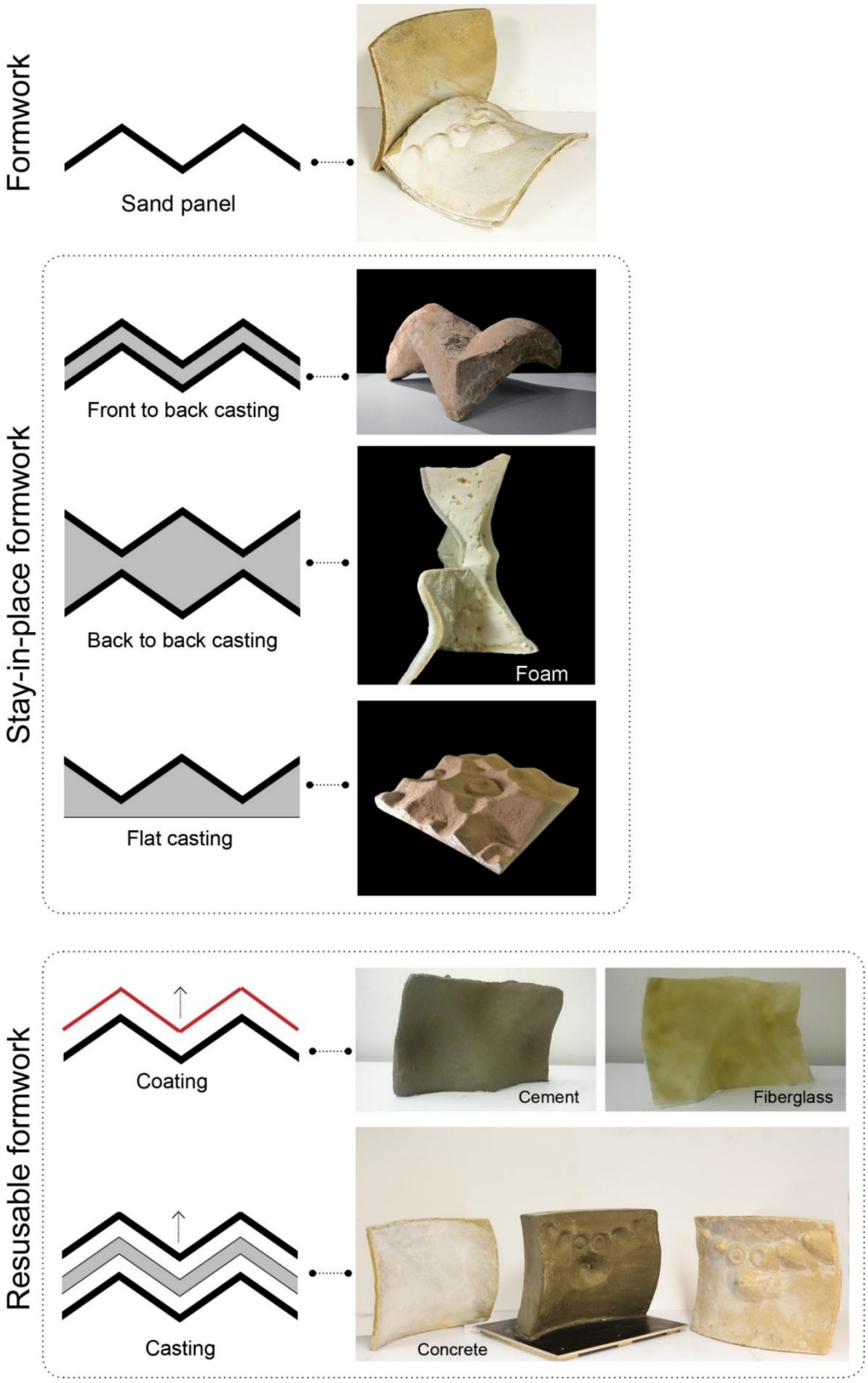


Figure 5.57 Casting techniques of sand panels either as stay-in or reusable formwork

#### 5.4.2.6 Formwork design and fabrication

The formwork has a twofold role in this work, a design tool, and a fabrication medium.

1. **From the design side**, the formwork is the tool by which the architect mediates the material behavior. Since sand slope is the constant of the formation process, then the design of formwork is the variable of the process that gives rise to the sand emergent forms.

2. **From the fabrication side**, the design and making of the formwork have to meet the following considerations to attain efficient workability:

    - **Accessibility**: the formwork must be designed for easy flow of sand to all parts, and at the same time, accessible for the progressive spraying process from the top.
    - **Tightness**: since sand acts like a liquid when dry, it easily leaks from the formwork if it is not tight. Hence a sealing material or interlocking assembly of sides should be considered.
    - **Stiffness**: since the load of the sand mass acts on the sides of the container more than the bottom (see § 2.3), it is essential to consider stiff materials and assemblies to sustain the sand load.
    - **Demountable** to easily take out the solidified sand panel without breaking it.
    - **Durable** to reuse the formwork for iterative experiments.
    - **Scale:** all the above consideration directly defines the possible scale of the models, which directly inform the design process.

The complexity of the design of the formwork in this work is due to considering all the above considerations in correspondence with the available material (cardboard) and machine (laser cutter 90 x 60cm) at hand before the design of the sand panels. The available resources at the time of this research have limited the size of the panels to what can be fabricated with cardboard. Undoubtedly, plywood and CNC machine would ensure the fabrication of larger models with higher qualities.

## 5.5 The Digital-physical workflow of sand tectonics

The digital-physical workflow aims at correlating the design and fabrication methods in a coherent process of production. It is developed as a flexible path rather than a hierarchical sequence to enable the interchange between the different phases of making. Such an understanding of physical production yield to consider fabrication not as a mere execution of form but rather as a design tool.

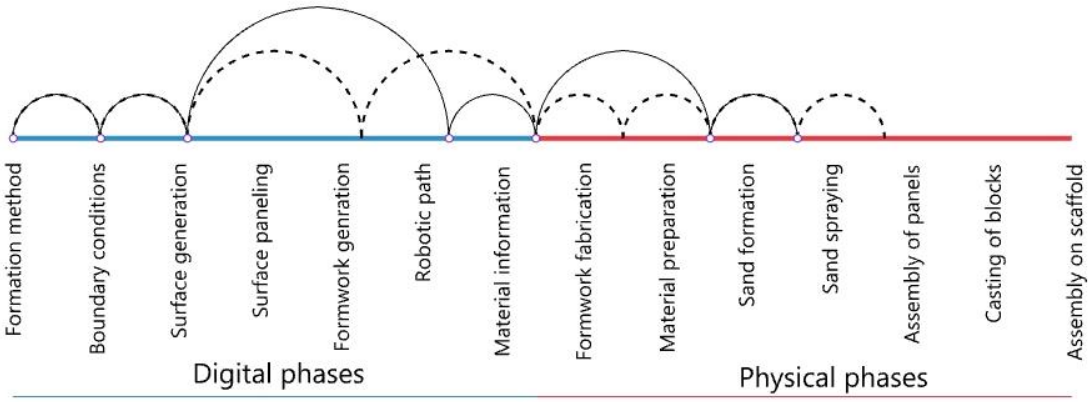


Figure 5.58 Diagram of the digital-physical workflow of making.

The workflow is introduced here using a 50x40x10cm block made by casting two hyperbolic paraboloid panels of sand. The stages of the workflow are summarized below with references to their illustrations in Figure 5.59 and to their detailing in their relevant subsections.

1. **Sand formation method:** the first step in the digital workflow is to select the sand formation method (§ 5.1.1) according to a design intention. Herein, a combination of Sweeping (§ 6.4) and Releasing (§ 6.1) methods of formation.
2. **Boundary conditions**: the boundary curves are then designed (§ 5.1.1) by drawing the sweeping curves of the surfaces and the releasing holes in Rhino. In this stage it is essential to consider the fabrication and the material constraints .
3. **Surface generation**: the input boundary curves are then used as inputs in a custom-made parametric algorithm, which generates sand surfaces from the input boundaries in respect to the slope of sand. At this point, there is the possibility to modify the input curves to attain a convenient model that meets the design intentions and the fabrication constraints.
4. **3D model:** the generated surfaces are then processed to generate the 3D model of the block in respect to the feasible physical thicknesses of the sand panels and block.
5. **Fabrication setup:** the essential information for manufacturing is then processed from the 3D model including the drawings of the formwork and the required quantities of materials.
6. **Formwork fabrication**: to initiate the physical workflow (§ 5.4.1), the formwork is first produced in cardboard using a laser cutting machine and then assembled.

7. **Material preparation:** the required quantities of sand, saline solution and the Hyposand mixture are prepared according to the materials preparation methods introduced in § 3.1.
8. **Sand formation:** the sand is then poured in the formworks and shaped into a hollow hyperbolic parabolic surface by sweeping the sand surface with a ruler following the formwork edges, then opening the holes at the bottom to release the sand and generates the conical formations on the surface.
9. **Sand spraying:** the emergent patterns of dry sand are then sprayed with the saline solution, which instantly binds the grains on the surface. Subsequently, layers of sand are spread and sprayed until the required thickness is achieved giving a solid panel in a short time (around 10 minutes).
10. **Demolding**: once the surfaces are solid, the panels are demolded and assembled.
11. **Block casting:** the Hyposand mixture is then poured in between the panels returning a solid block in around 3 hours.

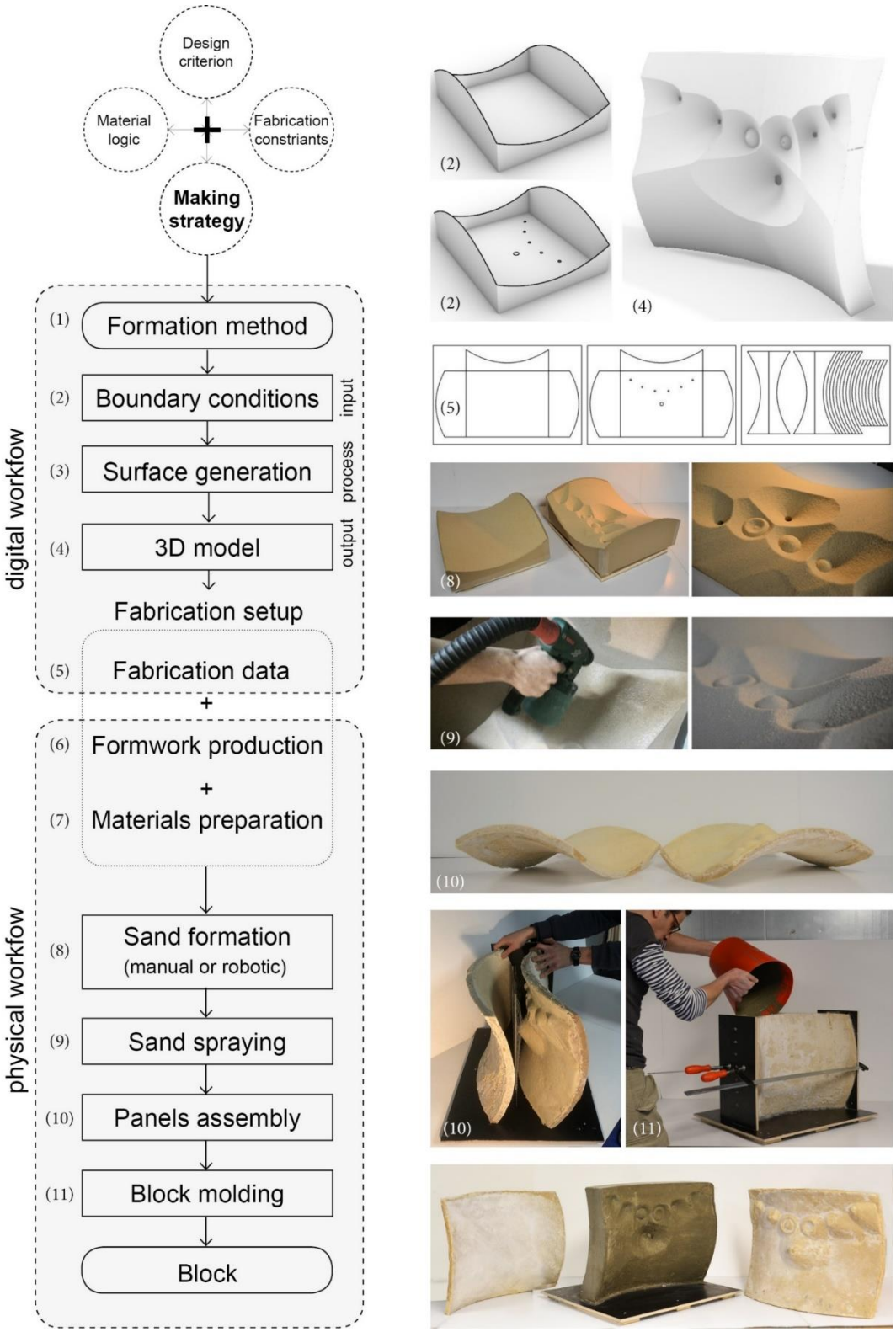


Figure 5.59 The digital-physical workflow of sand tectonics

## 5.6 The framework of methods

The objective of this work is not to construct a predefined form but rather to develop a methodology to tease out processes of formations from the sand capacities. It is then essential to construct the framework of the methodology as a flexible space of interchange to explore the possibilities of making allowed by the material. The framework of methods is an abstract reservoir of methods in which the interchanges can generate variations and rich tectonic articulations. It is the organizational space of the making methods and parameters which are organized in five groups: (i) formation methods, (ii) container types, (iii) generators types, (iv) fabrication, and (v) modeling methods. The framework is thought as a circular diagram, where the methods and parameters are clustered in groups around a circle in which the interchange between the methods are represented by curves (Figure 5.60).

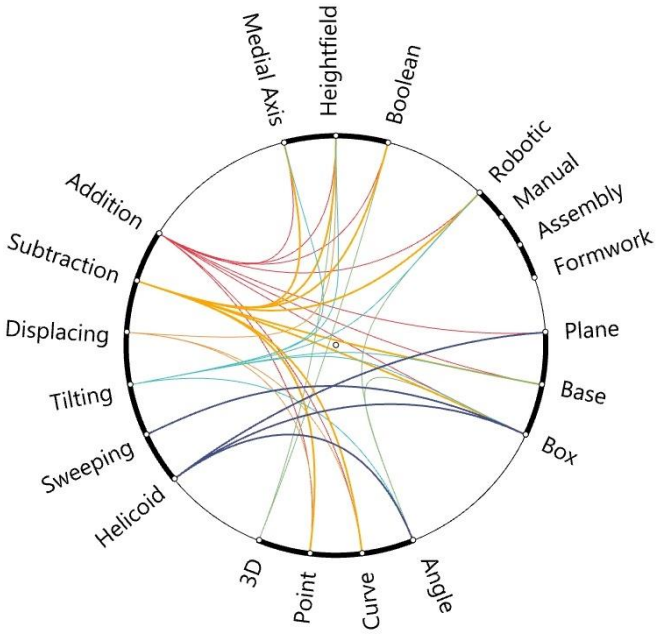


Figure 5.60 The framework of making methods

Such an understanding provides a model of design that is communicative, flexible, and explorative which promise to yield new possibilities that arise from the material logic and it formability. Thus, material behavior takes an active role in the genesis of forms along with the processes of formation. Combining the formation, modeling and fabrication methods establishes a complete table of parameters which can be used to describe the making system, and to develop its variations.

Until this point, the focus of this thesis has been to characterize the mechanical properties of the material, and to setup the material, design, and fabrication axes of the sand tectonics (ST). While these axes do not yet address the full potential of the ST, they do illustrate the material variability that can be achieved by shaping sand under different conditions. The following chapter demonstrates the making potentials of the ST through a number of digital and physical prototypes.

# Chapter 6

Prototyping

Design and fabrication experiments

# 6 Prototyping: design and fabrication techniques

The previous chapter developed the making system of sand tectonics by defining the methods of design, modeling, and fabrication. Collectively, they constructed the sand tectonics as an explorative framework, which essentially constitutes an open source of methods. This chapter applies the proposed making system through specific design and fabrication techniques to explore the capacities of sand self-formation in architecture.

In this chapter, five design and fabrication techniques of dry sand are presented according to the distribution methods introduced in § 5.1.1.1. In addition a formation technique of wet sand is presented.

- § 6.1 Addition and subtraction
- § 6.2 Tilting
- § 6.3 Displacing
- § 6.4 Sweeping
- § 6.5 Helicoid
- § 6.6 Pipe casting

For the purpose of clarity and coherence of this chapter, the techniques are introduced with a systemic and consistent structure, when possible. First, each technique is defined and the motivation behind it is discussed through an initial test. Second, the technique parameters, constraints, and geometrical principles are identified. Third, its custom-made algorithm is introduced. Finally, physical, and digital prototypes applying the technique are introduced. As the techniques vary greatly depending on their setup and constraints, they are presented at different degrees of detailing and applications.

*‘ Architecture is not about problem solving; rather, it should create desirable conditions and opportunities hitherto thought impossible*.’

Cedric Price, The Square Book,2003

Sand is unique in combining the flowability of fluids with the capacity to behave like a solid at certain conditions. Such liquid to solid reversible formability entails a design strategy that challenges the design approach of predefined forms and shifts the focus towards the observation of the material behaviour and the instrumentalization of its capacities as drivers of the formation processes.

Far from optimization and solving problem approaches of research, this chapter speculates what the sand wants to be. It explores the latent possibilities in the material morphogenesis through a bottom up design by research process from material to form. This chapter does not aim at designing a particular form but rather the process of making to unfold a space of possible forms allowed by the material. Such approach implies a close collaboration with the material through observation, analysis, and experimentation.

## 6.1 Addition and subtraction techniques

Addition and subtraction techniques refers to the deposition and releasing processes of sand distribution. They are presented together in this section as they are matching positive and negative forms and they share many of the morphological aspects, design parameters, modeling methods and fabrication techniques.

This section briefly recalls the work conducted by the 35 degree project in the subtraction technique, identifies specific design (§ 6.1.1) and fabrication (§ 6.1.2) limitations, and proposes further developments. In addition, a robotic deposition technique is studied (§ 6.1.3).

### 6.1.1 Parameters and design prototypes

The 35 degree project defined the parameters of the subtraction technique and their effect of the sand surface including the border shape, and the hole size, location, and height (Figure 6.1). Local and global organizations of holes were studied (Figure 6.2). A design strategy of holes distribution and nesting on curling and branching curves was developed and a generative design method of architectural forms for an ecolodge in the desert of Egypt was proposed (Figure 6.4) [1]. The design system proposed by the 35 degree allowed the articulation of the design parameters, and the development of complex articulations of sand forms with a tectonic language proper to the material behaviour and its formation method (Figure 6.3). The previous work established a design, modeling, and fabrication systems of the subtraction method and unfolded its morphological and architectural possibilities. Moreover, it showed that the design method holds great potential for further investigations.

The work developed by the 35 Degree project is introduced in Figure 6.1 to Figure 6.3 followed by a discussion of its limitations and the contributions of this thesis.

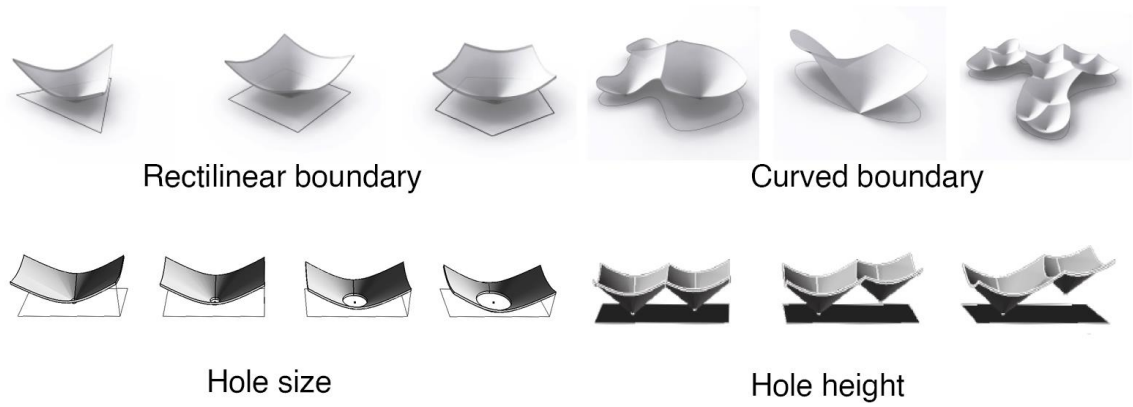


Figure 6.1 Parameters of the subtraction technique [1]

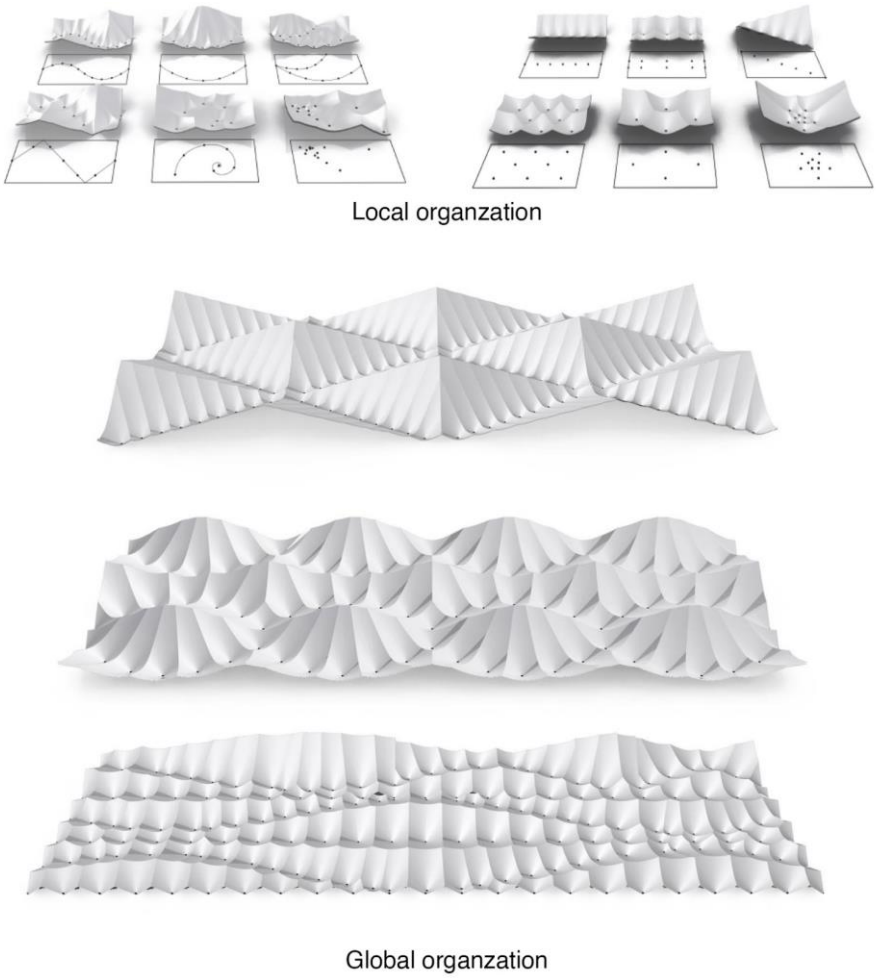


Figure 6.2 Local and global organizations of holes [1]

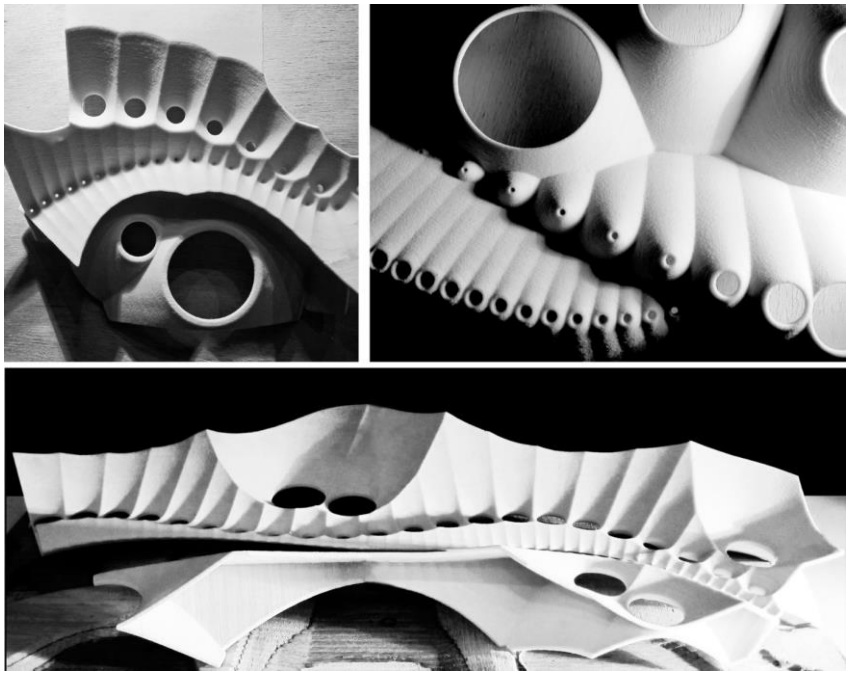

Figure 6.3 Tectonic articulations of conical forms [1]

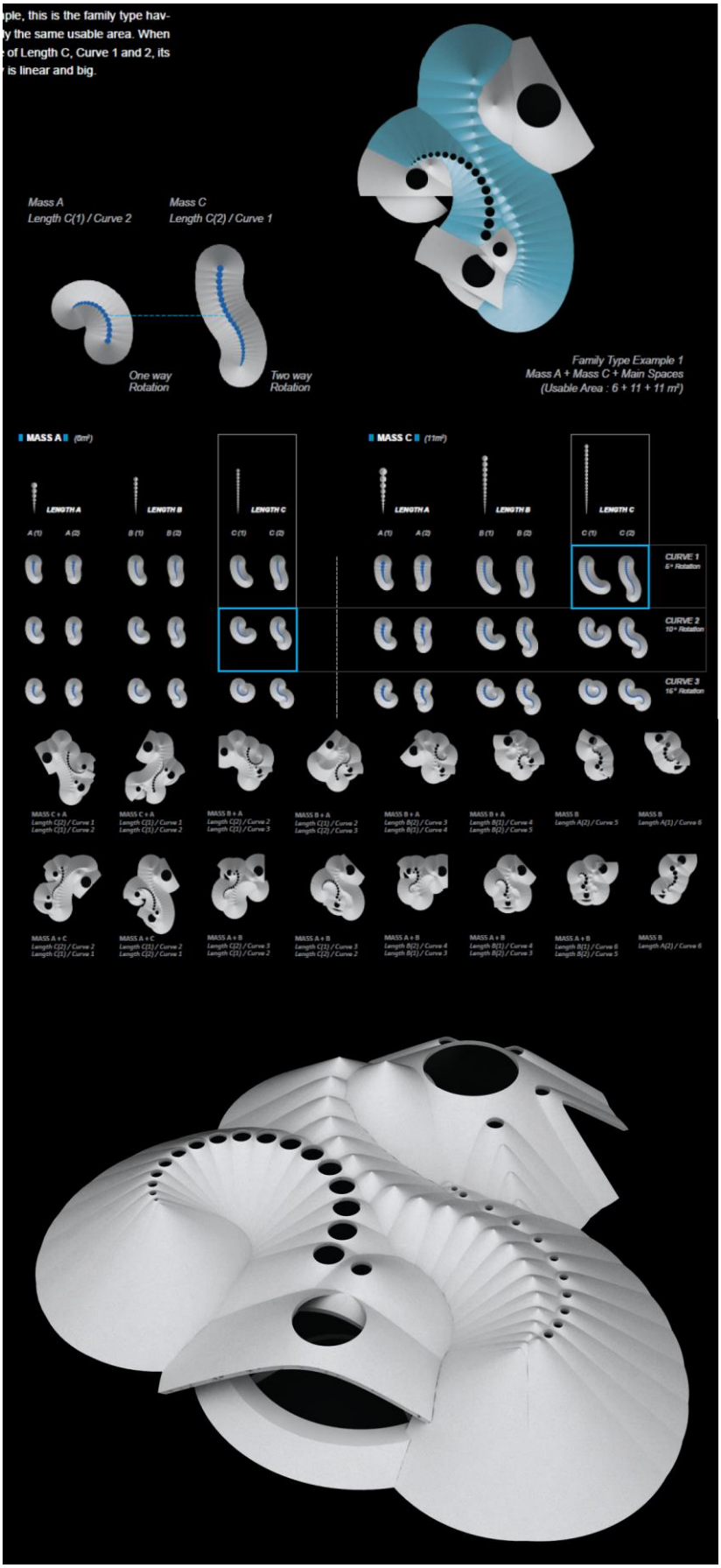


Figure 6.4 The generative design strategy for an ecolodge in the desert of Egypt [1]

The limitation of the design technique proposed by the 35 Degree project lies in twofold: first, the subtraction technique was limited to circular holes, and the modeling technique was based on the Boolean method of intersecting cones, which aligned with the design intention of the project, but restricted the design possibilities to conical surfaces and did not fully investigate the parameters and possibilities of the subtraction technique.

To overcome these limitations this thesis proposed integrated physical-digital solutions:

- The physical subtraction technique with a vacuum machine proposed in § 5.1.2 opens the possibilities for linear paths and eliminates the need for custom made formworks
- The parametric methods developed in § 5.3.2 and in § 5.3.3 allows the modeling of holes with different geometries including polygonal, linear, and curved shapes as well as solid piles.
- A robotic technique for sand deposition and subtraction (§ 6.1.3).

Together the developed solutions allowed to further investigate the parameters and morphological potentials of the addition and subtraction techniques.

Rather than considering the organization of the holes as the main design objective, this thesis focuses on the design of the emergent ridges as the main characteristics of the sand surface. The objective is to achieve certain ridges articulations by searching the distribution of holes that returns the desired ridges. For instance, diverging or converging ridges results from using concave or convex curves, respectively. While the densities of holes on the curves define the resolution of the ridges on the surface (see Figure 6.9). The design objective necessitated the study of the effect of holes parameters on the emergent ridges (see Figure 6.12).

Based on the design approach of ridge patterns, and by using the developed physical and digital methods of sand formation in this work the thesis examined the following parameters:

- Recursive branching distribution of sand deposition
- Generation of solid piles with different border shapes
- Combination of both the addition and subtraction techniques in hybrid formations
- The relationship between linear holes and the emergent pattern of ridges

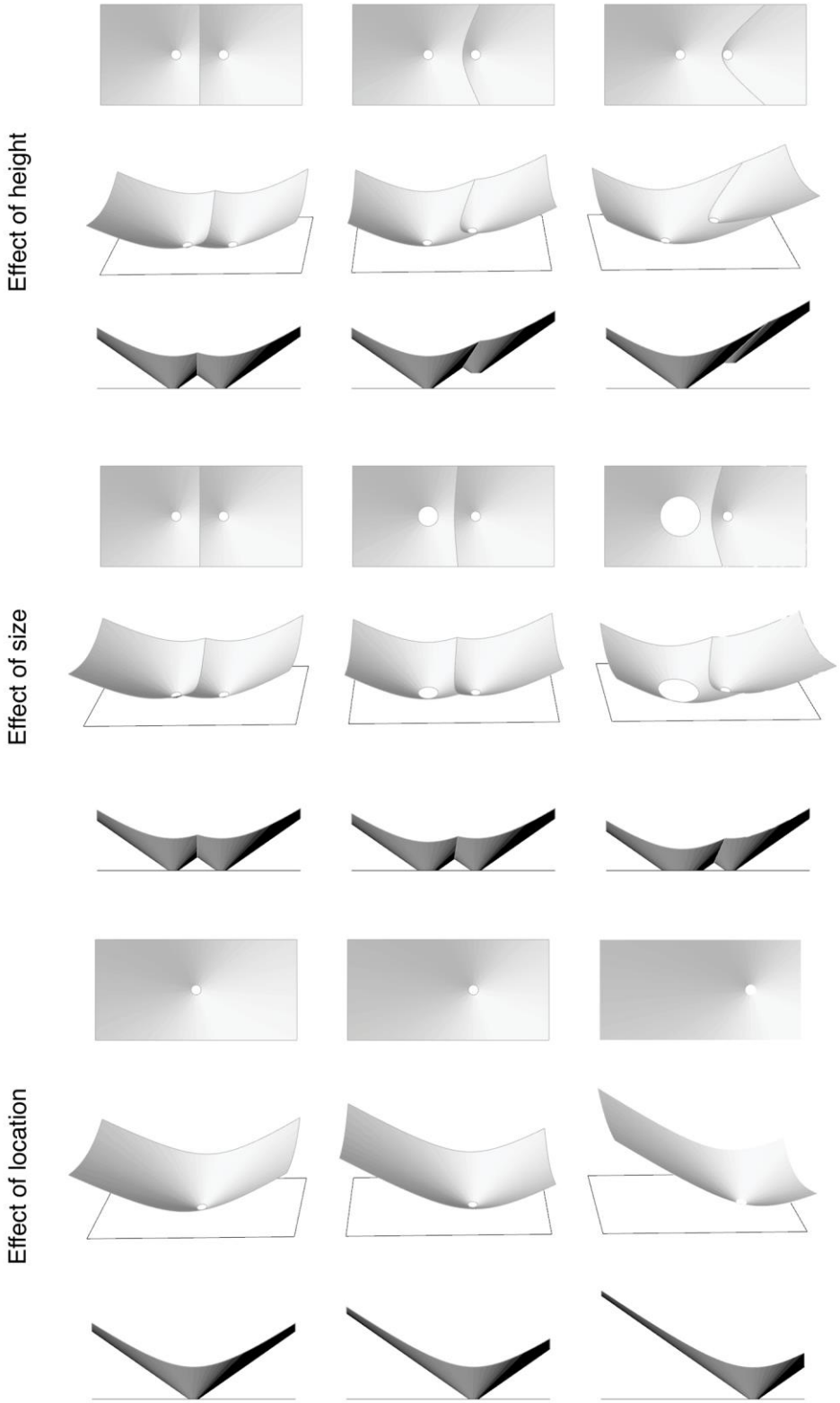


Figure 6.5 study of effect of holes height, size, and location on the ridge and surface form

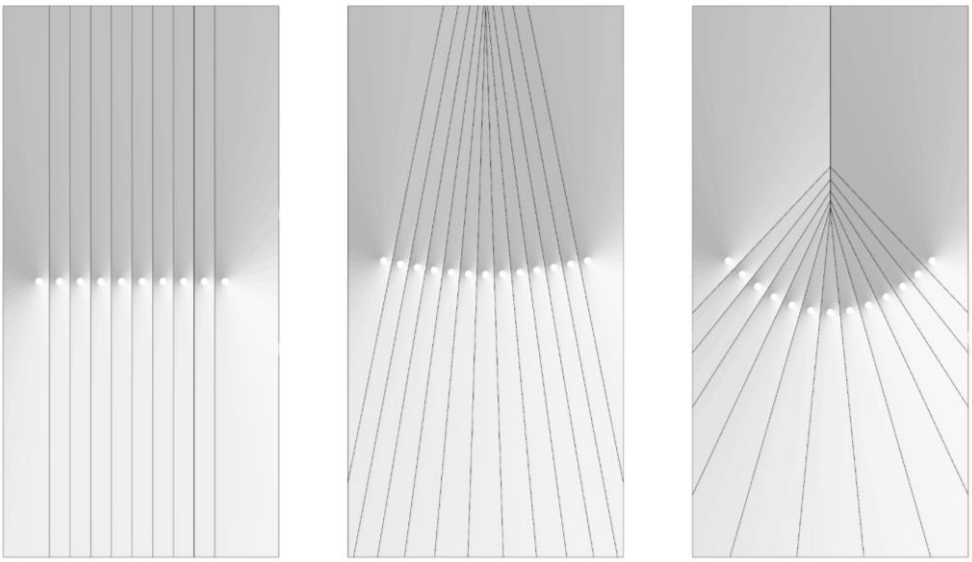

Figure 6.6 Study of effect of organization of holes on the directions of ridges

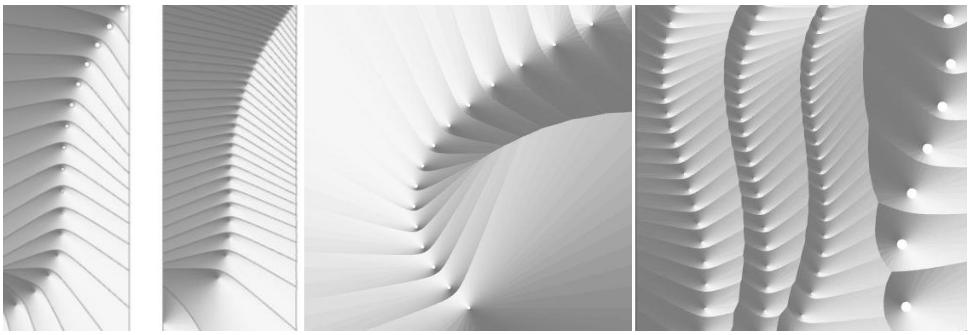

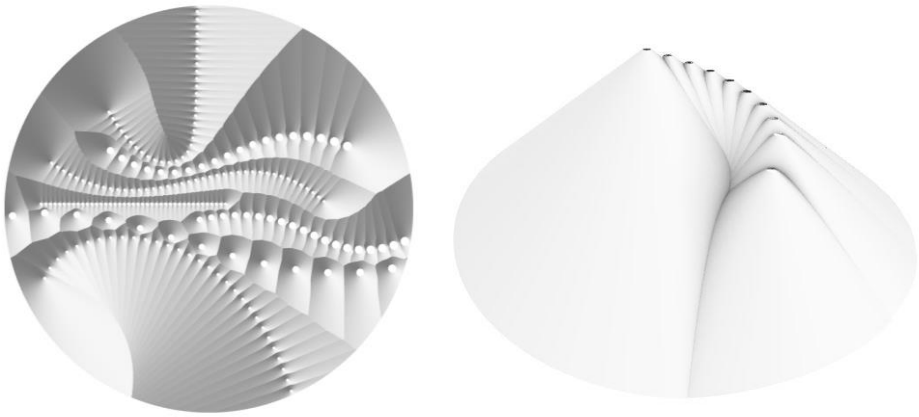

Figure 6.7 Articulations of curved organizations of holes at different heights and densities

**Recursing branching organization**

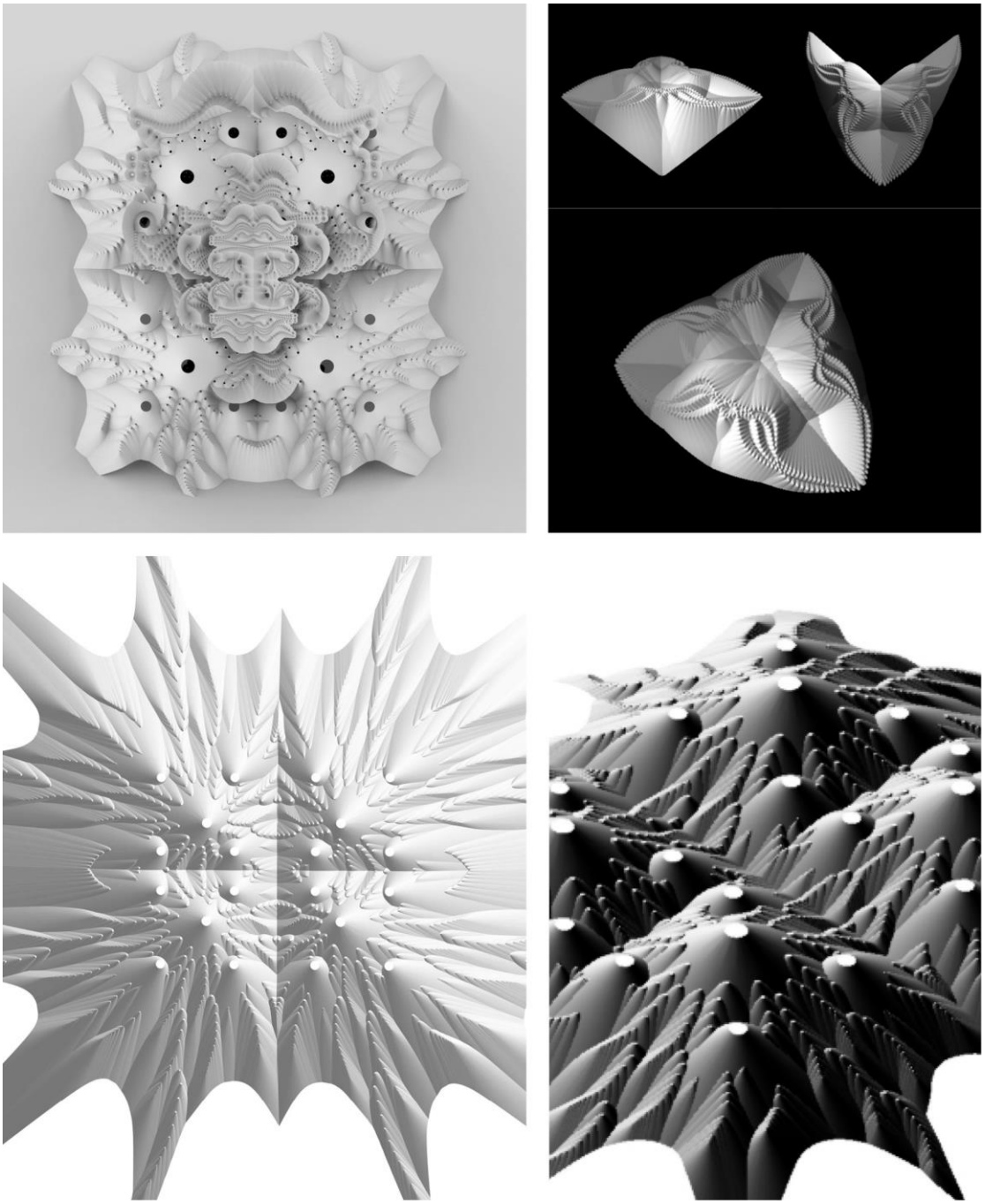

Figure 6.8 Recursive branching organizations

**Recursing branching organization**

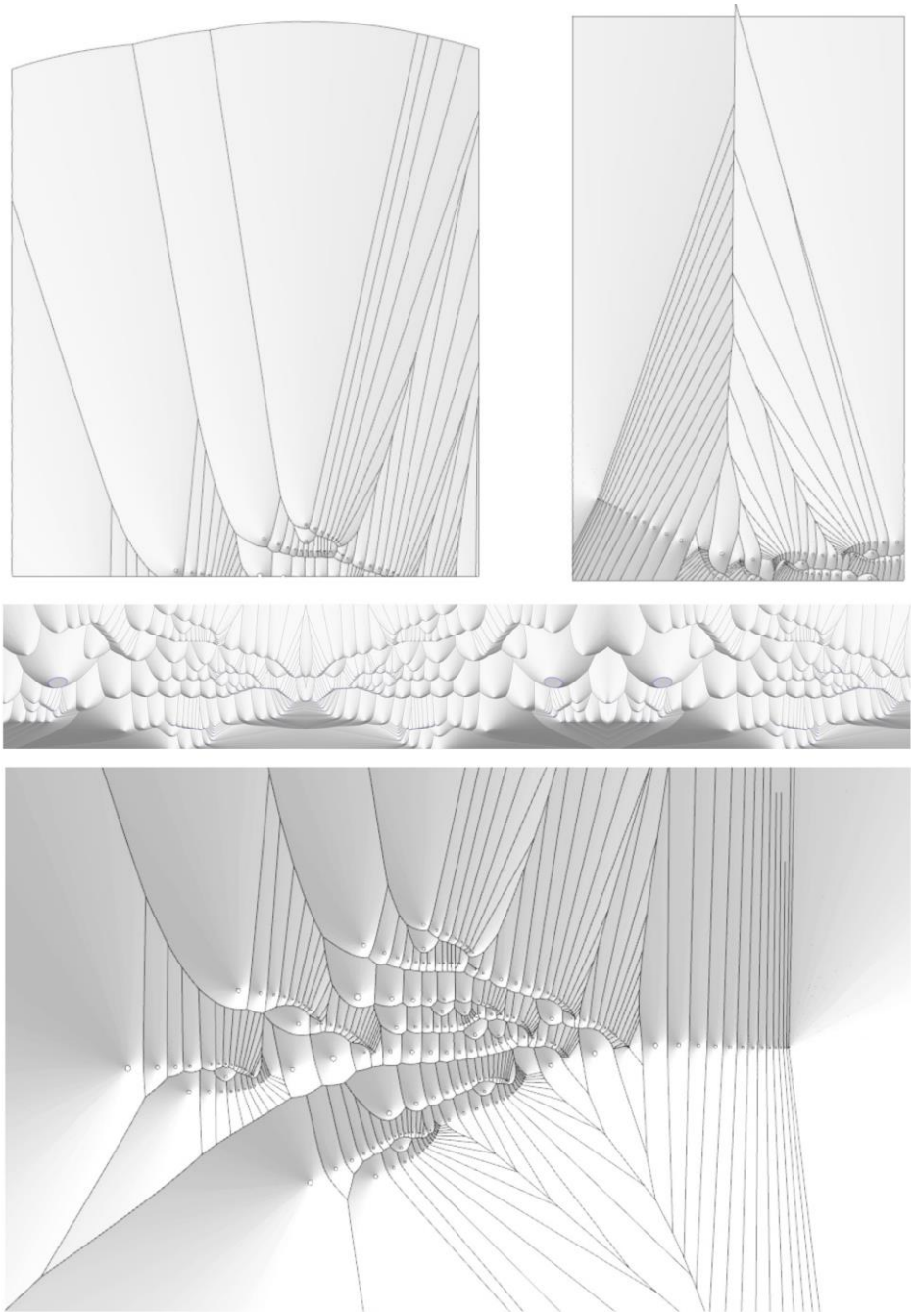

Figure 6.9 Study of the relationship between holes distribution and the directions of the ridges

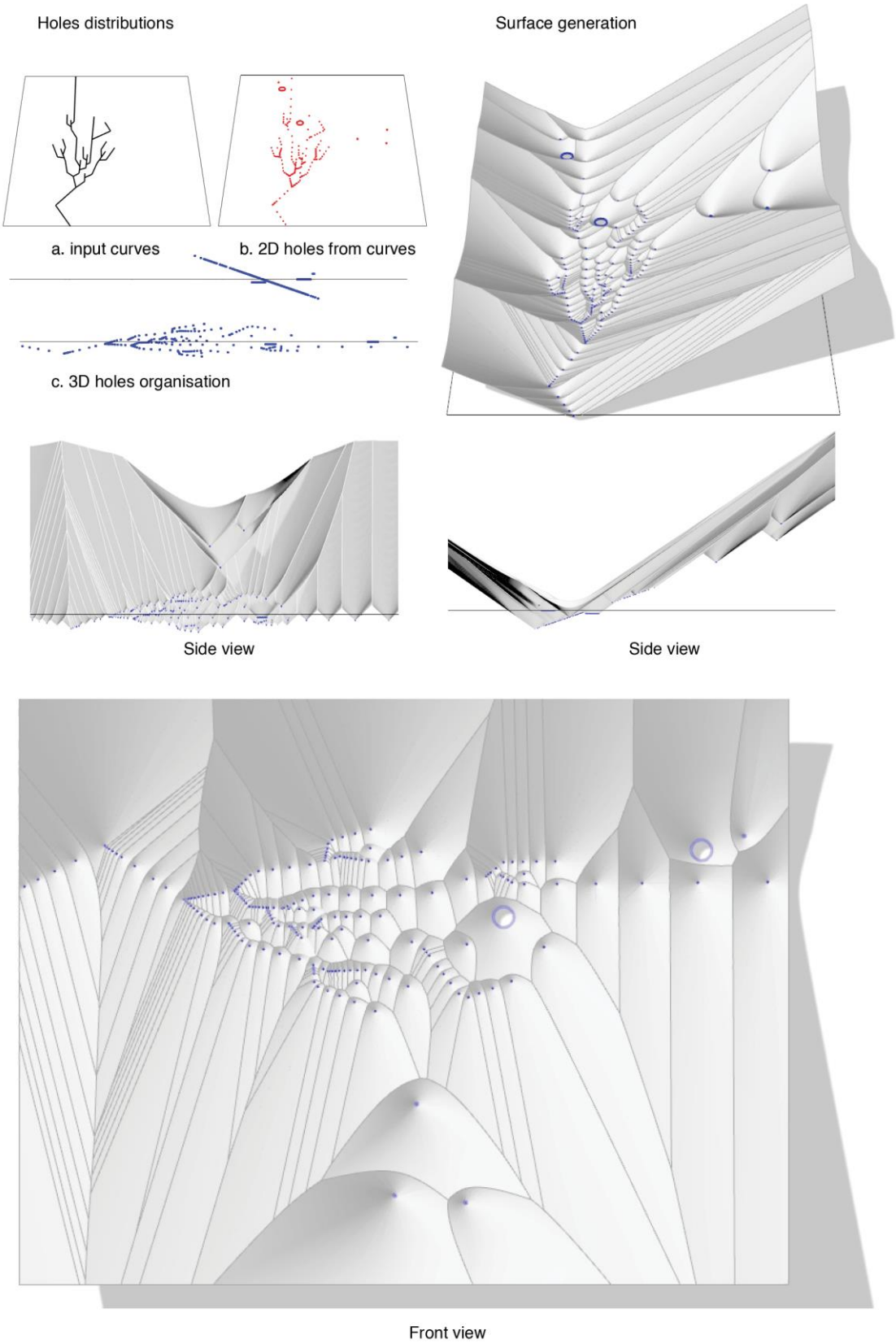


Figure 6.10 Design strategy of a proposed sand wall

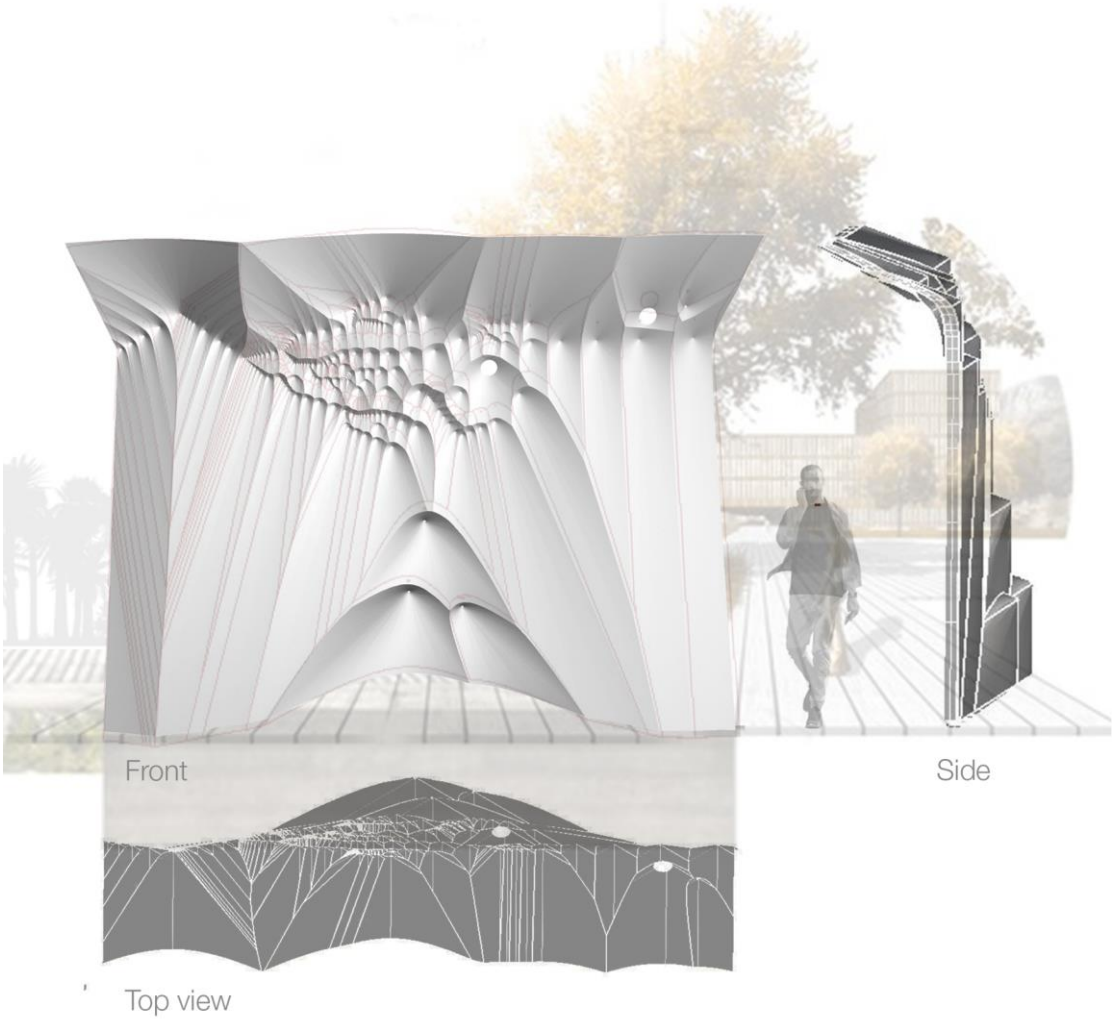


Front, top and side views of the proposed portion of the gate in context

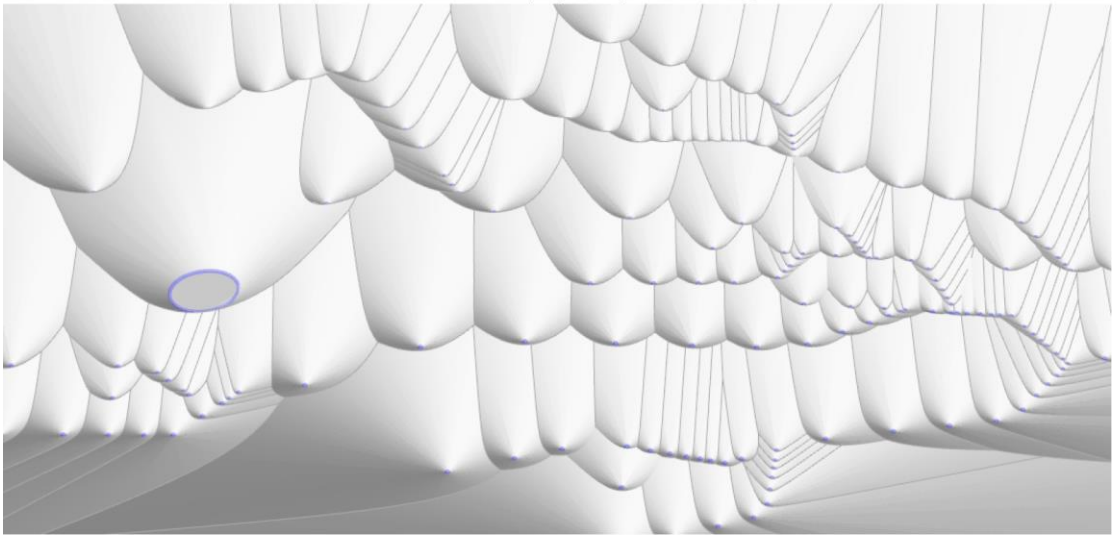

Figure 6.11 Model of the proposed sand wall

**Subtraction using linear holes**

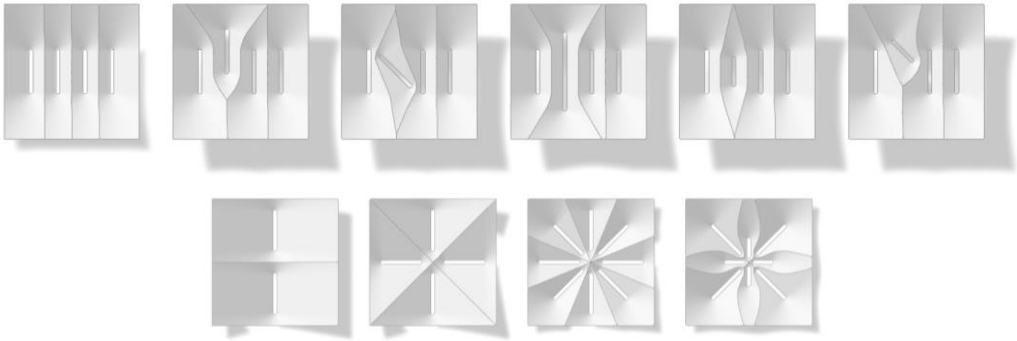

Figure 6.12 Study of the effect of linear hole location, rotation, and size on the emergent ridges

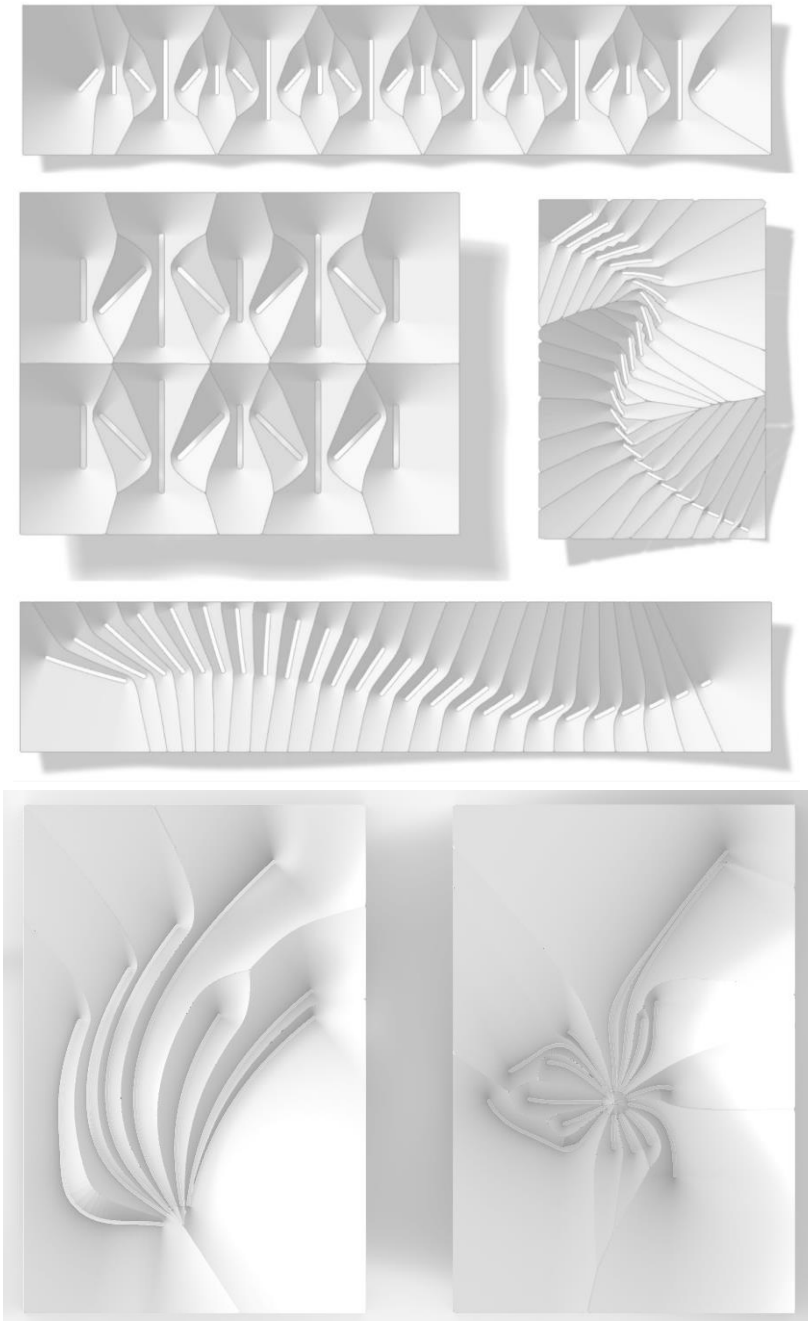

Figure 6.13 Models of different organizations of linear and curved holes

**Solid piles formed by deposition on predefined bases and planes**

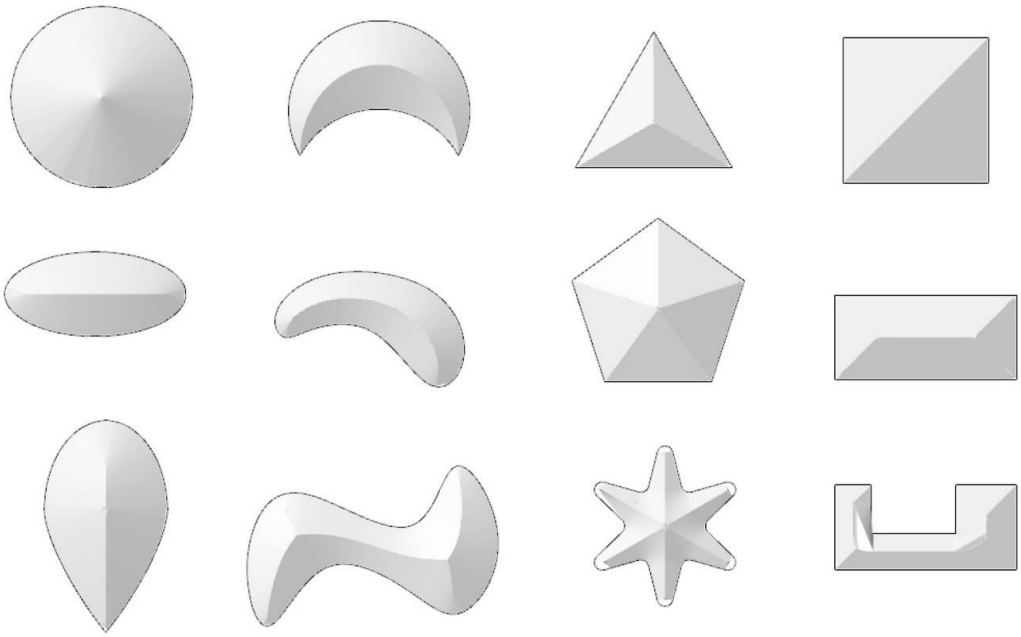

Figure 6.14 Models of solid piles formed by sand deposition on predefined bases. The models are generated by the boundary to ridge code based on the medial axis method.

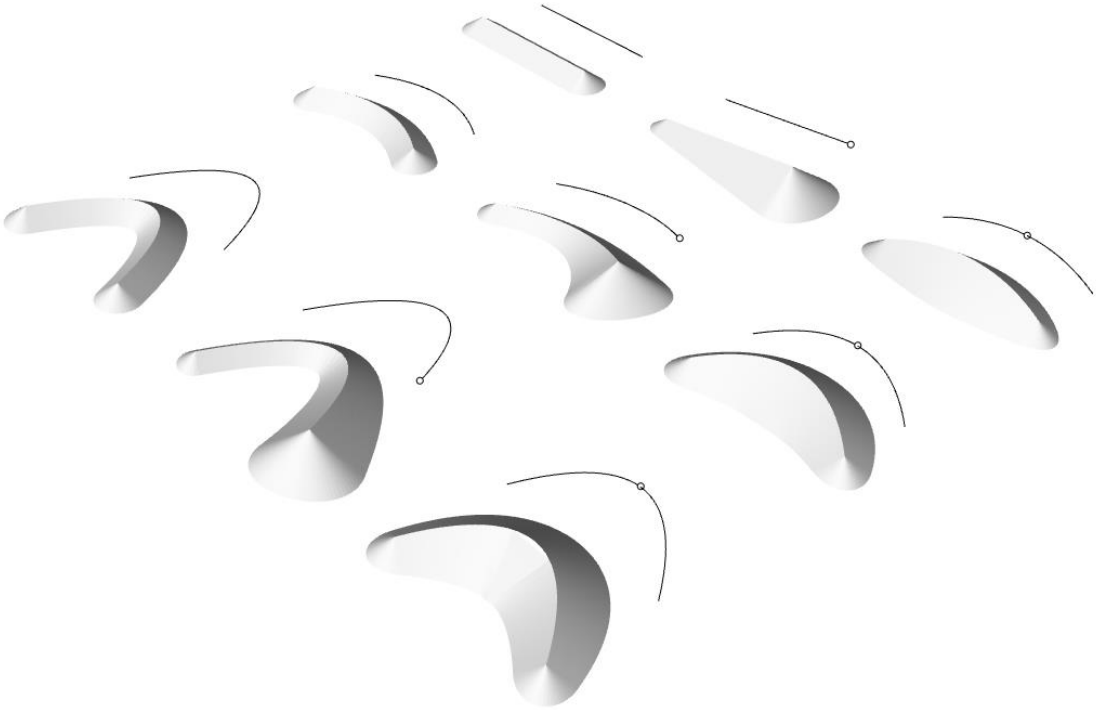

Figure 6.15 Models of sand piles formed by sand deposition on a plane. The models are generated by the ridge to border code based on the medial axis method

**Integrated addition and subtraction formations techniques**

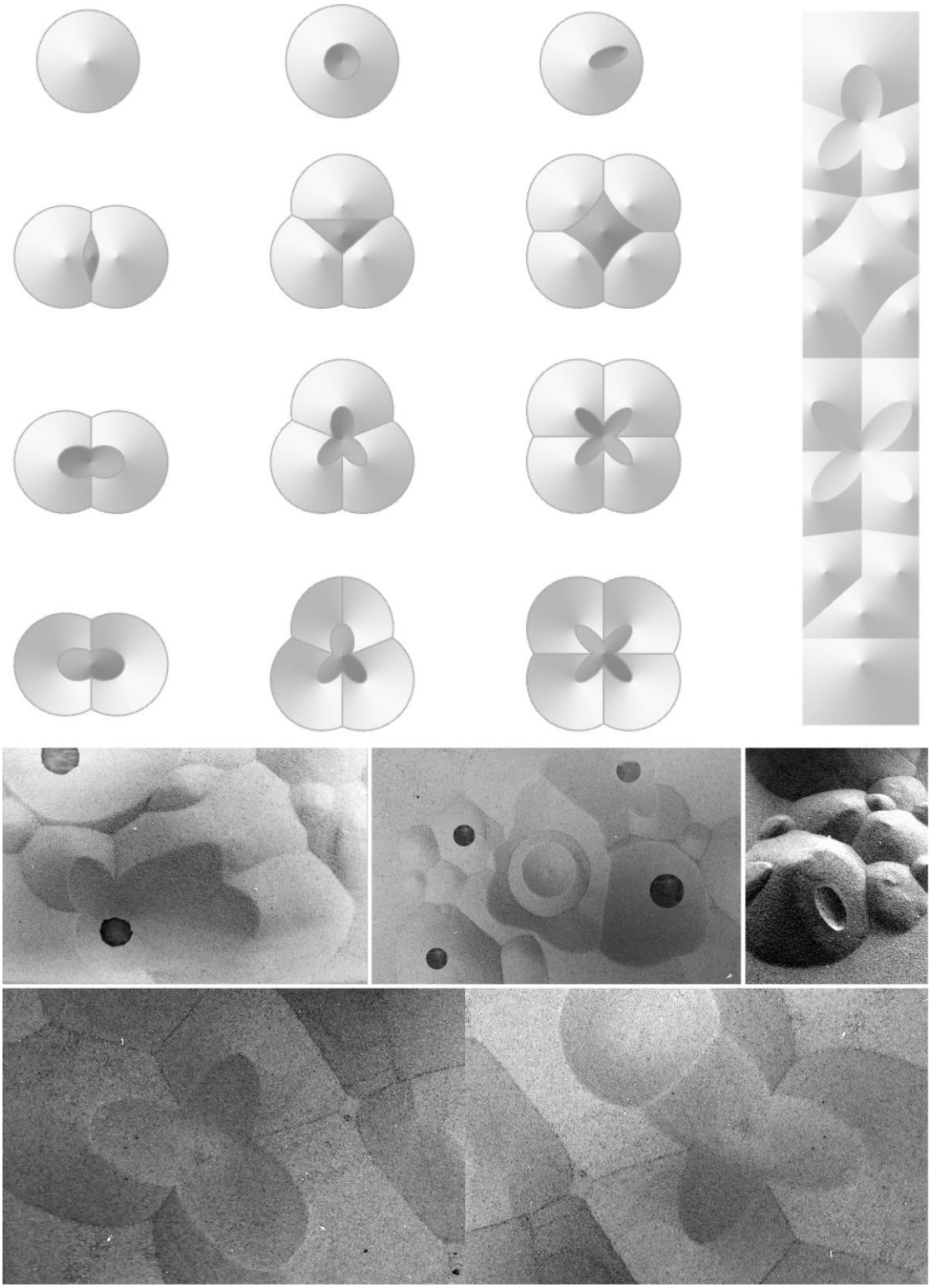

Figure 6.16 Digital and physical models of hybrid addition and subtraction of conical forms

### 6.1.2 Fabrication prototypes

The 35 Degree project proposed a method for the fabrication of sand blocks by casting Hyposand in between two panels (Figure 6.17). However, the assembly of more than two panels was not studied. For larger scale applications, this subsection introduces two prototypes of blocks making made of three tiles (model Alex-12) and 6 tiles (model D7-13).

Figure 6.17 The sand block of the 35 Degree project was made of two panels (20x40cm)[1]

**Model Alex-12**

In this work, a method of assembly is developed to enable the fabrication of sand blocks from more than two panels. Figure 6.18 shows the fabrication of 50x50x7cm sand block.

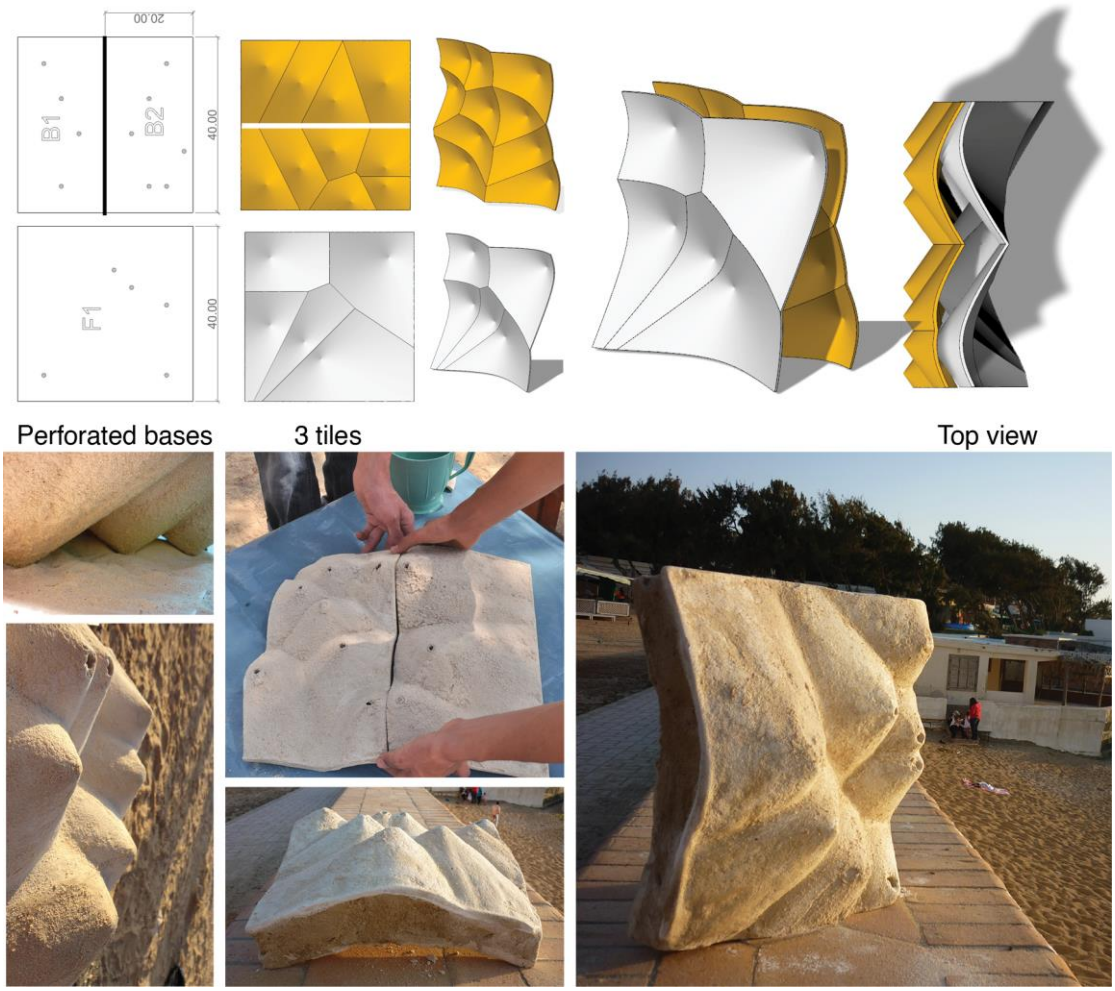


Figure 6.18 Drawings and making of the model Alex-12. The block is fabricated from three panels

**Model D7-13**

To overcome the limitation of model Alex-12, model D7-13[68] presented here proposes a technique of assembly based on modular overlapped tiles. A model composed of 10 panels of 20x40cm is thought. The panels are arranged vertically on the front side and horizontally on the back side to insure the interlock. Moreover, the seams of the tiles are shifted to afford a staggered assembly. The panels are assembled through common holes and molded in polystyrene for light purposes. The technique allows the assembly of unlimited number of panels to compose large formworks that are then molded with Hyposand to create a monolithic form.

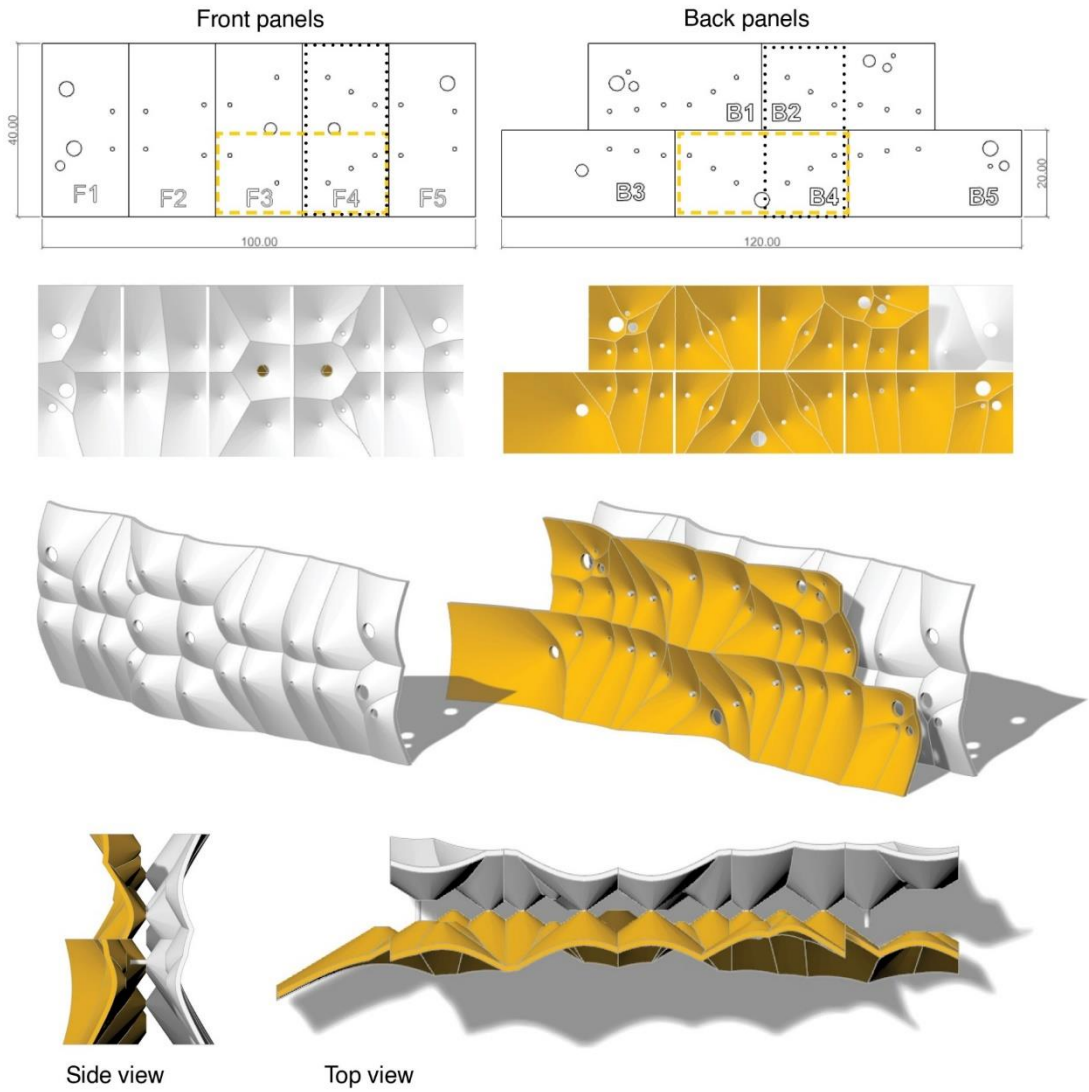


Figure 6.19 Drawings of the model D7-13.
The front and back panels are overlapped to provide an interlocked assembly.

[68] The model was developed within the short academic course 'Complex structure' of Professor Maurizio Brocato at ENSA Paris- Malaquais in 2013. The following students made part of the model design and fabrication: Beatriz Gomez, Stéphanie Guezenoc, Alienor Ibled, Eric le Mene, Laura Lapios, Clara le Bihanz Pauline Herbelor.

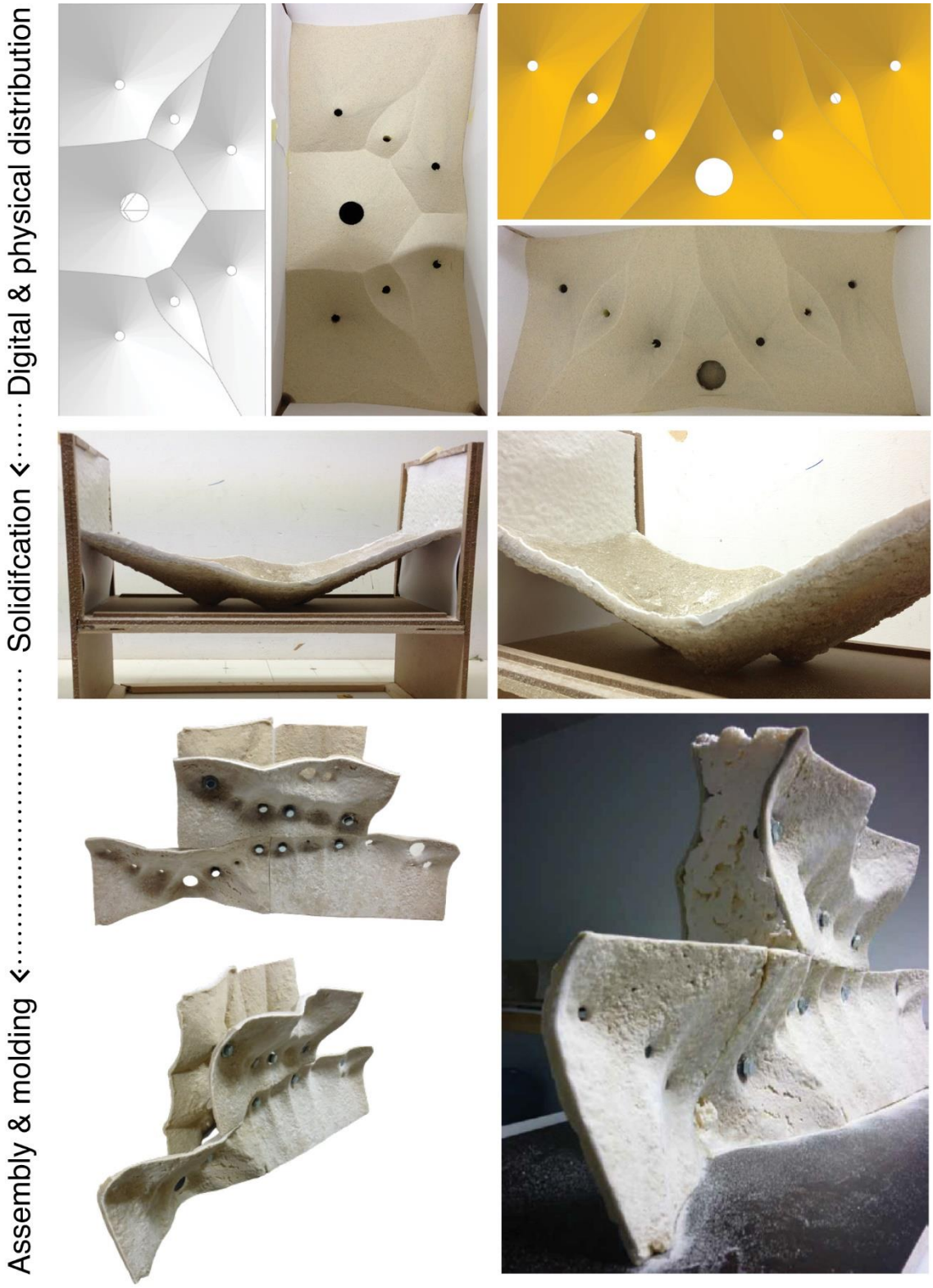


Figure 6.20 Process of making of model D7-12. The model tests the overlapping technique of assembly

### 6.1.3 Robotic deposition technique

In the last few years, there has been an increasing interest in developing architectural systems based on the robotic deposition of sand as previously discussed in chapter 1. The majority of prior research explored the robotic deposition of sand as a design tool for morphogenetic exploration. However, the data on the deposition parameters are limited and the digital modeling was not investigated.

This subsection aims at constructing the digital-physical workflow of the robotic deposition technique. In terms of modeling it aims at generating sand surfaces and robotic paths from the input deposition curve. Physically, the objective is to correlate the robotic parameters and the material behaviour. Finally, the digital and physical processes are correlated by the information of robot speed of movement. In this work, the medial axis (ridge to border) algorithm is used.

First, the sand and robot parameters are defined. Then, the parameters are studied to identify their interdependencies. Following, the modeling method is discussed in the light of to the acquired data. Finally, the digital-physical workflow is presented.

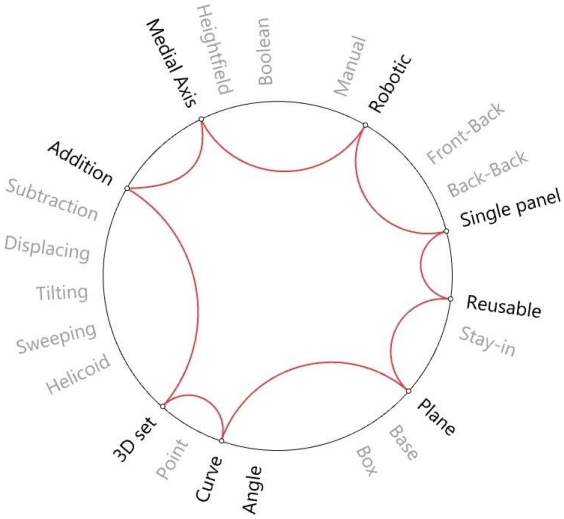


Figure 6.21 Diagram of methods for robotic deposition technique

A prerequisite to correlate the digital and physical methods is to define the relation between the speed of robot and the height of the resulting pile. To achieve this objective, the parameters of the method are defined and studied through digital and physical experiments.

Four parameters constitute the robotic deposition technique: (i) the flow rate of sand, (iii) the pouring height, (iii) the robot speed, and (iv) the input curve of deposition in the modeling algorithm. Each parameter is studied below to define the constants and variables of the system as well as the relationship between the robotic parameters and the emergent sand forms.

In the experiments, the same type of sand is used. and the deposition orifice is fixed. The robot is mounted with a simple deposition tube of 50 cm height and 10 cm width. At the bottom of the tube is a circular orifice of 10 mm diameter.

A. **The flow rate of sand**: the common knowledge in sand physics indicates that the flow rate of sand is constant[69] and depends on the orifice area [206]. Since the orifice area is fixed in this work , then the flow is considered as a constant in the process.
B. **The height of pouring**: upon the experiment showed in **Error! Reference source not found.**, it was found that the height of pouring does not affect the height of sand pile as much as it is close ridge of the of the pile.
C. **The speed of deposition path :** To define the relationship between the speed of robotic deposition and the height of the resulting pile, sand is poured along a path at different speeds. The path contains 4 segments of 40 cm , each is assigned to a robot speed value in (cm/second). Figure 6.22 shows the path with the different speed values for each segment. The trajectory is first assigned into the robotic control code and the speed values are then attributed between the endpoints of each segment.

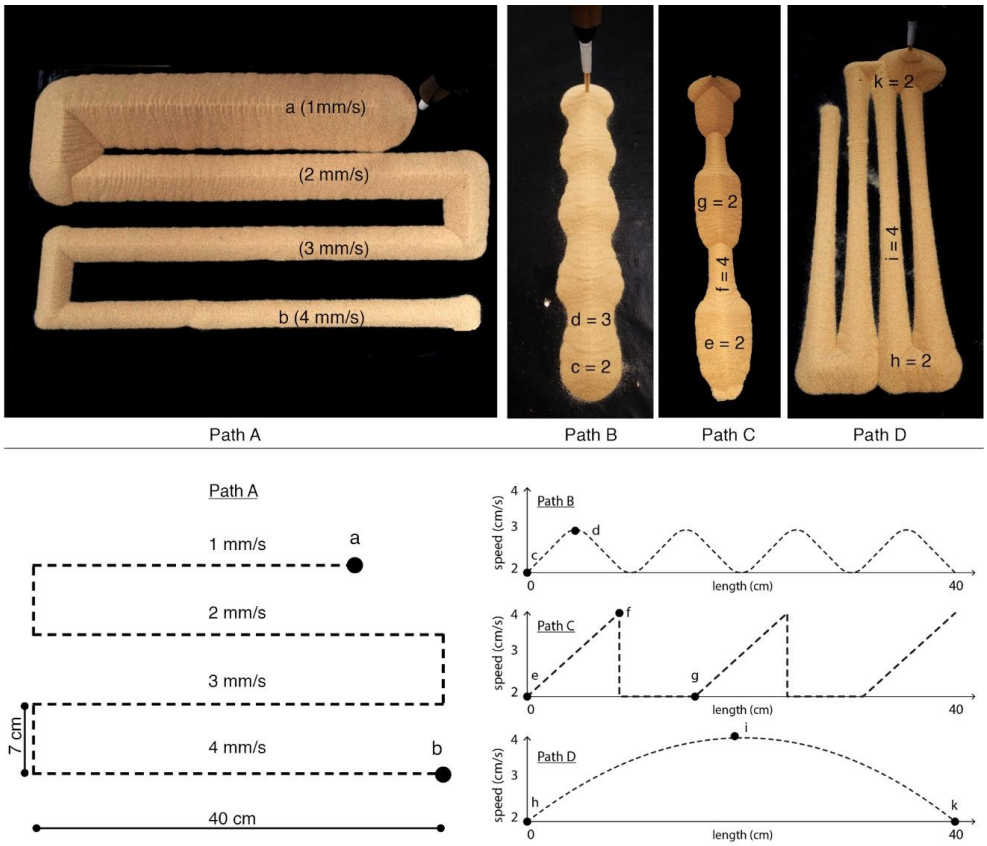


Figure 6.22 Robotic deposition: study of the robot speed vs. sand height

[69] Unlike water, the flow of sand is constant that is why sand is used in the hourglass instead of water to measure the passage of time. In the case of a liquid, the rate of flow is determined by the height of the liquid above. But, in the case of sand the pressure at the bottom of a container of sand is effectively constant and does not depend on the height of the grains above. The reason behind that is that the grains form chains and bridges that transmit their weight to the side of the container where they are supported by friction [205].

The results show that a 10 second deposition of sand from a fixed point returns a cone of 5 cm height (**Error! Reference source not found.**). While a moving deposition of 1 mm/ sec speed returns a pile of around 4 cm height (see point a, on path A in Figure 6.22). The acquired speed to height relation informs the modeling method where sand height is translated to robot speed in the generation of robotic path.

D. **The digital workflow:** Based on an input curve of deposition, the digital workflow generates the sand surface and produces the robotic path with its assigned speeds. The workflow correlates three methods developed in this work: (i) the Ridge to border modeling algorithm, (ii) the optimization of the deposition curve code, and the robotic control code. The typical digital process is as follow:

1. **Input path**: An input deposition path is given as a curve
2. **Path relaxation**: The curve is first relaxed to define the optimum ridge curve of the pile in respect to the slope of sand. The optimization is processed using the curve relaxation algorithm introduced in 5.3.5.2
3. **Surface generation**: The form of the pile is then generated from the ridge curve using the medial axis- ridge to border algorithm described in 5.3.5
4. **Robotic path**: Then the robotic path is generated from the relaxed curve according to the method described in the robotic control section (§ 5.3.7)
5. **Speed of movement**: the speed of the robot is then defined by assigning each target point on the robot trajectory to the height of its corresponding point on the ridge curve

Figure 6.23 Illustrates the process using a sandpile model generated by a circular path at different heights. The deposition curve is illustrated in black, the optimized curve, which is the pile ridge in red, and the robotic path in blue.

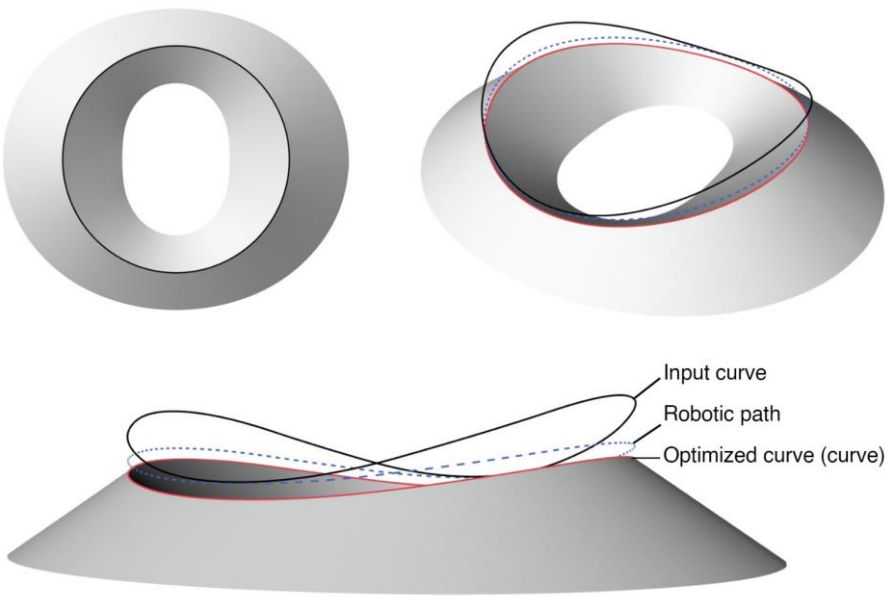


Figure 6.23 Optimization of input curve for robotic deposition process

Figure 6.24 Robotic deposition experiments of linear, linear then addition, curved, and overlapping curved paths.

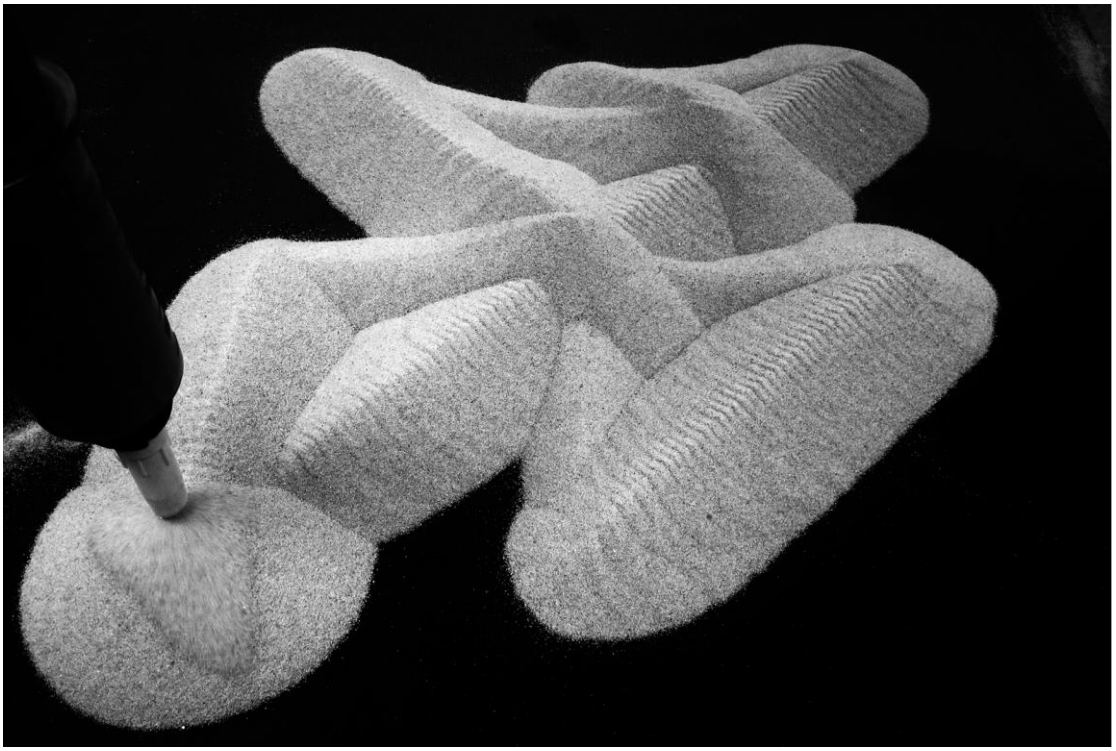

Figure 6.25  Physical model of overlapping deposition and a digital model of a curling path

## 6.2 Tilting technique

This section introduces the tilt method of sand distribution and proposes its application for the fabrication of non-standard 3D tiles. First, the motivation behind the method is discussed and the development methodology is defined. Secondly, the design and fabrication methods are identified through a first prototype. Finally, several prototypes are developed to examine the effect of the design parameters and to exhibit the potentials of the tilt method to produce efficiently non-standard tiles.

### 6.2.1 Method definition

As discussed along the research, the slope of a sand pile has a constant angle of repose of 35 degree[70]. However, the constancy of the angle limits the morphology of the piles to uniform slopes. This limitation raised the question of how to create a pile with different slopes and how that would open new morphological possibilities.

Certainly, the slope of sand cannot exceed the angle of repose, but it was noted during the work that decreasing the angle is possible if the pile is tilted, which opens the opportunity for different slopes, and accordingly different morphologies. This observation motivated the research to study the effect of tilting on the morphology of the sand piles and the fabrication possibilities that can be developed from this method of material distribution, herein the tilt method. The effect of tilt on liquid materials can be observed in daily life situations. For instance, when leaning a cup of water, the surface remains horizontal. However, sand behaves differently within the same situation, where the surface remains stable and parallel to the base of the cup despite tilting. But when the angle of tilt ($\alpha$) exceeds the maximum angle of repose of sand ($\Theta_{max}$) the surface undergoes an avalanche and slides to a stable slant. Note that in both cases, the tilt changes the area and form of the surface according to the angle of tilt and the form of the container.

Figure 6.26 Unlike water, the surface of sand remains stable until the tilt exceeds the angle of repose

[70] The angle of repose ranges from 30° to 40° depending on the morphology of the grain and the friction see §2.3

#### 6.2.1.1 Initial test

The initial test in Figure 6.27 studies the effect of the tilt angle *α* on the angle of repose *Θ*. First, a transparent box is partially filled with sand, which surface is flat and horizontal. Secondly, the box is tilted at four angles 30°,50°,60° and 70°, and finally *Θ* is measured for each tilt. It is observed that the surface of sand remains stable until *α* exceeds the *max*imum angle of repose *Θmax* after which the surface inclines with an angle of repose *Θ* that is equal to the difference between *α* and *Θmax* (*Θ* = *α* - *Θmax*).

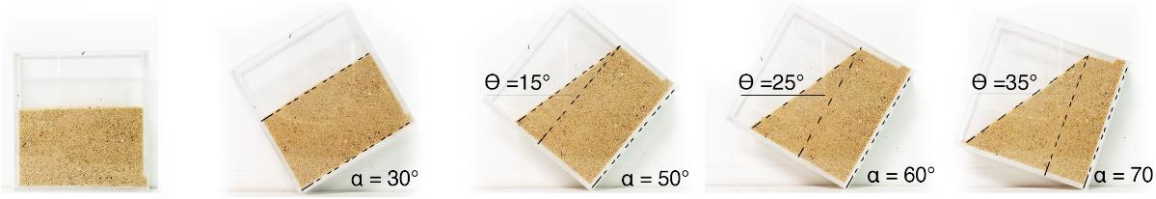


Figure 6.27 Measuring the angle of repose at different tilts

The initial test illustrates a simple model, where the sand has a single surface, but in the case of a pile with multiple surfaces (Figure 6.28) a study of the geometry and code are essentials to model complex aggregations.

Figure 6.28 Piles with multiple surfaces

#### 6.2.1.2 Application potentials

The advantage of the tilt method lies in the possibility of generating piles with different slopes from the same base by changing the angle of tilt. This advantage of material distribution when considered with the solidification method opens the opportunity for the fabrication of three types of non-standard tiles: one sided tile (hollow and solid), and two-sided tiles (solid block) as shown in Figure 6.29.

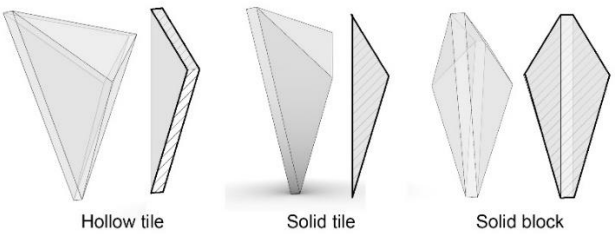


Figure 6.29 The tilt method allows the fabrication of three types of tiles: hollow tiles, solid tiles, and solid blocks.

The hollow and solid tiles are considered for 2D assemblies such as surface cladding, while the solid blocks are for 3D assemblies like for instance walls and vaults. Pre-cast 3D tiles are used as architectural elements in interior and exterior cladding for aesthetic, lighting, thermal

and acoustic purposes. Available fabrication methods of casted 3D tiles are based on the fabrication of formwork including milling of wood and polystyrene blocks: vacuum forming of plastic sheets, direct forming of clay, plaster, silicon, and rubber molds. However, the expensive cost of molds limits the design to standard tiles or a variation of few molds. For instance, only three variations of hexagonal ceramic tiles (flat, concave, and convex) are used for the exterior cladding of the museum Der kulturen in Basel by architects Herzog & de Meuron in 2011 (Figure 6.30). However, the tilt method introduced in this work enables the fabrication of non-standard panels at low-cost. The advantage of the sand mold lies in being a minimum waste method, recyclable and fast curing.

Figure 6.30 Standard 3D tiles are used for the exterior cladding of der Kulturen museum in Basel (left), Liverpool department Store in Querétaro City (middle) and for interior cladding (right)

#### 6.2.1.3 Methodology

To identify the potentials and process of the tilt method an experimental approach of study is considered in twofold: 1) the design method studies the geometry and defines the parameters and the algorithm of form generation 2) the fabrication method defines the process of making, solidification, and assembly. Finally, a series of prototypes are developed to examine the potentials of the tilt method to produce efficiently non-standard tiles.

#### 6.2.1.4 Design and fabrication method of 3d tiles and blocks

This subsection introduces the tilt method by first studying the geometry to define the calculations methods that are necessarily for coding, secondly the design parameters, algorithm and processes are discussed and finally the fabrication constraints and processes are introduced. It is essential to briefly describe the fabrication method first as it informs both the geometrical study and the design method. The fabrication process is applied firstly by pouring dry sand over a horizontal base that is tilted to achieve the desired form, then solidified by spraying the saline solution and finally re-titled to the horizontal plane for assembly.

The following terms of angles will be used along this section: 1- angle of tilt ($\alpha$) 2- angle of repose ($\Theta$) 3- *max*imum angle of repose ($\Theta max$), angle of vector rotation ($\beta$) and angle of axis rotation ($\Psi$).All angles are measured clockwise from the x axis.

### 6.2.2 Parameters and constraints

The geometrical study examines the deformation of the sand pile under tilting effect to define its parameters and constraints, which are essential for the development of the algorithm in the following subsection. The study aims at defining the method of calculation of two variables: (i) the **relaxed angle of repose *ϴ***, and (ii) the **angle of vector rotation *β*** . The calculations are based on the given inputs of: (i) the angle of tilt *α*, (ii) the *max*imum angle of repose of sand *ϴmax (*35°*)*, and (iii) the dimensions of the base.

To study the transformation of the pile over tilting, a pyramidal pile over a triangular base is analyzed. First the horizontal pile is tilted at 20° around the x-x' axis. Then re-tilted back to the horizontal plane (Figure 6.33). Section a-a of the tile is defined by the center of rotation O, the tilt angle *α*, the angle of repose *ϴ*, the *max*imum angle of repose *ϴmax*, the angle of vector rotation *β* and the base length AC. Figure 6.31 shows the sections of the horizontal pile (abc) and the tilted pile (ABC). It is noted that in ABC ∠ BCA remains constant at *ϴmax* but ∠BAC reduces as it exceeds the *ϴmax* to the horizontal axis AX. Consequently, the exceeded sand falls from point A until a new angle of repose *ϴ* is achieved making the stable pile AB'C. The new angle of repose *ϴ* is calculated as the difference between the *max*imum angle of repose *ϴmax* and the angle of tilt *α* (*ϴ* = *ϴmax* – *α*).

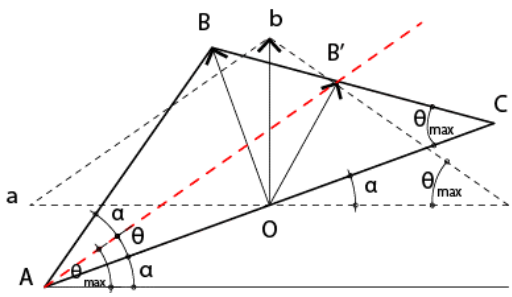


Figure 6.31 section through horizontal and tilted pile

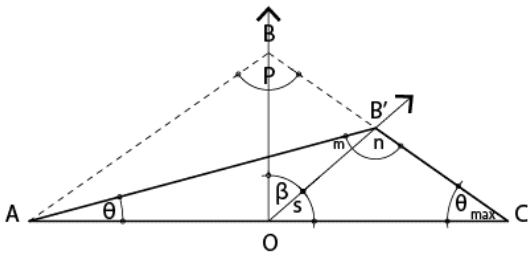


Figure 6.32 section through horizontal and re-tilted pile

In Figure 6.32 the tilted pile AB'C is re-titled to the horizontal plane and overlapped on the horizontal pile ABC. It is important for the algorithm to calculate the rotation angle *β* of the vector Ob to OB'. *β* is derived by defining: the angle *S*, and the lengths of the sides *OB'* and *B'C* through the sine and cosine rules of trigonometric functions (equations 1 to 4 respectively).

$$\beta = 90° - S \qquad \text{(Equation 6.1)}$$

$$S = sin^{-1}\left(\frac{(B'C)(Sin\,\theta_{max})}{OB'}\right) \qquad \text{(Equation 6.2)}$$

$$OB' = \sqrt{(B'C)^2 + (OC) - 2(B'C)(OC)(Cos\,\theta_{max})^2} \qquad \text{(Equation 6.3)}$$

$$B'C = \frac{(CA)(sin\,\theta)}{sin\,n} \qquad \text{(Equation 6.4)}$$

To verify the calculation method of $\beta$, equation 1 is applied on the tit angles $\alpha$ 0°,10°,20°,30° and 35°. The results show that at $\alpha$ = 0° the $\beta$ = 90° where the pile is horizontally stable and the vector is normal to the base, while at $\alpha$ = 35° the $\beta$ = 0° where no sand remains on the base and the vector is parallel to the base. The results justify the calculation method as the vector rotation angle $\beta$ range (0° to 90°) meets the range of the angle of repose (0° to 35°).

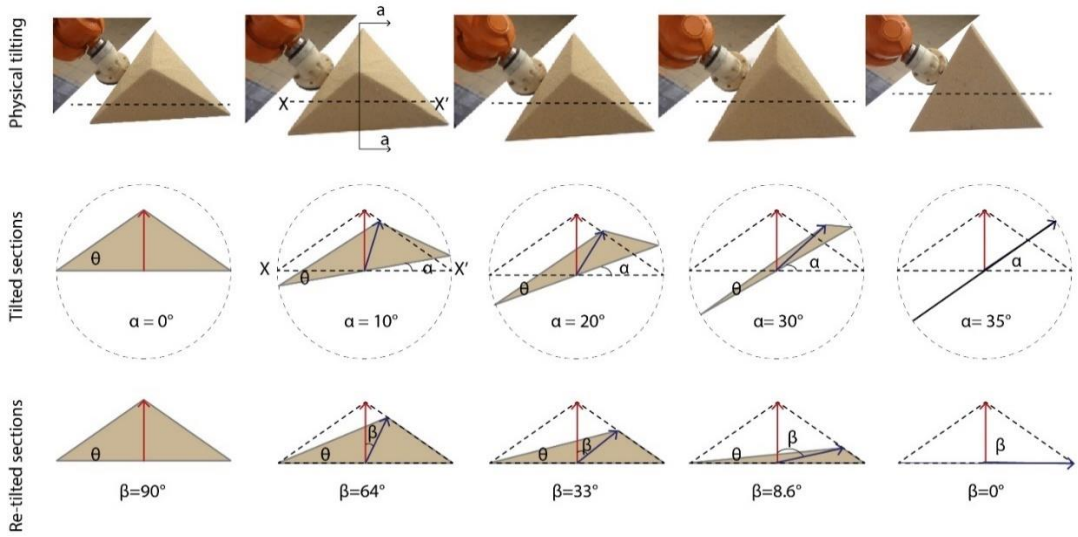


Figure 6.33 physical and geometrical analysis of the sequence of tilting from 0° to 35°

| Angle of tilt ($\alpha$) | Angle of repose ($\Theta$) | Angle of vector rotation ($\beta$) |
|---|---|---|
| 0° | 35° | 90° |
| 10° | 25° | 64° |
| 20° | 15° | 33° |
| 30° | 5° | 8.6° |
| 35° | 0° | 0° |

Table 6.1Values of $\Theta$ and $\beta$ according to $\alpha$

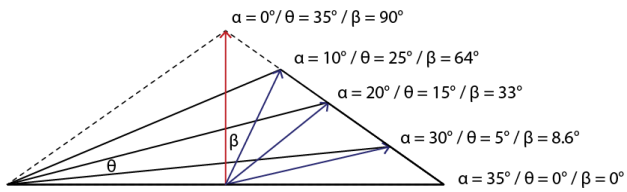


Figure 6.34 overlapped sections of piles at different angles of tilt

For the design consideration, it is important to note that the ridges displace in the opposite direction of titling, which decrease the area of the surfaces that are on the negative side of the rotation axe. The design and fabrication methods are introduced through a prototype of three hollow triangular tiles. To define the effect of tilting on the sand pile, the tiles are given a standard boundary (triangle of 15 cm side) with the same axis of rotation (the x axis), while being subjected to three different angles of tilt, 0°, 10° and 20°.

### 6.2.3 Algorithm of the tilting technique

The design technique studies the effect of tilting on the morphology of surfaces of constant slope. First, the design parameters are defined. Secondly, the algorithm of surface generation is detailed and finally, the design characteristics are discussed.

**Parameters :** based on the fabrication technique the design parameters are considered in two sets (i) The boundary condition: the shape of the base and the holes, and (ii) The rotation data: the axis and angle of rotation.

**Algorithm:** the objective of the tilt algorithm is to generate aggregations of tilted surfaces of constant slope. It is composed of three main parts:

1- **Input**: the given curves of the bases and the holes, the rotation axis, and angles.
2- **Process**: definition of the medial axe, the tilt vector, and the generation of the surfaces.
3- **Output**: the 3D model of the tiles and their associated information for fabrication including dimensions, rotation angles and axis.

The tilt algorithm is developed based on the '*border to ridge'* algorithm introduced in § 5.3.4. The algorithm uses the tilted vector (Vt) that considers the tilt and re-tilt angles as described above in the geometric study. The process of the tilt algorithm is illustrated Figure 6.35 :

1- The following parameters are given: boundary curves *Bc* and points *Bp*, the *max*imum angle of repose $\Theta max$, the tilt angle $\alpha$, the tilt axis *x-x'* and the rotation of the tilt axis $\Psi$.
2- The medial axis *Ma* and its points *Mp* are defined by the Voronoi tessellation of *Bp* points
3- The ridge points *Rp* are defined by moving the *Mp* points with the tilted vector *Vt*
4- The rulings are then generated between *Rp* points and their closest points on *Bc*
5- The surfaces of constant slope are then generated from the rulings

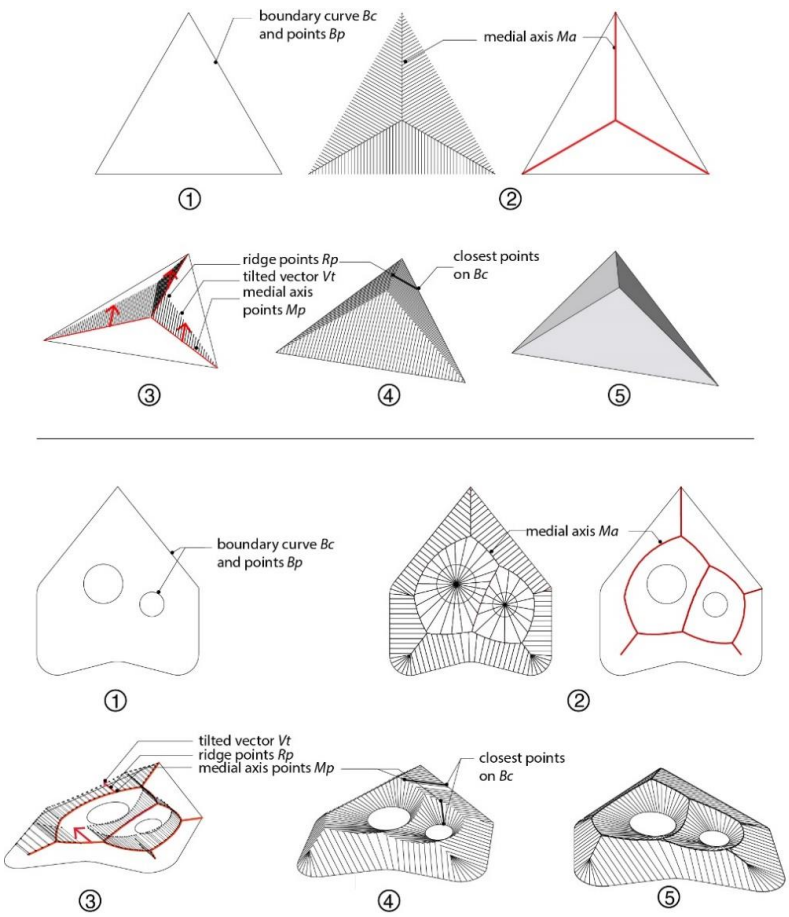


Figure 6.36 Process of tilt algorithm, steps 1 to 5 applied on a triangular base (top) and a hollowed freeform base (bottom)

### 6.2.4 Design and fabrication process

The design method provided the necessary information for manufacturing and assembly including: the shape and dimensions of the bases, the tilt angles and axis and finally the organization of the assembly. With this information, the fabrication method is applied on two sequential procedures: the formation of the pile by tilting the base then the solidification of the pile with the saline solution.

#### 6.2.4.1 The formation methods

The objective of the formation process is to tilt the sand pile to achieve the required slope while maintaining the sharpness of the sand ridges. Two methods of tilt are developed, a manual and a robotic method.

The strategy of the manual method is to pour the sand over a pre-tilted base. First, the base is fixed on a wood pivot, which top side is pre-cut according to the required angle. Secondly, the sand is poured over the base. Along pouring, the sand surface reaches the stable slope, and the required pile emerges with its distinct ridges while the excess sand trickle from the edges of the base.

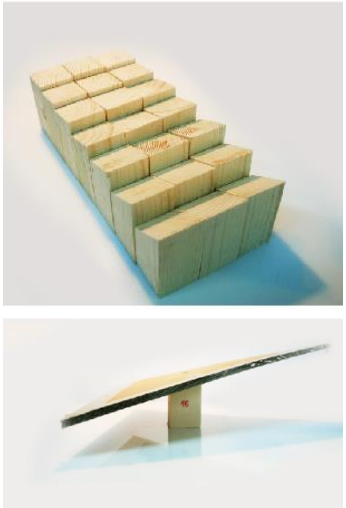

Figure 6.37
The top surfaces of the pivots are cut at different angles

The robotic method is based on first, fixing the base horizontally on the robotic arm, secondly, pouring the sand over the base until the pile is stable and the original pile is formed. Finally, the robot tilts the base according to the assigned axis, angle, and speed of rotation. Along the rotation, the pile releases the excess sand from the edges until it gets to the stable phase when the required angle is achieved.

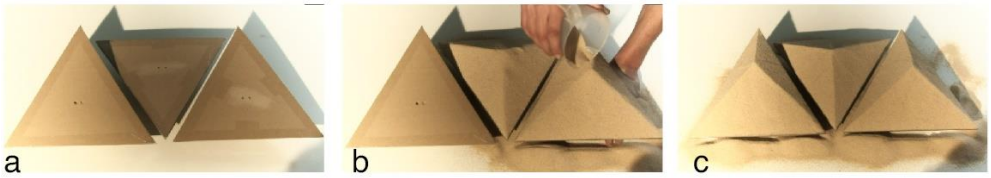


Figure 6.38 The manual method of tiles formation is based on pouring dry sand on pre-tilted bases

Figure 6.39 The robotic method of tiles formation is based on tilting a horizontal base up to the required tilt

#### 6.2.4.2 The solidification techniques

After the required pile of dry sand is formed, the surface is sprayed with the saline solution according to the spray method introduced in c3.3. Upon continuous spraying and addition of sand layers, a thin crust (around 1cm thickness) of the surface is solidified. The crust is then detached from the base giving a hollow tile, which can be used as a cladding element, or as a formwork for casting a solid tile or a solid block as introduced in § 6.2.1.2 (Figure 6.40).

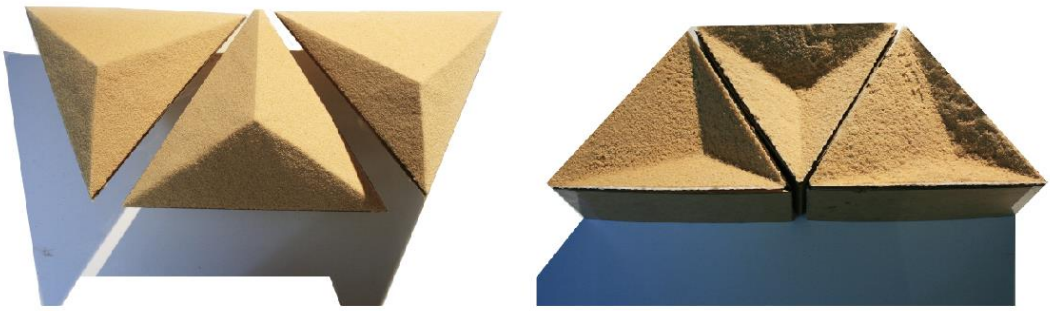

Figure 6.40: Solid triangular panels, top side (left) and back side (right)

#### 6.2.4.3 Characteristics of the tilt method

This subsection discusses the design and fabrication characteristics learned from the first prototype to develop the design of the prototypes in the following subsection. The below aspects are identified:

**Angle of tilt vs. light and shadows:** The morphology of the tilt method is characterized by a game of light and shadow that plays a key role in the design process. However, it is important to note that increasing the tilt angle reduces the height of the pile, which creates less remarkable shadows (Figure 6.41).

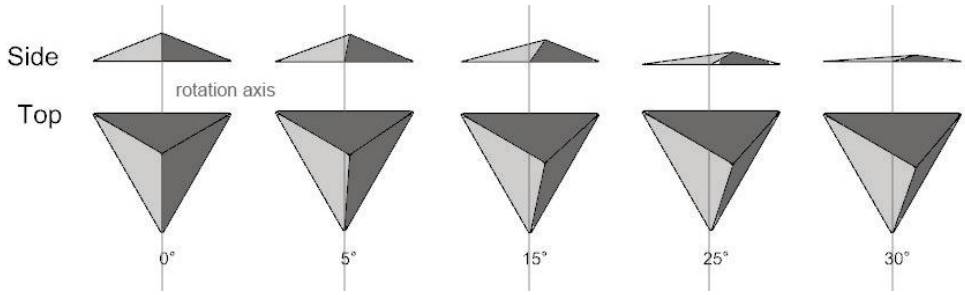


Figure 6.41 The volume and height of the tile decrease by tilting

**Tilt direction vs. ridges displacement:** The ridges of the surfaces displace in the opposite direction of the tilting axis, which increase the area of the surfaces that are on the side of tilting direction (Figure 6.42).

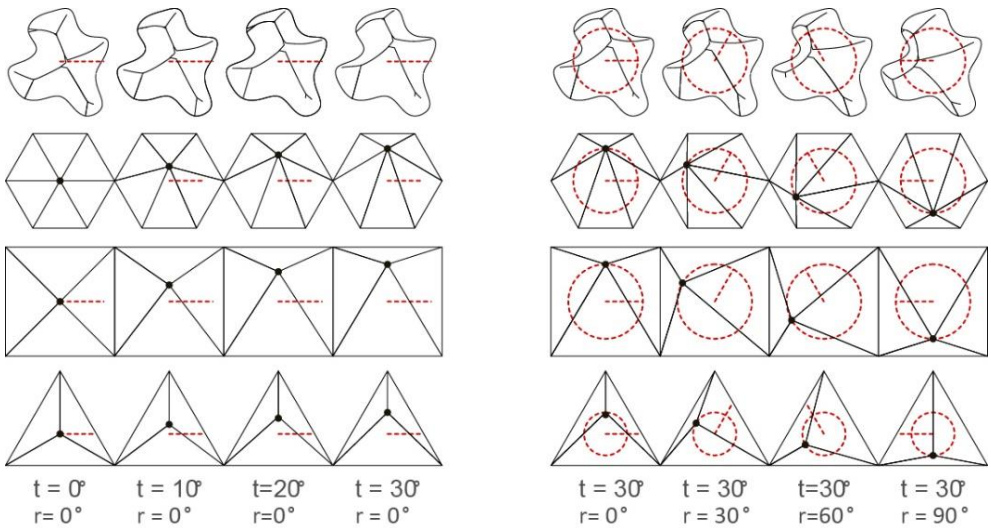


Figure 6.42 The ridges displace in the opposite direction of tilting. The predictability of the displacement decreases with the complexity of the shape

**Performative design:** The method studied the morphological aspects of tilting: however, future work can correlate the morphology of the tiles to acoustic and thermal performances.

**Design methods:** The design method considers the part to whole relationships of the entire assembly. Two design methods are distinguished based on the identified relationship between the tilt angles, axis, and the ridges:

- **Explicit design method:** the form of ridges is predefined, and the angles are experimented digitally until the desired form is achieved.
- **Implicit design method (Vector field):** the form of the ridges emerges from an input of gradient field of tilt vectors and angles.

#### 6.2.4.4 Fabrication constraints

1. The velocity of the manual sand pouring, or the robotic base tilting should be set at a steady slow rate to allows the formation of sharp ridges. However, the results show that the robotic method return more sharp edges.
2. On the design and precision levels, the robotic method is more viable as it allows the precise tilt at any angle in the possible range, while in the manual method it is necessary to fabricate a special pivot for each required angle. However, on the productivity level, the manual method allows the fabrication of many tiles simultaneously, while the robotic arm is limited to one tile at a time.
3. The hollow tile is lighter than the solid tile and the 3D block but it is less resistant.
4. The assembly techniques require further studies, which are not discusses in this work.

### 6.2.5 Physical and digital Prototypes

The design and fabrication methods presented above are used to develop two sets of prototypes introduced in this subsection. The first is a physical prototype fabricated during a workshop at Tu-Delft and the second set is a series of digital prototypes that explore the design potentials of the tilt method.

#### 6.2.5.1 Physical prototype

The physical prototype was fabricated during '*Sand: an (in)finite resource?*' summer school organized by Future Cities Laboratory-ETH-Zurich at TU-Delft in July 2016. The program revolves around the depleting resource sand and the question of how to develop alternative building materials for future cities. Three workshops were held during the summer school to explore alternative methods of sand binding: Bio-cementation, Crystallization, and 3D printing. My contribution was to conduct a one-day workshop on crystallization of sand with the saline solution.

The research objective was to examine the tilt method during the workshop through a large prototype. The workshop task required the participants to design and fabricate a 270x130 cm assembly of non-standard tilted triangular modules (Figure 6.43). To meet the objectives within the one-day time frame, the workshop considered the manual fabrication method as mean of production. After providing the participants with the required materials, they are introduced to the research background, the geometry of the tilt method and its design and fabrication techniques. The work was organized into two phases (i) **Design phase** that was looking at geometrical parameters and material techniques to define the distribution of angles for homogeneous assembly (Figure 6.43). (ii) **Fabrication phase** in which five tiles are fabricated per team, joined to a cardboard base, and assembled to create the triangular surface.

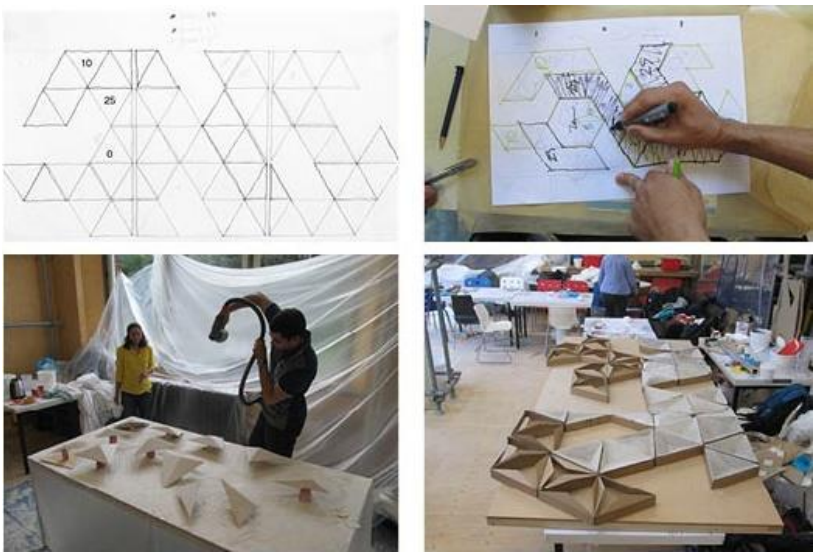


Figure 6.43 design of tilt angles (top), fabrication and assembly (bottom)

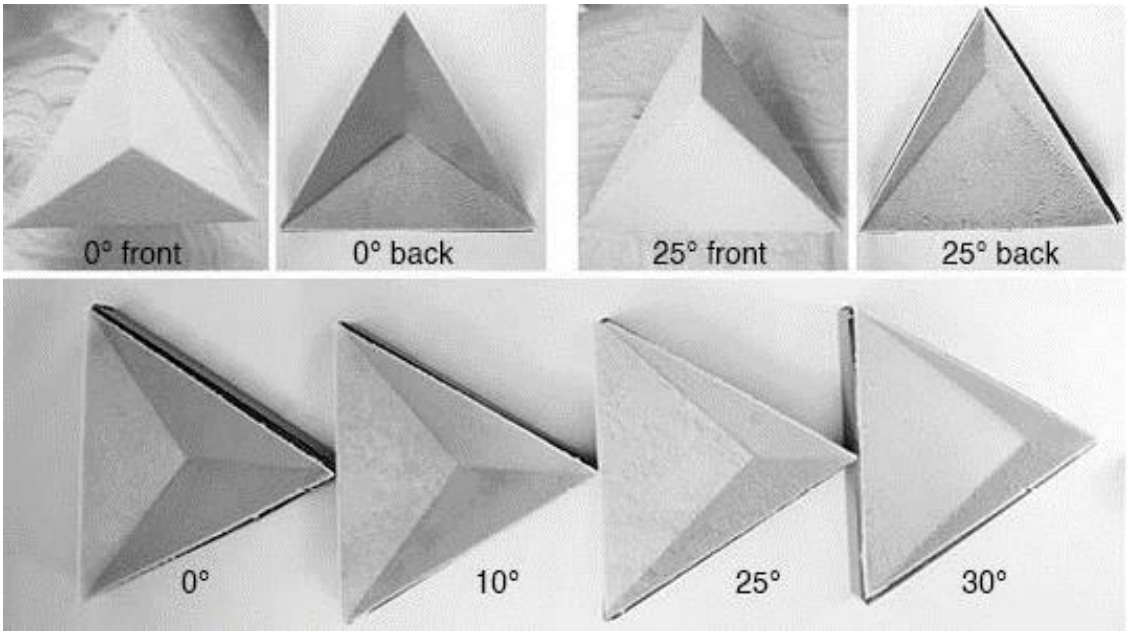


Figure 6.44 four solid panels at four tilt angles

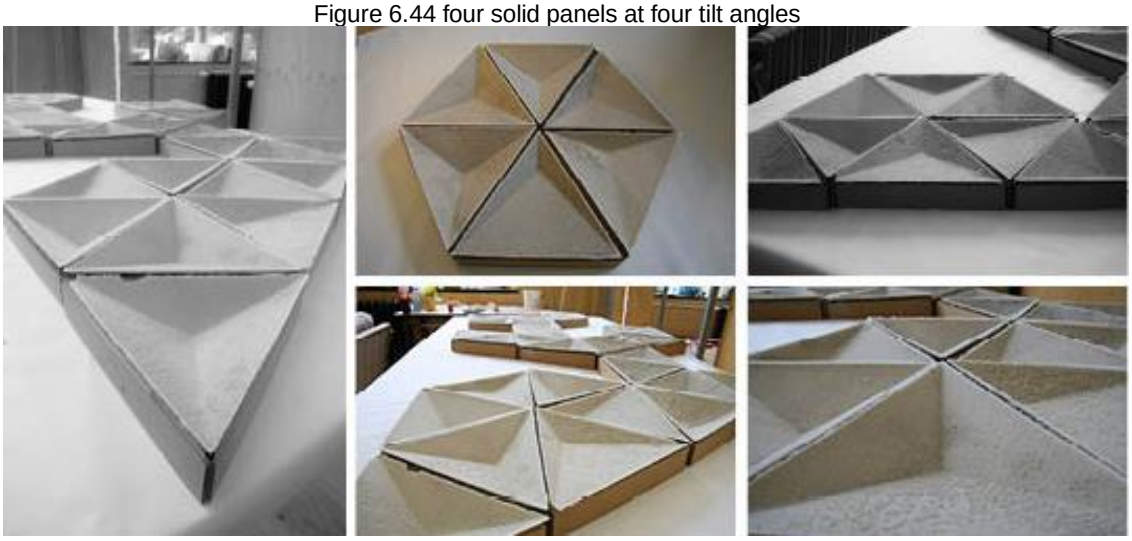

Figure 6.45 details of the triangular assembly

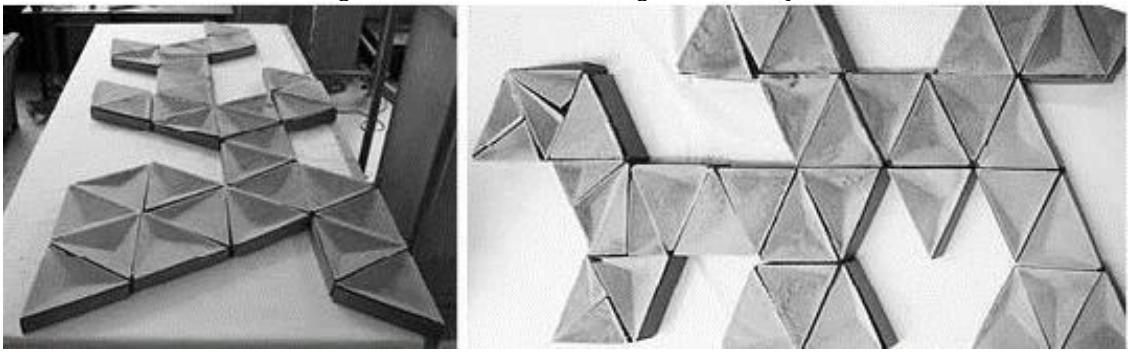

Figure 6.46 assembly of the panels

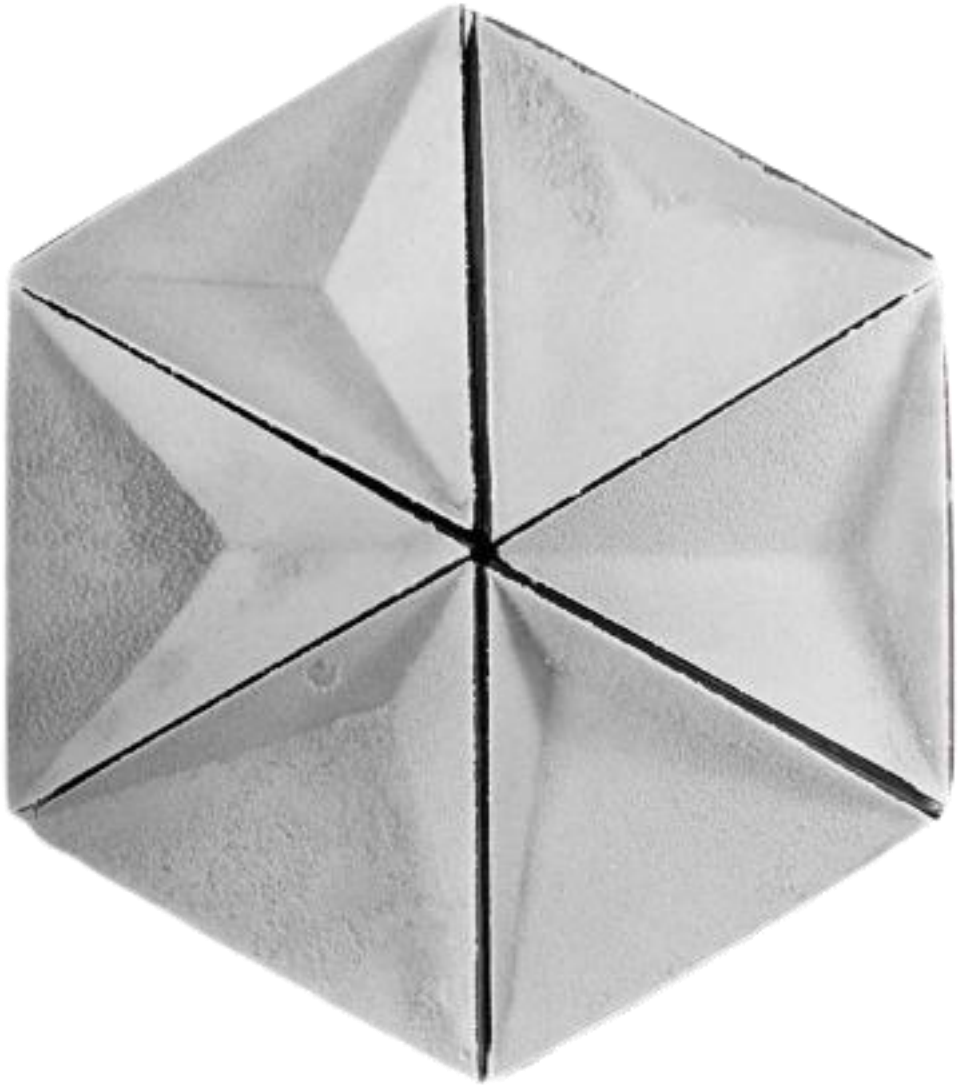

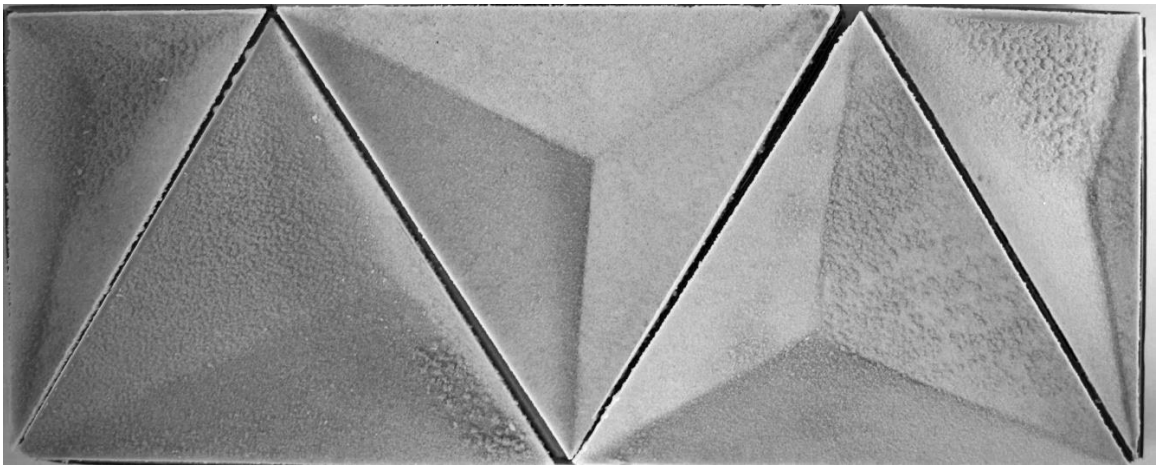

Figure 6.47 Details of the tilting model

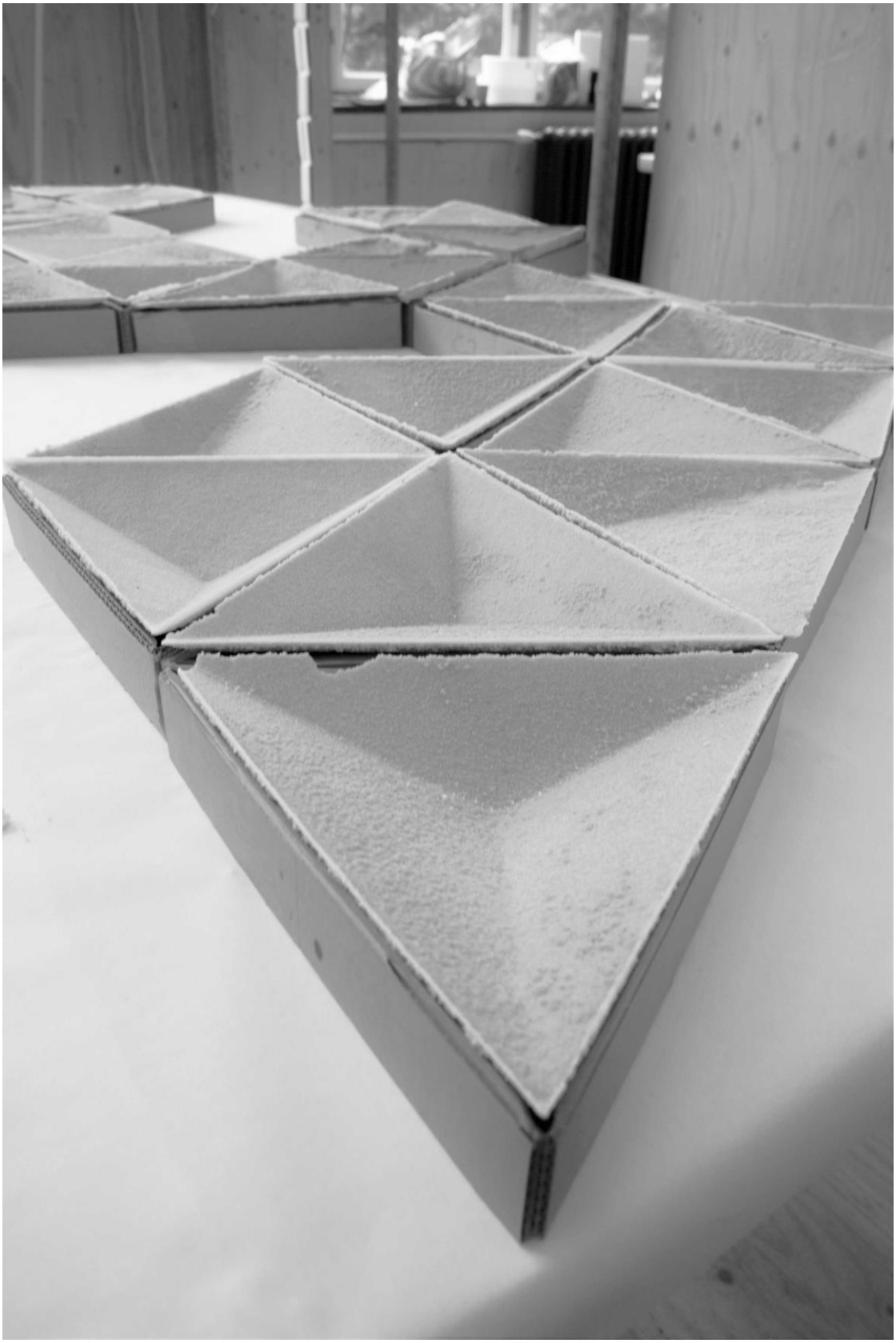

Figure 6.48 Shadow effect on the tilting model

#### 6.2.5.2 Digital prototypes

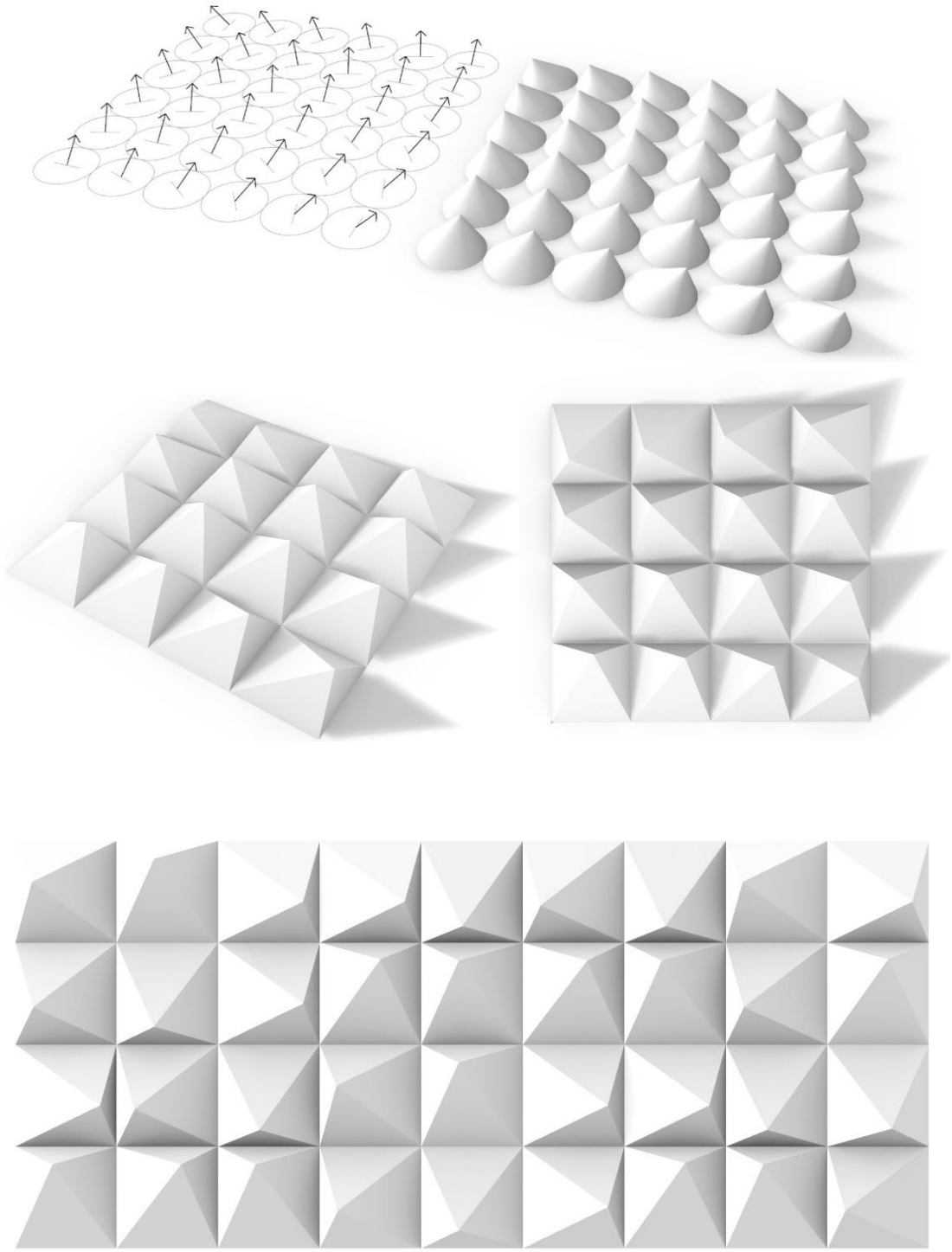

Figure 6.49 conical and square based panels with vector field distribution (top and middle) and random vector distribution (bottom)

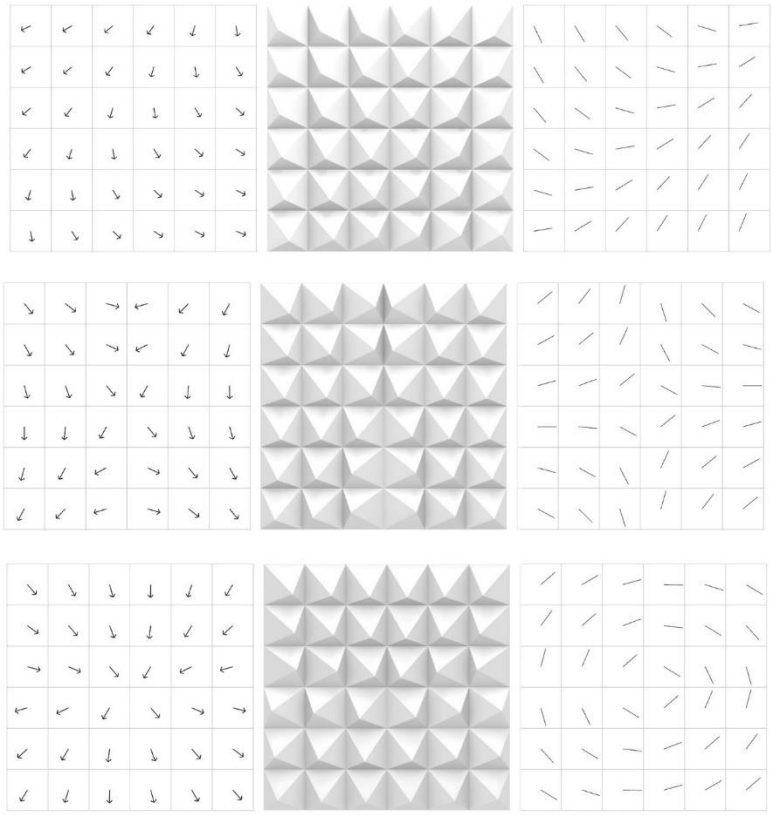

Figure 6.50 three distributions of tilt vectors at 20° (left) their emergent surfaces (middle) and axis (right).

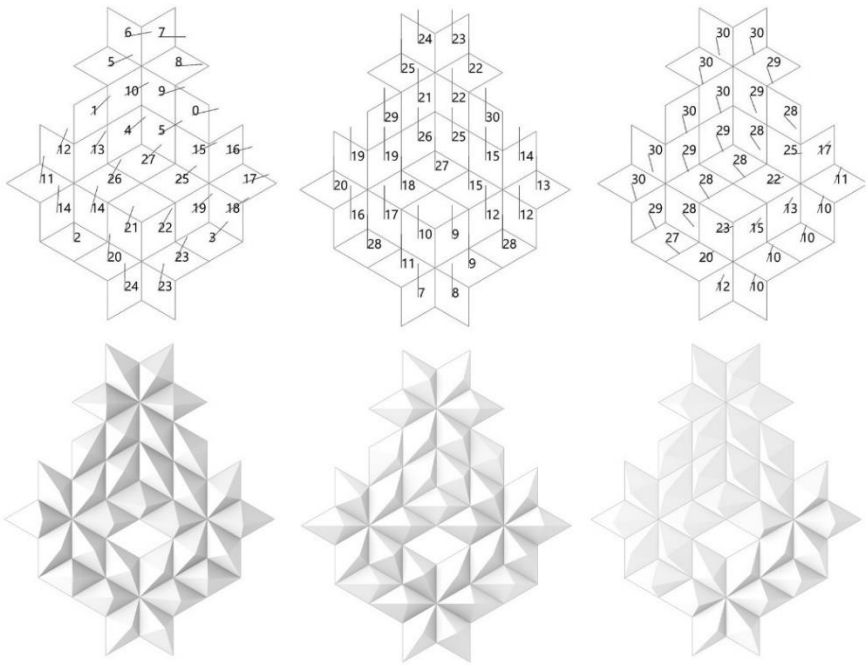

Figure 6.51 three angles distributions of rhombus shape

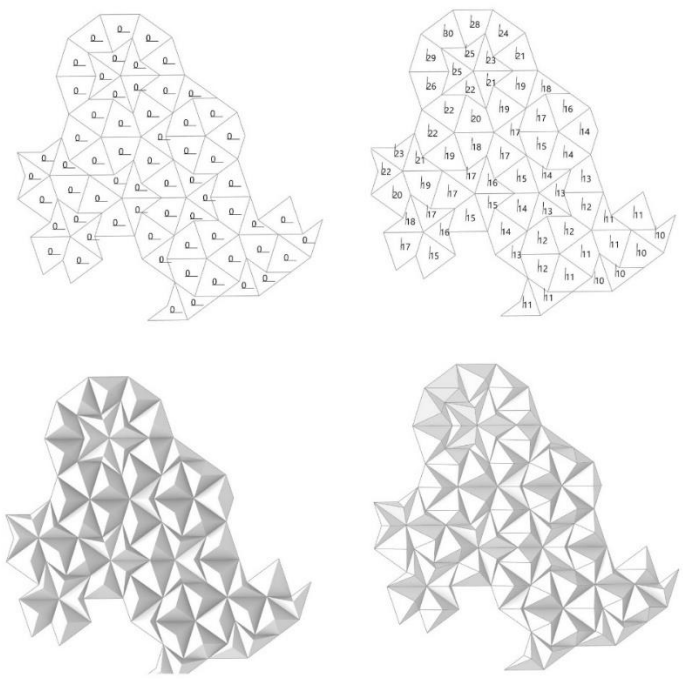

Figure 6.52 Penrose panels at 0° tilt (left) and at tilt range of 0°-30° (right)

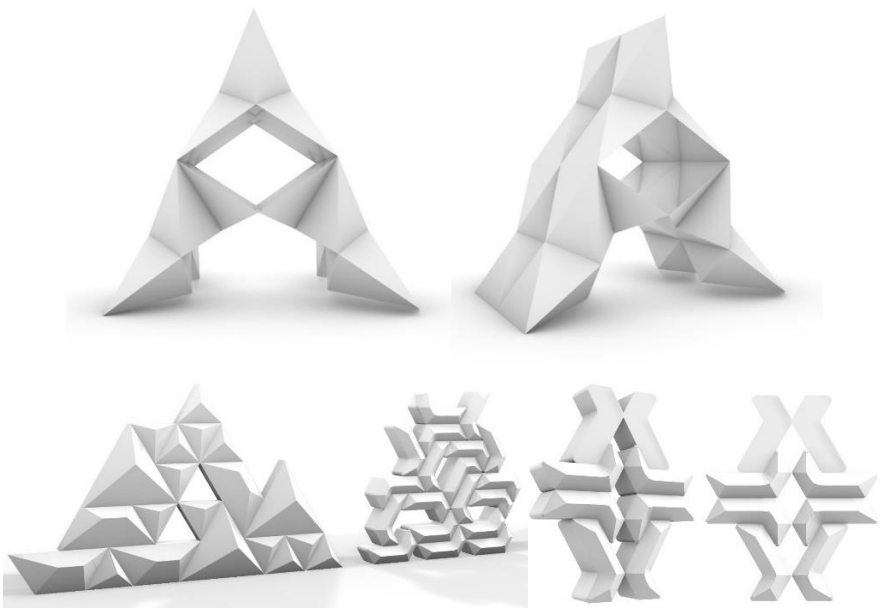

Figure 6.53 3D assemblies

## 6.3 Displacing technique

The design and fabrication technique presented here studies the robotic displacement of sand with simple tools on a predefined path. The process engraves sharp patterns of peaks and valleys. The manual displacement of sand with simple tools allows the creation of a whole spectrum of engraved patterns. Geometrical and almost natural-looking forms emerge from the interplay between the tool, the path, and the sand self-formation behavior. In the emergent patterns, it is important to observe the two juxtaposed states of order and disorder: the imprecision of the manual process and the precise formation due to the rigour behavior of sand self-organization.

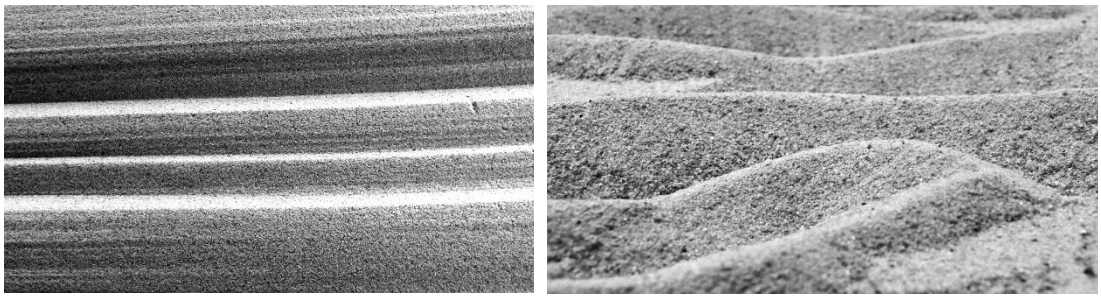

Figure 6.54 Manual displacement of sand creates geometrical and natural looking patterns. The emergent organizations are on the edge between the manual imprecision and the precise behavior of sand self-formation.

The rigour of the sand self-formation behavior under the displacement process drew the interest of the research to experiment with its potentials for design and fabrication processes. To explore the precise behavior of sand, it is essential to replace the manual process and its imprecision by digitally controlled machines.

The introduction of robotic process associates the machinic accuracy to the rigour of sand behavior, which returns highly precise patterns that are otherwise hard to achieve by the manual process. Previous studies at ETH[66], IAAC [207] and the Consortium for Research and Robotics[208] investigated the robotic displacement of sand within educational courses. The studies explored the fabrication of sand, clay and oil sand formworks through physical models hardened by silicon and an evaporative binder. Although the studies have explored the physical process, the analysis and modeling of the material behavior are still insufficiently explored. The objective of this section is the analysis of the self-organization behavior of sand under displacement effect to digitally approximate the behavior and to establish the digital and physical workflow of design and fabrication.

To identify the process and potentials of the displacement method an experimental approach of study is conducted in five parts. § 6.3.1 identifies the materials and tools of the method, 0 analyses the self-organization geometry and extracts the parameters of the method, which allows to develop the algorithm in § 6.3.4, and to establish the design and fabrication processes in §6.3.5. Finally, a series of prototypes exploit the design strategies, and potentials of the method in § 6.3.6.

### 6.3.1 Method definition

#### 6.3.1.1 Materials and tools

The materials being used are a box of dry loose sand for formation and the saline solution for solidification. A machinic process of formation is introduced through a robotic arm and a CNC machine at the end of which a designed end-tool is attached. Rhino and grasshopper platforms are used to generate the form, and to define the displacement path while the HAL and G-Code plugins are used to apply the robotic and the CNC processes, respectively.

#### 6.3.1.2 Process and prototype

The process of the method is detailed in §6.3.4 but it is important to outline it first here for analysis purposes. In brief, the process is applied by first drawing the context parameters in Rhino (displacement path, sandbox, and end-tool). From these inputs, the grasshopper algorithm generates the form of the pattern. Then, the context parameters are assigned to HAL to simulate the robotic movement, and to generate the robot control commands. Physically, the end-tool and the sandbox are prepared and calibrated with the robot. Based on the predefined path, the robot displaces the sand with the end-tool until the desired pattern is achieved. Finally, the emergent pattern of sand is sprayed with the saline solution to solidify a crust of the surface. The surface sets instantly after spraying and is used as a tile or a casting formwork. The following analysis and development of the method are studied through an initial prototype in Figure 6.55. It consists of a 60x60x3 cm bed of sand displaced, by a 4x4 cm end-tool on a predefined linear path of 4 cm length at 1 cm depth. To achieve an expressive pattern that exhibits the precision of both the machine and the sand self-formation behavior, a repetitive pattern of peaks and valleys is designed.

Figure 6.55: Initial prototype and pattern

### 6.3.2 Parameters and constraints

The method is governed by a set of constants and variables. Since the objective of the study is to examine the effect of displacement tool and path on sand self-organization, it considered the followings parameters of the system as constants: (1) the angle of repose of sand (35 degree), (2) the robot speed, (2cm/second), (3) the dimensions of the sandbox (60x60x5cm), and (4) the curvature of the sand surface (flat). Certainly, exploring curved surfaces as the first condition opens opportunities for curved formworks, but this work studies only flat surfaces to focus on the defined objectives. The following set of parameters are then considered as the variables (1) the shape the end-tool (profile, width, and angles), and (2) the path curve (shape, and depth).

### 6.3.3 Geometry analysis

The objective of this section is to first define the calculations methods of the pattern, which are necessary for modeling, and secondly to examine the effect of the tool and path parameters to establish the design and fabrication methods. The analysis method is based on measurements examination between the digital and the physical models, and the observation of the robotic displacement videos.

It is important to note that the sand distribution in the displacement method is more complex in comparison to the other methods introduced in this work. For instance, in the subtraction, tilting, and sweeping methods the behavior is simpler as it involves only erosion process (the released sand is not taken into consideration). However, in displacement, the complexity is due to the simultaneous processes of erosion, deposition and the avalanches involved in the method as will be detailed later. Analysis methods of fluid behavior of sand with great physical accuracy in the simulation have been reported in fluid dynamics and graphics of simulations disciplines. To overcome this complexity in this study, the geometrical analysis examines linear patterns that are to an extent simple. The objective of the method is not to define a general rule of analysis or modeling, but rather to approximate the behavior of a specific pattern, which applications are undoubtedly limited to certain displacement patterns introduced in this work.

#### 6.3.3.1 Sand displacement and self-organization

To study the pattern morphogenesis, the prototype introduced above is analyzed at three moments of formation: (1) at a single path to study the local behavior, (2) at two consecutive paths to study the effect of the second path on the first, and (3) at the aggregation of paths to study the global pattern.

Figure 6.56 shows the visual analysis of the three moments of the pattern, while Figure 6.57 illustrates the geometrical analysis of the single path to define the calculation method. In Figure 6.56, the sand surface is divided into a passive area (green) where no effect took place and active area (red and blue) where the sand is shaped. First, in the active area of the single path, the end-tool excavated a valley by compressing the sand below into a flat bottom (blue), then deposes the excavated volume in front of the end-tool as a peak over the sand bed (red). Simultaneously, the sides of the valley and the peak slipped in respect to the angle of repose of sand (red). Secondly, at the double path, two consecutive paths are employed at designed intervals. The displaced sand from the latter filled the flat bottom of the former making an inverted ridge at the bottom of the valley (black line). Finally, at the aggregation of paths, the intervals are reduced to create a pattern of positive and negative ridges. The aggregation pattern is studied in detail as a prototype to identify the design and fabrication methods in § 6.3.6.

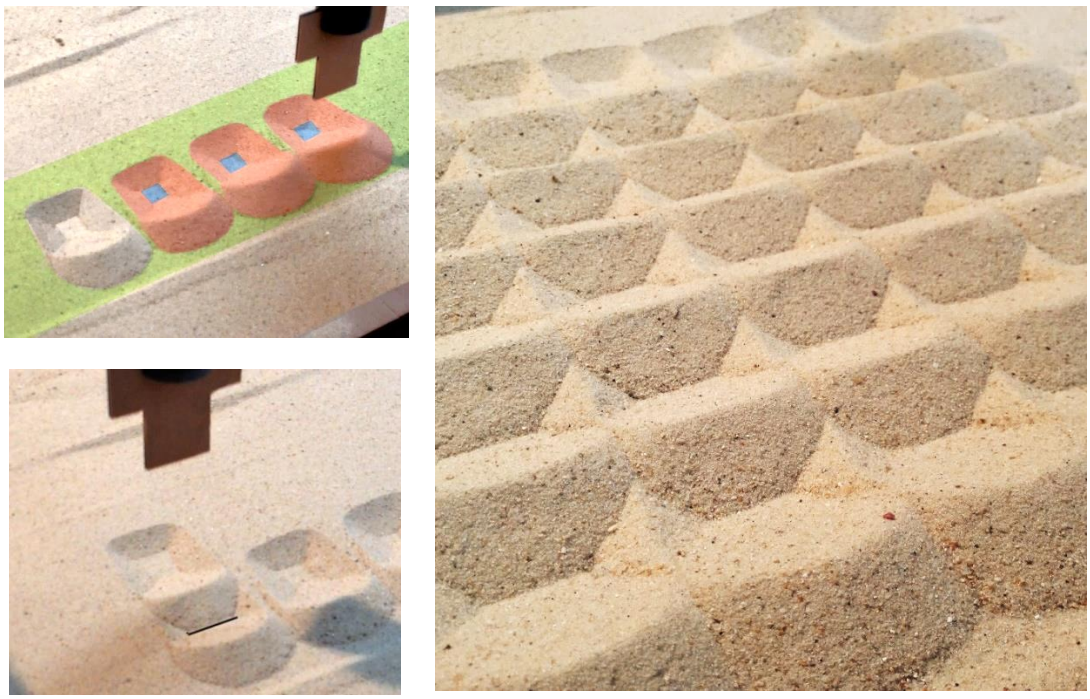

Figure 6.56 Pattern evolution, single path (top left), double path (bottom left), and aggregation of paths (right)

To define the calculation method of the pattern, it is essential to analyze the single path as shown in Figure 6.57. The end-tool of width *A* (4cm) moved over linear path $P_0$ to $P_4$ with a length *D* (4cm) at a depth *B* (2 cm). Based on A, D and B, the width $C_1$ of the flat bottom (blue), and the width $C_2$ of the sloped sides (red) of the valley are defined by the below trigonometric functions.

$$A = C_1 + 2\,C_2$$

$$C_2 = \frac{B}{Tan\,\theta}$$

$$C_1 = A - 2\left(\frac{B}{Tan\,\theta}\right)$$ Equation 6.5

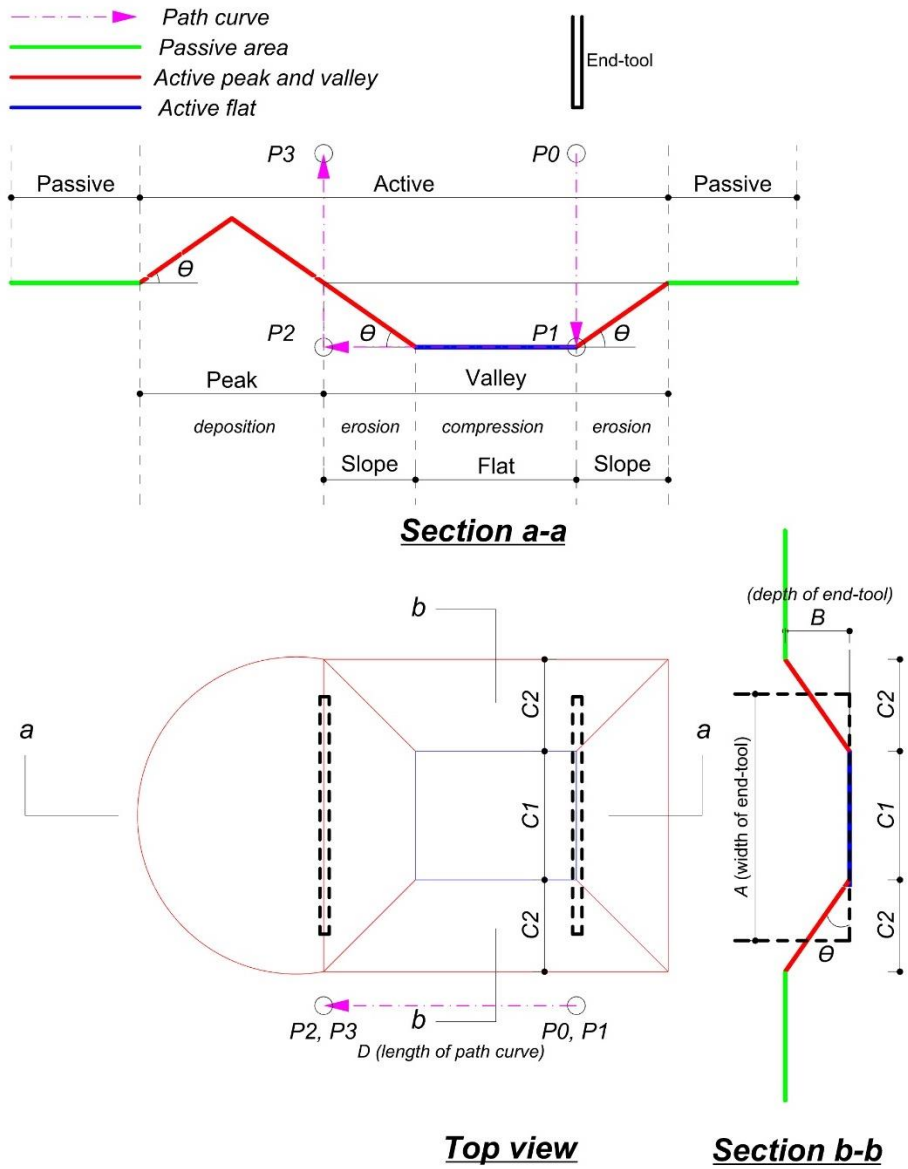


Figure 6.57 Top view, section a-a, and section b-b through the single path pattern

#### 6.3.3.2 Path curve parameters

The shape and depth of the path curve are essential parameters of the emergent pattern. In this work, the path shape is determined by its degree of curvature (linear or curved), continuity (continuous or dashed), rotation (around its Z-axis) and its global organization over the surface (repetition, spacing, self-intersection…). The depth of the path is correlated with the width *A* of the end-tool in determining the width $C_1$ of the flat bottom of the valley as described in the previous section. Finally, a variation of depth along the path returns curved surfaces.

With the decrease of depth D, the width of the flat part $C_1$ decreases while the width $C_2$ of the slope increases inward and outward of the flat part proportionally. In other words, more the end-tool immerse in the sand bed, more it generates slopes and the flat compressed surface decreases.

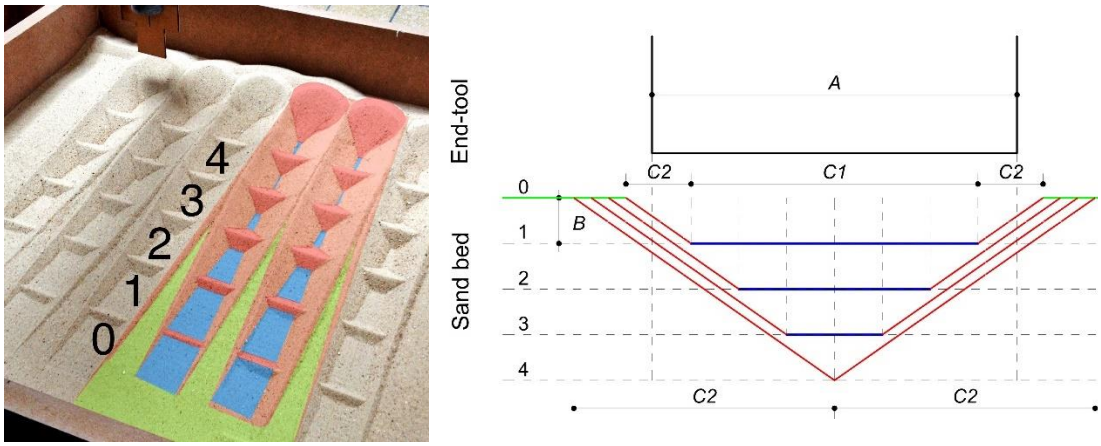


Figure 6.58 Study of the effect of path curve depth on the width of the pattern

#### 6.3.3.3 End-tool parameters

The shape, width, and angle of the end-tool play a key role in the formation process. The profile curve of the bottom edge informs the shape of the pattern. Figure 8.5 shows two sets of designed end-tools, set *S* of straight tools, and set *C* of curved tools. With predefined linear paths, the patterns emerge from the interplay of the tool and slope of sand. To create a compressed flat bottom of $C_1$ width at *B* depth, the minimum width *A* of the end-tool should be two times larger than the width of the sand slope $C_2$ (see Equation 6.5).

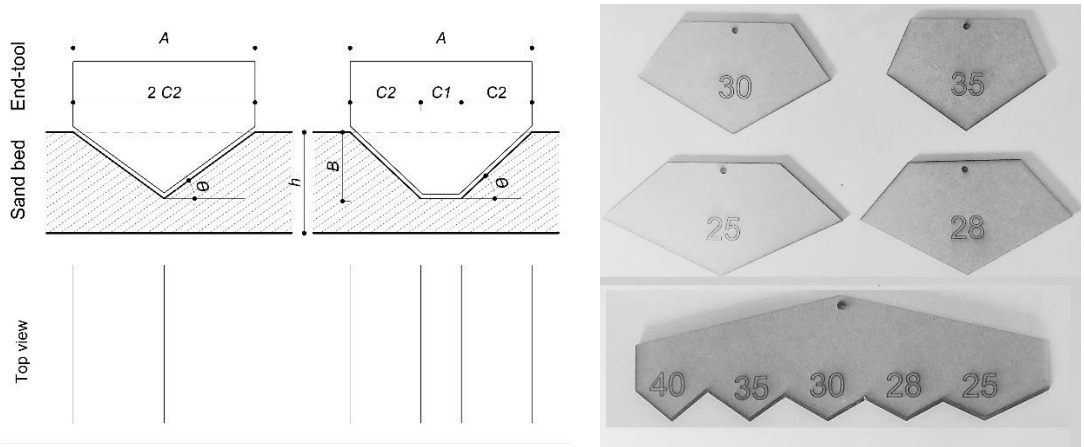


Figure 6.59 Study of the effect of the end-tool width and angle on the pattern

The angle of the end-tool *α* should not exceed the angle of repose of sand *Θ* to achieve the predefined slope of the pattern. If *α* exceeds *Θ* the slope of the pattern will be constant at *Θ.* Hence, it is ineffective to design the end-tool with angles larger than the angle of repose of sand-like for instance at 90 degrees as the self-organization behavior of sand will repose the slope.

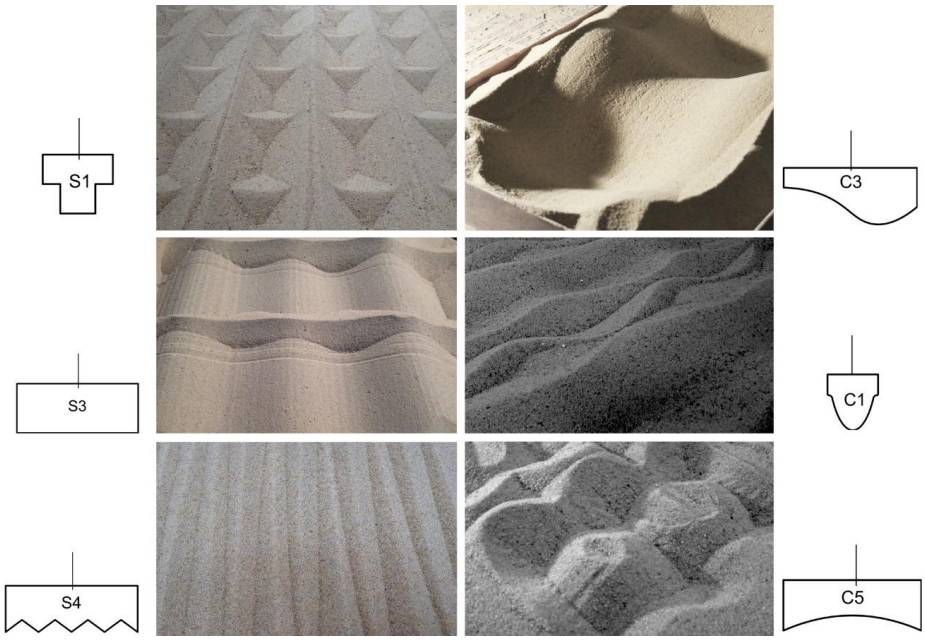


Figure 6.60 study of the effect of the tool profile on the form of the pattern

### 6.3.4 Algorithm

The previous subsection defined the displacement parameters and their calculation methods, which are essential for the development of the algorithm in this subsection. The objective of the algorithm is to generate the pattern and to produce the fabrication data for the robotic control. To meet these objectives, the algorithm is executed into two parts: (i) form generation, and (ii) robotic simulation. The inputs and processes of the two parts are detailed below through the case study used in the geometry subsection.

#### 6.3.4.1 Form generation

The algorithm of form generation is based on the Heightfield modeling method introduced in § 5.3.2. The Heightfield method models the sand surface by a grid of points, which heights are defined by their distance to the closest active boundary and the sand angle of repose. The form generation algorithm is processed in two phases: initialization, and surface generation.

1- **The Initialisation process** assigns the following inputs: (i) the predefined boundary and the initial height of the sand as a grid of points, (ii) the depth *B,* length *D*, and shape of displacement path as a curve, (iii) the end-tool width *A* and shape as a curve, and (vi) the angle of repose of sand $\Theta$ as a value.
2- **The generation process** creates a surface based on the previous inputs through three stages:
   a) **Definition** of the boundary curve $C_1$ (the flat area of the valley) based on *A, B*, *D*, and the boundary curve $C_2$ (the slope area of the valley and peaks) based on $C_1$ and $\Theta$.
   b) **Clustering** of the grid points *P* into groups $P_n$ based on their distances from $C_1$ and $C_2$. First, they are divided into two clusters: $P_p$ (passive points out of $C_2$ curve where no change takes action), and $P_a$ (active points in $C_2$ curve). Then, the active cluster $P_a$ is divided into $P_f$ (flat valley points in $C_1$), and $P_s$ (valley and peaks slope points in $C_2$ but out of $C_1$).
   c) **displacement** of the points in each cluster by updating their heights according to their distances from $C_1$ and $C_2$. The heights of the passive points $P_p$ remain stable (flat surface) and the heights of the flat valley points $P_f$ decrease according to the depth of the $C_1$ from the sand bed surface. While the heights of the valley and peaks slope points $P_s$ decrease and increase respectively according to their distance from $C_1$ and $C_2$ curves. A mesh is created from the updated points to represent the emergent pattern.

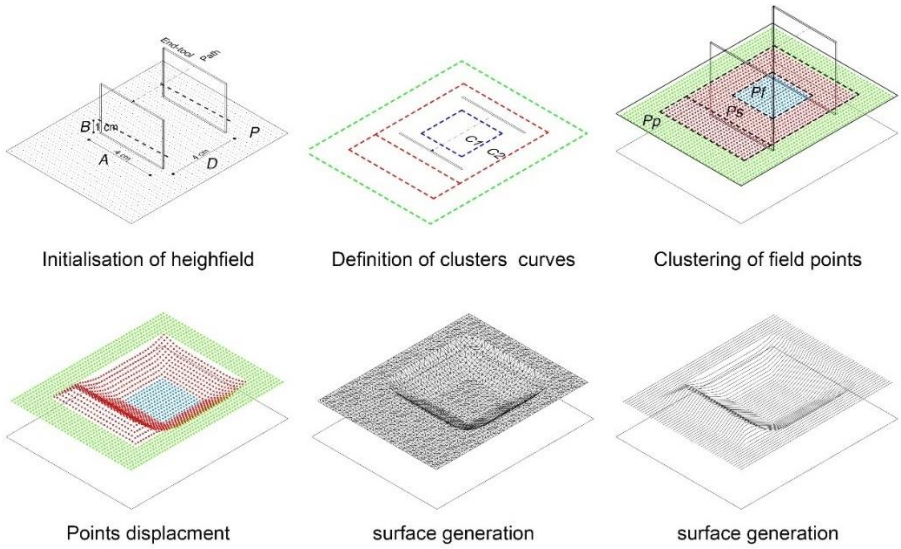


Figure 6.61 Displacement algorithm process

#### 6.3.4.2 Robotic simulation

The robotic simulation is the second part of the algorithm, it simulates the robotic process and generates the control commands for physical execution First, the forms of the physical materials (sandbox, sand bed, and end-tool) and the displacement paths are assigned into Rhino/Grasshopper platform and the robotic HAL environment. Then, the displacement path curve is divided into planes organized in the sequence in which they must be processed by the robot for fabrication. After the simulation of the robotic movement, the spatial position and orientation of each plane on the displacement curve are automatically translated into control commands for the robot physical execution.

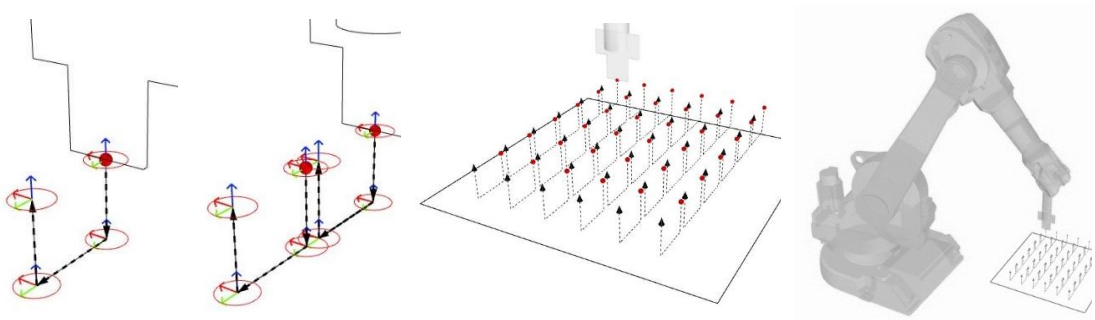

Figure 6.62 Robotic path simulation for single, double, and aggregate paths

### 6.3.5 Design and fabrication processes

After defining the method parameters, geometry, and algorithm in the previous sections, the design and fabrication techniques are established below following the same prototype used above. An aggregation version of the case study is conducted here to define the digital-physical workflow.

#### 6.3.5.1 Design process

The objective of the design process is to generate the emergent pattern, simulate the robotic path, and provide fabrication data. This is applied through the following four steps:

1- **Digital setup:** the fixed parameters of the method are first defined in Rhino-Grasshopper environment including the end-tool, the sand bed, and the angle of repose of sand.

2- **Path design**: the displacement path curve is the variable parameter, which design allows the parametric exploration of various patterns. The path curve and the boundary of the sand bed are drawn in 2D in Rhinoceros and then linked to the Grasshopper algorithm along with the inputs from step 1. The predefined displacement path in case study 1 is aggregated over the surface in successive rows at equal distances. This organization ensured the deposition of displaced sand of the peaks in the valleys giving a global pattern of positive and negative ridges.

3- **Surface generation**: the path curve and the inputs from step 1 are assigned to the code to generate the surface as previously detailed in the algorithm subsection (Figure 6.63).

4- **Robotic simulation**: first the form of the end-tool and the sand bed are assigned in the HAL plugin, then the speed and velocity are set. Secondly, the path curves are processed following the algorithm of robotic control explained above. Based on this setup, the simulation of the robot path is developed and the control commands for the robot physical execution are automatically generated (Figure 6.62).

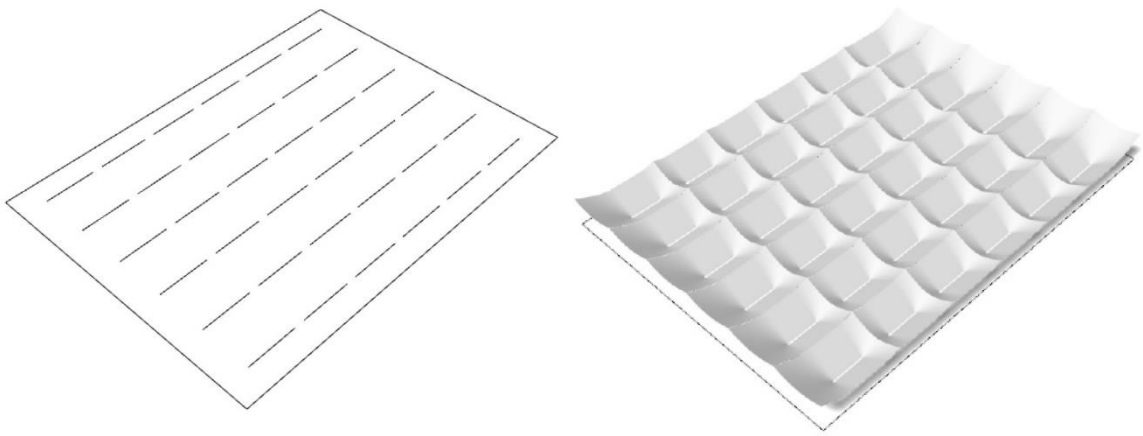

Figure 6.64 The input path curves and the generated surface.

#### 6.3.5.2 Fabrication process

1- **Physical setup:** the sand bed is placed in front of the robot as defined in the digital environment and the end-tool is mounted on the robot arm. The position of the tools is calibrated with the robot as the initial position.

2- **Robotic displacement:** based on the control commands, the robot trajectory is executed and the end-tool displaces the sand following the assigned sequential targets.

5- **Surface solidification:** after the required pattern of dry sand is formed, the surface is solidified by spraying the saline solution according to the method introduced in § 3.3. The solidification process returns a solid crust (around 2cm thickness) of the surface so materials can be cast on to it. Once the cast tile hardens, the formwork can be reused, recycled, or decomposed.

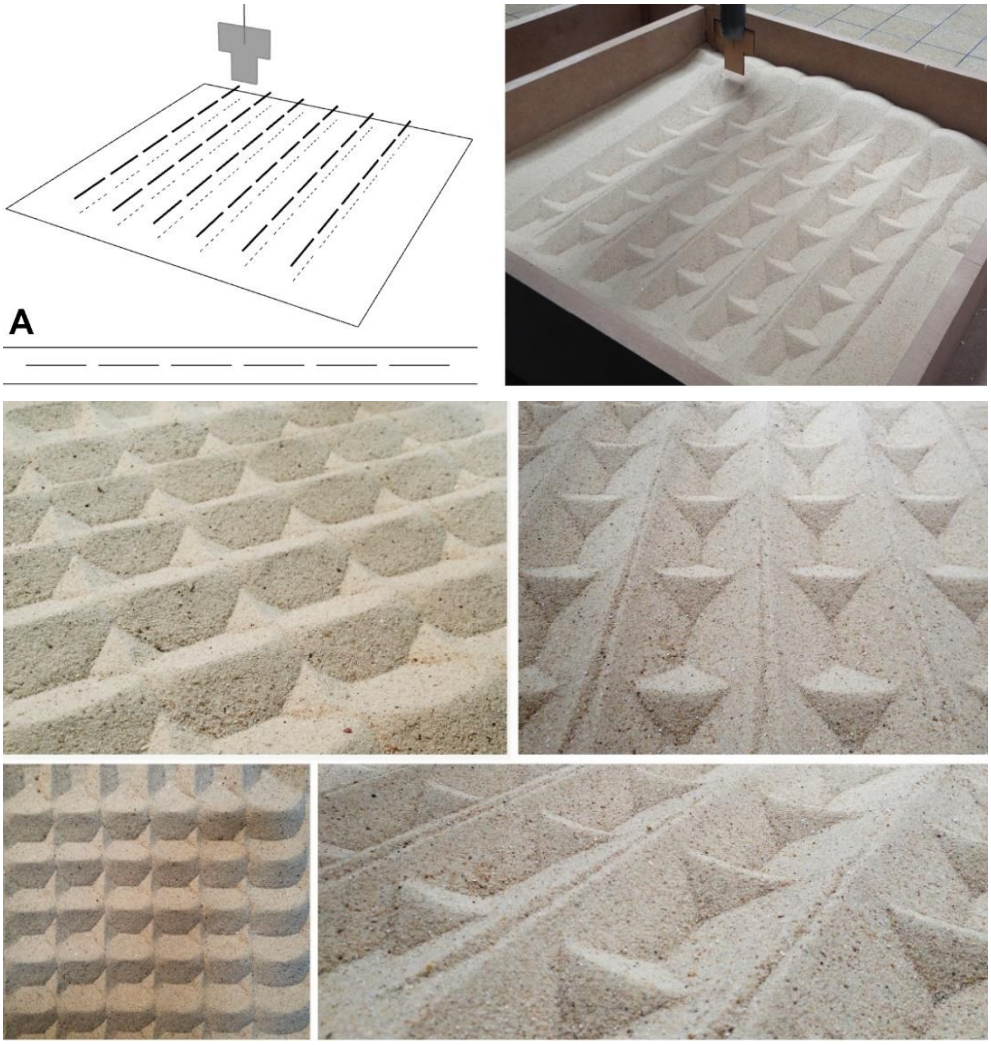


Figure 6.65 Robotic displacment experiments. Dashed pattern of dispalcment diagram (a) and physical test.

### 6.3.6 Physical and digital experiments

#### 6.3.6.1 Physical models

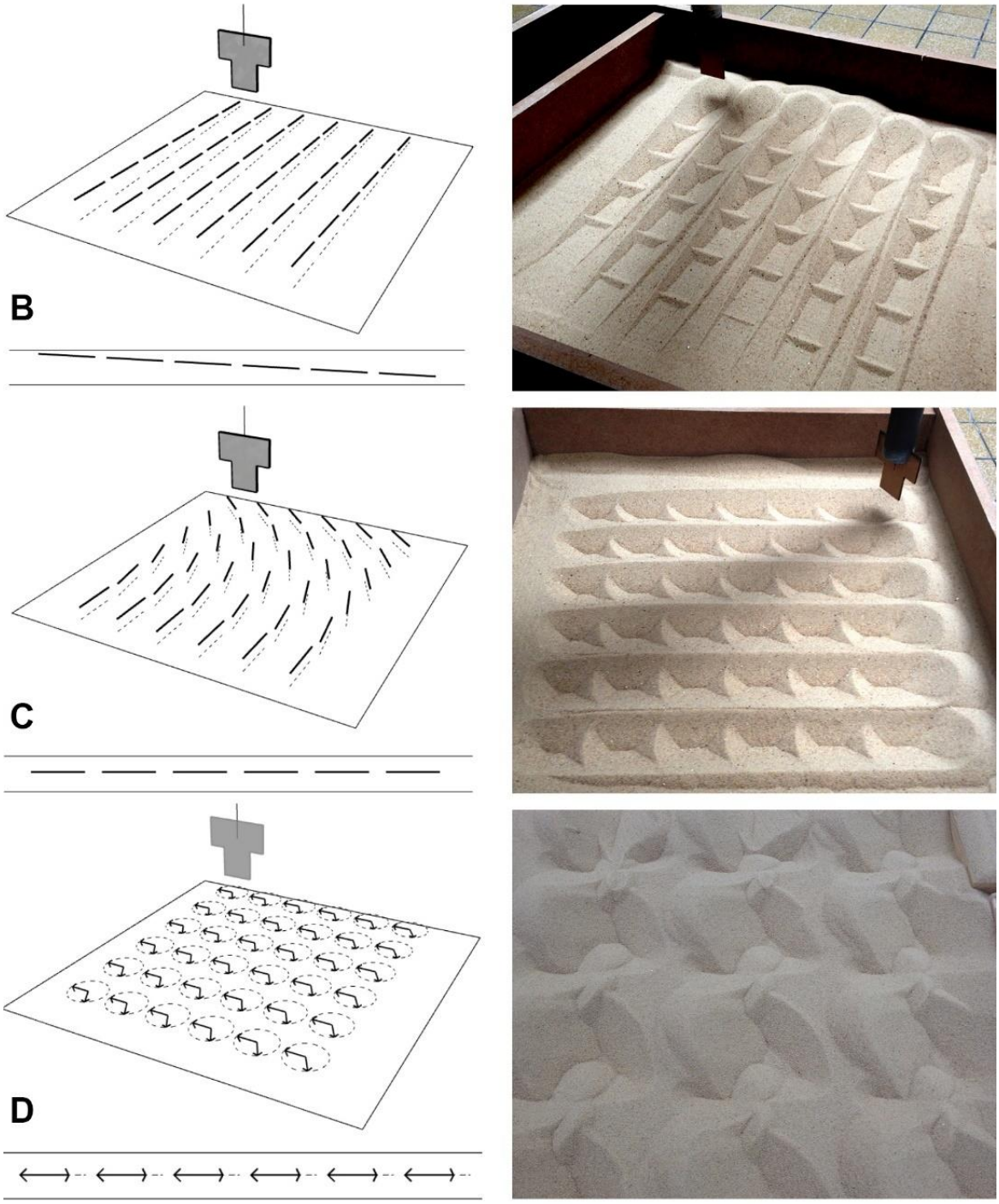


Figure 6.66 Robotic displacment experiments. dashed pattern with a fading slope (B), directionl paths (c), and rotational paths at fixed points.

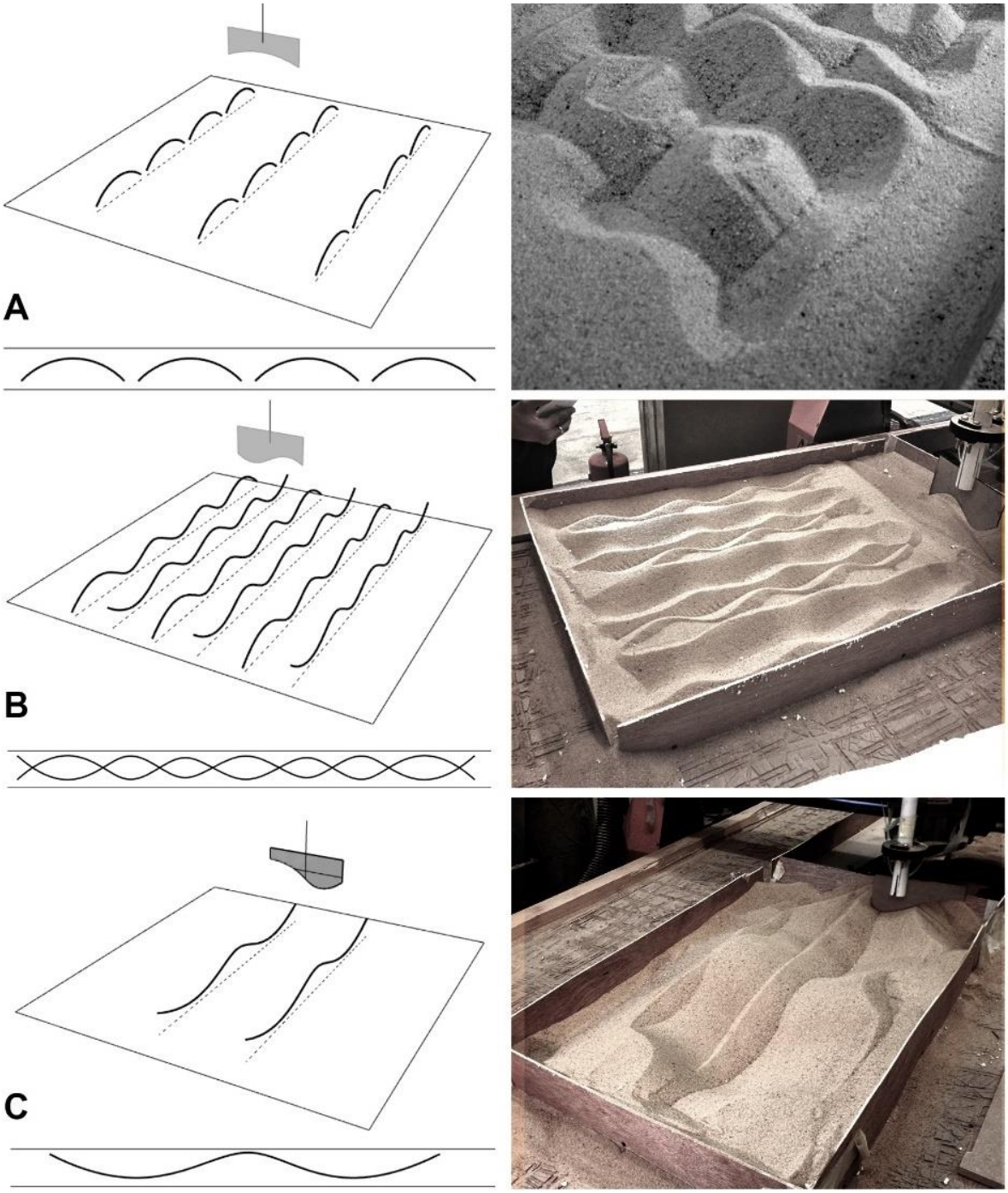


Figure 6.67 Physical experiments using a CNC machine. Repetitve curved pattern (a), dense organisation of opposite sine waves (b), double path of a single sine wave for the fabrication of a hyperbolic prabolid block (c).

#### 6.3.6.2 Digital models

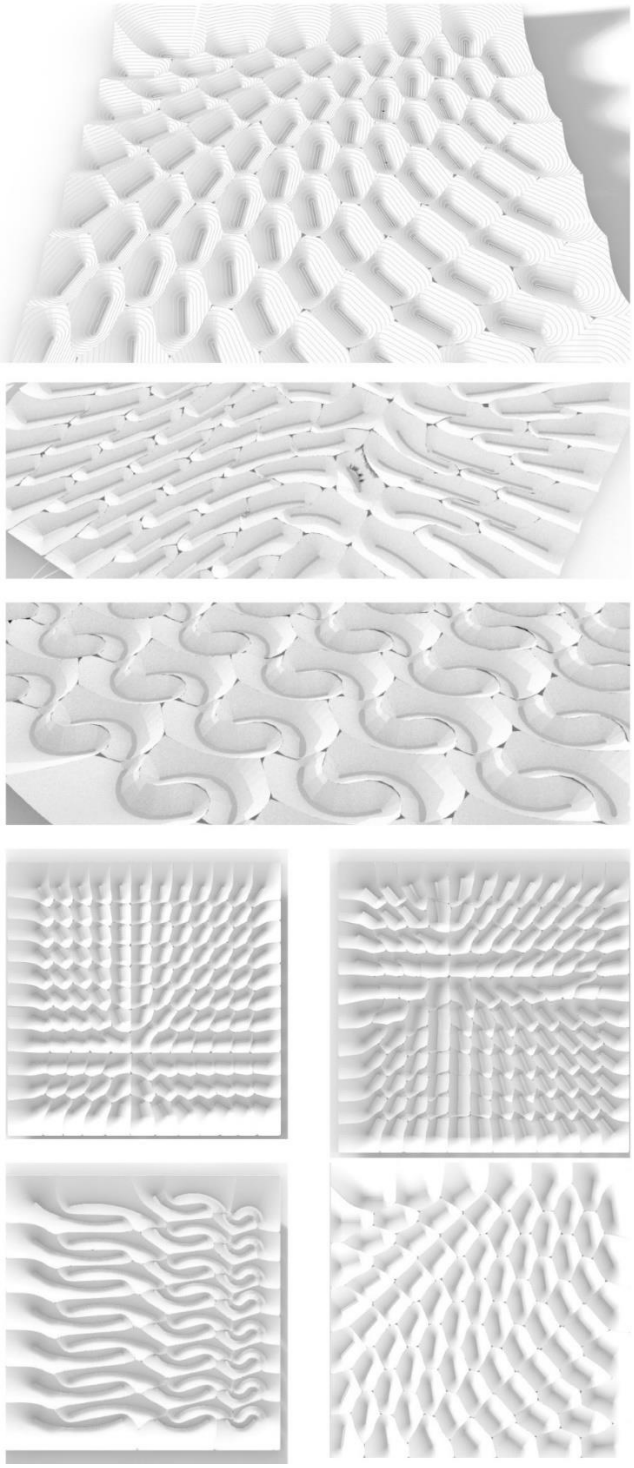

Figure 6.68 Digital models of the displacment method

## 6.4 Sweeping technique

The sweeping technique aims at making of single and doubly ruled sand panels by sweeping the sand surface with a ruler. The technique seeks to take advantage of the geometrical characteristics of surfaces of constant slope (SCS) generated by sand being ruled surfaces. The interest of the technique lies behind the possibility of approximating nonpositive Gaussian curved with ruled strips which yields easily-built panels as will be discussed. First the method is defined through initial experiments. Second, the physical and digital constraints are discussed, and their processes are presented. Finally, the technique is assessed through physical and digital prototypes.

### 6.4.1 Method definition

The sweeping technique proposes the formation of ruled surfaces by sweeping sand with a ruler over the edges of a predefined formwork. The formed surface is then sprayed and casted to fabricate sand panels that can be used as reusable formwork for casting. To examine the proposed technique initial experiments are conducted to test three phases of the process, (i) formation of dry sand, (ii) fabrication of solid panels, and (iii) design of large scale assemblies.

#### A. Formation experiment

An initial experiment of formation is performed on different typologies of ruled surfaces (Figure 6.69). The objective is to define the parameters and constraints of the technique and to evaluate its formation feasibility. First a ruled surface is modelled from two input curves while considering that the surface slope does not exceeds the sand slope. Secondly, a formwork is generated form the input surface profile. Next, the formwork is fabricated from a flat sheet material, assembled, and filled with sand. Finally, the sand surface is swept with a ruler over the edges the formworks.

The experiment returns clear single and double ruled sand surfaces, which proofs the feasibility of the formation process. The initial parameters of the technique are defined as (i) the shape of the generator curves, and (ii) the slope of the surface. Further morphological exploration of different curves typologies is conducted.

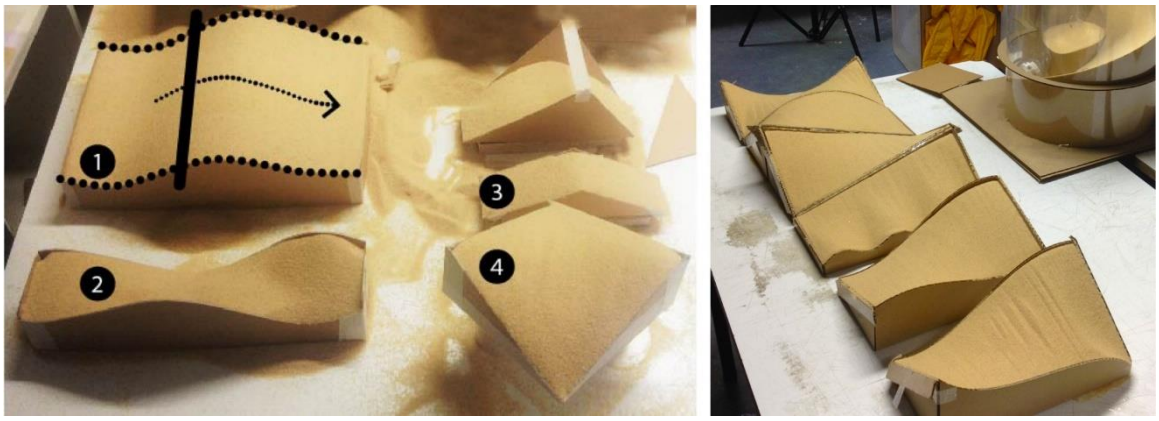


Figure 6.70 Initial experiment of the sweeping formation. The experiment returns single (1,2 - curved & 3- angular), and double ruled (4-Hyperbolic paraboloid) surfaces. Exploration of different typologies (right).

### B. Fabrication experiment

To extend the sweeping formation method into production, a fabrication method is developed. The swept sand surface is first sprayed with the saline solution. After hardening, a border with the same profile of the surface is laid over the formwork. Next, Hyposand mixture is casted and left to dry. After few minutes, the solid sand panel is demolded, and the formwork is used to cast another panel. The proposed fabrication process returns a straightforward procedure, a solid sand panel faithful to the initial input surface, and a reusable formwork (Figure 6.71).

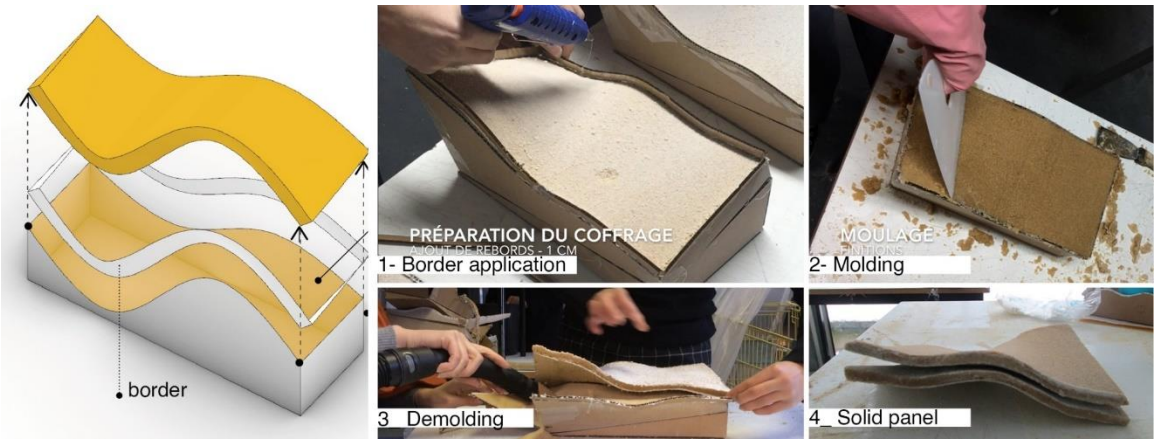


Figure 6.72 Initial experiment of the sweeping technique of fabrication. The developed formwork is composed of a box and a border (left). The procedure of making a panel (right)

### C. Paneling experiment

After setting the formation and fabrication processes of a single panel, the third experiment questions the possibility of using the sweeping technique for the design and fabrication of large scale surfaces. A set of simple and double ruled surfaces were subdivided to define the design constraints. The experiment raised two questions thar are discussed in the following subsections.

How to evaluate the surface slope and connect between the design and fabrication ?

What is the optimum discretization method that returns planar for the formwork ?

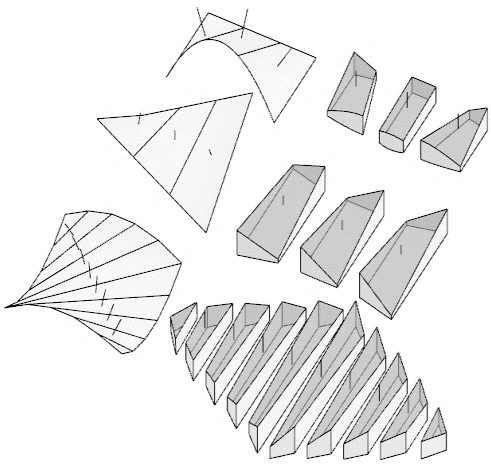

Figure 6.73 Paneling of single and doubly ruled surfaces according to the sweeping method

### 6.4.2 Curved surface discretization and fabrication

Architectural forms based on doubly curved surface are becoming increasingly common in architecture. While the digital modeling of freeform surfaces is easily achieved, the construction poses two key challenges: 1) the rationalization of the freeform surfaces into buildable parts: herein panels, and 2) the fabrication of the panels at the reasonable cost. The available methods of rationalization and fabrication of freeform surfaces are discussed briefly in this subsection.

The design of freeform in architecture commonly follows a similar workflow. The overall form is first defined by a surface. Then, the surface is subdivided by a network of curves into smaller segments suitable for fabrication and construction. This subdivision results in a network of faces, edges, and nodes. The subdivision of the surface is also called segmentation or discretization.

Available discretization[71] techniques of freeform surfaces include the approximation of the surface with: (i) planar polygonal panels, which is the most used method, (ii) ruled patches, which returns better approximation than the planar method while being less expensive than the doubly curved [209], and (iii) doubly curved panels, which returns the best approximation but with the highest cost.

The method of discretizing freeform surfaces with ruled patches enables adequate approximation with a smooth union of ruled patches. Two technique are reported: the first is the approximation with, single ruled, developable strip (D-Strip method) and with ruled panel (R- panel method). The RP method is to approximates a zero or negatively curved surface by its segmentation with strips or panels of ruled surfaces.

**Ruled panel method of paneling (R-Panel)**

The process of the R-Panel method [209,210] is employed on three stages (i) the analysis of the gaussian curvature,(ii) the definition of the asymptotic directions (rulings), and (ii) the reconstruction of the surface by ruled patches in between the rulings. Given a designed freeform surface Ś, the first step is the analysis of the gaussian curvature at a sufficient number of points over Ś. Only the regions with zero or negative curvature are considered in the paneling process as the positive curvature regions are not buildable with ruled panels. The second step is the extraction of the asymptotic curve network at predefined points P over Ś. At each point P

[71] Discretization refers to the geometrical process of segmenting a surface into smaller patches (panels) that can be manufactured according to a selected technology and when assembled they best approximate the original surface. In architecture, discretization is a fundamental process to procced from a designed surface towards feasible production, the challenge of discretization lies in the simultaneous interplay of the geometric constraints (surface topology and paneling algorithm) and the fabrication method (dimensions, material, cost) while respecting the design quality (surface smoothness and approximation).

two asymptotic directions are defined by two-unit vectors aV that bisector the principal curvature vectors pV at P. The asymptotic curve network is then generated as the integral curves of the vector field aV.

**Available fabrication methods**

The feasibility of the sweeping method is studied in this work by reviewing the available methods of casting curved surfaces in architecture. There is a long history of interest in shaping liquid materials, such as concrete, into curved surfaces. The interest in casting liquid materials lies on the opportunities behind their phase changing behavior as they go from fluid to solid state, which enables the casting of almost any shape while returning resistant results upon hardening. The efficiency of the casting techniques lies fundamentally on the design the formwork which determines the feasibility of the method and the quality of the final product. Reported reviews of available casting techniques studied the feasibility of formworks in terms of workability (labor needed), technology (low or high-tech tools and machines), speed of fabrication, cost, reusability of the formwork, recyclability of its raw materials, and finally the quality of the final curved surface (curvature degree). Within the scope of the sweeping method, the relevant casting techniques of curved surfaces are considered in three main categories: traditional timber, subtractive (CNC and Hotwire) and flexible formwork methods.

- **Timber formwork** is historically the traditional and most used method for casting curved surfaces in architecture. It is based on bending flat sheets of plywood on a substructure of wood shuttering that approximates the surface profile. The traditional method is low tech and applicable for precast and onsite fabrication. However, the method is limited to low curvature forms, time consuming, labour intensive (require highly qualified carpenters) while the reusability of its elements is limited, which increase the cost: especially for non-standard and not-repetitive surfaces.
- **Subtractive formwork** methods have been developed in recent decades due the introduction of CNC milling and robotic hotwire technologies in architecture. In the **CNC method**, a solid material, e.g. polystyrene foam, or wood, is milled according to the surface design returning accurate results. The CNC method is well proven in the contemporary construction of curved, freeform and complex structures. But an economic and sustainable construction still poses great challenges to the industry.
    - **The Hotwire method** is a subcategory of the subtractive fabrication methods for formworks, which allows a numerically control cutting of foam blocks, using a heated thin wire and 6 degrees of freedom robot arm. While this process used to be restricted to ruled surfaces, recent work showed the possibility of creating a free form surfaces by attaching the wire ends to two robot arms. This process is considered fast compared to other subtractive methods like CNC milling.

### 6.4.3 The making constraints.

**Slope analysis**

It is necessary first to define the reference plane of the surface to calculate the surface slope and to orient the surface to the fabrication plane in the next part. The reference plane (RF) is the plane to, which the slope and the orientation parameters are referred. It is considered in this work as the optimal plane that returns the minimum slope when the surface is oriented to the fabrication plane. To define the reference plane, the 'fit plane' component in GH is used, it generates the plane that best fit the UV coordinates of the surface with the least deviations (distance between points on surface and the reference plane). The fit plane component in GH is based on the least squares reference plane method, which provides a good approximation for the flatness deviation.

The analysis part of the code aims at evaluating the curvature and slope of surface to verify if it is ruled and that its slope does not exceed the angle of repose of sand. The gaussian curvature (K) is firstly analyzed by evaluating the surface curvature at sufficient {uv} coordinates (1 cm intervals), it is calculated as the multiplication of the maximum $K_1$ and minimum $K_1$ curvature at each point ($k=K_1xK_2$). The returned values of the gaussian curvature should be nonpositive in order to consider the surface as ruled and hence valid for the fabrication process.

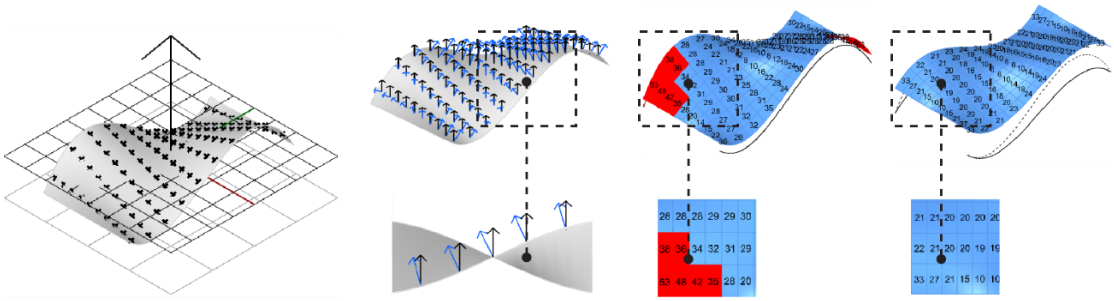

Figure 6.74 Surface slope analysis

The slope of the surface is defined by calculating the angle between the normal at the UV points and the normal of the XY plane (fabrication plane). A representation method of the slope is developed to visualize the slope on the surface. On each UV coordinate the value of the angle is indicated numerically and a color is assigned (blue ≤ angle of repose of sand > red). The results of the slope analysis return a feedback that indicates the areas of the surface that exceed the angle of repose of sand, which require the redesign of the panel to reduce its slope. After verifying the surface curvature and slope, the surface is considered as valid for fabrication. The next part details the process of generation of the formwork.

**Formwork constraints**

A major constraint that informs the surface discretization process in the sweeping technique is the fabrication method of the sand formwork. Since the formwork is fabricated by cutting flat sheets materials (cardboard or plywood), then the sides of the formwork should be designed either planar or single ruled without torsion to respect the possibilities of the flat sheet material. Following this consideration, different methods of surface discretization are studied.

**Surface discretization**

Among different methods of surface discretization, the asymptotic curves are the most efficient for the sweeping methods as they return flat right sides for the fabrication the formwork.

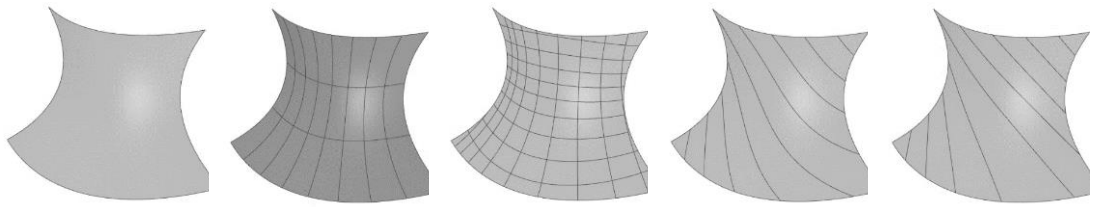

Origina surface Isometric Principal Geodesic Asymptotic

Figure 6.75 Evaluation of different discretization methods

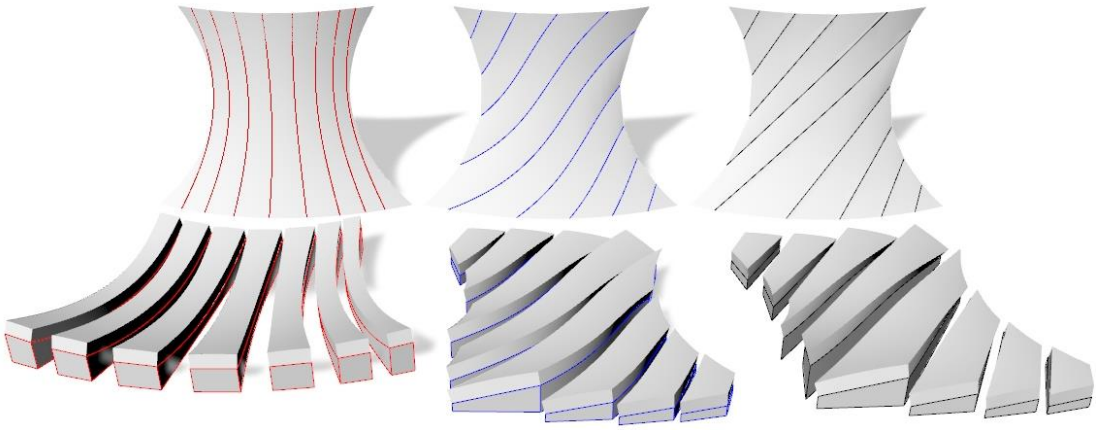

Figure 6.76 Evaluation of the flatness of boxes sides in principal, geodesic, and asymptotic curves

### 6.4.4 The making workflow

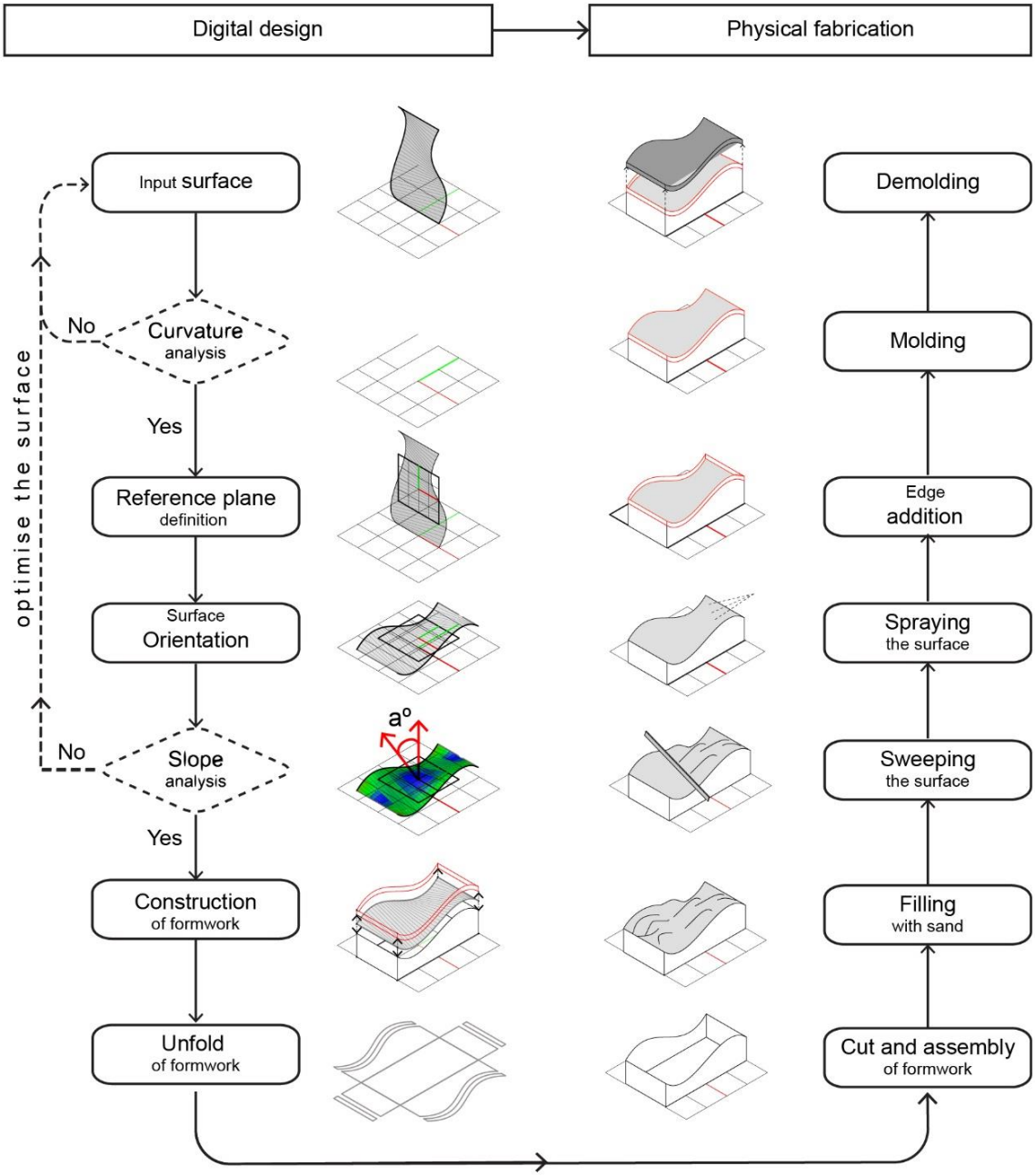


Figure 6.77 Digital / physical workflow of the sweeping method

#### 6.4.4.1 Digital workflow

The sweeping code aims at providing information for the fabrication process while considering the manufacturing and material constraints. A typical process of the sweeping technique is as follow:

1. An initial surface is given as an input of the algorithm.
2. The surface curvature is analyzed to ensure it is a nonpositive Gaussian curvature.
3. The surface is then subdivided into ruled panels with reasonable sizes for manufacturing.
4. The panels are then oriented to the ground, and their slope are analyzed.
5. If the slopes of the panels exceed the slope of the sand the surface is then relaxed.
6. The panels are offset normal to the large surface to define their thicknesses.
7. The formworks are then generated from the profile of the oriented panels.

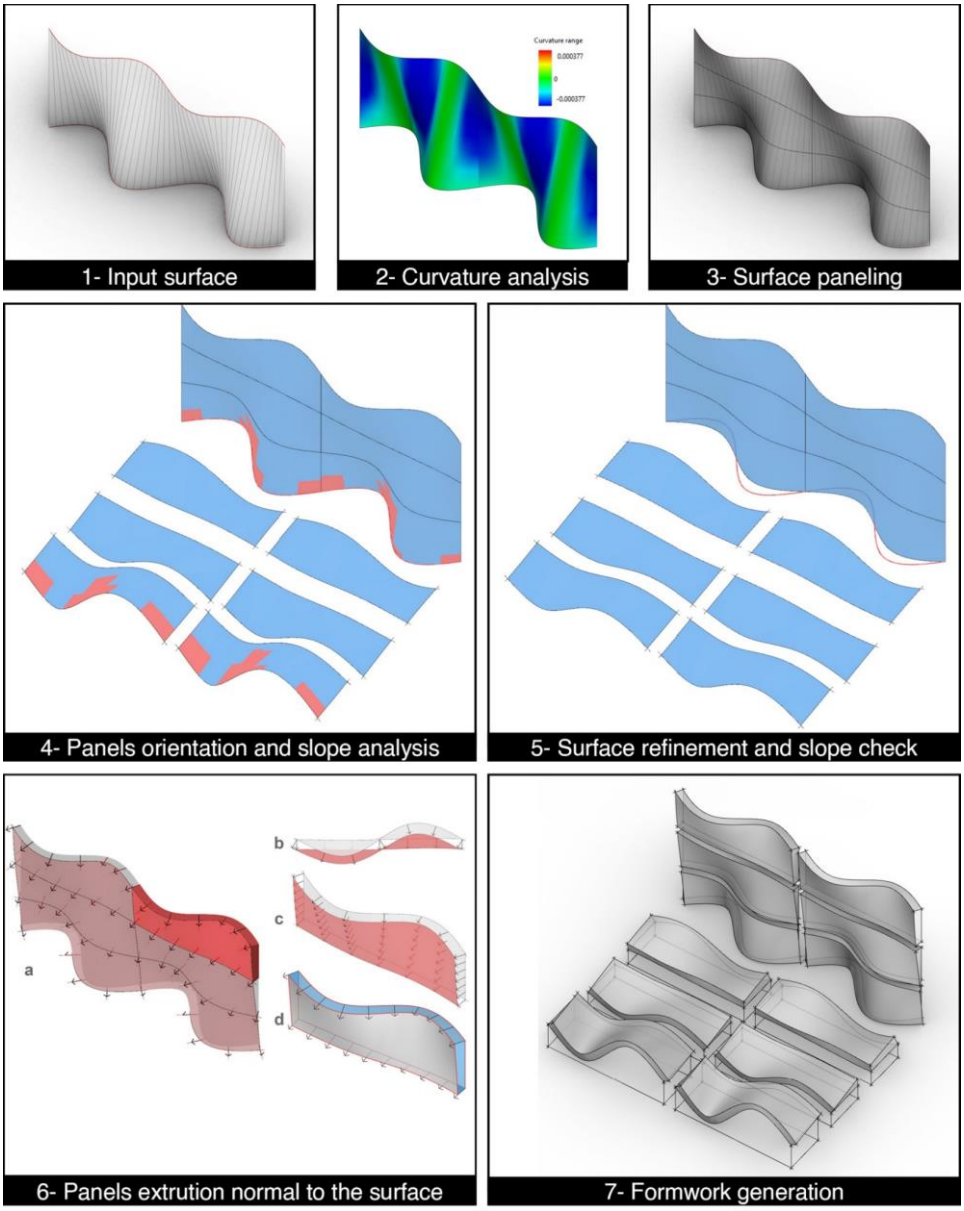


Figure 6.78 The digital workflow of the sweeping technique

**Generation of the formwork**

The fabrication part of the code aims at generating the drawings of the formwork. Firstly, the surface is oriented to the fabrication plane to return the minimum slope. To do so, the surface is oriented from the source plane (the reference plane with its origin placed in the center, which is already defined in the previous part) to the target plane of fabrication (world XY plane and its origin). After the orientation of the surface, the process of the fabrication is applied on three steps. Firstly, the surface is extruded the normal direction of the XY plane with the value of the thickness to generate the 3D model of the panel. Secondly, the sides of the extruded panel are extracted to generate the sides of the formwork thickness. Finally, the boundary curve (c) of the surface is projected to the XY plane to generate the base curve (d) of the formwork, curves c and d are then lofted to generate the sides and the bottom of the formwork. Now as the formwork is generated, the 3D model is unfolded to develop the 2D drawings for cutting the formwork.

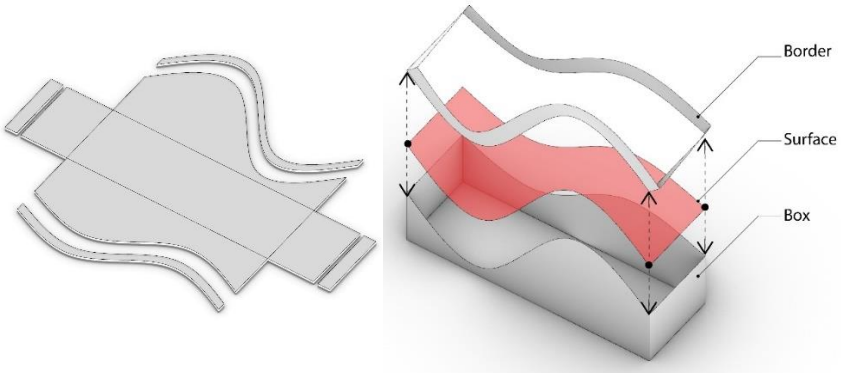


Figure 6.79 The sweeping formwork development and assembled.

#### 6.4.4.2 Physical workflow

The physical workflow of making is presented here through a 50x50x2cm hyperbolic paraboloid surface. Prior to fabrication, the HP surface is modeled, and the drawings of the formwork and the assembly scaffold are generated. The procedure is detailed below and illustrated in Figure 6.80.

1. The drawings of the unfolded formwork including the box and the border are cut on cardboard. The box is then assembled and filled with dry sand.
2. The surface of dry sand is swept with a ruler to create a smooth ruled surface.
3. The surface is solidified by spraying the saline solution. A thin solid layer is produced instantly, and the surface is used as the bottom side of the new formwork for molding.
4. The cardboard border is then fixed over the edge of the solidified sand surface.
5. The formwork is molded with a plastic mixture of Hyposand, swept with the ruler to make an even surface and left to dry for one hour.
6. After hardening the sand panel is demolded and the formwork is reused for remolding.
7. The produced panels are assembled on a scaffold

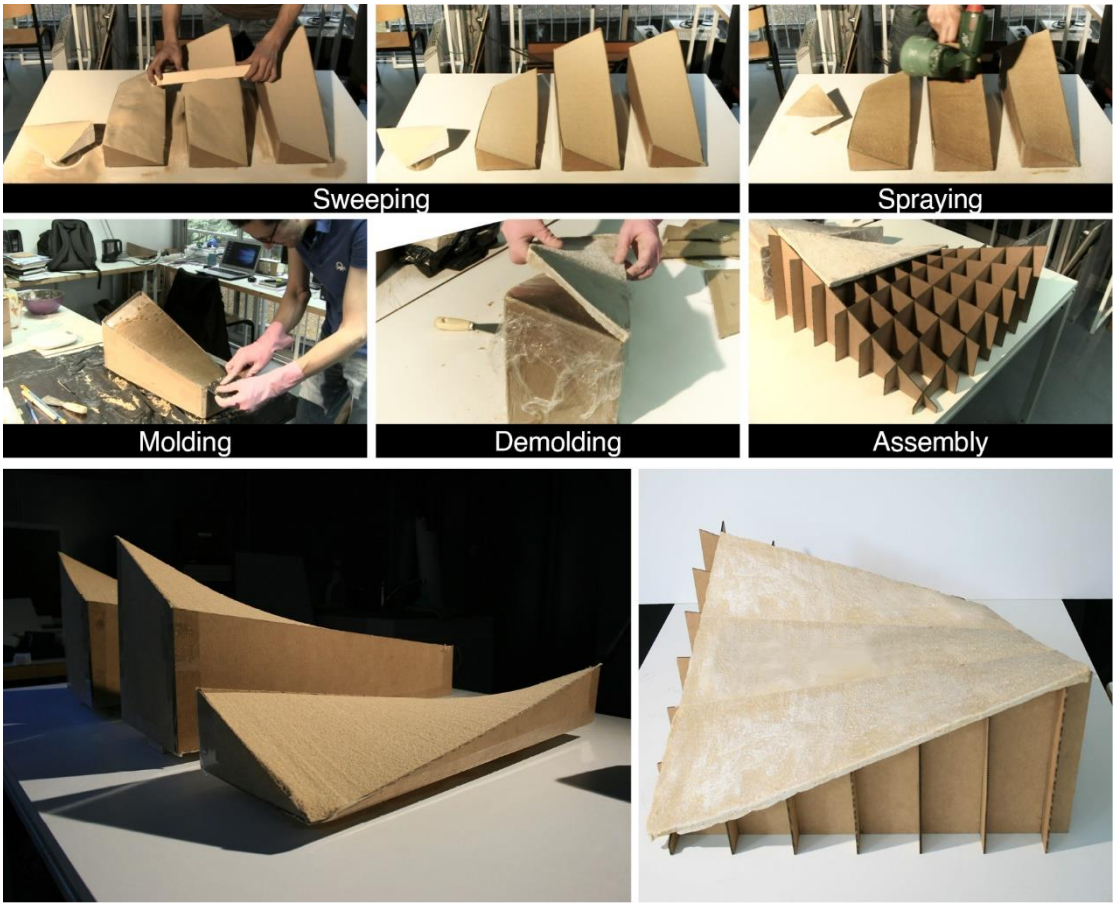


Figure 6.81: Fabrication process of a hyperbolic paraboloid surface from three panels.

The fabrication of the ruled panel is applied through four steps: the formwork assembly, filling with dry sand, solidification of the sand surface and finally the casting of the panel. At first, the drawing of the unfolded formwork is cut on cardboard or plywood by a laser machine, which returns fast and accurate results. After then, the formwork is assembled and filled with dry sand. The irregular surface of filled sand is swept with a ruler, which remove the exceed material and return the ruled surface smooth. The surface of dry sand is then solidified by spraying the saline solution evenly over the surface, which returns instantly a thin crisp (2-3 mm) of solid sand. The thin solid surface of sand is then considered as the base of the formwork and the cut borders are fixed on the edges of the formwork. Finally, the formwork is filled with the liquid mixture of sand and salt and swept with the ruler to make an even finishing of the surface. The mold is left to set for one hour after, which the panel is solid and can be demolded while the formwork can be reused to produce another panel.

### 6.4.5 Physical and digital experiments

The advantages of the sweeping method presented is being simple, low-cost, and reusable with minimum waste. The method consists of a precut formwork filled with dry sand that is swept along the profile of the box to create a ruled surface, then the exposed surface of sand is solidified by spraying the saline solution giving a solid crust of sand that acts as the base to cast the sand/salt mixture or other liquid material such as concrete or plaster. After removing the solidified panel from the mold, the sand can be reused for a new formwork. However, the plywood box can only be reused for identical panels.

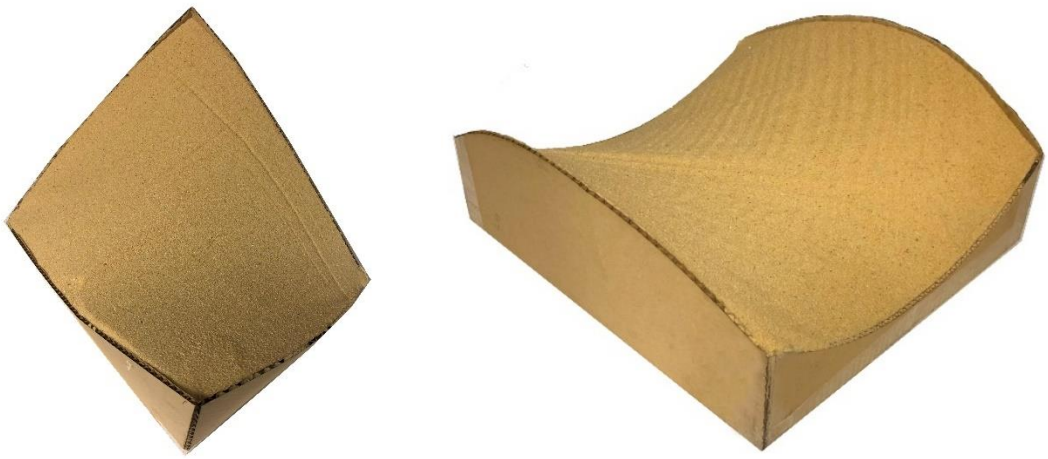

Figure 6.82 A Hyperbolic paraboloid and a saddle surface formed by sweeping in the direction of their rulings.

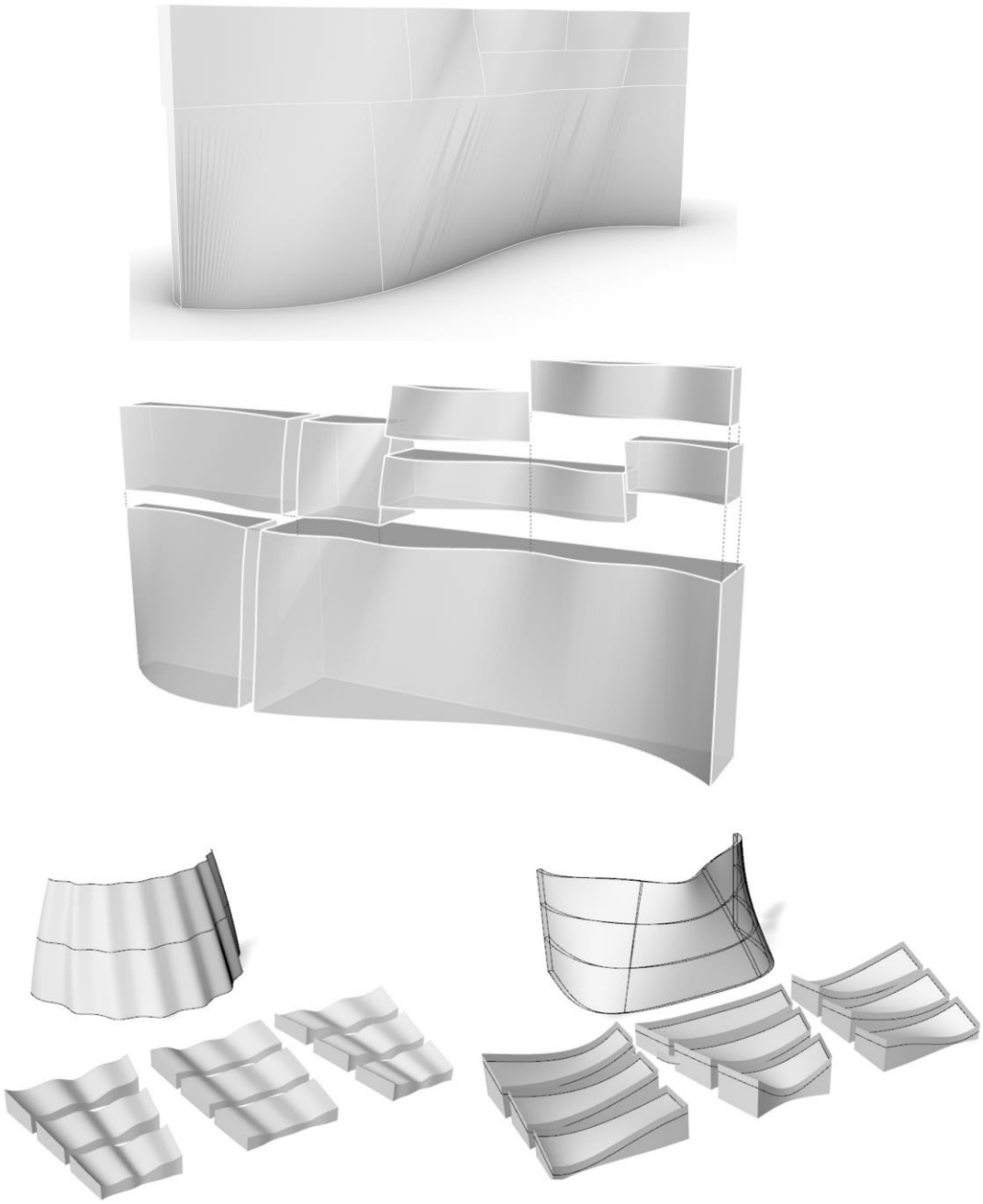

Figure 6.83 Models of curved walls subdivision into ruled panels

Figure 6.84 Digital and physical study of a twisted arch

**LF-20 prototype**

The LF-20 prototype examines three making techniques proposed in this work:

- The sweeping formation of negative ruled surface
- The combination of sweeping, addition, and substation formations
- The use of sand panels as a reusable formwork for casting concrete block

The sand is formed by first sweeping the surface following the direction of the rulings. Then, the sand surface was detailed with the engraved pattern through subtractive and additive processes. The detailed process of making this model is described in § 5.5.

Figure 6.85 LF-20 model : fabrication of a reusable casting formwork from two sand panels

Figure 6.86 Details of the panels ridges and edges

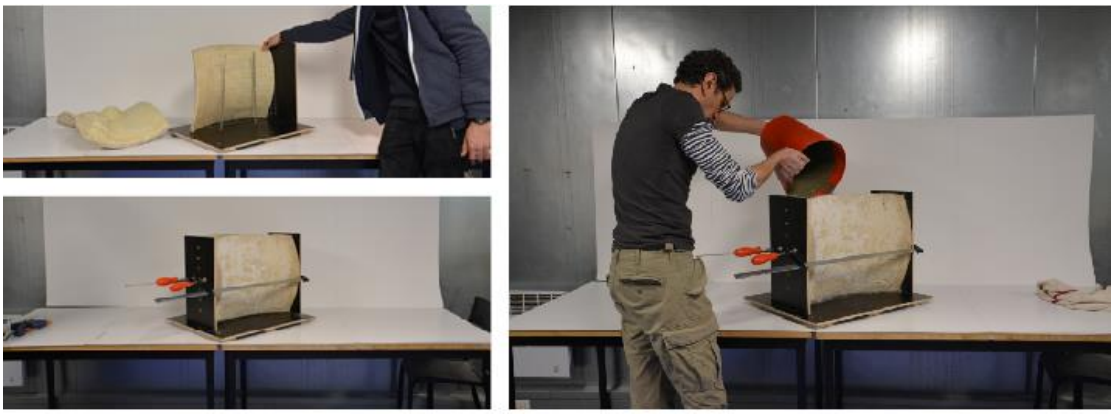

Figure 6.87 Assembly and casting of the panels with cement

Figure 6.88 Demolded cement block and reusable sand panels

## 6.5 Helicoid technique

The Helicoid technique aims at defining the making methods of developable helicoid surface from sand self-formation. The study's approach is based on the geometrical feature of the developable helicoid being a constant angle surface. The study questions the shape of the formwork and the process of making that allows the helicoid surface to emerge from sand self-formation.

### 6.5.1 Method definition

An integrated study of geometry, modeling, and physical experiments is conducted to identify the process and potentials of the helicoid method as briefed below:

1. An initial digital-physical test is conducted to explore the parameters and constraints of the proposed method (Figure 6.89).
2. The study of the geometrical properties of the developable helicoid surface identifies its key parameters and informs the algorithm and the making process (Figure 6.90).
3. Two making methods are proposed based on the design of the formwork:
    a. By releasing sand from a cylindrical formwork (Figure 6.91).
    b. By sweeping sand surface following the edges of a spiral formwork (Figure 6.94)
4. A method of making the helicoid surface in parts is tested to examine to examine larger scale applications (Figure 6.95)
5. A parametric modeling method is developed to generate the surface of the helicoid and the surface of the corresponding formwork. Moreover, the algorithm examines the possible morphogenetic variations that emerges from the differentiation of the input parameters (Figure 6.96).

The following figures demonstrate the helicoid technique with a brief description.

Figure 6.89 First test of helicoid fabrication for a spiral stair design

### 6.5.2 Geometrical principles

The developable helicoid is a surface of constant slope generated by the tangents to a circular helix. Figure 6.90 shows the geometrical principles of the developable helicoid *s* and the helix curve *r* (in red). The helical line is a curve in space situated on the surface of a circular cylinder, which intersects all generators at a constant angle. As a consequence, when unfolding the cylinder into a plane the helix becomes a straight line in this planar development.

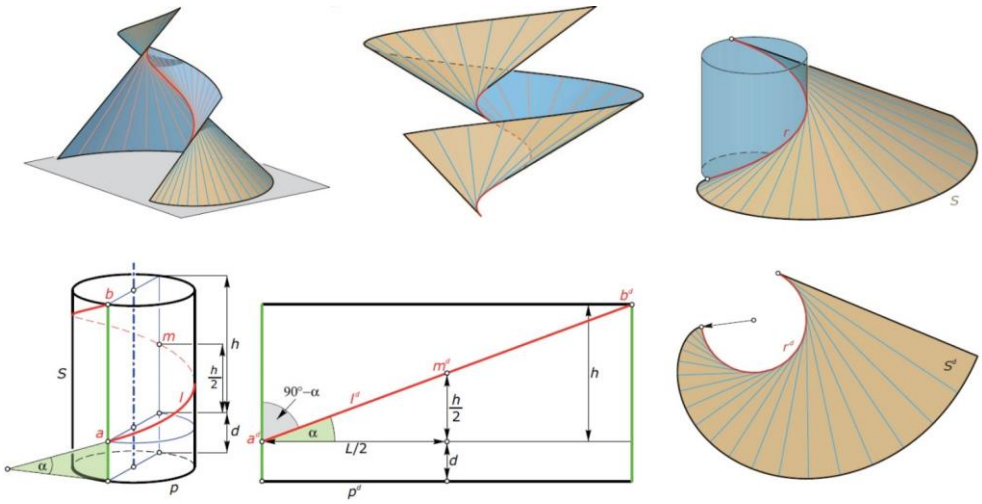


Figure 6.90 the geometrical principles of the developable helicoid and the helix curve of constant slope

### 6.5.3 Physical making method

Informed by the above geometrical description, a formwork is generated by the algorithm to physically make the helicoid by the self-formation behaviour of sand. The formwork consists of two cylinders, a vertical partition tangent to the interior cylinder, and a base with a hole adjacent to the partition. The formwork is first generated by the algorithm according to the designed surface. It is then developed, cut, and assembled. When filled with sand, the sand flows in the direction of the hole leaving behind a developable helicoid surface (Figure 6.91). The surface is then sprayed with the saline solution returning a solid helicoid (Figure 6.93).

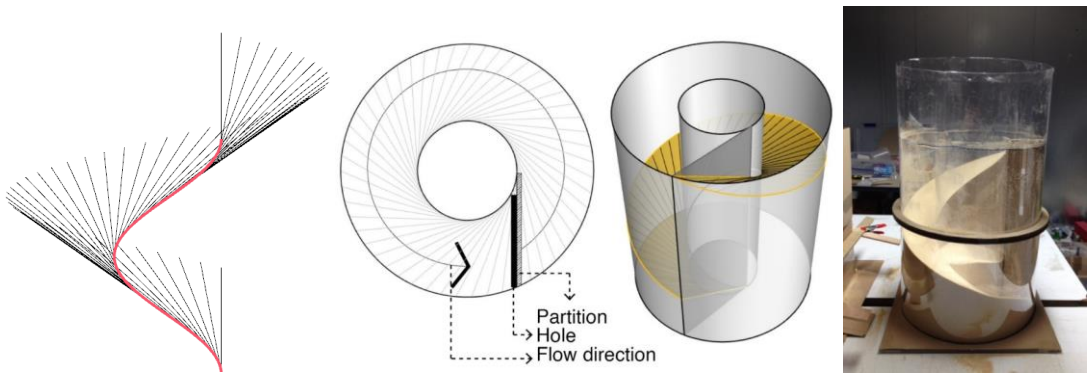


Figure 6.91 the cylindrical formwork for the generation of the helicoid surface

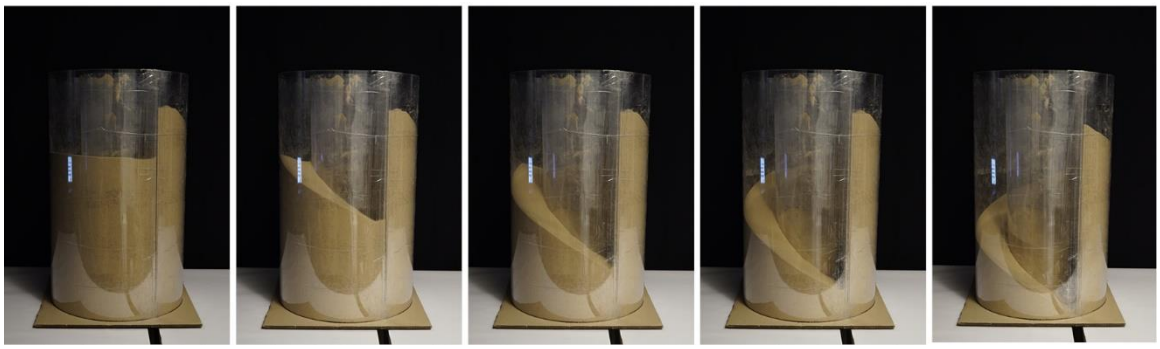

Figure 6.92 Process of formation of the helicoid surface using the cylindrical formwork

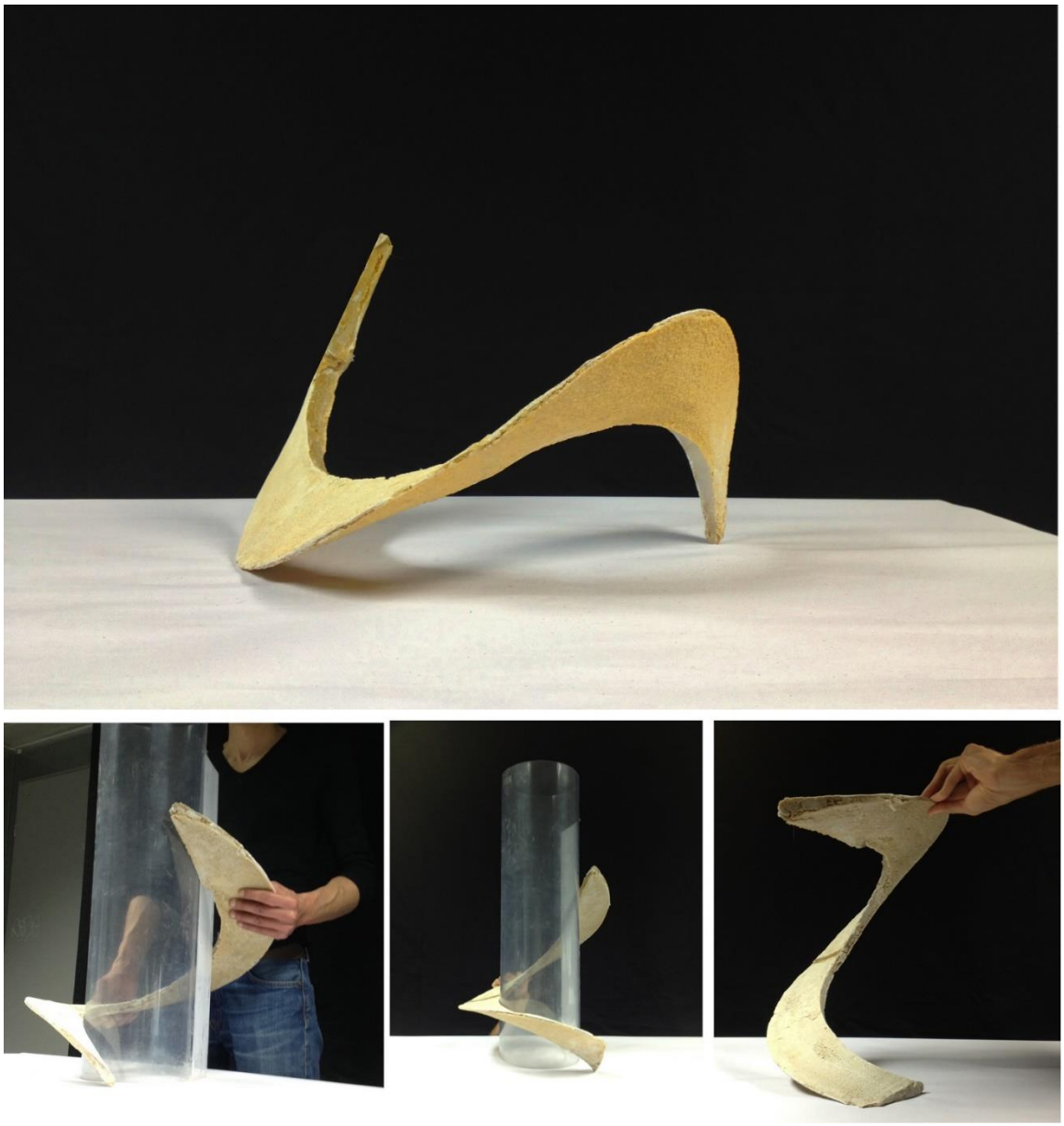

Figure 6.93 Solid helicoid surface made of sand. (height 30cm, radius 25cm, thickness 2cm)

Despite the successful process of formation using the cylindrical formwork it limits the spraying process in the fabrication phase. The lower part of the helicoid is at the bottom of the narrow space between the two cylinders, which is not accessible for spraying. To overcome this limitation, a spiral formwork using the sweeping method of formation is proposed.

The spiral formwork consists of two cylindrical sides cut following the helix curves and a vertical partition but without the hole at the bottom. The formation process is based on the sweeping technique. First the space in between the two spiral sheets is filled with sand. Then, the surface of sand is swept with a ruler guided by the edges of the spiral sheets. The process returns a developable helicoid that is more accessible for spraying and even molding.

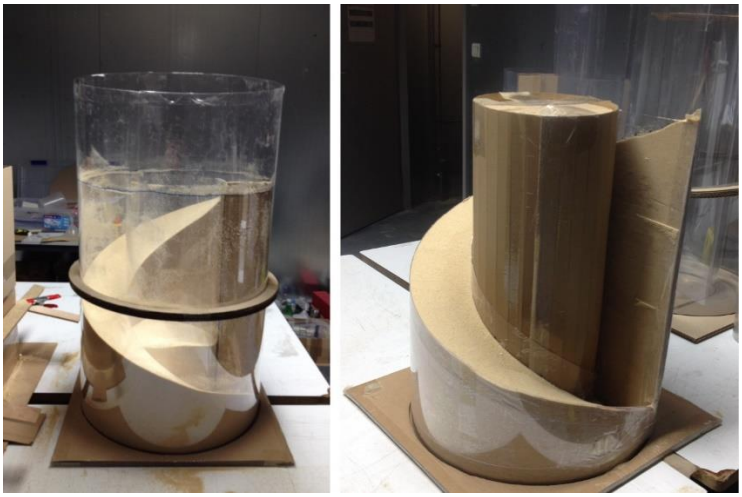

Figure 6.94 the cylindrical formwork (left) vs. the spiral formwork (right)

In term of scale, for the construction of a spiral stairs for instance, it is costly to construct large cylinders of sand due to the mass of the material. To overcome this limitation, a test is conducted to fabricate a part of the helicoid surface (Figure 6.95). The test returns a feasible method for the fabrication of a part of the helicoid, which opens the possibility for studying larger assemblies.

Figure 6.95 Fabrication test of a part of the helicoid surface for larger scale applications (left), and a physical model of a double helicoid 40x80x30 cm (right)

### 6.5.4 Digital making method

The above study and experiments of helicoid making defined the process of formation, its parameters, and the fabrication constraints. The acquired data is crucial for informing the parametric modeling technique. Based on the geometrical principles of the developable helicoid and the above physical experiments, four main parameters are defined:

- ***It*** & ***Ib***: the top and bottom radii of the interior envelop
- ***Et*** & ***Eb***: the top and bottom radii of the exterior envelop

The algorithm aims at modeling the helicoid surface and the formwork for physical production. Based on the input of the interior radius and the slope of sand, the surface, and the formwork according to the following procedure:

1- A cylindrical or conical helix curve is first generated with parametric equations [211–213] where the top *It* and/or bottom *Ib* radii of the interior envelop and the slope are given.
2- The tangents of the helix are then generated with a range of lengths corresponding to the top *Et* and bottom *Eb* radii of the exterior cylinder
3- The helicoid surface is generated from the tangents
4- The formwork is then defined from the profile curves of the helicoid
5- The formwork is then developed for fabrication

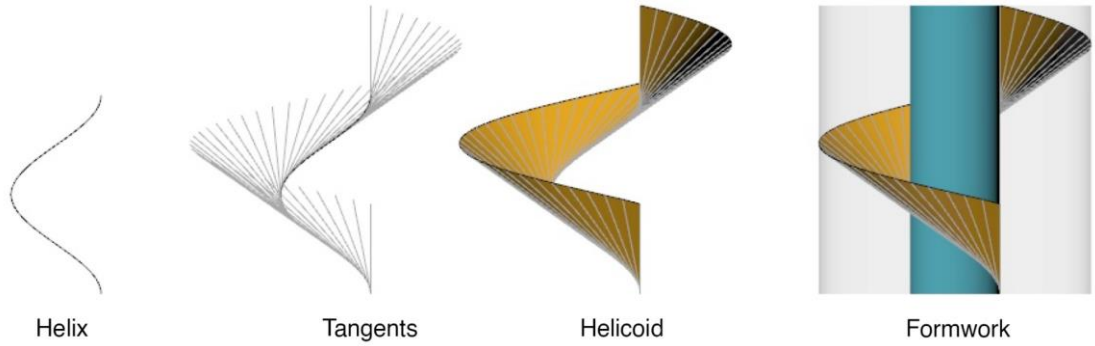


Figure 6.96 Digital process of helicoid and formwork generation

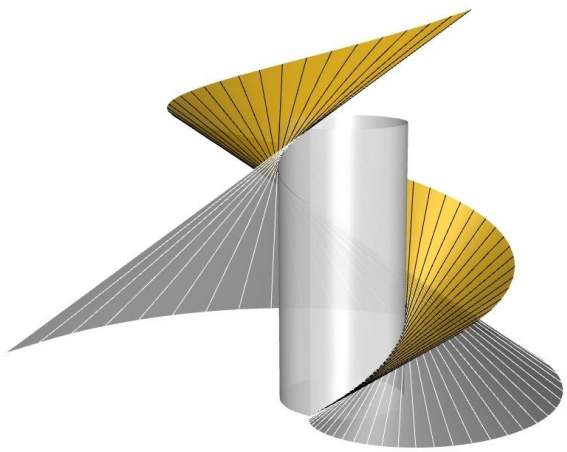

Figure 6.97 The direction of the tangents defines the direction of slope of sand either inward (yellow) in case of using interior and exterior envelops, or outward (gray) in case of using an exterior envelop only.

The algorithm allows the investigation of different configurations of helicoid by altering the input parameters of the diameters of the envelops. Figure 6.98 shows five possible variations of cylindrical and conical helicoids. At the bottom is a digital experiment of generating a helicoid on a cone with the same slope of sand as an interior envelope. It is necessary to verify the digital model with a physical experiment in future work to validate the method.

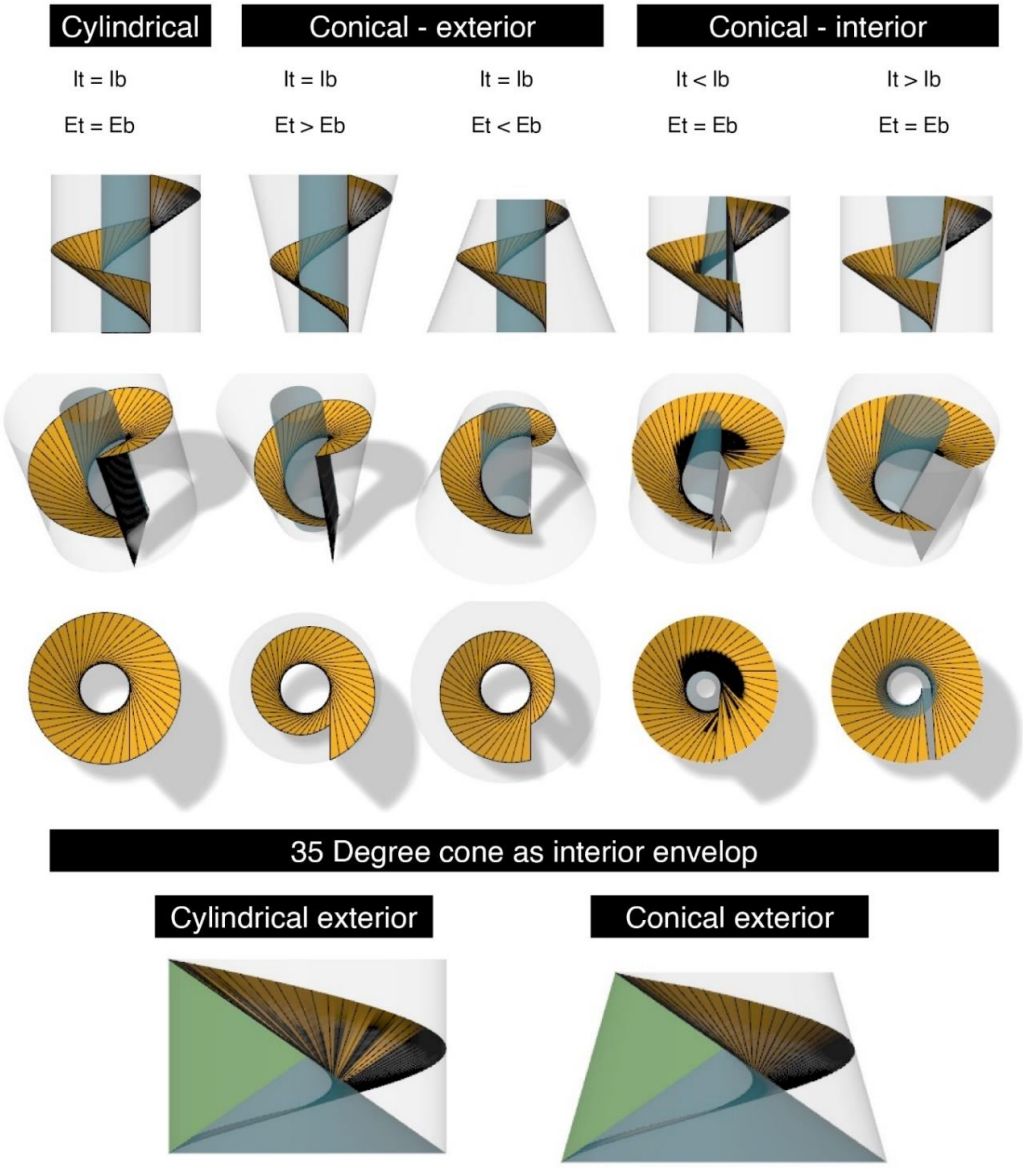


Figure 6.98 Possible variations of the helicoid surface

The shape of the interior and exterior envelop, and the use of multiple intersecting helicoids are not discussed in this thesis. However, they are considered for future work as they allow for hybrid helicoid surfaces and open further morphological investigations in both modeling and physical making (see Figure 6.95 above).

## 6.6 Pipe casting technique

This section introduces a formation method informed by the capacities of Hyposand[72]. In addition to the plasticity and the mechanical advantage of Hyposand, it exhibits a motivating hardening process: the capacity to solidify without air contact[73], i.e., in a vacuum container (see §3.5). Moreover, the application of a watertight membrane protects the material from humidity and extends its lifespan. Collectively, these capacities of the material motivate the research to examine a making technique where plastic sheaths are used as a stay-in-place formwork for casting Hyposand. The objective is to develop a linear tectonic from the material that synthesis form, structure, and ornament by the method of making.

### 6.6.1 Initial tests

To examine the proposed technique two initial tests are conducted. The first examines the making process with a single element (Figure 6.99), while the second explore the morphological possibilities with multiple elements (**Error! Reference source not found.**).

Figure 6.99 Formation of sand tubes: dry sand (left) and solidified and (right)

In test 1, two single tubes of 4cm diameter are filled with dry sand and Hyposand then formed. The dry sand returns a flexible tube that can be formed and reformed into a knot shape. The formability of the tube is due to the flexibility of the sheath and the phase changing behaviour of sand from liquid to solid states (see §2.2.1). In the same figure, the tube on the right is filled with Hyposand, and formed within the workability time of the material. The tube hardens relatively fast returning a solid form in 20 minutes. In test 2, the morphological possibilities of aggregation and assembly are investigated by weaving, branching, and twisting techniques (Figure 6.100).

[72] Although this research is concerned with the self-formation of dry sand, formation of wet sand is partially in the scope of experimentation to explore the capacities of Hyposand as a forming material rather than a mere filler. Some methods of formation with wet-sand are reviewed in the literature in § 2.2.2 , preliminary experiments with Hyposand such as printing, and injecting are conducted and briefly introduced in § 3.1.4 along with their advantages and limitations.

[73] The capacity of Hyposand to harden without air contact is acquired from the behaviour of the salt which can crystalizes in vacuum container if in contact with a nucleation agent like sand. As such, air contact is not essential for the crystallization process as discussed in section 2.6.1.

Figure 6.100 Investigations of sand tubes bundling, weaving, branching, and twisting morphologies.

According to the initial material exploration, two processes of formation are set to explore: (i) ‘casting-forming’ where the tubes are filled then formed, and (ii) ‘forming-casting’ where the tubes are hanged on a scaffold then casted. To develop the proposed technique it was essential to study the process of making in experiment 1 and the morphological possibilities and assembly methods in experiment 2. The technique implies a very particular morphology characterized by progressive combination and splitting of the tubes. Linear tectonics where discrete linear elements converge and diverge is a cross disciplinary morphological system.

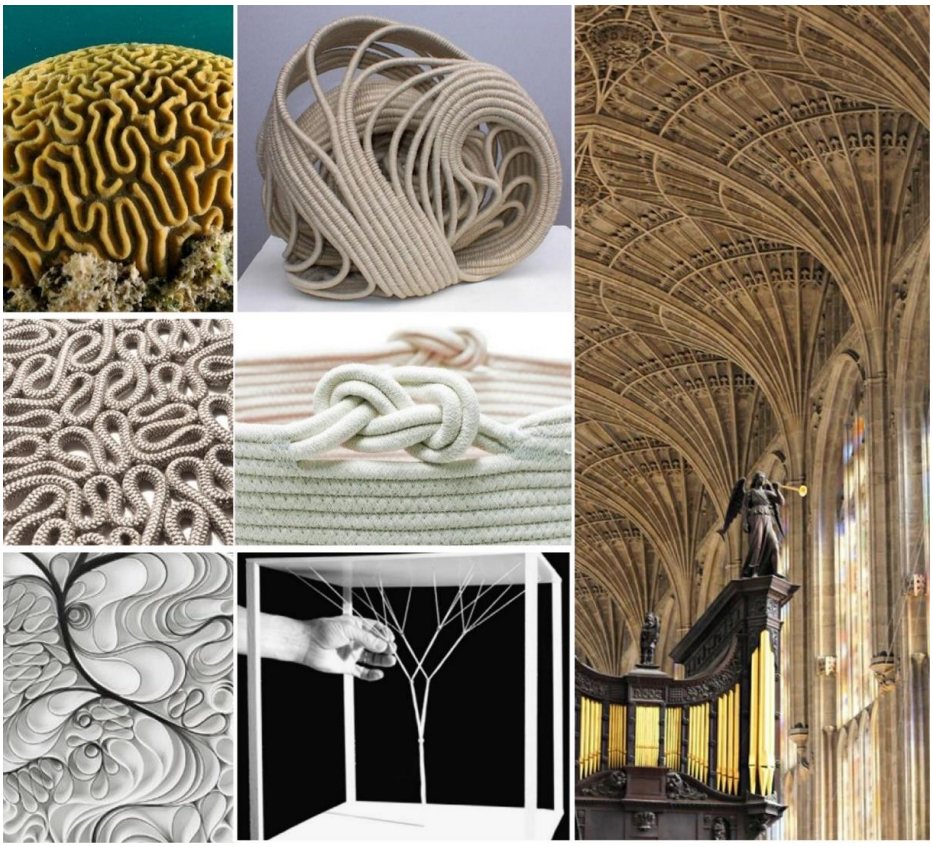

Figure 6.101 Examples of linear based tectonics in nature, art, craft, and architecture.

### 6.6.2 Experiment 1: the hanging model

The first experiment[74] aimed at determining the process of making and its constraints. A hanging model of a vault was though to return a pure compression structure which meets the advantage of Hyposand in compression. Prior to fabricating the model, an initial test defined the catenary curve of a hanged sheath when empty and when filled with Hyosand. A method of assembly by weaving was proposed to interlock the tubes after hardening. To fabricate the model, empty sheaths were hanged on a scaffold first then weaved. Following, Hyposand was poured from the two ends of each sheath at the same time and zip ties were used to temporarily hold the tubes in place. The model was then left to harden for one day then turned upside down.

Figure 6.102 Initial test to determine the catenary curve and the technique of making. (a) dry sand, (b) wet sand, (C) hanged plastic sheaths, and (d) organization of dry sand tubes.

[74] The first experiment was conducted within an academic workshop of 3 days at ENSA Paris-Malaquais by the group of students of Monica Klink, Joseph Melka, Hugo Suchet and Thibault Félix.

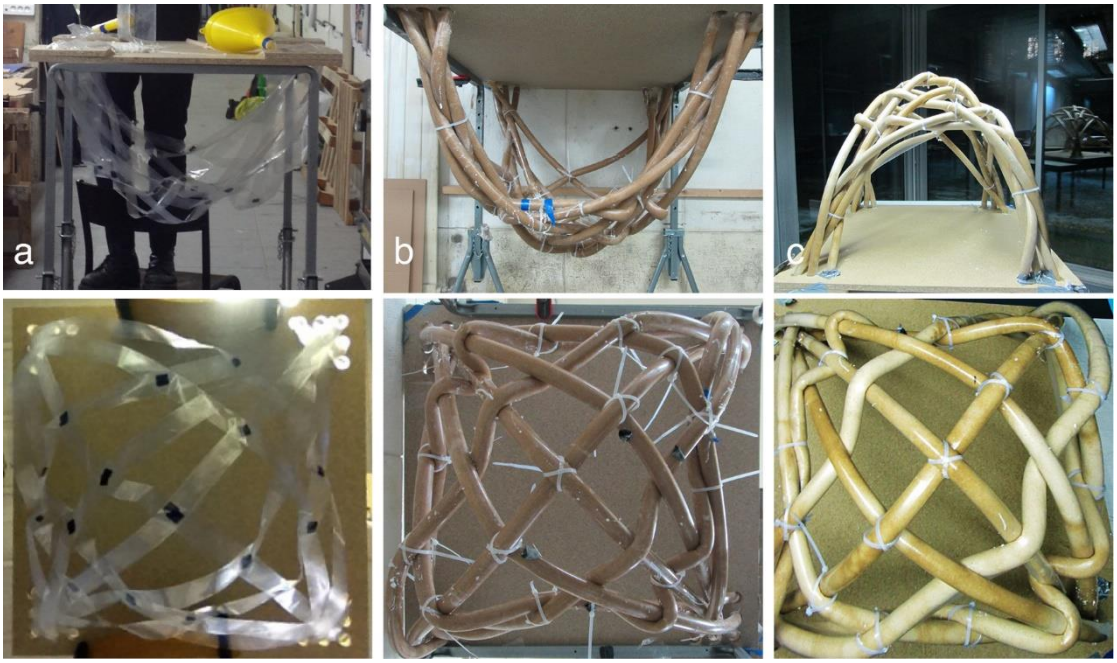


Figure 6.103 process the catenary technique. (a) hanging, (b) casting, and (c) reversing

Figure 6.104 The casting process. The model is casted simultaneously from the two ends of the tubes

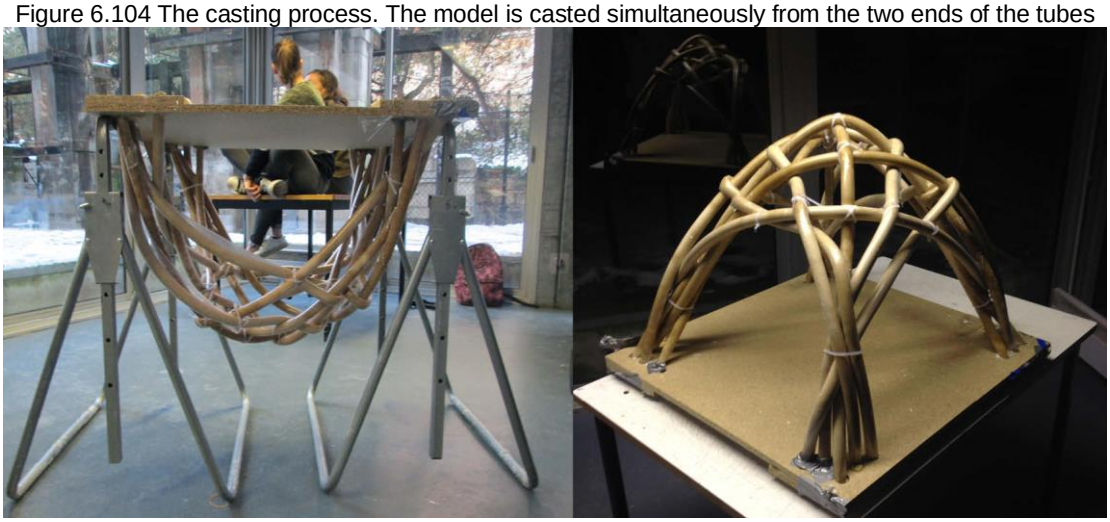

Figure 6.105 the solid catenary model (top), and the reversed model (bottom)

### 6.6.3 Experiment 2: the vertical model

The second experiment[75] studied the vertical bundling of tubes[76] with a prototype of 50x50x120 cm height. A wood scaffold with perforated planes was used to keep the sheaths in their places prior to casting. To assemble the tubes after hardening, custom 3D printed joints were used. The result showed the feasibility of the proposed fabrication process and the use of custom joints. However, buckling occurred at the bottom of the tubes under their weight.

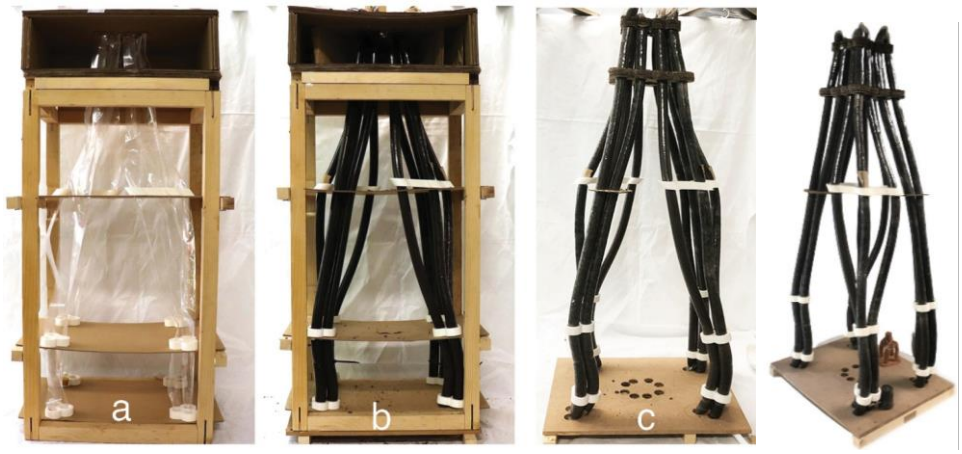


Figure 6.106 Making process of the tubular vertical structure (50x50x120 cm). Organization of the sheath in the scaffold (a), casting (b), removal of the scaffold.

Overall, the pipe casting technique proposes a linear tectonics system of compressive structures teased out from the capacities of Hyposand. It shows advantages in terms of morphological possibilities and productivity of making. However, the structural performance of the techniques requires the consideration of compression-only forms. A possible subject for future research is integrating form-finding methods of branching structures to generate compression-only forms. Nevertheless, it is important to note that a major difference with branching systems is that the sand tubes are not joined branches but discrete elements, which implies a different form generation and structural optimization approach. In terms of scale, sheaths of up to 20 cm diameter are available in the market, opening the possibility of introducing reinforcements in the tubes for tensile strength.

Finally, the development of an integrated computational tool that synthesis design morphogenesis, fabrication logics, and structural optimization would enable the construction of compressive sand forms characterized by a rich tectonic articulation of bundling, looping, weaving, twisting, and branching. Thus, a series of structures could be configured by interweaving the tubes.

---

[75] The model was developed within an academic design course, semester 6, at ENSA Paris Malaquais by the students Samir Boukhalifa and Yasmina Ayuch.

[76] A parametric algorithm for form generation was developed to investigate different bundling possibilities but it is not discussed in this work.

## 6.7 Discussion of the sand tectonics

**Time based**: Sand take time to settle do their work and, further, that this curing time is a necessary and productive delay.

the time taken by materials to do their work, e.g. flowing, curing, heating, or cooling;

## Conclusion and future work

This section concludes the dissertation and draws perspectives for future work. First, the research aims and methods are recalled. Then, a summary of the main contributions is given. Next, the findings, limitations, and future work of sand tectonics are discussed. Finally, final reflections and future perspectives are drawn.

The overall aim of the thesis was to develop the sand tectonics, a design to fabrication architectural system informed by sand self-organization and salt crystallization. To achieve the overall aim, an interdisciplinary framework of research was set to simultaneously develop material, design, and fabrication studies. In turn, material tests, geometrical analysis, physical experiments, and digital modeling are synthesized in a feedback loop to develop a digital-physical workflow of making. In support of the overall aim of the research, the following main contributions are achieved:

1. Development of an architectural material-based system where formation and materialization are inseparably related by sand self-organization behaviour.
2. Standardization of the processes of making of Hyposand and enhancement of its workability, quality, and strength.
3. Characterization of the key mechanical properties and microstructure of Hyposand.
4. Development of six manual and robotic formation methods of sand allowed by the material logic while considering the fabrication constraints.
5. Development of two parametric methods for modeling sand forms based on the geometrical principles of surfaces of constant slope.
6. Development of the fabrication methods and the digital-physical workflow of making from design to production.
7. Production of a large number of physical and digital prototypes implementing the developed sand tectonics methods.

Collectively, the contributions constructed the sand tectonics system which allowed the exploration of possible sand forms, their modeling, and production. The system was used efficiently to produce non-standard sand panels and blocks that can be assembled into a larger whole. Through a series of iterative experiments, a number of physical demonstrators supporting the thesis and demonstrating both its potential and limits, were produced.

The contributions of the thesis are discussed in the following subsections in two axes:

A. **Material system**: discusses the making methods of Hyposand and its characterization
B. **Making system**: discusses the design, geometry, modeling, and fabrication methods

## A. Material system

The 35 Degree project established the material system of the sand tectonics. It proposed a method to solidify sand with sodium thiosulfate salt by means of mixing and spraying. However, the methods of the material fabrication had limitations in workability, and the mechanical characteristics of the material were not studied. To deepens the knowledge of Hyposand and unfold its morphological and construction potentials, the material research in this work aims at:

1. Standardizing the processes of making of Hyposand to improve its workability
2. Characterizing the mechanical properties of Hyposand to define its structural capacities

A prerequisite for this investigation was the theoretical and experimental study of the fundamentals of sand and salt in chapter 2, including: (i) the sand physical characteristics, phase-changing behavior, self-organization behavior, and solidification methods, and (ii) the salt phase-changing behavior.

### *1. Standardization of the processes of making of Hyposand*

To improve the workability of Hyposand, it was necessary to develop the know-how of the material fabrication in chapter 3 by conducting several material experiments. On this basis, the following findings are drawn:

a) To overcome the limitations of the saline solution in the 35 Degree project, the crystal form of salt is used instead of the powder form to exclude the use of water in the preparation phase. Moreover, a kettle is used instead of a hotplate to heat the salt exactly up to its boiling point (100°C), which avoids the decomposition of the salt and the reduction of its strength if overheated. Furthermore, a spraying gun is used instead of manual sprayers to produce evenly sprayed surfaces, sharper sand patterns, and higher strength panels.

b) According to the study of the effect of water content on the formability of sand in § 3.2, three states of hydrated Hyposand and their formation possibilities are distinguished in this work: (i) plastic- moldable (50% salt), (iii) viscous- castable (55%), and (iii) liquid-pourable (60%). Altering the consistency of the material gives rise to new formation possibilities.

c) Following the study of the effect of sand grain characteristics on the workability of Hyposand, two types of sand are distinguished for casting and spraying processes:
   - Well graded fine to medium rounded sand is used to attain a workable mixture
   - Poorly graded fine rounded sand is used to achieve sharp patterns when formed

d) The examination of the STP phase changing behavior in § 2.5 leads to identify the following workability aspects of the saline solution:
   - The STP salt is a byproduct of industry, easily accessible, not expensive, and not harmful for health or the environment. It melts at a relatively low temperature (48°C), and when heated up to its boiling point (100°C) returns a supersaturated solution.

- The STP returns higher strength in bonding if used while hot (80°C to 100°C). This is due to that the STP saturation, which increases proportionally with its temperature.
- The STP is relatively fast hardening. Its rate of crystallization decreases proportionally with its temperature. It hardens instantly below 48°C (melting point) or lower, while at 80°C, a more workability time is given.
- The salt can be stored in its liquid state (in vacuum containers under 48°C), allowing the use of the salt in sites where no heating sources are available to melt the crystals. The storing possibility is due to the supercooling feature of the STP.
- The salt can be partially restored by melting the solid crystals due to its semi-congruent property. The restored salt is more viscous and less concentrated but can be used in the mixing technique.
- Overheating the saline solution or reheating the solid crystals cause the transition of the STP transition to lower hydrates that are less concentrated and therefore less effective in bonding.

Collectively, the above findings and the material experiments improve the workability of Hyposand and identify its aspects in § 3.6. To conclude, Hyposand is an accessible material that relies on limited resources being sand, STP salt, and heating energy to melt the salt. No water is needed for the process. It is a castable and sprayable material with remarkable strength in compression when solid. It is fast hardening at room temperature without the need for burning, additives, or air contact. The material is reusable by means of heating the solid conglomerate. It is semi-recyclable with minimum waste by means of water immersion, which allows the recovery of sand and the semi-recovery of salt at lower hydrates. Any type of sand can be used, including desert sand, which is widely available and has nowadays limited use in the construction industry.

### *2. Characterization of the Hyposand mechanical properties*

To identify the mechanical properties of Hyposand an experimental campaign was conducted in chapter 4 and returned the following findings:

- Hyposand has an average strength of 25 MPa in compression (19 to 31 MPa), and 7 MPa in flexure (4 to 10 MPa). The material shows a relatively low elastic modulus in the range of 0.2–2 GPa. In addition, the results demonstrate that Hyposand has a relatively low thermal conductivity of 0.58 W/(m.k) (0.45 to 0.7 W/(m.k)).

- The effect of grain size and shape, salt to sand proportion, heating temperature of the salt, temperature of the saline solution at mixing, setting time, and addition of gravel have been measured. As expected, rounded, fine and well-graded grains returned more homogeneous material with higher strength. Porosity affected strength almost linearly, a

low porosity being achieved using rounded and circular grains, enabling a good penetration of the saline solution through the interstices. Among the various salt to sand ratios tested, it was experimentally found that the 1:2 proportion of salt to sand returned the highest compression strength with a sufficient workable mixture for casting. Experimental evidence showed that heating the salt up to 100°C and mixing it at 80°C returned a more homogeneous and workable material and hence gave higher strength. The results shows that Hyposand archives the highest strength at the age of 3 days, while the addition of gravel reduces the material strength. The standard deviation test shows that the process of making is stable with a limited dispersion of 1.53 MPa. Together these results define the following the optimum mixing method that returns workable material with high strength:

| | |
|---|---|
| • **Type of sand:** quartz or carbonate | • **Salt to sand proportion:** 1:2 |
| • **Granulometry:** fine | • **Salt melting temperature:** 100 °C |
| • **Gradation:** well-graded | • **Salt mixing temperature:** 80 °C |
| • **Shape:** circular - rounded | • **Setting time:** 3 days |

- Any type of sand can be used, including desert sand, which is widely available and has nowadays limited use in the construction industry.

- The broad comparison of Hyposand compressive strength with existing conventional materials shows that it is comparable to normal weight concrete (strength class 20/25) and higher than masonry bricks. In terms of thermal conductivity, it is comparable to masonry bricks and lower than concrete.

**Limitations and future work of the material system**

- The mechanical characterization campaign was performed at the laboratory scale with around 300 specimens which returned an overview of the key mechanical characteristics, but to achieve more reliable results, the study should be repeated with a larger number of specimens.

- Further experimental investigations are needed to know the new material in detail: study the effect of temperature on the material resistance, improve the material tensile strength, assess the material lifecycle and impact on the environment, and above all, the material insulation and recyclability.

- The major limitation of Hyposand is its degradation if in contact with water or humidity, which reduces its life-span and limits its application for temporary structures. The flexural test results indicate that the flexural and compression strengths of Hyposand decreased by 37% and 41%, respectively, when subjected to 35 to 50% humidity for three days in a

controlled environment. To overcome the instability of Hyposand if in contact with water, small-scale experiments are conducted using natural and artificial water-repellant materials, but the degradation appeared to be unaffected (§ 3.5). For more durable applications, further studies are required to increase water resistance and identify a fit coating that protects the material against humidity and water. To achieve appropriate insulation methods, it is a prerequisite to better understand the phenomenon of water penetration into Hyposand. A neutron/x-ray imaging test is in the scope of future research to observe and quantify the imbibition of Hyposand and the dissolution of the binding salt. If an insulation method is achieved, it will extend the material life-span and allow its use for durable structures, which might be a turning point for the future of the material.

- Thanks to the decomposition weakness of hyposand, its recyclability by wetting can then be sought, separating sand by gravity, and recovering the salt from the water by some chemical or physical processes, which have not been discussed so far. The degradability of Hyposand with water facilitates the recycling of the material at a low-cost with minimum waste. Further studies need to be carried out to identify the recycling method and assess its impact on the environment. The results of the above proposed neutron/x-ray imaging test might help in designing appropriate recycling methods. Suppose the insulation and recyclability objectives are achieved, opportunities for a new architectural system with a designed lifecycle might arise, which returns the materials to their environments at the end of the building life-span for a reproduction phase. This would be a fruitful area for further work. Collectively, the above-discussed characteristics of Hyposand suggest its use in temporary structures in arid climates, recyclable formworks, or applications where a watertight coating can be applied to protect the material.

To conclude, the materials and fabrication processes were described in chapter 3, and the mechanical properties of Hyposand, obtained by different settings, were investigated in chapter 4. Overall, Hyposand seems to develop satisfactory strengths, promising technical accessibility, and minimal consumption of resources. However, further investigations are needed to know the material in detail, to improve its workability, and to extend its lifespan.

## B. Making system

The making system examined the formability of sand and the means by which it can be instrumentalized as a design and fabrication tool. It developed design and fabrication methods allowed by the material logic and associated them in a coherent digital-physical workflow for prototyping. To construct the making system the following studies were simultaneously developed:

1. **Design system:** defined the physical formation methods, their conditions, and tools
2. **Geometry**: analyzed the geometrical principles of surfaces of constant slope.
3. **Algorithm:** developed parametric methods of form generation and robotic control

4. **Fabrication system**: defined the fabrication process and constraints.

To systemize the processes and to establish order in the almost infinite range of making possibilities, it was necessary to associate the above studies through:

5. **The framework of methods** which integrates the methods as the toolbox of making
6. **The physical-digital workflow** which associates the design and fabrication processes in a coherent workflow of making.

To develop the making system, an empirical methodology of design by research was employed through physical and digital experiments integrating material behaviour, geometry, code, design, and fabrication constraints through a feedback study. The results of the above studies are discussed in the following paragraphs.

### *1. Design system*

What the sand wants to be ? was the central question addressed by the design research to examine the interplay between the material agency, the architect's authorship, and the emergent forms. The objective was to define the processes and conditions of sand formation which allows to unfold the morphogenetic possibilities of sand while remaining coherent with the material logic without forcing external ideas. To address the research question, iterative experiments of manual and robotic sand distribution were conducted. In parallel, some aspects of sand physics were studied, the forces and conditions that trigger sand morphologies in nature and technology were examined, the underlying geometry of surfaces of constant slope was studied, and the employment of sand self-organization in architecture was reviewed.

As a result, a) six formation methods were developed, b) the boundary conditions were defined by three types of containers and four typologies of generators, c) the interchanges between the parameters were specified, and d) their digital representation was defined.

**a) Formation methods:**

Manual and robotic distribution methods were developed based on the processes of: pouring, releasing, tilting, displacing, sweeping, and helicoid. Each method returns distinct morphological aspects while being able to correlate with other methods which enabled hybrid formations and extended the morphological possibilities.

**b) Boundary conditions:**

I. **The border**: Three types of container where sand is formed were defined: a box, a raised base, and a plane. The borders either

II. **The generators**: The geometrical characteristics of the elements that trigger the formation process (ex: deposition path or releasing holes) were identified in four aspects being rectilinear-curvilinear, open- closed, concave- convex, with acute, right, or reflex corner.

c) **The interchanges** between the design parameters were examined, and the possible combinations were defined and illustrated in a diagram of typologies (ex: deposition on a plane or releasing from a box).

d) **The digital representation** of the design parameters was thought as following to communicate them as inputs in the surface generation algorithms:

- The formation methods are represented by vectors to inform the direction of sand flow.
- The boundary conditions (border and generators) are assigned as points or curves

Although the slope of the sand is constant, the interchange between the formation methods and the container types in addition to the variations of the generators allowed the construction of a rich network of tools to unfold almost infinite formation possibilities. The definition of the range in which these parameters can be operated upon, and yet remain coherent with the material, fabrication, and construction constraints, is the critical task of the design system.

### *2. Geometry*

The design system allowed a wide variations of sand forms to emerge which necessitated the analysis of their underlying geometry to inform the modeling methods. The study of the geometrical principles of surfaces of constant slope in § 2.3.2, and the feedback analysis of the physical and digital models in § 5.2 defined four fundamental concepts of material geometry:

- **Constant slope**: The constant slope allowed the definition of the relationship between the boundary, ridge, and medial axis curves through trigonometric functions.
- **Ruled surface**: a surface of constant slope is a ruled and developable surface. The tangent plane intersects the surface at the rulings which are normal to the boundary and contour curves. The rulings connect the boundary and the ridge on the surface, and their projection connect the boundary and the medial axis. The contour lines form a family of offset curves whose common evolute is the ridge and its projection, the medial axis.
- **Cones intersections and Voronoi diagrams**: The intersections of cones with the same heights return right hyperbolic sections, which vertical projection yields straight lines (boundaries of ordinary Voronoi diagram). However, if the cones have different heights, their intersections are inclined hyperbolics, which vertical projection returns curves (boundaries of weighted Voronoi diagram). The projected curves point towards the higher cone.
- **Medial axis and boundary curves**: In this work, the medial axis is defined by three methods: (i) the Voronoi tessellation of points on the boundary curve, (ii) the locus of the centers of the maximal inscribed circles that are contained in a boundary curve and tangent to it in at least two points, and (ii) the trimmed offsets of the boundary curve. In correspondence, the boundary curve can be determined by the offset of the medial axis or the envelope of the inscribed circles.

Together, the above concepts established a complete set of geometrical parameters and methods which are used to parameterize the design system and to inform the digital modeling techniques.

### *3. Modeling methods*

To parametrically operate the making process from design to production a digital workflow was developed in four parts:

a) **Boundary design**: to input the data inferred from material, geometry, design, and fabrication.
b) **Form generation**: to explore the possible morphologies of the sand tectonics
c) **Manufacturing information**: to produce the formwork drawings and materials quantities
d) **Robotic control**: to generate the trajectories of the robotic arm.

To overcome the limitations of the Boolean method proposed by the 35 Degree project, two algorithms were developed in this work, Heightfield and Medial Axis, based on the geometrical logic of surfaces of constant slope. The algorithms were developed in Rhino and Grasshopper platform as a flexible computational framework to adapt to the different physical formation processes, and the variations of their boundary conditions, while considering the fabrication constraints and assembly logics.

1. **The Heightfield algorithm** models sand surface as a field of points which heights are defined by their distance to their closest boundary and the slope of sand. In this algorithm points clustering, and displacement are operated by the Weighted Voronoi method.

2. **The medial axis algorithm** models sand piles as patches of ruled surfaces. From the input of either the boundary (in case of sand releasing), or the ridge of the pile (in case of sand deposition) , the algorithm defines the medial axis, construct the rulings between the boundary and the ridge, and generates the surface from the rulings.

Both algorithms process the inputs of boundary condition to generate the sand surface and to produce the manufacturing information. For robotic fabrication, the algorithms connect to the robotic control algorithm, using Hal plugin, to assign the boundary, generate the toolpath, simulate the robot motion, and generate the control code for physical execution.

**<u>Limitations and future work</u>**

The evaluation of the algorithms adaptability to different inputs and productivity in term of time and accuracy showed that:

- Both algorithms are adaptable for modeling: (i) the four formation methods (addition, subtraction, tilting, and displacement), and (ii) the different curves typologies of boundary conditions for either solid or hollow piles.

- The main drawback of the Heightfield algorithm is its time consuming of calculation to model accurate surfaces due the required high-density of points.

- The major limitation of the Medial axis method is that it cannot consider 3D organizations of points due to the use of the Voronoi component in grasshopper, which operate only on 2d points. In future work this challenge must be overcome by developing a custom made Weighted Voronoi code to allow the design of surfaces with different heights of boundaries.

To conclude, the main contribution of the digital methods is that it allowed to go much further in terms of scale and complexity of experimentation than the physical models. A better understanding of the morphogenetic capacity of sand and its design potentials in architecture is thus acquired. The proposed algorithms successfully operated the interdependent parameters inferred from material, geometry, design, and fabrication, which allowed to explore the sand morphogenetic possibilities, to produce manufacturing information, and to execute robotic distribution of sand. As such, the digital workflow of sand tectonics is constructed efficiently for its use in prototyping.

### *4. Fabrication system*

The fabrication system is the third axis of the sand tectonics framework which extends the material and design systems to the materialization phase. From the outset, it is designed as a prefabrication system of non-standard sand panels and blocks that can be assembled into a larger whole. The study aims at defining the fabrication process enabled by the material logic and the formation methods, while considering feasible fabrication and assembly constraints.

**The fabrication process** was developed through technical studies and iterative experiments to improve the workability of each task, then merge them into a coherent process of four stages:

a) **Fabrication setup**: the formwork is fabricated, and the materials are prepared according to the data acquired from the digital model.
b) **Sand formation**: the sand is distributed in the formwork either manually or robotically
c) **Panels spraying**: the emergent forms of dry sand are then sprayed with the saline solution. After hardening, the panels are then demolded and assembled.
d) **Block casting**: Hyposand is poured between the panels producing a monolithic block.

**The fabrication constraints** were defined upon iterative experimentation and the feedback between physical and digital prototyping along this work. It was essential to incorporating the fabrication constraints at the early stages of design and modeling in this thesis to ensure the feasibility and quality of the making process.

- **The panel size** is determined by its thickness of and the maximum size of the formwork. In this work the maximum panel size is of 50x50x2cm

- **The panel shape** is determined by the material of formwork and its method of fabrication. Rectilinear shapes are easily fabricated but curvilinear side requires flexible sides which was not discussed in this work.
- **Large surface paneling** is essential for large scale fabrication to divide the surface into panels with feasible size and shape, then assemble them as a formwork for casting.
- **Large surface assembly**: to ensure the stability of the panels such that they form a stable formwork for casting, they should be laid following a staggered pattern to maintain an adequate lap between joints and to provide a necessary interlock between the panels.
- **Panels orientation in assembly**: In terms of orientation of the panels in assembly three techniques are proposed: front to back, back to back, and flat casting. The orientation of the panel in assembly should be considered early in the design and fabrication to ensure quality of production.
- **Casting techniques**: Sand panels might be used either as a stay-in-place formwork, as a reusable formwork for casting Hyposand or other materials such as concrete.

The architectural creative is nevertheless maintained in the flexibility of the fabrication workflow, the interchanges between its processes, and the variations of the assembly methods. Such an understanding of physical production yield to consider fabrication not as a mere execution of form but rather as a design tool.

The development of the fabrication process, along with the modeling process, allow the construction of the digital-physical workflow of making integrating design, modeling, and fabrication processes in a comprehensive yet flexible workflow.

Collectively the material and making systems accomplish the construction of the sand tectonics which allow the exploration of possible sand forms, their modeling and production in the prototyping phase of the research. Until this point, the focus of this thesis has been to setup the material, design, and fabrication axes of the ST. While these axes do not yet address the full potential of ST, they do illustrate the material variability that can be achieved by shaping sand under different conditions. Moreover. they provide an understanding of the material system, mechanical characteristics, and the making constraints.

## Final reflections and future perspectives

The sand tectonics system contributes to the field of material-based design in architecture by extending the role of material-self formation behaviour from design to the fabrication level. It proposes a method to employ sand formability and its mechanical strength, when bonded with salt, as drivers in the design and fabrication of compressive forms. This dissertation adds an additional value to the sand tectonic system, by improving the material system, and developing new design and fabrication methods based on the material logic and geometry. Such advantage opens new construction possibilities that ties together the sand morphological, mechanical, and ecological capacities.

- Some key aspects of Hyposand workability and mechanical characteristics were identified. The material seems to develop satisfactory compressive strength comparable to residential concrete, promising technical accessibility, different formation possibilities, and minimal consumption of resources. Further interdisciplinary research could be conducted to give further insight on the material insulation, recyclability, environmental impact, and structural possibilities.

In contrast to the optimization approach of the mechanical and workability studies, the design study did not aim to define an optimal form but rather it followed an explorative approach to explore possibilities of formations. Accordingly, the processes were the objective of design rather than the final form.

- The thesis systematically investigated the morphology of sand and unfolded dependencies of form and formation methods. For instance, it correlated the shape of displacement tool and path with the material geometry which enabled to foreseen and model the resulting patterns. It studied the relation between robotic speed in deposition and height of emergent sand forms.

- The developed framework of methods can be used to systematically deduce further parameters and methods combinations for sand morphologies and hybrid methods of making offering a vast field of research.

- The parametric modeling methods of surface of constant slope allowed to correlate the material, geometry, and fabrication constraints and provided an efficient design to production tool. As such, they allowed to go beyond the physical models in terms of scale and complexity giving a deeper understanding of the design potential of the material system.

- The design and fabrication techniques defined the parameters of the material formation methods, analyzed their geometrical principles, and examined the effect of their variation on the emergent forms. As such, a very particular tectonic language that is unique to sand and its formation techniques was unfolded. To an extent, the experiments in this work examined the differentiations of the design parameters and revealed the expressiveness of the formal articulations and the richness of the inner structure of the sand tectonics. The emergent design grammar of sand self-formation and its articulations proved to be aesthetically appealing, which can be used as a stand-alone design system in other disciplines and scales not necessarily related to sand.

- The sand tectonics employs low-tech and high-tech methods which open possibilities to adapt to different economical communities and local architectural contexts. The mechanical advantage of Hyposand in compression, its low thermal conductivity, and its workability with any type of sand offer great potential for applications in desert areas where the climate is arid, and sand has nowadays limited use in the construction industry. Further, the Hyposand minimal consumption of materials and energy, its semi-recyclability and reusability allow its application in desert areas and arid climates with minimum environmental impact. Finally, the formability and fast hardening of Hyposand hold promising potentials for future interdisciplinary research to investigate on-site 3D printing in desert areas. A prerequisite to unfold those potentials is to conduct further research on the material insulation, recyclability, and life-cycle assessment.

In pursuit of the aim for the construction of larger prototypes that responds to specific architectural contexts, the research aims at further investigating the material characteristics , formation processes , and construction techniques in future work.

Ultimately, this thesis has shown that synthesizing material self-formation, mechanical properties, and formation processes in line with digital technology extend the architectural design possibilities to the fabrication level. The thesis developed a material-driven design to fabrication methodology in which sand capacities and its formation processes inform both design and fabrication processes. As such, sand is no longer regarded in architecture as a mere aggregate for concrete but as a promising building material for the future.

## List of figures

Figure 0.1 The sand tectonics framework ..... 14
Figure 0.2 The organizational framework of the research ..... 15
Figure 1.1 Gottfried Semper, Illustrations of the Caribbean hut and study of flowers and snow ..... 25
Figure 1.2 Evolution of iron tectonic. ..... 28
Figure 1.3 The tectonic of concrete. ..... 29
Figure 1.4 Soap film and membrane model studies of the Basento Bridge ..... 31
Figure 1.5 Sand morphological studies by Jean-Marie Delarue. ..... 34
Figure 1.6 Morphological and geometrical analysis of sand piles by Jean-Marie Delarue ..... 35
Figure 1.7 The convertible membrane experiment, Frei Otto. ..... 36
Figure 1.8 The territorial expansion experiment, Frei Otto ..... 37
Figure 1.10 the loadbearing experiment, Frei Otto. ..... 37
Figure 1.11 Sand formations experiments by Achim Menges and Michal Hensel [65] ..... 38
Figure 1.12 The fabrication process proposed by the 35 Degree project [73]. ..... 39
Figure 1.13 Physical model 50x50x2cm [73]. ..... 39
Figure 1.14 Geometrical analysis and design explorations of the conical design system [73] ..... 39
Figure 1.15 Robotic sand forming techniques. ..... 40
Figure 1.16 Digitally controlled deposition of sand. ..... 41
Figure 1.17 The methodological framework of the sand tectonics ..... 42
Figure 2.1 Visual assessment of sand type ..... 45
Figure 2.2 Visual assessment of grain shape ..... 46
Figure 2.3 States of wet sand in physics ..... 49
Figure 2.4 Forms of wet sand ..... 49
Figure 2.5 Applications of wet sand in architecture. ..... 49
Figure 2.6 Forms of dry sand under different formation forces. ..... 50
Figure 2.7 The AR of different materials ..... 51
Figure 2.8 Sand piles formation ..... 52
Figure 2.9 Morphological and geometrical studies of sand piles by Jean-Marie Delarue ..... 52
Figure 2.10 General surface of constant slope ..... 53
Figure 2.11 Geometrical analysis of a hollow sand pile. ..... 54
Figure 2.12 Methods of generation of surfaces of constant slope ..... 54
Figure 2.13 Building strategies based on SSB in nature ..... 55
Figure 2.14 ‘Temps Imparti’, installation by Jean-Bernard Métais. ..... 55
Figure 2.15 Salt architecture in Siwa, Egypt. ..... 56
Figure 2.16 Forms of sodium thiosulfate salt. ..... 58
Figure 2.17 Crystallization process of STP ..... 59
Figure 2.18 Phase changing behavior of STP ..... 59
Figure 3.1 Sand grains and salt crystals ..... 63
Figure 3.2 Effects of sand characteristics on the emergent patterns ..... 64
Figure 3.3 The mixing technique of making. ..... 65
Figure 3.4 A thin crust of sand solidified by spraying ..... 66
Figure 3.5 process of the spraying method ..... 67
Figure 3.6 Spraying method of making. ..... 68
Figure 3.7 Experiments of other making techniques ..... 70

Figure 3.8 Hyposand life cycle ..... 71
Figure 3.9 Forms of crystalized STP salt. ..... 74
Figure 4.1 Cumulative curve of grain size distribution. ..... 81
Figure 4.2 Histogram graph of grain size distribution ..... 82
Figure 4.3 The scale of the Fineness Modulus ..... 83
Figure 4.4 Skewness and Kurtosis descriptions of frequency curves ..... 84
Figure 4.5 Percentage of grain size on Wentworth scale ..... 89
Figure 4.6 Frequency curves on Wentworth scale (Φ) ..... 89
Figure 4.7 Skewness vs kurtosis (Folk method) ..... 90
Figure 4.8 Sorting vs skewness ..... 90
Figure 4.9 sorting vs kurtosis ..... 90
Figure 4.10 The x-ray tomograph scanner at laboratory 3SR in Grenoble ..... 92
Figure 4.11 Sand specimen and the x-ray images ..... 93
Figure 4.12 Analysis process of one slide of Hyposand ..... 94
Figure 4.13: The problem of separation ..... 95
Figure 4.14 The problem of segmentation ..... 95
Figure 4.15 The 27 slides used in the Tomography analysis ..... 97
Figure 4.16 Average roundness and circularity ..... 99
Figure 4.17 Average roundness and circularity ..... 99
Figure 4.18 The analysis of one slide of each type of sand. ..... 100
Figure 4.19 The proportions of materials in each slide and their averages ..... 101
Figure 4.20 Porosity vs. grain shape (circularity and roundness) ..... 103
Figure 4.21 Porosity vs grain mean size and fineness modulus ..... 103
Figure 4.22 Porosity vs sorting ..... 104
Figure 4.23 Porosity vs. skewness and kurtosis ..... 104
Figure 4.24 The compression test machine ..... 105
Figure 4.25 Compressive strength of the four types of sand ..... 106
Figure 4.26 Compressive strength vs. Granularity of sand ..... 107
Figure 4.27 Compressive strength vs. proportion of salt to sand ..... 108
Figure 4.28 The segregation of salt on the top of the specimen. ..... 108
Figure 4.29 Compressive strength vs. salt mixing temperature ..... 109
Figure 4.30 Variation of compressive strength with the salt melting temperature ..... 110
Figure 4.31 Compressive strength vs. setting time ..... 111
Figure 4.32 Detail of a broken specimen of the mixture of Hyposand and gravel ..... 112
Figure 4.33 Compressive strength vs. Proportion of gravel in the Hyposand material ..... 112
Figure 4.34 Compressive strength dispersion (MPa) ..... 113
Figure 4.35 Compressive strength of each type of sand ..... 114
Figure 4.36 Compressive strength vs. Mean size and vs. porosity ..... 114
Figure 4.37 Compressive strength vs. Skewness and vs. Kurtosis ..... 115
Figure 4.38 compressive strength vs. porosity ..... 115
Figure 4.39 compressive strength vs. roundness and porosity ..... 115
Figure 4.40 Average of proportion of materials in the three types of sand ..... 116
Figure 4.41 Humidity conditions for the flexural test ..... 117
Figure 4.42 Set A in the dry box and set B in the humid ..... 117
Figure 4.43 Three-point flexural test ..... 117

Figure 4.44 Comparison between the results of the three-point flexural test.....118
Figure 4.45 The Hyposand specimen of the thermal conductivity test.....119
Figure 4.46 Results of the thermal conductivity test.....120
Figure 4.47 Thermal conductivity of the sodium thiosulfate pentahydrate salt.....120
Figure 4.48 The method of plotting the properties of Hyposand on Ashby plots.....121
Figure 4.49 Strength vs. Density of Hyposand.....122
Figure 4.50 Young's modulus vs density. of Hyposand.....122
Figure 4.51 Thermal conductivity of Hyposand.....123
Figure 4.52. Strength vs. relative cost of Hyposand.....123
Figure 4.53 Approximate cost per unit volume of Hyposand.....124
Figure 4.54 Approximate cost per unit mass.....124
Figure 5.1 Diagram of the framework of making methods.).....126
Figure 5.2 Diagram of the ST design parameters.....128
Figure 5.3 Sand formation methods.....129
Figure 5.4 Mixed formation methods.....130
Figure 5.5 The interrelation between the formation methods and boundary conditions.....131
Figure 5.6 An abstract shape that represents the different typologies of generators.....132
Figure 5.7 A vacuum machine is used for removing sand in the subtraction method of formation.....133
Figure 5.9 The six-axes robotic arm and the mountable end-effectors.....133
Figure 5.10 Robotic patterns generated by displacement, addition and tilting methods.....134
Figure 5.11 Trigonometric relationships between the ridge, boundary, and medial axis curves.....135
Figure 5.12 Types of conic sections that occur in sand formation.....136
Figure 5.13 The curvature of the hyperbola.....137
Figure 5.14 The intersection of cones with the same height.....137
Figure 5.15 Conic sections in sand models.....137
Figure 5.16 Sand falls in a linear path towards the closest hole.....137
Figure 5.17 Comparison of ordinary and Additively weighted Voronoi diagrams [193,194].....139
Figure 5.18 the lower envelope of intersecting cones.....139
Figure 5.19 Definition of the *Ma* curve by the Voronoi diagram method.....141
Figure 5.20 Definition of the *Ma* by the inscribed circles.....141
Figure 5.21 Physical illustration of the *Ma* by sand on a free-form base.....142
Figure 5.22 Geometrical construction of a hollowed sand pile from a given boundary.....142
Figure 5.23 The abstract boundary shapes for the assessment of the algorithms.....144
Figure 5.24 The trigonometric functions of the subtraction and addition methods of sand formation.....145
Figure 5.25 Sand formation methods modelled by the Boolean algorithm.....145
Figure 5.26 physical and digital models of the addition and subtraction mixed method of formation.....146
Figure 5.27 The intersection of cones with different radii.....146
Figure 5.28 The deposition path.....146
Figure 5.29 Effect of the size and height of the holes on their range of effect.....147
Figure 5.30 The construction of the mesh from the displaced points.....147
Figure 5.31 Diagram of the Heightfield algorithm showing the key operations.....148
Figure 5.32 The HF algorithm.....149
Figure 5.33 Evaluation of the adaptability of HF algorithm.....150
Figure 5.34 The mesh from points logic of the HF algorithm.....150
Figure 5.35 The sand physical model of a topographic surface by Jean-Marie De Larue.....150

Figure 5.36 The advantage of the HF method ..... 150
Figure 5.37 The trigonometric relationships ..... 151
Figure 5.38 Sand deposition methods. ..... 151
Figure 5.39 Voronoi tessellation of a hollowed pile, ..... 152
Figure 5.40 Diagram of the Boundary to ridge algorithm showing the key operations ..... 153
Figure 5.42 The B-R algorithm can model two formation methods ..... 154
Figure 5.43 Evaluation of the adaptability of B-R algorithm ..... 155
Figure 5.44 Weighted Voronoi method in Mathematica ..... 155
Figure 5.45 Procedure of the R-B algorithm ..... 156
Figure 5.46 Path curve relaxation. The deposition path is relaxed to define the optimum ridge. ..... 157
Figure 5.47 The R-B operates on different curve typologies ..... 157
Figure 5.48 The results of the comparative study ..... 159
Figure 5.49 The interrelation between the formation methodsand the modelling methods ..... 159
Figure 5.50 Tests of tuning the robot speed and wait duration with the flow of sand ..... 160
Figure 5.51 Diagram of fabrication process ..... 163
Figure 5.53 The size of panels is restricted by it thickness ..... 164
Figure 5.54 method of alignment of the panels edges [73]. ..... 165
Figure 5.55 Assembly techniques of sand panels for casting monolithic blocks ..... 166
Figure 5.56 the top side (left) and bottom side (right) of a sprayed sand panel. ..... 167
Figure 5.57 Casting techniques of sand panels either as stay-in or reusable formwork ..... 168
Figure 5.58 Diagram of the digital-physical workflow of making. ..... 170
Figure 5.59 The digital-physical workflow of sand tectonics. ..... 172
Figure 5.60 The framework of making methods ..... 173
Figure 6.1 Parameters of the subtraction technique [1] ..... 176
Figure 6.2 Local and global organizations of holes [1]. ..... 177
Figure 6.3 Tectonic articulations of conical forms [1] ..... 177
Figure 6.4 The generative design strategy for an ecolodge in the desert of Egypt [1] ..... 178
Figure 6.5 study of effect of holes height, size, and location on the ridge and surface form ..... 180
Figure 6.6 Study of effect of organization of holes on the directions of ridges ..... 181
Figure 6.7 Articulations of curved organizations of holes at different heights and densities ..... 181
Figure 6.8 Recursive branching organizations ..... 182
Figure 6.9 Study of the relationship between holes distribution and the directions of the ridges ..... 183
Figure 6.10 Design strategy of a proposed sand wall ..... 184
Figure 6.11 Model of the proposed sand wall ..... 185
Figure 6.12 Study of the effect of linear hole location, rotation, and size on the emergent ridges ..... 186
Figure 6.13 Models of different organizations of linear and curved holes ..... 186
Figure 6.14 Models of solid piles formed by sand deposition on predefined bases. ..... 187
Figure 6.15 Models of sand piles formed by sand deposition on a plane ..... 187
Figure 6.16 Digital and physical models of hybrid addition and subtraction of conical forms ..... 188
Figure 6.17 The sand block of the 35 Degree project was made of two panels (20x40cm)[1] ..... 189
Figure 6.18 Drawings and making of the model Alex-12. The block is fabricated from three panels ..... 189
Figure 6.19 Drawings of the model D7-13. ..... 190
Figure 6.20 Process of making of model D7-12. ..... 191
Figure 6.21 Diagram of methods for robotic deposition technique ..... 192
Figure 6.22 Robotic deposition: study of the robot speed vs. sand height ..... 193

Figure 6.23 Optimization of input curve for robotic deposition process....194
Figure 6.24 Robotic deposition experiments....195
Figure 6.25 Physical model of overlapping deposition and a digital model of a curling path....196
Figure 6.26 Sand tilting....197
Figure 6.27 Measuring the angle of repose at different tilts....198
Figure 6.28 Piles with multiple surfaces....198
Figure 6.29 The tilt method allows the fabrication of three types of tiles....198
Figure 6.30 Standard 3D tiles used for the exterior cladding of der Kulturen museum....199
Figure 6.31 section through horizontal and tilted pile....200
Figure 6.32 section through horizontal and re-tilted pile....200
Figure 6.33 physical and geometrical analysis of the sequence of tilting from 0° to 35°....201
Figure 6.34 overlapped sections of piles at different angles of tilt....201
Figure 6.36 Process of tilt algorithm....203
Figure 6.37 A model of tilt technique....204
Figure 6.38 The manual method of tiles formation is based on pouring dry sand on pre-tilted bases ..204
Figure 6.39 The robotic method of tiles formation....204
Figure 6.40: Solid triangular panels, top side (left) and back side (right)....205
Figure 6.41 The volume and height of the tile decrease by tilting....205
Figure 6.42 The ridges displace in the opposite direction of tilting....206
Figure 6.43 design of tilt angles (top), fabrication and assembly (bottom)....207
Figure 6.44 four solid panels at four tilt angles....208
Figure 6.45 details of the triangular assembly....208
Figure 6.46 assembly of the panels....208
Figure 6.47 Details of the tilting model....209
Figure 6.48 Shadow effect on the tilting model....210
Figure 6.49 conical and square based panels....211
Figure 6.50 three distributions of tilt vectors....212
Figure 6.51 three angles distributions of rhombus shape....212
Figure 6.52 Penrose panels at 0° tilt (left) and at tilt range of 0°-30° (right)....213
Figure 6.53 3D assemblies....213
Figure 6.54 Manual displacement of sand....214
Figure 6.55: Initial prototype and pattern....215
Figure 6.56 Pattern evolution....217
Figure 6.57 Top view, section a-a, and section b-b through the single path pattern....218
Figure 6.58 Study of the effect of path curve depth on the width of the pattern....219
Figure 6.59 Study of the effect of the end-tool width and angle on the pattern....220
Figure 6.60 study of the effect of the tool profile on the form of the pattern....220
Figure 6.61 Displacement algorithm process....222
Figure 6.62 Robotic path simulation for single, double, and aggregate paths....222
Figure 6.64 The input path curves and the generated surface....223
Figure 6.65 Robotic displacment experiments....224
Figure 6.66 Robotic displacment experiments....225
Figure 6.67 Physical experiments using a CNC machine....226
Figure 6.68 Digital models of the displacment method....227
Figure 6.70 Initial experiment of the sweeping formation. T....228

Figure 6.72 Initial experiment of the sweeping technique of fabrication....229
Figure 6.73 Paneling of single and doubly ruled surfaces according to the sweeping method....229
Figure 6.74 Surface slope analysis ....232
Figure 6.75 Evaluation of different discretization methods....233
Figure 6.76 Evaluation of the flatness of boxes sides in principal, geodesic, and asymptotic curves ...233
Figure 6.77 Digital / physical workflow of the sweeping method ....234
Figure 6.78 The digital workflow of the sweeping technique ....235
Figure 6.79 The sweeping formwork development and assembled. ....236
Figure 6.81: Fabrication process of a hyperbolic paraboloid surface from three panels. ....237
Figure 6.82 A Hyperbolic paraboloid and a saddle surface formed by sweeping ....238
Figure 6.83 Models of curved walls subdivision into ruled panels ....239
Figure 6.84 Digital and physical study of a twisted arch ....240
Figure 6.85 LF-20 model : fabrication of a reusable casting formwork from two sand panels ....241
Figure 6.86 Details of the panels ridges and edges ....242
Figure 6.87 Assembly and casting of the panels with cement....242
Figure 6.88 Demolded cement block and reusable sand panels....242
Figure 6.89 First test of helicoid fabrication for a spiral stair design ....243
Figure 6.90 the geometrical principles of the developable helicoid ....244
Figure 6.91 the cylindrical formwork for the generation of the helicoid surface....244
Figure 6.92 Process of formation of the helicoid surface using the cylindrical formwork ....245
Figure 6.93 Solid helicoid surface made of sand. (height 30cm, radius 25cm, thickness 2cm) ....245
Figure 6.94 the cylindrical formwork (left) vs. the spiral formwork (right) ....246
Figure 6.95 Fabrication test of a part of the helicoid surface for larger scale applications ....246
Figure 6.96 Digital process of helicoid and formwork generation ....247
Figure 6.97 The direction of the tangents defines the direction of slope of sand....247
Figure 6.98 Possible variations of the helicoid surface....248
Figure 6.99 Formation of sand tubes: dry sand (left) and solidified and (right)....249
Figure 6.100 Investigations of sand tubes bundling, weaving, branching, and twisting morphologies. .250
Figure 6.101 Examples of linear based tectonics in nature, art, craft, and architecture. ....250
Figure 6.102 Initial test to determine the catenary curve ....251
Figure 6.103 process the catenary technique. (a) hanging, (b) casting, and (c) reversing....252
Figure 6.104 The casting process....252
Figure 6.105 the solid catenary model (top), and the reversed model (bottom) ....252
Figure 6.106 Making process of the tubular vertical structure. ....253

## List of tables

Table 4.2 List of tests presented in this chapter and their variables ..... 76
Table 4.4 Standard materials and conditions followed in the tests ..... 77
Table 4.5: Results of the visual assessment of the four types of sand. ..... 79
Table 4.6 Measurement and results of the sieve analysis test ..... 81
Table 4.7: The verbal description of the sieve analysis results ..... 83
Table 4.8: Formulas and evaluation of the USCS method (after [186]) ..... 85
Table 4.9: Formulas and evaluation of Trask method (after [187]) ..... 86
Table 4.10: Folk and Ward statistical measures and evaluation criteria (after [185]) ..... 87
Table 4.11: Results of grain size statistics ..... 88
Table 4.12 The verbal description of grain size distribution ..... 91
Table 4.13 Results of the tomography analysis ..... 98
Table 4.14 Summary of the results of the tomography scan analysis ..... 98
Table 4.15 The factors which influence on the compressive strength are assessed ..... 105
Table 4.17 Results of Compressive strength of the four types of sand ..... 106
Table 4.18 Results of compressive strength vs. proportion of salt to sand. ..... 108
Table 4.19 Compressive strength vs. salt mixing temperature ..... 109
Table 4.20 Results of the variation of σ vs. the salt melting temperature ..... 110
Table 4.21 Fixed and variable parameters of the test and Compressive strength ..... 113
Table 4.22 Results of the flexural and compression tests ..... 118
Table 5.2 Evaluation of the feasibility and performance of the three modelling techniques. ..... 158
Table 6.1Values of $\Theta$ and $\beta$ according to $\alpha$ ..... 201

## Bibliography


[1] Hussein, A., Shahi, B., Lee, J., and Wong, P., 35 degree: Thesis book, Master thesis (unpublished), Architectural Association School of Architecture, DRL (Design Research Lab), London, 2011. https://issuu.com/home/published/sand_tectonics_.

[2] Frampton, K., Studies in Tectonic Culture: The Poetics of Construction in Nineteenth and Twentieth Century Architecture, Reprint edition, The MIT Press, Cambridge, Mass. London, 2001.

[3] Menges, A., and Ahlquist, S., Computational Design Thinking: Computation Design Thinking, 1 edition, Wiley, Chichester, UK, 2011.

[4] Frampton, K., Modern Architecture: A Critical History, Fourth edition, Thames & Hudson, London ; New York, N.Y, 2007.

[5] Picon, A., La matérialité de l'architecture, PARENTHESES, Marseille, 2018.

[6] His, G., Félix-Fromentin, C., and Mastrorilli, A., Cahiers thématiques n°15, Matérialités, Maison des sciences de l'homme/Lille, Maison des sciences de l'homme/Lille, Lille, France, 13AD. https://umrausser.hypotheses.org/4317 (accessed May 9, 2020).

[7] Loos, A., Ornament and Crime, Penguin Classics, 2019.

[8] Oxman, R., "*Informed tectonics in material-based design,*" Design Studies. 33 (2012).

[9] Schröpfer, T., Material design: informing architecture by materiality, Walter de Gruyter, 2012.

[10] Maulden, R., Tectonics in architecture: from the physical to the meta-physical, Massachusetts Institute of Technology, 1986.

[11] Schwartz, C., Introducing Architectural Tectonics: Exploring the Intersection of Design and Construction, 1 edition, Routledge, New York, 2016.

[12] De Mattia, D., "*The birth of the Tectonics: from the history of construction to the structural analysis and architectural design.,*" Structural Analysis of Historical Constructions. 2 (2012).

[13] Schwarzer, M., German Tectonics, in: Companion to the History of Architecture, American Cancer Society, 2016: pp. 1–13. doi:10.1002/9781118887226.wbcha088.

[14] Schwarzer, M., "*Ontology and representation in Karl Bötticher's theory of tectonics,*" Journal of the Society of Architectural Historians. 52 (1993).

[15] Schumacher, P., The Autopoiesis of Architecture, Volume I: A New Framework for Architecture, John Wiley & Sons, 2011.

[16] Chestnova, E., "*The House that Semper Built,*" Architectural Theory Review. 21 (2017).

[17] Hartoonian, G., and Frampton, K., Ontology of construction: on nihilism of technology in theories of modern architecture, Cambridge university press Cambridge, 1994.

[18] Semper, G., "*The Four Elements of Architecture and Other Writings (1851),*" Trans. HF Mallgrave and W. Hermann. Cambridge: Cambridge U. Press. (1989).

[19] Hildebrand, S., "*Concepts of creation: historiography and design in Gottfried Semper,*" Journal of Art Historiography. (2014).

[20] Semper, G., Style in the Technical and Tectonic Arts; or, Practical Aesthetics, 1 edition, Getty Research Institute, Los Angeles, 2004.

[21] Spuybroek, L., The architecture of continuity: essays and conversations, V2_ publishing, 2008.

[22] Oxman, N., Ortiz, C., Gramazio, F., et al., "*Material ecology,*" Computer-Aided Design. 60 (2015). doi:10.1016/j.cad.2014.05.009.

[23] Jones, W., "*Can Tectonics Grasp Smoothness?,*" Log. (2014).

[24] Leach, N., Turnbull, D., and Williams, C.J., "*Digital tectonics,*" (2004).

[25] Oxman, R., and Oxman, R., "*The New Structuralism: design, Engineering and Architectural Technologies,*" Journal of Architectural Education. 67 (2013).

[26] Carpo, M., The Alphabet and the Algorithm, 1 edition, The MIT Press, Cambridge, Mass, 2011.

[27] Scheer, D.R., The Death of Drawing: Architecture in the Age of Simulation, 1 edition, Routledge, London ; New York, 2014.

[28] Kieran, S., and Timberlake, J., Refabricating architecture: How manufacturing methodologies are poised to transform building construction, McGraw Hill Professional, 2004.

[29] Menges, A., Material Synthesis: Fusing the Physical and the Computational, John Wiley & Sons, 2015.

[30] Trummer, P., "*Associative design: from type to population,*" Computational Design Thinking: Computation Design Thinking. London: Wiley AD Reader. (2011).
[31] Salazar, J., "*Philosophies of Design: The Case of Modelling Software,*" Verb Architecture Boogazine: Authorship and Information. 1 (2002).
[32] DeLanda, M., "*The New Materiality,*" Architectural Design. 85 (2015). doi:10.1002/ad.1948.
[33] Kara, H., and Bosia, D., Design engineering refocused, John Wiley & Sons, 2016.
[34] Levine, N., "*The template of photography in nineteenth-century architectural representation,*" Journal of the Society of Architectural Historians. 71 (2012).
[35] Kotnik, T., and Weinstock, M., "*Material, form and force,*" Architectural Design. 82 (2012).
[36] Nervi, P.L., Aesthetics and Technology in Building, First Edition edition, Harvard University Press, 1966.
[37] "*SMART SLAB – DFAB HOUSE,*" (n.d.). https://dfabhouse.ch/smart-slab/ (accessed September 8, 2020).
[38] Reiser, J., Atlas of Novel Tectonics, 1 edition, Princeton Architectural Press, New York, 2006.
[39] Braham, W.W., and Hale, J.A., Rethinking technology: a reader in architectural theory, Routledge, 2006.
[40] DeLanda, M., "*Material complexity,*" Digital Tectonics. 14 (2004).
[41] Hoel, A., and Folkvord, I., eds., Ernst Cassirer on Form and Technology: Contemporary Readings, Palgrave Macmillan UK, 2012. doi:10.1057/9781137007773.
[42] Ingold, T., "*The textility of making,*" Cambridge Journal of Economics. 34 (2010).
[43] Kelly, K., What Technology Wants, Penguin Books, 2010.
[44] Gosden, C., "*What Do Objects Want?,*" J Archaeol Method Theory. 12 (2005). doi:10.1007/s10816-005-6928-x.
[45] Burry, J., and Burry, M., Prototyping for Architects: Real Building for the Next Generation of Digital Designers, 1 edition, Thames & Hudson, London, 2016.
[46] Sheil, B., ed., Design Through Making, 1 edition, Academy Press, Chichester, 2005.
[47] Oxman, N., Material-based design computation, Massachusetts Institute of Technology, 2010.
[48] Danilowitz, B., and Horowitz, F., "*Josef Albers: To Open Eyes: the Bauhaus, Black Mountain College, and Yale,*" 2006. (2006).
[49] Albers, J., "*Teaching Form through Practice,*" AA Files. (2013).
[50] Addis, B., "*'Toys that save millions'-A history of using physical models in structural design,*" The Structural Engineer. 91 (2013).
[51] Otto, F., and Rasch, B., Finding Form: Towards an Architecture of the Minimal, 3rd edition, Edition Axel Menges, Stuttgart?, 1996.
[52] Otto, F., Form, Kraft, Masse: Form, force, mass. Konstruktion, Institut für Leichte Flächentragwerke, Universität Stuttgart, 1992.
[53] West, M., "*Thinking with matter,*" Architectural Design. 78 (2008).
[54] Oxman, N., Material-based design computation, Thesis, Massachusetts Institute of Technology, 2010. http://dspace.mit.edu/handle/1721.1/59192 (accessed July 22, 2017).
[55] Geiser, K., Materials Matter: Toward a Sustainable Materials Policy, 1st edition, The MIT Press, Cambridge, Mass, 2001.
[56] Borden, G.P., and Meredith, M., Matter: Material Processes in Architectural Production, Routledge, 2012.
[57] Mindrup, M., The Material Imagination: Reveries on Architecture and Matter, Routledge, 2016.
[58] Tibbits, S., Active Matter, MIT Press, 2017.
[59] Gramazio, F., and Kohler, M., Digital Materiality in Architecture, 1 edition, Lars Muller, Baden, 2008.
[60] Menges, A., ed., Material Computation: Higher Integration in Morphogenetic Design, 1 edition, Academy Press, Hoboken, N.J.; Chichester, 2012.
[61] Carpo, M., The Second Digital Turn: Design Beyond Intelligence, 1 edition, The MIT Press, Cambridge, Massachusetts, 2017.
[62] Kolarevic, B., and Klinger, K., Manufacturing material effects: rethinking design and making in architecture, Routledge, 2013.
[63] Hensel, M., Menges, A., and Weinstock, M., eds., Techniques and Technologies in Morphogenetic Design, 1 edition, Academy Press, Chichester, 2006.

[64] Hensel, M., Menges, A., and Weinstock, M., Emergent Technologies and Design: Towards a Biological Paradigm for Architecture, Routledge, 2013.
[65] Evans, R., Difford, R., and Middleton, R., Translations from drawing to building and other essays, Architectural Association London, 1997.
[66] Gramazio, F., Kohler, M., and Willmann, J., The Robotic Touch: How Robots Change Architecture, Park Books, 2014. https://books.google.fr/books?id=LIGSngEACAAJ.
[67] De Landa, M., "*The machinic phylum,*" First Created Online. (1997).
[68] Leach, N., Matter Matters: A philosophical preface, in: Active Matter, MIT Press, 2017.
[69] Delarue, J.-M., Surfaces d'égale pente: morphogénèse et applications constructifs, Grands Ateliers, Unpublished manuscript, ENSA Paris Malaquais, Paris,France, 2001. http://surfacesdeveloppables.net/.
[70] Delarue, J.-M., "*Géométrie constructive des Surfaces développables : Voies d'expérimentations,*" Surfaces Developpables. (n.d.). http://surfacesdeveloppables.net/ (accessed January 11, 2021).
[71] Otto, F., Occupying and Connecting: Thoughts on Territories and Spheres of Influence with Particular Reference to Human Settlement, Edition Axel Menges, Stuttgart, 2009.
[72] Hensel, M., and Menges, A., "*Designing Morpho-Ecologies: Versatility and Vicissitude of Heterogeneous Space,*" Architectural Design. 78 (2008). doi:10.1002/ad.648.
[73] Hussein, A., Shahi, B., Lee, J., et al., 35 degree: Thesis booklet, Master thesis (unpublished), Architectural Association School of Architecture, DRL (Design Research Lab), London, 2011. https://issuu.com/home/published/aadrl_sand.
[74] Malé-Alema, M., and Portell, J., FAB bots: Research in Additive Manufacturing for Architecture, in: F, Gramazio, M, Kohler, S, Langenberg (Eds.), Fabricate 2014: Negotiating Design & Making, UCL Press, 2017.
[75] "*Norman Foster Foundation Atelier 2018—Robotics — Norman Foster Foundation,*" (n.d.). https://www.normanfosterfoundation.org/educational/norman-foster-foundation-atelier-2018-robotics/ (accessed July 4, 2020).
[76] "*S.10 Robotic Sand/Clay forming - Presentations,*" IAAC Blog. (2012). http://www.iaacblog.com/2012/05/18/s-10-robotic-sandclay-forming-presentations/ (accessed December 21, 2018).
[77] "*The Urburb - Patterns of Contemporary Living | MIT Architecture,*" (n.d.). https://architecture.mit.edu/history-theory-and-criticism/lecture/urburb-patterns-contemporary-living (accessed August 10, 2018).
[78] Harmon, B.A., Petrasova, A., Petras, V., et al., "*Tangible topographic modeling for landscape architects,*" International Journal of Architectural Computing. 16 (2018). doi:10.1177/1478077117749959.
[79] "*SandScape,*" (2003). http://tangible.media.mit.edu/project/sandscape (accessed July 4, 2020).
[80] SCIArcLens, SCI-Arc Presents "Advances in Architectural Geometry" Film, Centre Pompidou, Paris, n.d. https://www.youtube.com/watch?v=iKFZO75BmLA (accessed August 10, 2018).
[81] "*Tellart creates topographic sandpit table that lets you move mountains,*" Dezeen. (2018). https://www.dezeen.com/2018/06/01/tellart-terraform-table-topographic-sandpit-move-mountains-technology/ (accessed August 7, 2018).
[82] Pettijohn, F.J., Potter, P.E., and Siever, R., Sand and Sandstone, Springer Science & Business Media, 2012.
[83] Sherzer, W.H., "*Criteria for the recognition of the various types of sand grains,*" Geological Society of America Bulletin. 21 (1910). doi:10.1130/GSAB-21-625.
[84] Alexander, M.G., and Mindess, S., Aggregates in concrete, Taylor & Francis, London ; New York, 2008.
[85] Neuendorf, K.K.E., Glossary of Geology, Springer Science & Business Media, 2005.
[86] "*World Atlas of Sands » Sand,*" (n.d.). http://www.sand-atlas.com/en/sand/ (accessed July 17, 2017).
[87] Hasdemir, S., Tuğrul, A., and Yılmaz, M., "*The effect of natural sand composition on concrete strength,*" Construction and Building Materials. 112 (2016).
[88] "*ASTM C136 / C136M-14, Standard Test Method for Sieve Analysis of Fine and Coarse Aggregates, ASTM International, West Conshohocken, PA, 2014, www.astm.org,*" (n.d.).
[89] Tsiskreli, G.D., and Dzhavakhidze, A.N., "*The effect of aggregate size on strength and deformation of concrete,*" Hydrotechnical Construction. 4 (1970). doi:10.1007/BF02376145.

[90] Schindelin, J., Rueden, C.T., Hiner, M.C., et al., "*The ImageJ ecosystem: An open platform for biomedical image analysis,*" Mol. Reprod. Dev. 82 (2015). doi:10.1002/mrd.22489.
[91] ASTM, "*Standard specification for standard sand,*" C778-13. (2013).
[92] "*Sand, Rarer than One Thinks,*" Environmental Development. 11 (2014). https://wedocs.unep.org/handle/20.500.11822/8665 (accessed June 9, 2020).
[93] Programme, U.U.N.E., Sand and Sustainability: Finding New Solutions for Environmental Governance of Global Sand Resources, UNEP, 2019.
[94] Duran, J., Sables, poudres et grains: Introduction à la physique des milieux granulaires, Eyrolles, Paris, 1999.
[95] Duran, J., Sables émouvants : La physique du sable au quotidien, Belin, Paris, 2003.
[96] Claudin, P., La physique des tas de sable. Description phenomenologique de la propagation des contraintes dans les materiaux granulaires, These de doctorat, Paris 11, 1999. http://www.theses.fr/fr/1999PA112006 (accessed June 27, 2020).
[97] Claudin, P., La Physique des tas de sable (Volume 24 n°2): Annales de Physique (Volume 24 n°2), EDP Sciences, 2012.
[98] Ball, P., Flow: Nature's patterns: a tapestry in three parts, OUP Oxford, 2009.
[99] Ball, P., Patterns in Nature: Why the Natural World Looks the Way It Does, University Of Chicago Press, Chicago, 2016.
[100] Anger, R., and Fontaine, L., Bâtir en terre, Belin litterature et revues, Paris, 2009.
[101] Ensag, Cra., Anger, R., and Laetitia, F., Grains de Bâtisseurs, CRATerre, 2005. http://www.grainsdebatisseurs.com/references/livre-grains-de-batisseurs/ (accessed March 8, 2016).
[102] "*(9) Grains de bâtisseurs : expériences scientifiques autour de la matière en grains - YouTube,*" (n.d.). https://www.youtube.com/playlist?list=PLr_Fjwu4UMLE9-fQjWs6LR45UWRU2XAIf (accessed June 27, 2020).
[103] Baule, A., Morone, F., Herrmann, H.J., et al., "*Edwards statistical mechanics for jammed granular matter,*" Reviews of Modern Physics. 90 (2018).
[104] Jaeger, H.M., Nagel, S.R., and Behringer, R.P., "*Granular solids, liquids, and gases,*" Reviews of Modern Physics. 68 (1996).
[105] Jaeger, H.M., Murphy, K., and Roth, L.K., Architectured Particulate Materials, in: 2018.
[106] BENEDETTI, B.C., and JORGE, J.T., "*EFFECT OF MOISTURE CONTENT ON COEFFICIENTS OF FRICTION AND ANGLE OF REPOSE FOR DIFFERENT TYPES OF GRAINS,*" (n.d.).
[107] Fall, A., Weber, B., Pakpour, M., et al., "*Sliding Friction on Wet and Dry Sand,*" Phys. Rev. Lett. 112 (2014). doi:10.1103/PhysRevLett.112.175502.
[108] Mitarai, N., and Nori, F., "*Wet granular materials,*" Advances in Physics. 55 (2006).
[109] Hornbaker, D.J., Albert, R., Albert, I., et al., "*What keeps sandcastles standing?,*" Nature. 387 (1997). doi:10.1038/42831.
[110] Halsey, T.C., and Levine, A.J., "*How Sandcastles Fall,*" Phys. Rev. Lett. 80 (1998). doi:10.1103/PhysRevLett.80.3141.
[111] Rovero, L., Tonietti, U., Fratini, F., et al., "*The salt architecture in Siwa oasis – Egypt (XII–XX centuries),*" Construction and Building Materials. 23 (2009). doi:10.1016/j.conbuildmat.2009.02.003.
[112] Nijsse, R., Rebuilding Le Corbusier'sWorld Exhibition Pavilion-Electronique in Brussels, 1958, in: Tailor Made Concrete Structures, CRC Press, 2008: pp. 68–70.
[113] "*Growing Islands,*" Self-Assembly Lab. (n.d.). https://selfassemblylab.mit.edu/growingislands (accessed July 2, 2020).
[114] Hensel, M., and Menges, A., "*Aggregates,*" Architectural Design. 78 (2008). doi:10.1002/ad.645.
[115] Weinstock, M., The Architecture of Emergence: The Evolution of Form in Nature and Civilisation, 1st edition, Wiley, Chichester, U.K, 2010.
[116] Malm, H., Joyce, S., Tsigkari, M., et al., Designing the Desert, in: Modelling Behaviour, Springer, 2015: pp. 159–168.
[117] Wheatstone, C., "*On the Figures Obtained by Strewing Sand on Vibrating Surfaces, Commonly Called Acoustic Figures,*" Philosophical Transactions of the Royal Society of London. 123 (1833).
[118] Ernst Florens Friedrich Chladni, Traité d'acoustique, Chez Courcier, 1809. http://archive.org/details/traitdacoustiqu00chlagoog (accessed August 21, 2018).

[119] Stöckmann, H.-J., "*Chladni meets Napoleon,*" Eur. Phys. J. Spec. Top. 145 (2007). doi:10.1140/epjst/e2007-00144-5.
[120] Faraday, M., "*XVII. On a peculiar class of acoustical figures; and on certain forms assumed by groups of particles upon vibrating elastic surfaces,*" Phil. Trans. R. Soc. Lond. 121 (1831). doi:10.1098/rstl.1831.0018.
[121] van Gerner, H.J., van der Weele, K., van der Meer, D., et al., "*Scaling behavior of coarsening Faraday heaps,*" Physical Review E. 92 (2015). doi:10.1103/PhysRevE.92.042203.
[122] Jenny, H., Cymatics: A Study of Wave Phenomena & Vibration, 3rd edition, MACROmedia Publishing, Newmarket, NH, 2001.
[123] Zhou, Q., Sariola, V., Latifi, K., et al., "*Controlling the motion of multiple objects on a Chladni plate,*" Nature Communications. 7 (2016). doi:10.1038/ncomms12764.
[124] Ochiai, Y., Hoshi, T., and Rekimoto, J., "*Three-dimensional mid-air acoustic manipulation by ultrasonic phased arrays,*" PloS One. 9 (2014).
[125] Çalışır, P., "*FORM-FINDING WITH EXPERIMENTATION ON NATURAL PERIODIC FORCES: THE SOUND MOTION STREAKS PROJECT,*" (n.d.).
[126] Leach, N., "*Digital Cities,*" Architectural Design. 79 (2009). doi:10.1002/ad.911.
[127] McLaren, C.P., Kovar, T.M., Penn, A., et al., "*Gravitational instabilities in binary granular materials,*" Proceedings of the National Academy of Sciences. 116 (2019).
[128] Caballero, G., Bergmann, R., van der Meer, D., et al., "*Role of Air in Granular Jet Formation,*" Phys. Rev. Lett. 99 (2007). doi:10.1103/PhysRevLett.99.018001.
[129] Huijben, F., "*Vacuumatic formwork: a novel granular manufacturing technique for producing topology-optimised structures in concrete,*" Granular Matter. 18 (2016). doi:10.1007/s10035-015-0602-0.
[130] Beakawi Al-Hashemi, H.M., and Baghabra Al-Amoudi, O.S., "*A review on the angle of repose of granular materials,*" Powder Technology. 330 (2018). doi:10.1016/j.powtec.2018.02.003.
[131] Liu, Z., "*Measuring the angle of repose of granular systems using hollow cylinders,*" (2011). /paper/Measuring-the-angle-of-repose-of-granular-systems-Liu/7a19190118884bd83555ae80ed0faca622fca745 (accessed June 18, 2020).
[132] Pottmann, H., Asperl, A., Hofer, M., et al., Architectural Geometry, 1st edition, Bentley Institute Press, Exton, Pa, 2007.
[133] "*MATHCURVE.COM,*" (n.d.). https://www.mathcurve.com/ (accessed August 13, 2019).
[134] Kawase, H., Okata, Y., and Ito, K., "*Role of Huge Geometric Circular Structures in the Reproduction of a Marine Pufferfish,*" Scientific Reports. 3 (2013). doi:10.1038/srep02106.
[135] Du, Q., Faber, V., and Gunzburger, M., "*Centroidal Voronoi Tessellations: Applications and Algorithms,*" SIAM Rev. 41 (1999). doi:10.1137/S0036144599352836.
[136] Barlow, G.W., "*Hexagonal territories,*" Animal Behaviour. 22 (1974). doi:10.1016/0003-3472(74)90010-4.
[137] Callan, J., "*Untitled-1997,*" Jonathan Callan. (1997). http://www.jonathancallan.com/ (accessed August 16, 2018).
[138] Métais, J.-B., "*Temps Imparti,*" (1999). http://www.jbmetais.com/index-fr.php?act=article&id=22 (accessed August 7, 2018).
[139] Knipe, J., "*Julia Parkinson,*" Wall Street International. (2018). https://wsimag.com/art/35590-kiting (accessed August 7, 2018).
[140] Weber, K., "*Sandfountain,*" (2012). https://www.contemporaryartdaily.com/2012/11/klaus-weber-at-herald-st-2/ (accessed August 12, 2018).
[141] Malouin, P., "*TIME ELAPSED,*" Philippe Malouin. (2011). http://philippemalouin.com/ (accessed August 12, 2018).
[142] "*felippe moraes makes geometric drawings using pendulum,*" Designboom | Architecture & Design Magazine. (2014). https://www.designboom.com/art/felippe-moraes-pendular-movement-drawings-order-07-29-2014/ (accessed August 7, 2018).
[143] Gijs, van B., "*Skryf,*" Gijs van Bon. (2014). http://www.gijsvanbon.nl/skryf.html (accessed August 16, 2018).
[144] "*Jean Bernard Metais,*" (n.d.). http://www.jbmetais.com/index-fr.php?act=article&id=1 (accessed July 17, 2017).

[145] Dosier, G.K., Methods for making construction material using enzyme producing bacteria, 2011. https://patents.google.com/patent/US8728365B2/en (accessed July 8, 2017).
[146] Dini, E., Method and apparatus for quick production of a conglomerate building structure, WO2011021080A2, 2010. https://patents.google.com/patent/WO2011021080A2/en (accessed July 9, 2017).
[147] Rong, H., Qian, C.-X., and Li, L., "*Study on microstructure and properties of sandstone cemented by microbe cement,*" Constr. Build. Mater. 36 (2012). doi:10.1016/j.conbuildmat.2012.06.063.
[148] Jonkers, H.M., Thijssen, A., Muyzer, G., et al., "*Application of bacteria as self-healing agent for the development of sustainable concrete,*" Ecological Engineering. 36 (2010). doi:10.1016/j.ecoleng.2008.12.036.
[149] Achal, V., Mukherjee, A., Kumari, D., et al., "*Biomineralization for sustainable construction – A review of processes and applications,*" Earth-Science Reviews. 148 (2015). doi:10.1016/j.earscirev.2015.05.008.
[150] Achal, V., and Kawasaki, S., "*Biogrout: A Novel Binding Material for Soil Improvement and Concrete Repair,*" Front Microbiol. 7 (2016). doi:10.3389/fmicb.2016.00314.
[151] Bernardi, D., DeJong, J.T., Montoya, B.M., et al., "*Bio-bricks: Biologically cemented sandstone bricks,*" Constr. Build. Mater. 55 (2014). doi:10.1016/j.conbuildmat.2014.01.019.
[152] Jason T. DeJong, Michael B. Fritzges, and Klaus Nüsslein, "*Microbially Induced Cementation to Control Sand Response to Undrained Shear,*" J GEOTECH GEOENVIRON. 132 (2006). doi:10.1061/(ASCE)1090-0241(2006)132:11(1381).
[153] Jonkers, H.M., Healing agent in cement-based materials and structures, and process for its preparation, 2008. https://patents.google.com/patent/EP2082999A1/en (accessed July 8, 2017).
[154] Abo-El-Enein, S.A., Ali, A.H., Talkhan, F.N., et al., "*Application of microbial biocementation to improve the physico-mechanical properties of cement mortar,*" HBRC Journal. 9 (2013). doi:10.1016/j.hbrcj.2012.10.004.
[155] Cheng, L., and Cord-Ruwisch, R., "*In situ soil cementation with ureolytic bacteria by surface percolation,*" Ecological Engineering. 42 (2012). doi:10.1016/j.ecoleng.2012.01.013.
[156] Brown, J.R., ed., Chapter 14 - Sodium silicate bonded sand, in: Foseco Ferrous Foundryman's Handbook (Eleventh Edition), Butterworth-Heinemann, Oxford, 2000: pp. 204–215. doi:10.1016/B978-075064284-2/50015-6.
[157] Imagawa, N., Silicon carbide structure and method of producing the same, US20130292704 A1, 2013. http://www.google.com/patents/US20130292704.
[158] Dillenburger, B., and Hansmeyer, M., Printing architecture: castles made of sand, in: FABRICATE 2014, 2014.
[159] MEIBODI, M.A., BERNHARD, M., JIPA, A., et al., THE SMART TAKES FROM THE STRONG:: 3D PRINTING STAY-IN-PLACE FORMWORK FOR CONCRETE SLAB CONSTRUCTION, in: A, MENGES, B, SHEIL, R, GLYNN, M, SKAVARA (Eds.), Fabricate 2017, UCL Press, 2017: pp. 210–217. http://www.jstor.org/stable/j.ctt1n7qkg7.33.
[160] "*Binders | ExOne,*" (n.d.). http://www.exone.com/Resources/Binders (accessed July 8, 2017).
[161] "*Sand | voxeljet sand casting,*" Voxeljet.Com. (n.d.). https://www.voxeljet.com/materials/sand/ (accessed July 8, 2017).
[162] Gardiner, J., Exploring the emerging design territory of construction 3D printing - project led architectural research, RMIT University, 2011. https://researchbank.rmit.edu.au/view/rmit:160277 (accessed July 9, 2017).
[163] Wang, Y., Fred, C., Magda, S., et al., "*Characterization of Hydrocarbon Emissions from Green Sand Foundry Core Binders by Analytical Pyrolysis (PDF Download Available),*" ResearchGate. (n.d.). doi:http://dx.doi.org/10.1021/es071657o.
[164] "*Advances Made in Mega Freeform Construction,*" (n.d.). http://www.rapidtoday.com/freeform-construction.html (accessed July 9, 2017).
[165] Richthofen, A. von, and Hebel, D.E., "*Constructing Sand: Exploring Alternatives,*" FCL Magazine Special Issue. (2015). doi:10.3929/ethz-a-010636984.
[166] "*Kayser Works,*" Kayser Works. (n.d.). https://kayserworks.com (accessed July 6, 2020).

[167] Kenisarin, M., and Mahkamov, K., "*Salt hydrates as latent heat storage materials:Thermophysical properties and costs,*" Solar Energy Materials and Solar Cells. 145 (2016). doi:10.1016/j.solmat.2015.10.029.
[168] Garg, H.P., Mullick, S.C., and Bhargava, V.K., Solar Thermal Energy Storage, Springer Science & Business Media, 2012.
[169] Kośny, J., Short History of PCM Applications in Building Envelopes, in: PCM-Enhanced Building Components, Springer, Cham, 2015: pp. 21–59. doi:10.1007/978-3-319-14286-9_2.
[170] Hadjieva, M., Stoykov, R., and Filipova, T., "*Composite salt-hydrate concrete system for building energy storage,*" Renewable Energy. 19 (2000). doi:10.1016/S0960-1481(99)00024-5.
[171] Garg, H.P., and Nasim, M., "*Studies on low-temperature salt-hydrate for thermal storage applications,*" Energy Conversion and Management. 21 (1981). doi:10.1016/0196-8904(81)90033-9.
[172] Stunić, Z., Djuričković, V., Majstorović, S., et al., "*Study of multicycle melting and freezing of sodium thiosulphate pentahydrate,*" J. Chem. Technol. Biotechnol. 32 (1982). doi:10.1002/jctb.5030320205.
[173] Young, S.W., and Burke, W.E., "*FURTHER STUDIES ON THE HYDRATES OF SODIUM THIOSULPHATE.,*" J. Am. Chem. Soc. 28 (1906). doi:10.1021/ja01969a002.
[174] Sharma, A., Tyagi, V.V., Chen, C.R., et al., "*Review on thermal energy storage with phase change materials and applications,*" Renewable and Sustainable Energy Reviews. 13 (2009). doi:10.1016/j.rser.2007.10.005.
[175] Sharma, S.K., Jotshi, C.K., Kumar, S., et al., "*Dehydration kinetics of sodium thiosulphate pentahydrate in thermal energy storage,*" ResearchGate. (1985). https://www.researchgate.net/publication/256512939_Dehydration_kinetics_of_sodium_thiosulphate_pentahydrate_in_thermal_energy_storage (accessed August 11, 2017).
[176] Llorens, J., Fabric Structures in Architecture, Elsevier, 2015.
[177] Magnaval, T., "*Le sable et le sel comme nouveau matériau de coffrage,*" Matériaux Pour l'éco-Conception. (2018). https://seminairemateriaux.wordpress.com/2018/01/06/le-sable-et-le-sel-comme-nouveau-materiau-de-coffrage/ (accessed December 3, 2020).
[178] Hussein, A., Lipo, B., Dal Pont, S., et al., "*Mechanical characterization of Hyposand: A new material of sand solidified by sodium thiosulphate salt,*" Construction and Building Materials. 221 (2019).
[179] Besler, H., The Great Sand Sea in Egypt: Formation, Dynamics and Environmental Change - a Sediment-analytical Approach, Elsevier, Oxford, 2011.
[180] El-Bayomi, G.M., "*Coastal Environmental Changes Along the North Western Coast of Egypt Case Study from Alexandria to El Alamein Coast,*" Forum Geografic. VIII (2009).
[181] Wentworth, C.K., "*A Scale of Grade and Class Terms for Clastic Sediments,*" The Journal of Geology. 30 (1922).
[182] Powers, M.C., "*A new roundness scale for sedimentary particles,*" Journal of Sedimentary Research. 23 (1953). doi:10.1306/D4269567-2B26-11D7-8648000102C1865D.
[183] Hryciw Roman D., Zheng Junxing, and Shetler Kristen, "*Particle Roundness and Sphericity from Images of Assemblies by Chart Estimates and Computer Methods,*" Journal of Geotechnical and Geoenvironmental Engineering. 142 (2016). doi:10.1061/(ASCE)GT.1943-5606.0001485.
[184] Folk, R.L., Petrology of Sedimentary Rocks, Cambridge University Press, 2009.
[185] Blott, S.J., and Pye, K., "*GRADISTAT: a grain size distribution and statistics package for the analysis of unconsolidated sediments,*" Earth Surf. Process. Landforms. 26 (2001). doi:10.1002/esp.261.
[186] Holtz, R.D., Kovacs, W.D., and Sheahan, T.C., An Introduction to Geotechnical Engineering, 2 edition, Pearson, Upper Saddle River, NJ, 2010.
[187] Selley, R.C., Applied Sedimentology, Elsevier, 2000.
[188] Friedman, G.M., "*On Sorting, Sorting Coefficients, and the Lognormality of the Grain-Size Distribution of Sandstones,*" The Journal of Geology. 70 (1962).
[189] Krumbein, W.C., and Sloss, L.L., "*Stratigraphy and Sedimentation,*" Soil Science. 71 (1951).
[190] Cao, V.D., Pilehvar, S., Salas-Bringas, C., et al., "*Microencapsulated phase change materials for enhancing the thermal performance of Portland cement concrete and*

*geopolymer concrete for passive building applications,*" Energy Conversion and Management. 133 (2017). doi:10.1016/j.enconman.2016.11.061.
[191] Ashby, M.F., and Cebon, D., "*Materials selection in mechanical design,*" MRS Bull. 30 (2005).
[192] "*Wolfram MathWorld,*" (n.d.). http://mathworld.wolfram.com/ (accessed November 7, 2019).
[193] Deza, M.M., and Deza, E., Encyclopedia of Distances, Springer-Verlag, Berlin Heidelberg, 2009. doi:10.1007/978-3-642-00234-2.
[194] Dobrin, A., "*A review of properties and variations of Voronoi diagrams,*" Whitman College. (2005).
[195] Aurenhammer, F., Klein, R., and Lee, D.-T., Voronoi Diagrams and Delaunay Triangulations, 1 edition, World Scientific Publishing Company, Hackensack, New Jersey, 2013.
[196] Hoff III, K.E., Keyser, J., Lin, M., et al., Fast computation of generalized Voronoi diagrams using graphics hardware, in: Proceedings of the 26th Annual Conference on Computer Graphics and Interactive Techniques, ACM Press/Addison-Wesley Publishing Co., 1999: pp. 277–286.
[197] Thamsonglar, C., Algorithm for computation and visualization of weighted constrained Voronoi diagrams, University of Missouri--Columbia, 2009.
[198] Attali, D., Boissonnat, J.-D., and Edelsbrunner, H., Stability and computation of medial axes-a state-of-the-art report, in: Mathematical Foundations of Scientific Visualization, Computer Graphics, and Massive Data Exploration, Springer, 2009: pp. 109–125.
[199] Siddiqi, K., and Pizer, S., Medial representations: mathematics, algorithms and applications, Springer Science & Business Media, 2008.
[200] Zhu, Y., Sun, F., Choi, Y.-K., et al., "*Computing a compact spline representation of the medial axis transform of a 2D shape,*" Graphical Models. 76 (2014).
[201] Au, C., "*A simple algorithm for medial axis transform computation,*" Engineering with Computers. 29 (2013).
[202] Kosinka, J., and Lávička, M., "*A unified Pythagorean hodograph approach to the medial axis transform and offset approximation,*" Journal of Computational and Applied Mathematics. 235 (2011).
[203] Calvache, P., Dune Surfaces: A Spatial Visualization Technique for Medial Axes in the Plane or on the Sphere, in: Proceedings of Bridges 2012: Mathematics, Music, Art, Architecture, Culture, Tessellations Publishing, 2012: pp. 439–442.
[204] "*Surface d'égale pente,*" (n.d.). https://mathcurve.com/surfaces/talus/talus.shtml (accessed August 30, 2020).
[205] Aguirre, M.A., Grande, J.G., Calvo, A., et al., "*Pressure independence of granular flow through an aperture,*" Physical Review Letters. 104 (2010).
[206] Flores, J., Solovey, G., and Gil, S., "*Flow of sand and a variable mass Atwood machine,*" American Journal of Physics. 71 (2003).
[207] "*SCULPTING with kuka - robotic sand forming,*" IAAC Blog. (n.d.). http://www.iaacblog.com/programs/sculpting-with-kuka-robotic-sand-forming/ (accessed July 26, 2019).
[208] "*The Consortium for Research and Robotics,*" The Consortium for Research and Robotics. (n.d.). https://consortiumrr.com/ (accessed July 26, 2019).
[209] Flöry, S., Nagai, Y., Isvoranu, F., et al., Ruled Free Forms, in: L, Hesselgren, S, Sharma, J, Wallner, N, Baldassini, P, Bompas, J, Raynaud (Eds.), Advances in Architectural Geometry 2012, Springer Vienna, Vienna, 2013: pp. 57–66. doi:10.1007/978-3-7091-1251-9_4.
[210] Flöry, S., Pottmann, H., Mitani, J., et al., "*Ruled Surfaces for Rationalization and Design in Architecture,*" LIFE in:Formation, On Responsive Information and Variations in Architecture: Proceedings of the 30th Annual Conference of the Association for Computer Aided Design in Architecture (ACADIA). 1 (2010). https://cumincad.architexturez.net/doc/oai-cumincadworks-id-acadia10-103 (accessed January 27, 2019).
[211] Lazureanu, C., "*Spirals on surfaces of revolution,*" (n.d.).
[212] "*Circular helix,*" (n.d.). https://www.mathcurve.com/courbes3d.gb/helicecirculaire/helicecirculaire.shtml (accessed October 18, 2019).

[213] "*Conical helix,*" (n.d.). https://www.mathcurve.com/courbes3d.gb/heliceconic/heliceconic.shtml (accessed October 18, 2019).